Seismic Evaluation of Older Concrete Buildings for Collapse Potential

FEMA P-2018 / December 2018

FEMA

nehrp

Seismic Evaluation of Older Concrete Buildings for Collapse Potential

Prepared by

APPLIED TECHNOLOGY COUNCIL
201 Redwood Shores Parkway, Suite 240
Redwood City, California 94065
www.ATCouncil.org

Prepared for

FEDERAL EMERGENCY MANAGEMENT AGENCY
Michael Mahoney, Project Officer
Robert D. Hanson, Technical Monitor
Washington, D.C.

APPLIED TECHNOLOGY COUNCIL
Jon A. Heintz, Project Manager

PROJECT TECHNICAL COMMITTEE
William T. Holmes (Project Tech. Director)
Abbie Liel
Michael Mehrain
Jack P. Moehle
Peter Somers

WORKING GROUP MEMBERS
Saman A. Abdullah
Carlos Arteta
Supratik Bose
Panagiotis Galanis
Cody Harrington
Travis Marcilla
Pablo Parra
Siamak Sattar
Andreas Stavridis
Duy Vu To

PROJECT REVIEW PANEL
Terry Lundeen (Chair)
Michael Cochran
Gregory G. Deierlein
Ken Elwood
Josh Gebelein
Laura N. Lowes
Khalid Mosalam
Robert Pekelnicky
Pui-Shum Shing
Bill Tremayne
Fred Turner
John W. Wallace

Notice

Any opinions, findings, conclusions, or recommendations expressed in this publication do not necessarily reflect the views of the Applied Technology Council (ATC), the Department of Homeland Security (DHS), or the Federal Emergency Management Agency (FEMA). Additionally, neither ATC, DHS, FEMA, nor any of their employees, makes any warranty, expressed or implied, nor assumes any legal liability or responsibility for the accuracy, completeness, or usefulness of any information, product, or process included in this publication. Users of information from this publication assume all liability arising from such use.

Cover photograph – Older concrete building damaged in the 2010 Maule earthquake, located in Vina del Mar, Chile (photo courtesy of J. Heintz).

Foreword

The Federal Emergency Management Agency (FEMA) has the goal of reducing the ever-increasing cost that disasters inflict on our country. Preventing losses before they happen by designing and building to withstand anticipated forces from these hazards is one of the key components of mitigation, and is the only truly effective way of reducing the cost of disasters.

As part of its responsibilities under the National Earthquake Hazards Reduction Program (NEHRP), and in accordance with the National Earthquake Hazards Reduction Act of 1977 (PL 94-125, as amended), FEMA is charged with supporting activities necessary to improve technical quality in the field of earthquake engineering. The primary method of addressing this charge has been supporting the investigation of seismic technical issues as they are identified by FEMA, the development and publication of technical design and construction guidance products, the dissemination of these products, and support of training and related outreach efforts.

One of the issues still of significant concern for the Program is the risk presented by older, seismically vulnerable concrete buildings, known as non-ductile concrete buildings. These are concrete frame buildings constructed prior to the mid-1970s, including archaic designs dating back to the early 1900s. One of the lessons to come out of the 1971 San Fernando earthquake was the poor performance of concrete frame buildings and how design codes of that era did not provide for sufficient steel reinforcing to confine the concrete within the building columns during earthquake shaking. The most famous example of this type of failure was the partial collapse of the new Olive View Hospital in Sylmar. By the mid-1970s, design codes had increased the amount and detailing of steel reinforcing to prevent this type of failure. However, these buildings still exist in great numbers and still pose significant risk.

Although retrofitting criteria for seismically deficient non-ductile concrete buildings has been developed, the problem remains one of efficient identification of the most hazardous buildings. Not all pre-1970s concrete buildings are equally hazardous; generally, only those with columns that would fail in shear and/or compression. It is often difficult to visually determine which of these buildings are collapse hazards and which are not. Although some non-ductile concrete buildings may not be collapse hazards, this construction type includes some of most seismically dangerous buildings because of their potential occupancy load.

This report, *Seismic Evaluation of Older Concrete Buildings for Collapse Potential* (FEMA P-2018), provides a simplified methodology for evaluating collapse resistance using simplified estimates of drift demand. The calculations have been intentionally simplified; however, the underlying criteria are based on probabilistic concepts and structural reliability theory. Development of the procedures included testing of the methodology by practicing engineers in several rounds of trial evaluations, and vetting of the methodology in a series of annual workshops. All of this was used to adjust and improve the methodology throughout the development process.

This project also coordinated with, and included, the results of other ongoing research in this area. This includes the National Science Foundation's Network for Earthquake Engineering Simulation (NSF/NEES) Grand Challenge Project with the Pacific Earthquake Engineering Research Center (PEER). In addition, this project also worked closely with the Concrete Coalition, a group formed by the Earthquake Engineering Research Institute (EERI) to coordinate low-cost mitigation of the risks from this building type.

FEMA is indebted to the leadership of Bill Holmes, Project Technical Director, and to the members of the project technical team, trial evaluators, and workshop participants, for their efforts in the development of this methodology. The Project Management Committee, consisting of Abbie Liel, Mike Mehrain, Jack Moehle, and Peter Somers, led the technical development efforts, and guided the investigations of the Project Working Groups.

FEMA also wishes to thank the Project Review Panel, which consisted of Terry Lundeen (Chair), Mike Cochran, Greg Deierlein, Ken Elwood, Josh Gebelein, Laura Lowes, Khalid Mosalam, Bob Pekelnicky, Benson Shing, Bill Tremayne, Fred Turner, and John Wallace. This group provided significant technical advice and consultation over the duration of the work. The names and affiliations of all who contributed to this report are provided in the list of Project Participants at the end of this report.

Without their dedication and hard work, this publication would not have been possible.

Federal Emergency Management Agency

Preface

In 2009, the Applied Technology Council (ATC) was awarded the first in a series of contracts with the Federal Emergency Management Agency (FEMA) for “Identification and Mitigation of Non-Ductile Concrete Buildings,” identified as the ATC-78 Project Series. The overall purpose of this series of projects was to develop an evaluation methodology that could be used to identify and prioritize the most seismically hazardous non-ductile concrete buildings in an inventory of buildings in a way that was easier and less expensive to apply than evaluation and retrofit methodologies currently available and in use at the time.

The need to address non-ductile concrete buildings was identified as a national imperative in the early 2000s, and the work on this project was coordinated with results from related projects funded by the National Earthquake Hazards Reduction Program (NEHRP), the National Institute of Standards and Technology (NIST), and the National Science Foundation (NSF), as well as other FEMA-sponsored projects, published in 2010 and later.

The resulting methodology is based on the evolution of procedures as outlined in the ATC-78 series of reports published between 2011 and 2017. In the methodology, collapse is defined as the global loss of vertical load-carrying ability at a story, possibly leading to the collapse of other stories. Procedures for evaluating collapse resistance require simplified estimates of drift demand to implement. Although the calculations are intentionally simplified, the underlying criteria are based on probabilistic concepts and structural reliability theory. The methodology and calculation procedures are based on detailed analytical study, and have taken years to develop. A key aspect of the developmental process has included testing of the methodology by practicing engineers and researchers in several rounds of trial evaluations, and vetting of the methodology in annual workshops. The trial evaluations and workshop discussions were used to adjust and enhance the methodology along the way, and the results have significantly impacted the final product.

ATC is indebted to the leadership of Bill Holmes, Project Technical Director, and to the members of the ATC-78 Project Team, trial evaluators, and workshop participants, for their efforts in the development of this methodology. The Project Management Committee, consisting of Abbie Liel, Mike Mehrain, Jack Moehle, and Peter Somers, led the technical development efforts, and guided the investigations of the Project Working Groups, which included Saman Abdullah, Carlos Arteta, Supratik Bose, Panagiotis Galanis, Cody Harrington, Travis Marcilla, Pablo Parra, Siamak Sattar, Andreas Stavridis, and Duy Vu To.

The Project Review Panel, consisting of Terry Lundeen (Chair), Mike Cochran, Greg Deierlein, Ken Elwood, Josh Gebelein, Laura Lowes, Khalid Mosalam, Bob Pekelnicky, Benson Shing, Bill Tremayne, Fred Turner, and John Wallace provided technical advice and consultation over the duration of the work. The names and affiliations of all who contributed to this report are provided in the list of Project Participants at the end of this report.

ATC also gratefully acknowledges Michael Mahoney (FEMA Project Officer) and Robert Hanson (FEMA Technical Monitor) for their input and guidance in the conduct of this work, and Carrie Perna for ATC report production services.

Jon A. Heintz
ATC Executive Director

Table of Contents

Foreword iii

Preface v

List of Figures xv

List of Tables xxvii

1. Introduction 1-1
- 1.1 ATC-78 Project Series 1-1
- 1.2 Evaluation Methodology 1-3
- 1.3 Comparison with ASCE/SEI 41 1-5
- 1.4 Policy Implications 1-6
- 1.5 Report Organization and Content 1-9

2. Evaluation Methodology 2-1
- 2.1 Scope and Applicability 2-1
  - 2.1.1 Applicability 2-1
  - 2.1.2 Seismic Deficiencies that are not Considered in the Methodology 2-3
  - 2.1.3 Buildings with Concrete Components that are not Considered in the Methodology 2-3
- 2.2 Overview of the Evaluation Methodology 2-4
  - 2.2.1 Overview of Key Calculation Procedures 2-5
  - 2.2.2 Early Identification of Lower Seismic Risk Buildings 2-7
  - 2.2.3 Early Identification of Exceptionally High Seismic Risk Buildings 2-7
- 2.3 Use of Alternate Analysis Procedures 2-8

3. General Requirements 3-1
- 3.1 As-Built Information 3-1
- 3.2 Site Investigation 3-2
- 3.3 Seismic Hazard 3-2
- 3.4 Material Properties 3-3
  - 3.4.1 General 3-3
  - 3.4.2 Concrete and Reinforcing Steel 3-3
  - 3.4.3 Masonry Infill 3-3
- 3.5 Condition of Structural Components 3-5
- 3.6 Structural Load Path Requirements 3-5
  - 3.6.1 Diaphragm Continuity 3-5
  - 3.6.2 Concrete Element Interconnectivity 3-6
- 3.7 Penthouse and Other Rooftop Structures 3-7

4. Component Strengths..4-1
4.1 Introduction..4-1
4.2 Axial Loads on Columns and Walls..4-1
  4.2.1 Expected Gravity Loads..4-1
  4.2.2 Earthquake Axial Loads..4-1
  4.2.3 Load Combinations..4-2
4.3. Component Strength Calculations..4-2
  4.3.1 General..4-2
  4.3.2 Concrete Column Strength..4-3
  4.3.3 Beam-Column Joint Shear Strength..4-4
  4.3.4 Slab-Column Frame Strength and Integrity Requirements..4-5
  4.3.5 Concrete Wall Strength..4-6
  4.3.6 Infilled Frame Strength..4-6
4.4 Column Shear Strength Ratio..4-9
  4.4.1 Column Shear Capacity in a Typical Story..4-9
  4.4.2 Slab-Column Frames..4-10

5. Structural Classification..5-1
5.1 Introduction..5-1
5.2 Classification of Concrete Components..5-2
  5.2.1 Reinforced Concrete Columns..5-2
  5.2.2 Reinforced Concrete Structural Walls..5-2
5.3 Classification of Building Systems..5-3
  5.3.1 Frame Systems..5-3
  5.3.2 Frame-Wall Systems..5-3
  5.3.3 Bearing Wall Systems..5-4
  5.3.4 Infilled Frame Systems..5-4
5.4 Wall Index and Wall Strength Index..5-5
  5.4.1 Wall Index..5-5
  5.4.2 Wall Strength Index..5-6
  5.4.3 Identification of Lower Seismic Risk Buildings using the Wall Strength Index..5-6
5.5 Effective Yield Strength..5-7
  5.5.1 Plastic Mechanism Base-Shear Strength for Frames and Walls..5-7
  5.5.2 Plastic Mechanism Base-Shear Strength for Infilled Frame Systems..5-15
  5.5.3 Plastic Mechanism Base-Shear Strength for Mezzanines and Other Configurations..5-17
  5.5.4 Three-Dimensional Considerations..5-18
  5.5.5 Base Shear Ratio..5-19
5.6 Effective Fundamental Period..5-19
  5.6.1 Determination of Effective Period by Formula..5-20
  5.6.2 Determination of Effective Period by Structural Analysis..5-21
5.7 Global Demand-to-Capacity Ratio..5-21
5.8 Identification of Lower Seismic Risk Buildings..5-22
  5.8.1 Essentially Elastic Buildings..5-22
5.9 Identification of Exceptionally High Seismic Risk Buildings..5-22
  5.9.1 Exceptionally Weak Buildings..5-22

5.9.2 Discontinuous Walls Supported on Columns, Wall Piers, or Girders 5-23
5.10 Pounding 5-25
5.10.1 Shorter Interfering Building 5-25
5.10.2 Taller Interfering Building 5-25

6. Evaluation Procedure for Frame Systems 6-1
6.1 Introduction 6-1
6.2 Identify Critical Stories 6-1
6.3 Identify Critical Components 6-2
6.3.1 Critical Columns 6-2
6.3.2 Critical Slab-Column Connections 6-2
6.3.3 Critical Beam-Column Corner Connections 6-3
6.3.4 Discontinuous Columns 6-3
6.4 Calculate Global Seismic Drift Demand 6-3
6.5 Calculate Story Drift Demand 6-4
6.5.1 Adjustment of Story Drift Demand for P-Delta 6-5
6.6 Calculate Drift Demands on Critical Components 6-6
6.6.1 Adjusted Drift Demand on Critical Components 6-6
6.6.2 Torsional Amplification Factor 6-6
6.6.3 Drift Factor 6-6
6.7 Calculate Drift Capacity of Critical Components 6-7
6.7.1 Drift Capacity of Critical Columns 6-7
6.7.2 Drift Capacity of Critical Slab-Column Connections 6-9
6.7.3 Drift Capacity of Critical Beam-Column Corner Connections 6-10
6.8 Determine Column Ratings 6-10
6.8.1 Discontinuous Columns 6-12
6.9 Determine Story Ratings 6-12

7. Evaluation Procedures for Frame-Wall Systems 7-1
7.1 Introduction 7-1
7.2 Identify Critical Stories 7-1
7.3 Identify Critical Components 7-2
7.3.1 Critical Columns 7-2
7.3.2 Critical Walls and Vertical Wall Segments 7-3
7.3.3 Critical Slab-Column Connections 7-3
7.3.4 Critical Beam-Column Corner Connections 7-4
7.3.5 Discontinuous Columns 7-4
7.4 Calculate Global Seismic Drift Demand 7-4
7.5 Calculate Story Drift Demand 7-5
7.6 Calculate Drift Demands on Critical Components 7-6
7.6.1 Adjusted Drift Demand on Critical Components 7-6
7.6.2 Torsional Amplification Factor 7-7
7.6.3 Drift Factor 7-8
7.7 Calculate Drift Capacity of Critical Components 7-9
7.7.1 Drift Capacity of Critical Columns 7-9
7.7.2 Drift Capacity of Critical Slab-Column Connections 7-11
7.7.3 Drift Capacity of Critical Beam-Column Corner Connections 7-12

7.7.4 Drift Capacity of Critical Walls and Vertical Wall Segments....7-12
7.8 Determine Column and Wall Ratings....7-15
7.8.1 Discontinuous Columns....7-17
7.9 Determine Story Ratings....7-17

8. Evaluation Procedures for Bearing Wall Systems....8-1
8.1 Introduction....8-1
8.2 Identify Critical Stories....8-1
8.3 Identify Critical Components....8-2
8.3.1 Critical Walls and Vertical Wall Segments....8-2
8.3.2 Other Critical Components....8-3
8.4 Calculate Global Seismic Drift Demand....8-3
8.5 Calculate Story Drift Demand....8-4
8.6 Calculate Drift Demands on Critical Components....8-5
8.6.1 Adjusted Drift Demand on Critical Components....8-5
8.6.2 Torsional Amplification Factor....8-5
8.6.3 Drift Factor....8-5
8.7 Calculate Drift Capacity of Critical Components....8-6
8.7.1 Drift Capacity of Critical Walls and Vertical Wall Segments....8-6
8.7.2 Drift Capacity of Other Critical Components....8-9
8.8 Determine Wall and Column Ratings....8-9
8.8.1 Determine Wall Ratings....8-9
8.8.2 Determine Column Ratings....8-9
8.9 Determine Story Ratings....8-9

9. Evaluation Procedures for Infilled Frame Systems....9-1
9.1 Introduction....9-1
9.2 Identify Critical Stories....9-2
9.3 Identify Critical Components....9-2
9.3.1 Critical Columns in Infilled Frame Systems....9-2
9.3.2 Other Critical Components....9-2
9.4 Calculate Global Seismic Drift Demand....9-3
9.5 Calculate Story Drift Demand....9-4
9.6 Calculate Drift Demands in Critical Components....9-4
9.6.1 Adjusted Drift Demand on Critical Components....9-4
9.6.2 Torsional Amplification Factor....9-5
9.6.3 Drift Factor....9-6
9.7 Calculate Drift Capacity of Critical Components....9-7
9.7.1 Drift Capacity of Critical Columns in Infilled Frame Systems....9-7
9.7.2 Drift Capacity of Other Critical Components....9-9
9.7.3 Drift Capacity of Critical Walls and Vertical Wall Segments....9-9
9.8 Determine Column and Wall Ratings....9-10
9.8.1 Determine Ratings for Columns in Infilled Frame Systems....9-10
9.8.2 Determine Ratings for Other Critical Components....9-11
9.9 Determine Story Ratings....9-11

10. Determination of Building Rating 10-1
10.1 Introduction 10-1
10.2 Determine Building Rating 10-1
10.3 Recommended Building Risk Levels 10-1
    10.3.1 Exceptionally High Seismic Risk Buildings 10-2
    10.3.2 High Seismic Risk Buildings 10-2
    10.3.3 Lower Seismic Risk Buildings 10-2

Appendix A: Development of Column Drift Capacities A-1
A.1 Introduction A-1
A.2 Column Plastic Rotation Capacity Determination A-1
    A.2.1 Plastic Rotation Capacities for Flexure-Critical Columns A-2
    A.2.2 Plastic Rotation Capacities for Flexure-Shear and Shear-Critical Columns A-2
    A.2.3 Bias in Plastic Rotation Capacity Predictions A-2
    A.2.4 Comparison of Plastic Rotation Capacity Prediction Methods A-4
    A.2.5 Uncertainty in Plastic Rotation Capacities A-6
    A.2.6 Elastic Component of Column Drift Capacity A-7
    A.2.7 Drift Capacity of Columns with Inadequate Lap Splices A-7
A.3 Slab-Column Connection Drift Capacity Determination A-7

Appendix B: Development of Method for Determining Column Ratings B-1
B.1 Overview B-1
B.2 Structural Reliability Methods for Computing the Column Rating B-1

Appendix C: Development of Method for Determining Story Ratings C-1
C.1 Overview C-1
C.2 Probability Theory for Determining Probability of Story Collapse C-1
C.3 Development of Story Ratings C-2

Appendix D: Wall Strength Index (WSI) Method D-1
D.1 Overview D-1
D.2 Numerical Simulation D-2
    D.2.1 Buildings Analyzed D-2
    D.2.2 Modeling D-3
    D.2.3 Ground Motion Selection and Scaling D-4
    D.2.4 Collapse D-4
    D.2.5 Results D-5
D.3 Analytical Investigation of WSI D-7
D.4 Limitations D-9
D.5 Conclusions D-10

Appendix E: Exceptionally Weak Building Criteria E-1
E.1 Overview E-1
E.2 Modeling E-2
E.3 Ground Motion Selection and Scaling E-2

E.4 Collapse E-2
E.5 Development of Criteria for Exceptionally Weak Frame Buildings E-2
E.6 Investigation of Criteria for Exceptionally Weak Frame-Wall Buildings E-5

Appendix F: Beam-Column Joints F-1
F.1 Introduction F-1
F.2 Performance of Connections with Discontinuous Beam Bottom Longitudinal Reinforcement F-1
F.3 Strength of Joints in Beam-Column Connections without Joint Transverse Reinforcement F-2
F.4 Effect of Joint Eccentricity on Joint and Column Behavior F-3
F.5 Axial Failure of Beam-Column Connections F-5

Appendix G: Effective Fundamental Period G-1
G.1 Frame Buildings G-1
G.2 Frames with Deep Spandrels G-4
G.3 Pier-Spandrel Systems G-4
G.4 Wall and Frame-Wall Buildings G-8

Appendix H: Development of Procedures to Estimate Story Drift Demands H-1
H.1 Introduction H-1
H.2 Studies of the SDOF Drift Demand H-1
  H.2.1 Basic Procedure to Calculate SDOF Drift Demand H-1
  H.2.2 Comparison with Results of Nonlinear Response History Analyses H-2
H.3 Studies of the Story Drift Demand H-5
  H.3.1 Basic Procedure to Calculate Story Drift Demand H-5
  H.3.2 Bare Frames H-5
  H.3.3 Frames and Walls H-14
  H.3.4 Frames with Walls Discontinuous in the First Story H-19
  H.3.5 Frames with Walls Discontinuous in Upper Stories H-22
  H.3.6 Buildings with Shear-Critical Walls H-27

Appendix I: Torsion Studies I-1
I.1 Introduction I-1
I.2 Identify Critical Stories I-2
I.3 Simulation of Collapse of Torsionally-Sensitive Buildings I-4
  I.3.1 Buildings Analyzed I-4
  I.3.2 Modeling I-6
  I.3.3 Analysis Procedures I-7
  I.3.4 Detailed Results for Selected Buildings I-8
  I.3.5 Normalization of Results for Comparison between Buildings I-9
I.4 Extreme Torsion I-10
I.5 Neglecting Torsion I-11
I.6 Torsional Amplification I-13
  I.6.1 Torsional Amplification Overview I-13
  I.6.2 Extraction of Torsional Amplification from Analytical Models I-13

I.6.3 Torsional Amplification Results I-15
I.6.4 Torsional Amplification Calculations in Each Column I-16
I.7 Comparison of Results to Other Torsion Studies I-16

Appendix J: Determination of Drift Factors J-1
J.1 Overview J-1
J.2 Drift Factor for Critical Columns J-1
J.2.1 Buildings Analyzed J-1
J.2.2 Results J-1
J.3 Drift Factor for Critical Slab-Column Connections and Beam-Column Corner Connections J-3
J.4 Drift Factor for Critical Wall and Wall Segments......J-3

Appendix K: Archetype Building Analysis Methods...... K-1
K.1 Introduction K-1
K.2 Nonlinear Static Analysis...... K-1
K.3 Incremental Dynamic Analysis K-1
K.4 Dynamic Analyses with Hazard-Consistent Ground Motions...... K-4
K.5 Dynamic Analyses for Torsion Studies...... K-9

Appendix L: Frame and Wall Modeling Procedures......L-1
L.1 Introduction L-1
L.2 Bare Frames Models......L-1
L.2.1 Building with Flexure-Controlled Columns......L-2
L.2.2 Building with Shear-Critical Columns L-3
L.3 Modeling Criteria of Frame-Wall Systems L-3
L.3.1 Frame-Wall Definition L-4
L.3.2 Wall Modeling Approach for Frame-Wall Systems....L-5
L.3.3 Frame Modeling Approach for Frame-Wall Systems......L-11

Appendix M: Column Shear Strength M-1
M.1 Column Shear Strength Equation M-1

Appendix N: Development of Wall Drift Capacities...... N-1
N.1 Introduction N-1
N.2 Expected Wall Behavior and Failure Mode N-1
N.3 Drift Capacity of Poorly Detailed Flexure-Controlled Walls...... N-3
N.4 Drift Capacity of Shear-Controlled Walls/Piers...... N-6
N.5 Drift Capacity of Walls with Inadequate Lap Splices N-9
N.6 Drift Capacity of Walls with L-Shaped, T-Shaped, and Half-Barbell Cross-Sections N-9
N.7 Drift Capacity of Walls Spirally Reinforced Columns at the Boundary Regions N-10
N.7.1 Flexure-Controlled Walls with Spirally Reinforced Columns N-11
N.7.2 Shear-Controlled Walls with Spirally Reinforced Columns N-11

Appendix O: Studies on Infilled Frames O-1
O.1 Introduction..O-1
O.2 Simulation of Collapse of Buildings Infilled with Solid Infills..O-2
O.2.1 Details of the Prototype Buildings...............................O-2
O.2.2 Development of Numerical Models............................O-4
O.2.3 Nonlinear Time-History Analyses...............................O-6
O.2.4 Detailed Results for Prototype Buildings O-7
O.3 Calculation of Strength of Infilled Frame Buildings O-9
O.3.1 Default Material Properties...O-9
O.3.2 Plastic Mechanism of Infilled Frames O-10
O.3.3 Column Effective Length O-10
O.3.4 Classification of Infilled Frames based on Failure Mechanism...O-12
O.3.5 Strength of Single Infilled Bay with Solid Panel......O-13
O.3.6 Strength of Single Infilled Bay with Openings.........O-15
O.3.7 When to Ignore Infills in Strength O-19
O.3.8 Calculation of Story-Shear Strength.........................O-21
O.4 Estimation of Effective Periods O-23
O.5 Determination of Story-Drifts..O-24
O.6 Impact of Infill on Column Ratings......................................O-25

Symbols P-1

References Q-1

Project Participants...R-1

List of Figures

Figure 4-1 Illustration of slab-column structural integrity requirements 4-5

Figure 4-2 Illustration of symbols defining the geometry of masonry infill panels 4-7

Figure 5-1 Illustration of terms in Equation 5-4 and Equation 5-5 5-8

Figure 5-2 Mechanism 1 for calculation of plastic mechanism base-shear strength..................... 5-9

Figure 5-3 Mechanism 2 for calculation of plastic mechanism base-shear strength..................... 5-10

Figure 5-4 Mechanism 3 for calculation of plastic mechanism base-shear strength..................... 5-12

Figure 5-5 Mechanism 4 for calculation of plastic mechanism base-shear strength..................... 5-14

Figure 5-6 Possible mechanisms for calculation of plastic mechanism base-shear strength of frames with mezzanines..................... 5-17

Figure 5-7 Kinematically compatible three-dimensional plastic mechanisms..................... 5-18

Figure 5-8 Mechanisms in buildings with extreme torsion............... 5-18

Figure 5-9 Force-displacement curve, showing the definition of effective stiffness, K_e, for calculation of the effective fundamental period..................... 5-19

Figure 6-1 Illustration of possible critical conditions for a column in a slab-column frame 6-12

Figure 7-1 Illustration of possible critical conditions for a column in a slab-column frame 7-16

Figure A-1 Ratio of measured to predicted plastic rotation at axial failure for columns other than spirally-reinforced circular columns as a function of: (a) axial load ratio; (b) transverse reinforcement ratio; and (c) V_p/V_n.............. A-3

Figure A-2 Ratio of measured to predicted plastic rotation at axial failure for spirally-reinforced circular columns as a function of: (a) axial load ratio; (b) transverse reinforcement ratio; and (c) V_p/V_n A-4

Figure A-3 Comparison of relationship between axial load ratio and plastic rotation capacity using different prediction methods for columns other than spirally-reinforced circular columns with transverse reinforcement ratio equal to: (a) 0.002; and (b) 0.006 .... A-5

Figure A-4 Comparison of relationship between axial load ratio and plastic rotation capacity using different prediction methods for spirally-reinforced circular columns with transverse reinforcement ratio equal to: (a) 0.002; and (b) 0.006 .... A-6

Figure A-5 Relationship between gravity shear ratio and drift capacity for slab-column connections A-8

Figure A-6 Ratio of measured versus predicted drift at punching shear failure for slab-column connections with different gravity shear ratios A-9

Figure C-1 Assumed model of correlation in column/wall drift capacities for failure of columns *i* and *j*, as a function of column/wall separation distance C-2

Figure C-2 Relationship between adjusted average column rating, R_{avg}, and the story rating, *SR,* for frame structures C-3

Figure C-3 Relationship between adjusted average column and wall rating, CR_{avg}, and the story rating, *SR,* from Monte Carlo simulation, and showing the simplified equation developed for the purpose of this methodology................ C-3

Figure D-1 Modeling overview for pure frame buildings D-4

Figure D-2 Modeling overview for frame-wall buildings D-4

Figure D-3 Collapse definition for 6-story, 6-bay, frame-wall system with a single 20 ft wall and shear critical columns D-5

Figure D-4 Relationship between WSI and probability of collapse for 32 building models D-6

Figure D-5 Relationship between WSI and probability of collapse for wall-frame buildings with flexurally-governed columns D-6

Figure D-6 Relationship between WSI and probability of collapse for wall-frame buildings with shear-controlled columns D-7

Figure E-1 Collapse fragilities for pure frame buildings from Table E-1 plotted as a function of $\mu_{strength}$ E-3

Figure E-2 Limiting values of V_p/V_n and $\mu_{strength}$ that identify exceptionally weak pure frame buildings E-4

Figure E-3 Collapse fragilities for frame-wall buildings plotted as a function of: (a) spectral acceleration at each building's fundamental period, shown in Table E-2; and (b) $\mu_{strength}$ E-5

Figure E-4 Relationship between WI and: (a) V_y/W; (b) median collapse $S_a(T_1)$; and (c) the ratio of median collapse $S_a(T_1)$ to V_y/W E-6

Figure F-1 Shear strength of unreinforced interior joints F-2

Figure F-2 Measured and calculated strengths for exterior joints loaded perpendicular to the edge, including corner joints F-3

Figure F-3 Measured and calculated strengths for exterior joints loaded perpendicular to the edge, including corner joints F-3

Figure F-4 Force transfer at eccentric beam-column connections F-4

Figure F-5 Maximum observed drift ratios and axial load ratios of corner beam-column connections F-5

Figure G-1 Example planar frame and fishbone idealizations of a four-story building G-2

Figure G-2 Calculated periods for all buildings studied G-3

Figure G-3 Comparison of calculated periods G-4

Figure G-4 Example of pier-spandrel system and model idealizations of a four-story building G-5

Figure G-5 Illustration of variables and constants in the parametric study G-6

Figure G-6 Comparison of calculated periods G-7

Figure H-1 Schematic elevation of the simulated 4-story frames H-2

Figure H-2 Ratio of (maximum displacement at effective modal height of non-linear analysis) / (estimated displacement at effective modal height) for different $\mu_{strength}$ values H-4

Figure H-3 Alpha factor story profiles for different variations of the 4-story idealized building H-6

Figure H-4 Alpha factor mean value at 1st story for different variations of the 4-story idealized building H-6

Figure H-5 Alpha factor story profiles for different variations of the 8-story idealized building H-7

Figure H-6 Alpha factor mean value at 1st story for different variations of the 8-story idealized building H-7

Figure H-7 Alpha factor story profiles for different variations of the 6-story idealized building with a critical 4th story H-9

Figure H-8 Alpha factor mean value at 1st story for different variations of the 6-story idealized building with a critical 4th story H-10

Figure H-9 Alpha factor mean value at 4th story for different variations of the 6-story idealized building with a critical 4th story H-10

Figure H-10 Zero-length plastic hinge rotational behavior for adequate and inadequate lap splicing conditions H-10

Figure H-11 Alpha factor story profiles for different variations of the 8-story building with and without inadequate lap-splicing conditions H-11

Figure H-12 Alpha factor story profiles for different variations of the 8-story building with and without inadequate lap-splicing conditions H-12

Figure H-13 Alpha factor story profiles for different variations of the 8-story building with inadequate lap-splicing conditions at the 1st and 4th critical story H-13

Figure H-14 Schematic elevation view of the simulated 8-story frame plus one rectangular wall H-14

Figure H-15 Typical wall cross section H-14

Figure H-16 Collapse mechanism for a 4-story structure H-16

Figure H-17 Schematic elevation view of the simulated 4-story frame plus two rectangular walls H-18

Figure H-18 Schematic elevation view of the simulated 8-story frame plus two rectangular walls, one discontinuous in the first story H-20

Figure H-19 8-story frame plus two 50 in. walls building, one discontinuous and supported by discontinuous columns H-21

Figure H-20 8-story frame plus two 50 in. walls building, one discontinuous and supported by ductile columns H-22

Figure H-21 Schematic elevation view of the simulated 8-story frame plus two rectangular walls, one discontinuous in upper story H-22

Figure H-22 Schematic elevation view of an 8-story wall with a shear critical story H-28

Figure H-23 (a) Two-spring in series model. (b) Response of each individual component representing flexure and shear H-28

Figure H-24 Response of the 8-story archetype frame-wall structure for wall length L_w = 200 in. with a shear critical section at the wall base. Simulation for a strong spring $V_{ns}/V_{spr,min} = 1.5$ H-30

Figure H-25 Response of the 8-story archetype frame-wall structure for wall length L_w = 200 in. with a shear critical section at the wall base. Simulation for $V_{ns}/V_{spr,min} = 1.1$ H-30

Figure H-26 Response of the 8-story archetype frame-wall structure for wall length L_w = 200 in. with a shear critical section at the wall base. Simulation for a weak spring $V_{ns}/V_{spr,min} = 0.5$ H-31

Figure H-27 Earthquake scenarios for shear critical models evaluation H-32

Figure H-28 Dynamic response of the BWS model under the LH set H-32

Figure H-29 Dynamic response of the BAS model under the LH set H-33

Figure H-30 Dynamic response of the BAS model under the IH set H-33

Figure H-31 Dynamic response of the BAS model under the HH set H-34

Figure H-32 Dynamic response of the BSS model under the LH set H-35

Figure H-33 Dynamic response of the BSS model under the IH set H-35

Figure H-34 Dynamic response of the BSS model under the HH set H-36

Figure H-35 Dynamic response of the BWS, BAS and the BSS models under the LH, IH, and HH sets H-37

Figure I-1 Illustration of the calculation of the center of strength for an example frame line I-3

Figure I-2 Illustration of the calculation of torsional capacity I-4

Figure I-3 Buildings analyzed in torsional study, showing variation in Torsional Ratio due the length of the walls I-5

Figure I-4 Diagram of 3D models used for torsional simulation I-6

Figure I-5 Steel material behavior used in fiber models I-7

Figure I-6 Response of columns in a torsionally-irregular building model, showing how the 1% story drift collapse definition was determined I-8

Figure I-7 Pushover results for case E, deaggregated to show contributions from frame and wall lines I-8

Figure I-8 Incremental dynamic analysis results for Case E, showing response of the building with the symmetrically-placed wall and the asymmetrically-placed wall, and the lower collapse capacity of the torsionally-irregular building I-9

Figure I-9 Median collapse capacities of all the building cases analyzed in this study I-10

Figure I-10 Collapse fragility for the torsionally-irregular buildings shown in Figure I-3, plotted in terms of $\mu_{Strength}$ I-10

Figure I-11 Buildings that are define to have “Extreme Torsion” are shown in the shaded area, identifying cases that may exceed 70% collapse probability I-11

Figure I-12 Buildings for which torsional effects can be neglected are shown in the shaded area as a function of the torsional ratio I-12

Figure I-13 Buildings for which torsional effects can be neglected are shown in the shaded area as a function of the wall index I-12

Figure I-14 Buildings that are required to undergo a full torsional analysis are defined by the shaded area I-13

Figure I-15 Column drift amplification due to torsion is the multiplier required to convert story drift to edge drift I-14

Figure I-16 3D portal frame used to examine estimates of *e* I-14

Figure I-17 Difference between stiffness based eccentricity and strength based eccentricity compared to eccentricity extracted from a model 3D portal frame with a wall on one side I-15

Figure I-18 Torsional amplification curve I-15

Figure I-19 Illustration of torsional amplifications computed for earthquake loading in the N-S direction I-16

Figure I-20 Collapse capacities from buildings analyzed by DeBock (2017), compared to the results of this study I-17

Figure J-1 Portion of drift taken by the column, γ, during nonlinear response from incremental dynamic analysis of selected 6-story buildings J-2

Figure J-2 Portion of drift taken by the column, γ, assuming a linear relationship with $\Sigma M_c/\Sigma M_b$ J-2

Figure K-1 IDA results and corresponding fragility curve estimation K-2

Figure K-2 Incremental Dynamic Analysis (IDA) curves for an 8-story modern code design building model K-3

Figure K-3 Collapse fragility functions for the "modern code design" building models K-4

Figure K-4 Scenario spectra K-5

Figure K-5 Hazard curves at different periods recovered with the CSS set K-5

Figure K-6 Static and dynamic response of two 8-story buildings K-6

Figure K-7 Risk curves of maximum roof drift ratio for two 8-story buildings K-7

Figure K-8 Fragility curves construction K-8

Figure K-9 Dynamic alphas, 4-story building K-8

Figure K-10 Dynamic alphas, 8-story building K-9

Figure L-1 Beam column element with concentrated flexural plasticity at the ends L-2

Figure L-2 Backbone and cyclic response rule of the rotational spring representative of the flexural plastic hinge region L-2

Figure L-3 Limit state shear-axial-spring material introduced L-3

Figure L-4 Elevation and wall reinforcement detailing of the frame-wall structure used for this study L-4

Figure L-5 Nonlinear force-based element with distributed plasticity formulation for the wall L-6

Figure L-6 Wall response under triangular load pattern for Gauss-Lobatto rule with three integration points L-8

Figure L-7 Wall response under triangular load pattern for Gauss-Lobatto rule with four integration points L-8

Figure L-8 Wall response under triangular load pattern for Gauss-Lobatto rule with five integration points L-8

Figure L-9 Wall response under triangular load pattern for Gauss-Radaue rule with two integration points in the first story and three Gauss-Legendre integration points upstairs L-9

Figure L-10 Wall response under triangular load pattern with a reversed load at the roof for Gauss-Radaue rule with 2IPs at the first story, and 3 Gauss-Legendre IPs upstairs L-9

Figure L-11 Normalized curvature demand at the first integration point (critical section at the base) for the inverted triangular load pattern L-10

Figure M-1 Column shear strength M-1

Figure N-1 Definition of flexure-controlled and shear-controlled walls based on results from a dataset of 990 wall tests N-2

Figure N-2 Histograms of the reduced dataset of 80 flexure-controlled walls N-3

Figure N-3 Variation of drift capacity at axial failure as a function of λ_b and $P / A_g f_c'$ N-4

Figure N-4 Drift capacity at axial failure for poorly detailed flexure-controlled walls N-5

Figure N-5 Comparison of predicted drift capacities from Equation N-1 and Figure N-4 with experimentally obtained drift capacities N-5

Figure N-6 Comparison of neutral axis depth, c, computed from Equation N-2 with that from detailed sectional analysis N-6

Figure N-7 Drift capacity of shear-controlled walls/piers as a function of $P / A_g f'_c$ and minimum web reinforcement ratio N-7

Figure N-8 Drift capacity of shear-controlled walls/piers as a function of $P / A_g f'_c$ with a natural log fit N-7

Figure N-9 Drift capacity of shear-controlled walls/piers as a function of $P / A_g f'_c$ with a bi-linear fit N-8

Figure N-10 Comparison of predicted drift capacities from Equation N-4 with experimentally obtained drift capacities at axial failure N-9

Figure N-11 Examples of asymmetric wall cross-sections N-10

Figure N-12 Damage in walls with asymmetric wall cross-sections N-10

Figure N-13 Drift capacity of flexure-controlled walls with spirally reinforced boundary columns N-11

Figure N-14 Damage of shear-controlled walls with spirally reinforced boundary columns at some level of lateral strength loss N-12

Figure N-15 Drift capacity of shear-controlled walls with spirally reinforced boundary columns N-13

Figure O-1 Building details of the six-story San Diego warehouse with infilled RC frames O-3

Figure O-2 Floor plans of the prototype structures and design details of the columns and the beams of the first two stories of the 4-story prototype O-3

Figure O-3 Lateral force-drift ratio curves for the infilled bays and calibration of struts O-5

Figure O-4 Three-dimensional numerical model with infill struts O-6

Figure O-5 Pushover analyses results of the models (M1 to M5) and deaggregated response of interior and exterior frames for models M1 and M3 .... O-8

Figure O-6 Incremental dynamic analysis results of the infilled frame models M1 to M6 .... O-9

Figure O-7 Displacement profiles of the buildings M1 to M6 just before collapse O-10

Figure O-8 Damage in infill panel with opening causing shear failure in bounding column O-11

Figure O-9 Classification of infills based on relative stiffness of infill and bounding frame O-12

Figure O-10 Classification of infills based on relative strength of infill and bounding frame O-12

Figure O-11 Results of detailed FE analyses single-story single bay frames for the prototypes structures considered here O-13

Figure O-12 Deformed meshes at 1.0% drift of panels with openings for $f'_m = 0.4$ ksi O-17

Figure O-13 Deformed meshes at 1.0% drift of panels with openings for $f'_m = 0.8$ ksi O-17

Figure O-14 Deformed meshes at 1.0% drift of panels with openings for $f'_m = 1.4$ ksi O-18

Figure O-15 Lateral force-vs.-drift behavior of the infilled panels with openings of different size and locations O-18

Figure O-16 Strength reduction of infilled frames as a function of opening location compared to the frame with a solid panel O-19

Figure O-17 Strength reduction of infilled frames as a function of opening area compared to the frame with a solid panel O-19

Figure O-18 Comparison of strength of infilled bays with openings obtained from Equation O-3 and detailed FE analyses in FEAP O-19

Figure O-19 Contribution of non-infilled columns at the peak strength of infilled frames O-22

Figure O-20 Variation of T_e with increase in seismic excitation of the infilled frame models M1 to M6 .... O-24

Figure O-21 Estimation of effective period of infilled frames O-24

Figure O-22 Normalized displacement profile of the infilled frame buildings with $\delta_{eff} = 1.0$.. O-25

Figure O-23 Damage to an infilled frame building, showing severely damaged columns, but no collapse.................. O-26

List of Tables

Table 3-1 Default Expected Properties for Masonry Infill................ 3-4

Table 5-1 Classification of Infill 5-5

Table 5-2 Drift at which Infill is Assumed to Reach Peak Lateral Strength, Δ_{peak} (in Percent Drift Ratio)............................ 5-17

Table 5-3 Values for Effective Mass Factor, C_m 5-21

Table 6-1 Values of Coefficient a for Frame Systems 6-5

Table 6-2 Drift Factor, γ, for Columns.. 6-7

Table 6-3 Plastic Rotation Capacities for Tied Columns 6-8

Table 6-4 Plastic Rotation Capacities for Spiral-Reinforced Columns 6-9

Table 6-5 Drift Capacity of Critical Slab-Column Connections 6-9

Table 6-6 Column Rating, CR 6-11

Table 7-1 Values of Coefficient α for Frame-Wall Systems 7-6

Table 7-2 Drift Factor, γ, for Columns.. 7-9

Table 7-3 Plastic Rotation Capacities for Tied Columns 7-10

Table 7-4 Plastic Rotation Capacities for Spiral-Reinforced Columns 7-11

Table 7-5 Drift Capacity of Critical Slab-Column Connections 7-11

Table 7-6 Drift Capacity of Flexure-Critical Walls or Vertical Wall Segments 7-13

Table 7-7 Drift Capacity of Shear-Critical Walls or Vertical Wall Segments 7-13

Table 7-8 Coefficients for Calculation of Neutral Axis Depth, c..... 7-14

Table 7-9 Minimum Transverse Reinforcement in Integral Columns or Boundary Elements Required to be Classified as Confined 7-15

Table 7-10 Column Rating, *CR*, and Wall Rating, *WR* 7-16

Table 8-1 Values of Coefficient α for Bearing Wall Systems............ 8-4

Table 8-2 Drift Capacity of Flexure-Critical Walls or Vertical Wall Segments 8-6

Table 8-3 Drift Capacity of Shear-Critical Walls or Vertical Wall Segments 8-7

Table 8-4 Coefficients for Calculation of Neutral Axis Depth, c 8-7

Table 8-5 Minimum Transverse Reinforcement in Integral Columns or Boundary Elements Required to be Classified as Confined... 8-8

Table 8-6 Wall Rating, *WR*.. 8-9

Table 9-1 Values of Coefficient α for Infilled Frame Systems 9-4

Table 9-2 Effective Height of Columns in Infilled Frame Systems 9-7

Table 9-3 Plastic Rotation Capacities for Tied Columns 9-8

Table 9-4 Plastic Rotation Capacities for Spiral-Reinforced Columns 9-9

Table 9-5 Column Rating, *CR* 9-10

Table 9-6 Assistance to Column Ratings Based on Infill Panel Response 9-11

Table 9-7 Drift at Onset of Residual Strength, Δ_{res}, for Infilled Bays.. 9-11

Table A-1 Uncertainty in Predictions of Column Plastic Rotation Capacity, Obtained from Comparison with Experimental Data.. A-6

Table D-1 Frame-Wall Building Properties D-2

Table D-2 WSI Required to Satisfy ASCE 41-13 Tier 1 Shear Stress Check D-9

Table E-1 Properties of Pure Frame Building Set............................. E-1

Table E-2 Properties of Frame-Wall Building Set E-2

Table E-3 Table of Collapse Probabilities (from ATC-78-1) for Pure Frame Buildings... E-4

Table H-1 Coefficients C_0, C_1, and C_2 of the Studied Buildings........ H-3

Table H-2 Average Ratio of (Maximum Displacement at Effective Modal Height of Non-Linear Analysis) / (Estimated Displacement at Effective Modal Height) for Different V_p/V_n and M_c/M_b Ratios of the 6-Story Idealized Building H-3

Table H-3 Mean Values for $\boldsymbol{\alpha}$ Factor for the 1st Story only for a 6-story Idealized Building with Critical 1st Story H-8

Table H-4 Values of Coefficient α Estimated from Pushover Analysis for a 4-Story Archetype Frame Plus One Continuous Wall H-15

Table H-5 Values of Coefficient α Estimated from Pushover Analysis for a 4-Story Modified Frame I Plus One Continuous Wall H-15

Table H-6 Values of Coefficient α Estimated from Pushover Analysis for a 4-Story Modified Frame 2 Plus One Continuous Wall H-16

Table H-7 Values of Coefficient α Estimated from Pushover Analysis for an 8-Story Archetype Frame Plus One Continuous Wall H-17

Table H-8 Values of Coefficient α Estimated from Pushover Analysis for an 8-Story Modified Frame I Plus One Continuous Wall H-17

Table H-9 Values of Coefficient α Estimated from Pushover Analysis for an 8-Story Modified Frame II Plus One Continuous Wall H-18

Table H-10 Values of Coefficient α Estimated from Pushover Analysis for a 4-Story Archetype Plus Two Continuous Walls H-19

Table H-11 Values of Coefficient α Estimated from Pushover Analysis for an 8-Story Archetype Plus Two Continuous Walls H-19

Table H-12 Values of Coefficient α Estimated from Pushover Analysis for a 4-Story Archetype Plus One Continuous Wall and One Discontinuous Wall in the First Story H-20

Table H-13 Values of Coefficient α Estimated from Pushover Analysis for an 8-Story Archetype Plus One Continuous Wall and One Discontinuous Wall in the First Story H-20

Table H-14 Values of Coefficient α Estimated from Pushover Analysis for a 4-Story Archetype Plus One Continuous Wall and One Wall That Ends in the Third Story H-23

Table H-15 Values of Coefficient α Estimated from Pushover Analysis for a 4-Story Archetype Plus One Continuous Wall and One Wall That Ends in the Second Story H-23

Table H-16 Values of Coefficient α Estimated from Pushover Analysis for a 4-Story Archetype Plus One Continuous Wall and One Wall That Ends in the First Story............ H-23

Table H-17 Values of Coefficient α Estimated from Pushover Analysis for an 8-Story Archetype Plus One Continuous Wall and One Wall That Ends in the Seventh Story H-24

Table H-18 Values of Coefficient α Estimated from Pushover Analysis for an 8-Story Archetype Plus One Continuous Wall and One Wall That Ends in the Sixth Story H-24

Table H-19 Values of Coefficient α Estimated from Pushover Analysis for an 8-Story Archetype Plus One Continuous Wall and one Wall That Ends in the Fifth Story H-25

Table H-20 Values of Coefficient α Estimated from Pushover Analysis for an 8-Story Archetype Plus One Continuous Wall and One Wall That Ends in the Fourth Story H-25

Table H-21 Values of Coefficient α Estimated from Pushover Analysis for an 8-Story Archetype Plus One Continuous Wall and One Wall That Ends in the Third Story H-26

Table H-22 Values of Coefficient α Estimated from Pushover Analysis for an 8-Story Archetype Plus One Continuous Wall and One Wall That Ends in the Second Story H-26

Table H-23 Values of Coefficient α Estimated from Pushover Analysis for an 8-Story Archetype Plus One Continuous Wall and One Wall That Ends in the First Story H-27

Table N-1 Neutral Axis Depth (c) Parameters Used in Equation N-2 .... N-6

Table N-2 Drift Capacity for Shear-Controlled Walls/Piers at Axial Collapse N-8

Table O-1 Details of the Archetype Models Considered in This Study to Evaluate Seismic Behavior of Infilled Buildings O-2

Table O-2 Column Dimensions and Design Details of the Prototypes O-4

Table O-3 Calibrated Concrete and Strut Properties of the Models' Elements O-5

Table O-4 Collapse Potential of the Infilled Buildings and Frame Counterparts O-8

Table O-5 Collapse Potential of the Infilled Buildings and Frame Counterparts O-8

Table O-6 Effective Height of Columns in Infilled Frame O-11

Table O-7 P_{inf}^{grav} and $P_{inf}^{\max}$ Values of the Models O-13

Table O-8 Comparison of Strength of Single Infilled Bays Obtained O-14

Table O-9 Geometric Details of the Openings Considered in the Parametric Study O-15

Table O-10 Classification of Infill in Each Infilled Bay O-20

Table O-11 When Infill Panels with Openings Can Be Ignored for Calculation of Strength? O-20

Table O-12 Collapse Potential of the Infilled Buildings and Frame Counterparts O-23

Table O-13 Fraction of the Drift Demand in the First Story O-25

Chapter 1

Introduction

A wide variety of concrete buildings exist in regions of significant seismicity in the United States, and many were constructed prior to the enactment of modern seismic provisions in building codes. Known as non-ductile concrete buildings, these buildings were constructed prior to the late-1970s, and include archaic construction dating back to the early 1900s. Problematic issues include inadequate steel reinforcing details, system irregularities, and element discontinuities that can result in sudden failure and loss of vertical load-carrying ability. Large earthquakes have demonstrated the seismic vulnerability of these older, concrete buildings, but not all such buildings are at risk of global collapse.

Following the 1971 San Fernando earthquake, the 1976 *Uniform Building Code* (ICBO, 1976) introduced requirements for more robust detailing of reinforced concrete systems along with larger seismic design loads than in previous editions of the UBC. As a result, the 1976 UBC is often used as a benchmark, and concrete buildings that were designed and constructed in accordance with codes prior to the 1976 UBC are considered to be high seismic risk buildings that should be evaluated and potentially retrofitted.

Visual inspection alone, as is performed in FEMA P-154 *Rapid Visual Screening of Buildings for Potential Seismic Hazards: A Handbook, Third Edition* (FEMA, 2016) cannot reliably evaluate the significance of seismic deficiencies that are often present in older concrete buildings. In most cases, an engineer must perform a detailed analytical evaluation to differentiate the potential collapse vulnerability among concrete buildings subjected to strong ground shaking. Because current evaluation methods and retrofit techniques are complex and expensive to perform, a new evaluation methodology was needed to more efficiently screen an inventory of older concrete buildings for potential collapse risk.

1.1 ATC-78 Project Series

The purpose of the FEMA-funded ATC-78 Project Series, "Identification and Mitigation of Non-Ductile Concrete Buildings," is to develop an evaluation methodology that will: (1) identify the most seismically hazardous non-ductile concrete buildings; and (2) be easier and less expensive to apply than the detailed analysis procedures of ASCE/SEI 41-17, *Seismic Evaluation and Retrofit of Existing Buildings* (ASCE, 2017b).

The efforts to develop this methodology were coordinated with, and built on, the results of related projects funded by the National Earthquake Hazards Reduction Program (NEHRP), the National Institute of Standards and Technology (NIST), the National Science Foundation (NSF), and other FEMA-sponsored work, including the following:

- The *NEES Grand Challenge for the Mitigation of Collapse Risk of Older Concrete Buildings* (NEES, 2010), identified the extent of the collapse hazard present in existing reinforced concrete buildings, conducted laboratory testing of selected concrete building systems and components, and developed an inventory of older concrete buildings.
- The NIST GCR 10-917-7 Report, *Program Plan for the Development of Collapse Assessment and Mitigation Strategies for Existing Reinforced Concrete Buildings* (NIST, 2010b), defined a broad program to systematically investigate and mitigate the vulnerability of non-ductile concrete buildings. The NIST *Program Plan* also suggested a methodology for determining the relative importance of various conditions known to be deficient, termed *collapse indicators*.
- The NIST-funded project conducted by the Building Seismic Safety Council (BSSC) of the National Institute of Building Sciences (NIBS) identified subclasses of non-ductile concrete buildings with common and quantifiable characteristic deficiencies in the NIST GCR 10-917-6 Report, *Concrete Model Building Subtypes Recommended for Use in Collecting Inventory Data* (NIST, 2010a).

Early phases of development investigated the collapse indicator concept identified in the NIST *Program Plan*, with the purpose of calculating a probability of collapse based on the severity of a collapse indicator. Although the collapse indicator concept proved insightful for the prediction of global collapse, use of collapse indicators as a predictive tool was more complex than originally envisioned and found to be impractical for the purposes of a simplified evaluation methodology for all types of concrete buildings (ATC, 2012; NIST, 2014).

As a result, later phases of development focused on story drifts and their relation to the collapse potential of concrete components such as columns and walls, and on developing criteria for linking component collapse to global collapse of concrete buildings overall. Project findings and evolving efforts defining the evaluation methodology have been documented in the ATC-78 series of reports:

- ATC-78, *Identification and Mitigation of Seismically Hazardous Older Concrete Buildings: Interim Methodology Evaluation* (ATC, 2011);
- ATC-78-1, *Evaluation of the Methodology to Select and Prioritize Collapse Indicators in Older Concrete Buildings* (ATC, 2012);
- ATC-78-2, *Seismic Evaluation for Collapse Potential of Older Concrete Frame Buildings* (ATC, 2013);
- ATC-78-3, *Seismic Evaluation of Older Concrete Frame Buildings for Collapse Potential* (ATC, 2015);
- ATC-78-4, *Seismic Evaluation of Older Concrete Frame and Shear Wall Buildings for Collapse Potential* (ATC, 2016);
- ATC-78-5, *Seismic Evaluation of Older Concrete Frame, Wall, and Frame-Wall Buildings for Collapse Potential* (ATC, 2016); and
- ATC-78-6, *Seismic Evaluation of Older Concrete Frame, Frame-Wall, and Bearing Wall Buildings for Collapse Potential* (ATC, 2017).

1.2 Evaluation Methodology

This report presents an evaluation methodology intended to determine the relative risk of collapse of older concrete buildings in strong earthquake shaking. The purpose of this methodology is to enable identification of the subset of buildings in this class that are expected to have a high risk of collapse without the need for extensive testing or nonlinear analysis. Significant features of the evaluation methodology are:

- Definition of collapse as a global loss of gravity support at a story, possibly leading to the collapse of other stories.
- Singular intent of determining the relative risk of global collapse among an inventory of older concrete buildings. Other performance measures, (e.g., extent of damage, functionality, or downtime) are not considered.
- Probabilistic characterization of demand (as story drift) and the capacity limit (as column or wall collapse), allowing estimation of the probability of collapse for column or wall components in each story.
- Estimation of the probability of collapse in a given story through consideration of global criteria based on the collapse probability of column and wall components in that story.

- Use of the probability of story collapse as a relative measure for ranking the seismic risk and screening an inventory of older concrete buildings to set priorities for further action.

For the purposes of this methodology, all concrete buildings designed to codes that are not equivalent to the 1976 *Uniform Building Code*, or not known to meet other locally accepted evaluation or retrofit standards, are considered *high seismic risk buildings*. This evaluation methodology is intended to identify the subsets of these buildings that are of lower relative risk of collapse, termed *lower seismic risk buildings*, or are considered to be of significantly higher relative risk of collapse, termed *exceptionally high seismic risk buildings*.

The evaluation methodology addresses reinforced concrete frame, frame-wall, bearing wall, and infilled frame structures with rigid diaphragms and heights less than 160 feet. The resulting methodology is based on the evolution of procedures as outlined in the ATC-78 series of reports, and have been refined by results obtained from trial evaluations and testing of the methodology. Collapse is defined as the global loss of vertical load-carrying ability at a story, possibly leading to the collapse of other stories. Procedures for assessing collapse in this methodology require simplified estimates of drift demand to implement. Although the resulting calculations are intentionally simplified, the underlying criteria are based on probabilistic concepts and structural reliability theory.

A mechanism-based method for estimating base shear strength, which can be generally applied to different concrete building types and configurations, has been incorporated in the methodology. This has the added advantage of identifying potential lateral mechanisms that influence story drifts. Procedures to identify conditions under which concrete columns and concrete walls will lose vertical load-carrying capacity have been based on limited available test data and structural reliability concepts.

Story drift demand is calculated probabilistically and combined with a capacity limit, resulting in a probabilistic measure of collapse for critical column and wall components in each story, and for the collapse of a story as a whole. Because extensive testing and nonlinear analysis is not required by the calculation procedures, the engineering time for evaluation is expected to be no greater than that for a Tier 2 evaluation in accordance with ASCE/SEI 41-17, and significantly less than Tier 3 nonlinear analysis procedures.

Other estimates of drift demand that are more extensive (and presumably more accurate) than the procedures recommended in this report can be used in the methodology. Similarly, other, more detailed methods of estimating the effective building period can be used. It is unclear at this time if risk ratings obtained using input parameters from other engineering procedures would be consistent with ratings obtained using the calculation procedures defined herein. For decision making at the public policy level, and implementation in mandatory evaluation and retrofit programs, it is recommended that the complete methodology be used with input parameters from a common engineering basis to ensure consistency in the relative rankings across an inventory of buildings.

1.3 Comparison with ASCE/SEI 41

Until recently, ASCE/SEI 31-03, *Seismic Evaluation of Existing Buildings* (ASCE, 2003), has been the standard for seismic evaluation, and ASCE/SEI 41-06, *Seismic Rehabilitation of Existing Buildings* (ASCE, 2007) has been the standard for seismic retrofit. In the 2013 update of these standards, the evaluation (ASCE/SEI 31) and retrofit (ASCE/SEI 41) standards were combined into a single standard (ASCE/SEI 41-13), and made more internally consistent (ASCE, 2013). The current version of these standards is ASCE/SEI 41-17 (ASCE, 2017).

The protection of life safety has been used as a seismic evaluation and retrofit performance objective for decades. Current standards for seismic evaluation and retrofit were originally developed with "life safety" as a conceptual basis, although higher and lower performance objectives have also been defined. Historically, the level of risk to life safety for existing buildings has been permitted to be somewhat higher than for new buildings due to the anticipated cost and disruption of retrofit. This elevated level of risk for existing buildings, however, has not been quantitatively defined in life-safety terms (i.e., acceptable risk of incurring serious injuries or deaths). Quantification and calibration of acceptable risk among different design and evaluation methods may eventually be possible with the FEMA P-58 *Seismic Performance Assessment of Buildings, Methodology and Implementation* (FEMA, 2012 and 2018).

Separate from the notion of "life safety," the "collapse prevention" performance level in ASCE/SEI 41 is based on the prevention of structural collapse. The criteria used to define "collapse prevention" are based on the performance of individual building components (e.g., beams, columns, walls, and slabs) rather than global collapse. Often, the failure of one or more components relative to ASCE/SEI 41 criteria is not expected to result in global collapse, and some engineers experienced in evaluation and retrofit of older concrete buildings estimate that only a small percentage of concrete buildings that fail the criteria in ASCE/SEI 41 will actually collapse, even in very rare earthquake shaking. Recent studies of building collapse performance, such as those embodied in the FEMA P-695 Methodology (FEMA, 2009), consider global collapse more explicitly and describe collapse performance probabilistically. These studies recognize that most serious injuries and deaths in earthquakes are caused by global structural collapse.

This evaluation methodology focuses on structural failures in vertical load-carrying elements that are expected to lead to global collapse. As a result, it does not directly address other seismic deficiencies that have been observed to cause structural damage (but not necessarily collapse) in past earthquakes. Evaluation using this methodology will result in an approximation of the probability of collapse of a building, subject to a specified ground motion. This result is not directly related to "collapse prevention" as defined in ASCE/SEI 41 because it is an approximation of *global* structural collapse. Results are considered approximate because of significant uncertainties in the determination of ground motion, the methods used to calculate story drifts, the prediction of the probability of failure of individual column and wall components, and the criteria used to estimate story collapse based on column and wall component collapse. Although approximate, the results of individual building evaluations within a group of buildings are expected to provide a useful indication of the relative potential for collapse across an inventory of buildings.

This evaluation methodology was developed for use as a screening tool. It is intended as a complement to, not a replacement for, ASCE/SEI 41, and results can be used to prioritize buildings for more detailed evaluation using ASCE/SEI 41. It is expected that results could eventually be used in future calibration of ASCE/SEI 41 evaluation and retrofit criteria for structural collapse, through comparisons with the probabilistic results obtained from this methodology.

1.4 Policy Implications

Application of this evaluation methodology is expected to include use by political jurisdictions in setting priorities for mandatory seismic risk reduction within their communities, considering collapse as the overriding loss to be avoided.

Concrete buildings designed and constructed to codes that are not equivalent to the 1976 *Uniform Building Code*, or not known to meet other locally accepted evaluation or retrofit standards, are considered to be highly vulnerable to earthquake shaking and are herein classified as *high seismic risk buildings*. The methodology described in this report is intended to enable relatively efficient identification of older concrete buildings with a high probability of collapse, termed *exceptionally high seismic risk buildings*, as well as those with a probability of collapse lower than most older concrete buildings, termed *lower seismic risk buildings*.

For any level of earthquake ground motion selected, this methodology can be used to rank buildings based on an approximate probability of collapse. The probability of collapse for any building is highly dependent on the severity of ground motion expected at the site, and the probability of occurrence for the selected ground motion, which can include smaller, more frequent earthquakes (72-year return period), or larger, less frequent earthquakes (500-year, 1000-year or 2500-year return periods).

The Basic Safety Earthquake, BSE-2E, from ASCE/SEI 41-17 is the seismic hazard level recommended herein for measuring collapse performance. In general, more intense (i.e., less frequent) ground motions will increase the collapse probability of all buildings in a region, but the relative ranking between buildings is expected to be the same. This general trend, however, may not be the case in areas with a steeply sloping hazard curve, such as the New Madrid seismic hazard region in and around Memphis, Tennessee. This region has a relatively low threat from frequent earthquakes, but the ground motion intensity for very rare earthquakes is very high. In areas with special seismic hazard concerns, selection of an earthquake hazard level that is most representative of the local seismic hazard setting should be considered.

A threshold for defining *exceptionally high seismic risk*, which presumably would identify the highest priority buildings for mitigation, has been judgmentally set in this methodology to be a building rating greater than or equal to 0.7, approximately corresponding to a 70% (or higher) probability of collapse given the selected ground motion level. Based on observed performance of U.S. style construction in past earthquakes, it is expected that a relatively low percentage of buildings will be placed in the *exceptionally high seismic risk* category, however, this percentage is not known. More extensive evaluation using the nonlinear analysis methods of ASCE/SEI 41 could be used to further evaluate, and possibly reclassify, buildings that have been identified as *exceptionally high seismic risk* using this methodology.

Threshold rankings that would define “acceptable” levels of collapse risk have not been established. Levels of collapse risk that would be deemed acceptable are difficult to determine, and complicated by societal needs and differences between the definition of collapse used in this methodology and those used in current codes and standards for new and existing buildings. It is anticipated that use of this methodology on buildings with known collapse characteristics (i.e., from analysis, laboratory testing, or observed performance) will help in setting threshold values for acceptable risk in the future.

A reasonable approach for using this methodology in a program for reducing the seismic risk associated with older concrete buildings could include the following:

- Using sidewalk surveys, assessors' files, or other available jurisdictional records, develop a preliminary inventory of older concrete buildings (i.e., buildings not conforming to the 1976 *Uniform Building Code*, or not meeting other locally accepted evaluation or retrofit standards).
- Within the first year of a program, require building owners in the preliminary inventory to submit a simple building data collection form, with input from an engineer or architect, to confirm the building status, and possibly identify additional risk factors. For example, such a form could be used to confirm that the building is of concrete construction, does not comply with acceptable building codes, and has not be retrofitted to acceptable standards. In addition, the form could also be used to identify the building height, area, and occupancy, as well as other risk factors, such as unstable soil conditions and structural irregularities. Owners of older concrete buildings that were not included in the preliminary inventory should also be required to submit a form, but identification and enforcement of such a requirement would require more effort, such as ongoing monitoring of building permit applications.
- Develop a refined inventory of older concrete buildings based on information contained in building data collection forms.
- Within approximately three years, require building owners in the refined building inventory to evaluate and classify their buildings using this methodology.
- Develop a prioritized inventory of older concrete buildings based on information obtained from the building evaluations.
- Within approximately five years, require mitigation of the risk associated with *exceptionally high seismic risk buildings* through more detailed evaluation or retrofit, if needed, using ASCE/SEI 41 or other locally accepted evaluation or retrofit standards.
- Over a longer period of time, require mitigation of the risk associated with *high seismic risk buildings* and *lower seismic risk buildings* through

more detailed evaluation or retrofit, if needed. It is expected that the state of knowledge in ASCE/SEI 41 will continue to evolve over time, and that many buildings in lower seismic risk categories could be deemed to be acceptably safe in the future. It is also possible that additional information gained from the use of this methodology over time will demonstrate that the criteria are sufficiently reliable for identifying buildings that are acceptably safe without further evaluation (at least in the case of *lower seismic risk buildings*).

Because this methodology has not been calibrated to traditional life safety standards, it is not intended, and should not be used, to determine retrofit requirements.

1.5 Report Organization and Content

This report outlines a methodology to evaluate the collapse potential of older concrete frame, frame-wall, bearing wall, and infilled frame buildings.

Chapter 2 outlines the evaluation methodology, including applicability and limitations on its use.

Chapter 3 defines the general requirements for use of the methodology.

Chapter 4 defines the recommended methods for calculating component strengths that are part of the methodology.

Chapter 5 includes guidance for classifying building systems based on their expected response characteristics. The primary response characteristic of interest is the lateral deformation pattern, which is used to estimate story drift. Based on the classification of a system, methods for calculating the structural period are provided, along with simplified methods for identifying certain *exceptionally high seismic risk buildings*, or buildings judged to be of *lower seismic risk*, relative to other older concrete buildings.

Chapter 6 describes the method of evaluation for concrete frame systems.

Chapter 7 describes the method of evaluation for concrete frame-wall systems.

Chapter 8 describes the method of evaluation for concrete bearing wall systems.

Chapter 9 describes the method of evaluation for concrete systems with masonry infill walls.

Chapter 10 describes the method of assigning building ratings based on the results of Chapters 5, 6, 7, 8, and 9.

The appendices to this report provide additional information on the background and derivation of the calculation procedures and criteria comprising the methodology.

A list of symbols used throughout this report, along with a list of references, are provided at the end of this report.

Chapter 2

Evaluation Methodology

Older concrete buildings not in compliance with the strength and detailing requirements of the 1976 or later editions of the *Uniform Building Code* (ICBO, 1976), and not otherwise determined to have acceptable seismic performance through evaluation or retrofit to locally accepted standards, could be susceptible to significant structural damage in an earthquake and should be considered *high seismic risk buildings*.

This chapter provides an overview of an evaluation methodology that can be used to identify subsets of these buildings that are of lower relative risk of collapse, termed *lower seismic risk buildings*, or are considered to be of significantly higher relative risk of collapse, termed *exceptionally high seismic risk buildings*. It describes the intended scope, summarizes limitations on applicability, and identifies explicit exclusions for use of the evaluation methodology.

Buildings categorized as *exceptionally high seismic risk* using this methodology should be prioritized for more detailed seismic evaluation or seismic retrofit.

2.1 Scope and Applicability

This evaluation methodology is intended for use in determining the relative risk of collapse within an inventory of buildings, prioritizing buildings for further evaluation, and guiding prudent risk-reduction policy decisions. It is not intended for use in developing or implementing seismic retrofits to improve the seismic performance, or reduce the risk of collapse, of an individual building.

2.1.1 Applicability

This methodology is applicable to reinforced concrete buildings 160 feet or less in height, with concrete diaphragms, and with or without structural load-bearing walls, reinforced concrete shear walls, or masonry infill walls. Reinforced concrete elements that can be evaluated using this methodology include:

- frame lines (or bays) that are designed to resist gravity loads, including beam-column systems, slab-column systems, or joist-column systems;

- frame lines (or bays) that are designed to resist gravity plus lateral loads, regardless of the level of ductile detailing;
- frame lines with masonry infill walls of hollow clay tile, brick masonry, or concrete masonry units (CMU), with or without openings (note: infill masonry panels that have been previously retrofitted or reinforced are outside the scope of application of the infill procedures in this methodology);
- wall lines with structural reinforced concrete walls, generally 4 inches or greater thickness and with a horizontal reinforcement ratio equal or greater than 0.0015 (see also Section 5.2.2);
- concrete elements retrofitted using materials and components that are compatible with concrete behavior and strength calculation procedures, and compatible with the mechanism analysis procedures of Section 5.5;
- post-tensioned concrete systems with reinforced concrete columns. In such cases, procedures for determining column capacity as a function of the beam or slab capacity, and any other calculation related to the capacity of beams and slabs, must be appropriately determined from ACI 318-14, *Building Code Requirements for Structural Concrete and Commentary* (ACI, 2014).

Additional requirements for use of this methodology include:

- a complete load path that includes diaphragms and adequate connections between lateral force-resisting elements, including adequate reinforcing at construction joints in walls and at column and wall connections to foundations; and
- beam-column joints with limited eccentricity, in which the centerline of the beam is located within the width of the column and at least some of the beam longitudinal reinforcement passes within the column core (as defined by the boundaries of the column longitudinal reinforcement). Up to 10% of the beam-column joints may exceed this requirement if it is judged that overall building response will not be adversely affected.

The evaluation methodology is not applicable to precast frame or wall structures in which the capacity of a system or component is limited by its connection to other structural elements.

Older concrete buildings that do not qualify for evaluation using this methodology should be considered to be *exceptionally high seismic risk buildings*, and prioritized for detailed seismic evaluation by other means.

2.1.2 Seismic Deficiencies that are not Considered in the Methodology

Because the evaluation methodology is focused on structural collapse, certain characteristics considered in other seismic evaluation procedures (e.g., ASCE/SEI 41), which identify sources of potential seismic damage, are not evaluated in this methodology. These include:

- Nonstructural components and systems (see section 5.2.2 for nonstructural walls that may affect response).
- Prescriptive minimum reinforcing ratios and configurations (the effects of these characteristics on component strengths, however, are considered in this methodology).
- Prescriptive minimum requirements on foundation configuration. For example, the effect of foundation ties on collapse probability is difficult to define and has not been considered.
- Precast concrete or stone cladding with brittle or drift-intolerant connections (note: estimated story drifts can be used to evaluate potential damage to the panels or their connections; however, potential falling hazards due to cladding are not considered in the ratings of this methodology).
- Geologic site hazards associated with earthquake-induced ground failure or tsunami effects. Such hazards require detailed analysis to determine the potential for collapse or other life safety risks. For the purposes of ranking an inventory of buildings, these buildings could initially be rated *exceptionally high seismic risk* requiring further detailed analysis.

2.1.3 Buildings with Concrete Components that are not Considered in the Methodology

The evaluation methodology is intended to address specific classes of reinforced concrete buildings. There are other types of pre-1976 UBC buildings with concrete components that are not considered in this methodology. For the purposes of ranking an inventory, individual buildings of the following types could be a collapse risk, and might be considered *exceptionally high seismic risk*; however, the unique conditions associated with these types of buildings are not addressed by the procedures in this methodology.

2.1.3.1 Tilt-Up Buildings

Tilt-up buildings are one to three stories tall with walls (normally exterior walls, but sometimes also interior walls) precast on the ground and “tilted up" into place. The connections between the tilt-up walls and the diaphragms are often poor, and walls have often been observed to be collapsed or leaning outward following an earthquake. This type of failure is a load path issue that is not covered by this methodology.

2.1.3.2 Residential Bearing Wall Buildings with Precast Slabs

Residential bearing wall buildings are typically motels, hotels, or apartments with demising walls of concrete or concrete masonry. When floors are constructed of precast concrete planks, with or without a concrete topping slab, the plank-to-wall bearing connection is often inadequate and can fail, leading to collapse of the floors. This type of failure is a load path issue that is not predictable by global building analysis, and is not covered by this methodology.

2.1.3.3 Lift-Slab Buildings

Lift-slab buildings typically have a concrete core tower and are constructed by casting the floors stacked on the ground. Steel or concrete columns are erected, and the floor slabs are lifted into place, sliding up the columns. A gravity connection is then added at each column at each level. These gravity connections often have little or no drift tolerance and can fail, leading to collapse of the floors. Connections between the floor slabs and the concrete core are variable in quality. The drift tolerance of the column-to-slab gravity connections is building-specific, and not covered by this methodology.

2.2 Overview of the Evaluation Methodology

The evaluation methodology is intended to rate the relative probability of global structural collapse of older concrete buildings subjected to earthquake shaking at a specified seismic hazard level. Implementation of this methodology does not require a structural analysis model, instead relying on approximate period and strength calculations that are intended to require less effort to implement than other more detailed seismic evaluation procedures (e.g., ASCE/SEI 41). These features are intended to ensure, through prescriptive criteria, that results for one building can be easily compared to results for another building, enabling consistent ranking of a building inventory in terms of relative collapse risk. By evaluating the likelihood of global collapse, rather than individual component failures, this methodology attempts to avoid some of the conservatisms inherent in other seismic evaluation procedures, such as ASCE/SEI 41.

The evaluation methodology uses a mechanism-based procedure to estimate strength and period, along with a prescribed approximation of story drifts as a function of global roof drifts derived from spectral displacements. Torsion, along with other considerations, are used to estimate inelastic rotation demands on individual columns and drift demands on walls, including consideration of uncertainty. Drift capacities and uncertainties for each column and wall have been based on experimental data (where available) quantifying the failure of different types of reinforced concrete components with varying levels of axial load and ductile detailing, including consideration of lap splice deficiencies.

Drift demands and drift capacities are used to compute column and wall ratings, which are then used to determine story ratings, and finally, an overall building rating. These ratings represent the likelihood of collapse, and vary between 0.1 and 0.9, with 0.1 representing a low likelihood of collapse and 0.9 representing a high likelihood of collapse. Numerical building ratings can then be used to rank a group of buildings, or to separate the inventory into classes (i.e., groups) of *lower seismic risk buildings*, *high seismic risk buildings*, and *exceptionally high seismic risk buildings*, for the purposes of setting risk mitigation priorities.

Certain buildings can be quickly classified as *lower seismic risk* (relative to all older concrete buildings), and others as *exceptionally high seismic risk*, using global considerations, including strength and configuration. Other buildings may undergo a more complete, but still abbreviated, evaluation procedure. The following sections highlight key calculation procedures for full application of the evaluation methodology, and summarize criteria used for early identification and classification of buildings.

2.2.1 Overview of Key Calculation Procedures

Full application of the evaluation methodology consists of the following steps:

- Complete the general requirements including a site visit.
- Classify the structural system among pure frame, frame-wall, bearing wall, and infilled frame systems.
- Identify *lower seismic risk buildings* and *exceptionally high seismic risk buildings* using approximate global characteristics.
- Determine global lateral mechanisms and the governing base shear strength.
- Estimate the effective period of vibration.
- Estimate global drift demands based on the spectral demands at the site.
- Estimate story drift demands as a function of global drift demands.

- Evaluate column and wall components for collapse based on drift demand to drift capacity ratios, and assign column and wall component ratings.
- Establish the story rating as a measure of story collapse probability based on the ratings of all gravity load-carrying components.
- Determine building rating and risk classification based on the largest story rating in either direction.

The methodology also includes special procedures for evaluating pounding between buildings, slab-column frames, corner-column conditions, discontinuous columns, and mezzanines. Key calculation procedures are provided in the following chapters and sections:

- Chapters 2 through 4 provide scope, applicability, general requirements, and general strength calculations for basic application of the methodology.
- Chapter 5 covers procedures for classifying building type, configuration, and behavior, which are critical and necessary for application of the methodology. It includes a mechanism procedure for estimating the effective base shear strength (Section 5.5), which is used to estimate the effective fundamental period (Section 5.6). It also includes estimation of a global demand-to-capacity ratio (Section 5.7), which is used as a key indicator of behavior, and is also used in early identification and classification of buildings (Sections 5.8 and 5.9).
- Chapters 6, 7, 8, and 9 provide system-specific evaluation procedures for frame, frame-wall, bearing wall, and infilled frame systems, respectively, based on the classification of buildings in Chapter 5. Each of these chapters is parallel in content and organization, and information is repeated so that each chapter is largely self-contained and essentially complete for evaluation of the system of interest. System-specific evaluation procedures include: identification of critical components (Section ∗.3), estimation of global drift demand (Section ∗.4), calculation of story and component drift demands (Sections ∗.5 and ∗.6), calculation of drift capacities (Section ∗.7), and determination of component and story ratings (Sections ∗.8 and ∗.9).
- Chapter 10 describes the determination of the overall building rating, and classification of buildings based on building rating.

2.2.2 Early Identification of Lower Seismic Risk Buildings

Buildings can be identified as *lower seismic risk buildings* with limited effort, and without the need for further evaluation, based on criteria in the following sections:

- Section 5.4.3 – identifies frame-wall or wall systems with regular configurations that can be classified as *lower seismic risk buildings* if a parameter called the wall strength index (WSI) meets certain requirements.
- Section 5.8.1 – identifies strength requirements for buildings to be classified as exceptionally strong (i.e., essentially elastic), and, therefore, *lower seismic risk buildings*.

2.2.3 Early Identification of Exceptionally High Seismic Risk Buildings

Buildings can be identified as *exceptionally high seismic risk buildings* with limited effort, and without the need for further evaluation, based on criteria in the following sections:

- Section 3.1 – specifies that concrete buildings for which detailed structural drawings are not available should be considered *exceptionally high seismic risk buildings* by default, unless structural details can be confirmed by other means.
- Section 3.6 – identifies structural load path requirements along with conditions that, if present, result in the designation of an *exceptionally high seismic risk building*.
- Section 5.9.1 – identifies strength requirements for buildings to be classified as exceptionally weak, and, therefore, *exceptionally high seismic risk buildings*.
- Section 5.9.2 – identifies conditions for discontinuous walls supported on columns, wall piers, or girders that, if present, can result in the designation of an *exceptionally high seismic risk building*; also provides criteria for further evaluation of elements supporting discontinuous walls.
- Section 7.6.2.3 and Section 9.6.2.3 – identifies criteria for extreme torsion resulting in the designation of an *exceptionally high seismic risk building*.

2.3 Use of Alternate Analysis Procedures

The evaluation methodology includes simplified calculation procedures for estimation of important structural properties and response characteristics, such as building strength, period of vibration, and drift demands. Although it is intended to be easier and less expensive to implement than other evaluation and retrofit methods, it does not preclude the use of alternate analysis procedures for determining structural parameters used in the evaluation methodology.

The use of alternate procedures is permitted, as long as the resulting structural parameters are compatible and consistent with the basis of this methodology, as follows:

- **Effective Fundamental Period.** Use of an accepted analysis procedure, such as the Nonlinear Static Procedure in ASCE/SEI 41-17 Section 7.4.3, is permitted for computing the effective fundamental period of the structure. The elastic period is not an acceptable substitute for the effective period.
- **Effective Yield Strength.** Use of an accepted analysis procedure, such as the Nonlinear Static Procedure in ASCE/SEI 41-17 Section 7.4.3, is permitted for computing the effective yield strength of the structure.
- **Story Drift Demand**. Use of an accepted analysis procedure, such as the Nonlinear Static Procedure in ASCE/SEI 41-17 Section 7.4.3, or the Nonlinear Dynamic Procedure in ASCE/SEI 41-17 Section 7.4.4, is permitted for determining the story drift demand including torsional effects, where required, in lieu of the approximate procedure in this methodology. Column drift demands may be determined directly from the analysis or from the procedures in this methodology.

It is unclear at this time if risk ratings obtained using input parameters from other engineering procedures would be consistent with ratings obtained using the calculation procedures defined herein. For decision making at the public policy level, and implementation in mandatory evaluation and retrofit programs, it is recommended that the complete methodology be used with input parameters from a common engineering basis to ensure consistency in the relative rankings across an inventory of buildings.

Chapter 3

General Requirements

The evaluation methodology requires specific knowledge of the as-built configuration and condition of in-place materials and components. This chapter describes the general requirements for use of the methodology, including the presence of a complete load path.

3.1 As-Built Information

Documentation of the as-built configuration of a building is necessary for implementation of the evaluation methodology. Required as-built information includes: (a) building size and configuration; (b) structural component size, reinforcement, and detailing; material properties; and (c) site and foundation information. This information is best obtained from complete structural design drawings or as-built drawings. Other potential sources of information include construction specifications, geotechnical reports, structural calculations, and shop drawings.

In the case of older concrete buildings, sources of as-built information are often not available. Because it is potentially misleading to make assumptions regarding reinforcement details and member proportioning, it is recommended that any concrete building for which detailed structural drawings are not available should be considered an *exceptionally high seismic risk building* by default, unless structural details can be confirmed by other means (e.g., destructive and non-destructive site investigations).

An exception to the need for complete data as described above is contained in Section 5.4.3, where certain buildings could be classified as *lower seismic risk* based on the ratio of cross sectional area of structural walls and total building area.

Where concrete buildings contain masonry infill, the configuration of the masonry (e.g., thickness and dimensions of openings) is often shown only in architectural drawings, specifications, or shop drawings, which may not be available with the structural drawings. In addition, masonry material properties are seldom identified in any construction documents. In the absence of available construction documents or material tests, estimates for default masonry material properties are provided, but should be considered as highly uncertain.

3.2 Site Investigation

A site investigation consists of visual observation of the condition of the building to verify that as-built information is representative of the existing conditions. The following should be confirmed as part of a site investigation: (a) building configuration, including the presence (or not) of structural additions, alterations, or modifications; (b) layout, proportioning, and condition of structural components; (c) site characteristics; (d) foundation conditions; and (e) where present, infill characteristics (e.g., infill panel locations, materials, thickness/number of wythes, and size of openings).

It is intended that site investigations be performed using non-destructive means. Concealed conditions should be exposed where feasible and practical (e.g., above suspended ceilings). In general, destructive removal of finishes and in-situ testing of materials are not required as part of the methodology, although information from destructive investigations could be used to enhance available as-built information. The condition of masonry infill can have a significant influence on the response of buildings with infill walls. Site investigation of masonry infill materials, including characterization of the mortar with a scratch test, is necessary for determining infill material properties.

3.3 Seismic Hazard

Seismic hazard due to ground shaking is defined as an acceleration response spectrum based on either a probabilistic or deterministic assessment of hazard presented in United States Geological Survey (USGS) seismic maps.

The recommended seismic hazard level for evaluation is the ASCE/SEI 41-17 Basic Safety Earthquake BSE-2E, which corresponds to a 5% probability of exceedance in a 50-year period. The USGS National Seismic Hazard Mapping Project provides spectral response acceleration parameters (S_S, S_1) adjusted for site class at the latitude and longitude of the building. Site class (A through F) should be determined in accordance with ASCE/SEI 7-16, *Minimum Design Loads and Associated Criteria for Buildings and Other Structures, Provisions* (ASCE, 2017a). Site class as documented in a geotechnical report is acceptable for use. If insufficient information is available to classify the site, default Site Class D shall be used.

For the purposes of this methodology the BSE-2E parameters (S_{XS}, S_{X1}) need not be greater than those for the risk-targeted maximum considered earthquake (MCE_R) ground motion (also modified for site class) determined in accordance with ASCE/SEI 7-16.

Evaluation using this methodology at other levels of seismic hazard is permitted.

3.4 Material Properties

3.4.1 General

Properties of cast-in-place concrete, reinforcing steel, and masonry infill materials shall be taken from design drawings or other as-built information. Physical testing of in-situ materials is not required as part of the methodology.

Although not required, testing can result in higher material strengths than minimum values specified on the drawings or default values provided in ASCE/SEI 41-17 or as part of this methodology. As a result, physical testing could be used to improve material strength values, and could be considered as part of an enhanced investigation of as-built information. Regardless of the source of material property information and level of testing and investigation performed, the methodology does not incorporate the use of a knowledge factor as prescribed in ASCE/SEI 41-17.

3.4.2 Concrete and Reinforcing Steel

If material properties are not identified in the design drawings or documented in other as-built information, default material properties may be used in accordance with ASCE/SEI 41-17 Section 10.2.2.5.

Concrete and reinforcing steel properties used in component strength calculations shall be expected material properties, determined as follows:

- expected compressive strength of concrete, f'_{ce}, taken as the specified or nominal compressive strength, f'_c, multiplied by 1.5; and
- expected yield strength of reinforcement, f_{ye}, taken as the specified or nominal yield strength, f_y, multiplied by 1.25.

3.4.3 Masonry Infill

Properties of infill masonry panels shall be taken from design drawings, other as-built information, or site investigation. At a minimum, information on infill panel locations, masonry unit material (clay or concrete) and type (brick, hollow clay tile, concrete masonry unit), thickness and number of wythes, confinement, and mortar condition are necessary.

Masonry infill properties used in component strength calculations shall be expected material properties, determined as follows:

- Expected cohesion of the masonry-mortar interface, C, defined in ASCE/SEI 41-17 Section 11.4.2.3. If no information is available, expected values can be taken from Table 3-1.
- Expected initial friction coefficient of masonry mortar joints, μ, defined in ASCE/SEI 41-17 Section 11.4.2.3. If no information is available, expected values can be taken from Table 3-1.
- Expected compressive strength of the masonry assembly, f'_m. If the mortar and masonry units are in good condition, and information about the type of mortar and the strength of the masonry units are available, f'_m is taken as the specified or nominal compressive strength, or from the unit strength method in Section 1.4 of TMS 602-13/ACI 530.1-13/ASCE 6-13 *Specification for Masonry Structures* (MSJC, 2013). If no other information is available, expected values can be taken from Table 3-1.

Table 3-1 Default Expected Properties for Masonry Infill

Mortar Description	C (psi)	μ	f'_m		
			Solid Fired Clay Brick	Concrete Masonry Unit (CMU)	Hollow Clay Tile [(1)]
Raked out by finger pressure (i.e., very soft/ lime mortar)	15	0.3	400	n/a	200
Scratches easily with finger nails (i.e., soft)	45	0.3	850	n/a	500
Scratches with finger nails (i.e., medium)	70	0.6	1000	1600	500
Scratches using aluminum pick or does not scratch with tools (i.e., hard/very hard)	100	0.8	1200	2000	600

(1) Hollow clay tile refers to clay tile in architectural or nonstructural applications. Structural clay tile should use the values under solid fired clay brick.

Default properties in Table 3-1 were developed as described in Appendix O. Significant uncertainties are present in masonry infill properties, which are not captured in the values provided in Table 3-1. Although physical testing is not explicitly required as part of this methodology, other information (if available), or results from physical tests (even if limited), should be used in lieu of the values in Table 3-1. Evaluation of infilled frame systems using default properties should consider the potential impact of variation in masonry infill parameters. Users are cautioned that it is not always conservative to assume the weakest (worst) condition for masonry infill.

3.5 Condition of Structural Components

The methodology assumes that the building and structure are in generally good condition. Although site investigations do not require destructive investigation or detailed condition assessment, visual observations should include assessment of the general condition of significant structural component in accessible areas. If the overall building or significant structural components are judged to be in poor condition, then the evaluation results should be adjusted to characterize the potentially weakened state of the building.

Concrete buildings constructed in the 1940s and earlier are particularly likely to have experienced inadequate quality control on concrete mixing and placement procedures during construction. As a result, the as-built condition of such buildings, and the condition of the concrete columns in particular, should be investigated in greater detail. Guidance on more detailed condition assessment is available in ASCE/SEI 41-17 Section 10.2.3, FEMA 306, *Evaluation of Earthquake Damaged Concrete and Masonry Wall Buildings* (FEMA, 1998), or ACI 201.2R, *Guide to Durable Concrete* (ACI, 2008).

3.6 Structural Load Path Requirements

The evaluation methodology assumes the existence of a complete load path. Prior to implementing the methodology, it is important to understand the load path for lateral and vertical forces. Significant gaps in the load path can lead to catastrophic failure even if most structural components would remain undamaged. Assessment of the load path is primarily qualitative in nature, based on identification of gaps in the seismic-force resisting system rather than quantitative analysis of structural elements. This is consistent with the philosophy of the Tier 1 Screening assessment in ASCE/SEI 41-17 Chapter 4.

Load path deficiencies that would cause an older concrete building to be considered an *exceptionally high seismic risk building* are identified in the following sections. Other load path considerations, such as discontinuous wall or frame elements, or excessive weakness in wall or frame elements, are explicitly addressed in the evaluation methodology.

3.6.1 Diaphragm Continuity

Except for buildings classified as frame structures, buildings should be evaluated for adequate connection between the diaphragms and shear walls. In general, it is assumed that frame structures have distributed lateral systems and that there is sufficient interconnection between the frames and floor slabs to provide at least a nominal load path for transferring diaphragm forces to the frame elements.

If any of the following conditions are present, the building should be considered an *exceptionally high seismic risk building*:

- Any individual shear wall or combined shear core that is located at the exterior of the building with less than 50 percent of the total wall length engaging the diaphragm at any level in either primary direction, unless collector reinforcing is present with minimum tensile capacity of $0.10S_{XS}$ times the weight of the floor tributary to the wall. S_{XS} is the spectral response acceleration parameter at 0.2 second period using the seismic hazard determined in Section 3.3.
- Diaphragm openings immediately adjacent to interior shear walls exceeding 75 percent of the shear wall length on both sides of the wall, unless collector reinforcing is present with minimum tensile capacity of $0.10S_{XS}$ times the weight of the floor tributary to the wall.
- Diaphragms lacking a positive connection to shear walls by means of reinforcing steel dowels between the wall and slab.
- Diaphragms in ramped parking structures, or buildings with ramped parking levels above grade, that consist of split-level floors in which the sections of the diaphragm are not engaged by seismic force-resisting elements on at least three sides of each section.

If individual walls with inadequate engagement to diaphragms exist in a building, the *exceptionally high seismic risk* designation can be set aside and the full methodology can be used to evaluate the building if the walls are not considered in the analysis and it can be shown that the presence of the walls does not result in any negative impacts on building response, such as a soft or weak story or significant torsion.

3.6.2 Concrete Element Interconnectivity

Basic interconnection of concrete frame and wall elements is necessary for a complete load path. If present in a building, the following conditions are indications of poor interconnectivity, but are not necessarily an indication of *exceptionally high seismic risk buildings*. The evaluating engineer should determine the effects of such conditions on the expected seismic performance of the building under consideration.

- Concrete columns are not doweled into foundations with a minimum of four dowels.

- Concrete walls are not doweled into foundations with vertical dowels equal to the size and spacing of vertical wall reinforcement immediately above the foundation.

3.7 Penthouse and Other Rooftop Structures

Penthouses and other rooftop structures need not be explicitly evaluated in this methodology if the weight is no more than 25 percent of the effective seismic weight of the main roof level, and the area of the footprint is no more than 30 percent of the total area of the main roof level. Where these conditions are not met, a penthouse or rooftop structure shall be considered a story and evaluated as such using this methodology.

Chapter 4

Component Strengths

This chapter specifies methods for determining the strengths of individual concrete components.

4.1 Introduction

For most concrete components, strengths are determined in accordance with ASCE/SEI 41-17 and ACI 318-14, *Building Code Requirements for Structural Concrete and Commentary* (ACI, 2014). Because of differences in proportioning and detailing between older concrete structures and current construction practices, clarifications and alternate provisions for some types of concrete components are provided. Because the strength of some concrete components depends on axial load, procedures for determining axial load are also provided.

4.2 Axial Loads on Columns and Walls

4.2.1 Expected Gravity Loads

For the purposes of this methodology, the determination of expected gravity loads on concrete columns, concrete walls, concrete slab-column connections, and masonry infill panels shall be determined in accordance with this section. Dead loads include the structure self-weight and appropriate superimposed dead loads. Live loads shall be taken as 25% of the unreduced design live loads listed in ASCE/SEI 7-10 Table 4-1. Vertical loads due to expected gravity load effects, P_g, are calculated as:

$$P_g = P_D + 0.25P_L \tag{4-1}$$

where P_D is the axial load due to tributary dead loads, and P_L is the axial load due to unreduced tributary live loads.

4.2.2 Earthquake Axial Loads

Consideration of column and wall component axial loads due to earthquake, P_{eq}, is required only where explicitly specified. Column axial load due to earthquake overturning effects, P_{eq}, at each story x is calculated as:

$$P_{eq} = \frac{V_y (h_{eff} - h_x)}{L} \tag{4-2}$$

where:

V_y = base shear strength of a structure

h_{eff} = effective height of the building, defined as the height from the base to the centroid of lateral forces (same as the effective height of an equivalent single-degree-of-freedom system, which may be taken as $0.7h_n$ in multistory buildings having uniform distribution of effective weight over the building height, and h_n in single-story buildings)

h_n = height from the base of the building to the highest level of the seismic force-resisting system (i.e., level n)

h_x = height from the base of the building to level x (i.e., the bottom of story x)

L = plan dimension between the outermost frame columns in the direction of interest at story x

Axial load, P_{eq}, is taken as positive in compression, and can be distributed in proportion to contribution of each frame line to total building V_y. Tension loads due to earthquake overturning are not critical and need not be considered. For columns located in a story above the effective height of the equivalent single-degree-of-freedom system, or for interior columns in a frame line (i.e., not the outermost columns in the frame line), P_{eq} may be taken as zero. If h_{eff} falls within a story, P_{eq} should be computed for the columns within that story.

Where explicitly required in the methodology, axial loads due to earthquake overturning effects on walls and vertical wall segments shall be estimated by accepted principles of mechanics.

4.2.3 Load Combinations

Where gravity loads are combined with earthquake forces, all load combinations shall be unfactored, with gravity loads determined in accordance with Equation 4-1. Evaluation of components for gravity loads in the absence of earthquake forces is beyond the scope of this methodology.

4.3 Component Strength Calculations

4.3.1 General

Component strengths used in this evaluation methodology shall be taken as expected strengths. Expected strengths shall be calculated using expected material properties, determined in accordance with Section 3.4.

Concrete column, beam, slab, joint, and wall component strengths shall be determined using expected material properties and accepted principles of mechanics. Unless specifically indicated otherwise in the sections that follow, the procedures of ACI 318-14 may be used to calculate the strength of concrete components, except that the strength reduction factor, ϕ, should be taken as unity (i.e., $\phi = 1.0$). For components constructed using lightweight concrete, strength calculations should be modified in accordance with ACI 318-14 procedures for lightweight concrete.

Expected strength of masonry infill panels shall be determined in accordance with Section 4.3.6.

4.3.2 Concrete Column Strength

4.3.2.1 Column Shear Strength

Column shear strength, V_n, is calculated based on ASCE/SEI 41-17, as follows:

$$V_n = k\left(\frac{A_v f_{ye} d}{s} + \lambda\left(\frac{6\sqrt{f'_{ce}}}{l_{inf}/d}\sqrt{1+\frac{P_g}{6\sqrt{f'_{ce}}A_g}}\right)0.8A_g\right) \tag{4-3}$$

where:

k = factor related to displacement ductility demand; can be taken as 1.0 for the purpose of calculating column shear strength in this methodology

s = spacing of transverse reinforcement

A_v = area of transverse reinforcement within spacing s

d = effective depth of the column section

f_{ye} = expected yield strength of reinforcement

λ = 0.75 for lightweight concrete, and 1.0 for normal weight concrete

f'_{ce} = expected compressive strength of concrete

l_{inf} = clear height of an equivalent cantilever column from the face of a joint to the point of inflection (or zero moment); in a typical story, l_{inf} may be taken as half of the column clear height, l_u

P_g = column axial load (in compression) due to expected gravity load effects (equal to zero if in tension)

A_g = gross area of concrete column section

It is permitted to assume $d = 0.8h_c$, where h_c is the overall dimension of the column in the direction of shear. The ratio l_{inf}/d should not be taken greater than 4, nor less than 2. For columns satisfying the detailing and proportioning requirements of ACI 318-14 Chapter 18, the shear strength equations of ACI 318-14 Chapter 22 are permitted.

Where the longitudinal spacing of transverse reinforcement is less than the component effective depth measured in the direction of shear, transverse reinforcement is assumed to be fully effective in resisting shear, and the limitations in ASCE/SEI 41-17 Section 10.3.4 related to spacing of transverse reinforcement need not apply.

4.3.2.2 Column Flexural Strength

The expected flexural strength of a column section, M_n, is calculated in accordance with ACI 318-14 Chapter 22 using expected material properties and $\phi = 1.0$. The axial load for determining flexural strength shall be the expected gravity loads on the column determined in accordance with Section 4.2.1.

4.3.2.3 Effects of Column Lap Splices on Flexural Strength

For the purpose of determining the effective base shear strength and controlling building mechanism in accordance with Section 5.5, if the lap splices in the vertical reinforcement of the columns do not meet the minimum length requirements in ASCE/SEI 41-17 Section 10.3.5, the expected flexural strength shall be modified to account for a reduction in the strength of vertical reinforcement in accordance with ASCE/SEI 41-17 Section 10.5.3.

4.3.3 Beam-Column Joint Shear Strength

Beam-column joints satisfying the following conditions may be assumed to have sufficient strength to develop the flexural strength of the beams and columns framing into the joint:

- interior beam-column joints where beams frame into all four faces of the joint; and
- any joint with hoop reinforcement within the joint at a spacing not exceeding the lesser of: $h/3$, where h is the overall dimension of the column in the direction of shear, or 8 inches.

For other joints, shear strength should be calculated in accordance with ASCE/SEI 41-17 Section 10.4.2.2, except that the joint shear strength, V_{nj}, need not be taken less than:

$$V_{nj} = 10\lambda\sqrt{\frac{h_c}{h_b}}\sqrt{f'_{ce}}A_j \tag{4-4}$$

where:

h_c = overall dimension of the column in the direction of shear

h_b = overall depth of the beam

A_j = effective cross-sectional area of the beam-column joint

The ratio h_c/h_b shall be taken less than or equal to 1.0. The effective area of the joint, A_j, can be taken as $h_c\ (b_c + b'_w)/2$, where b_c is overall width of the column in the direction perpendicular to joint shear; and b'_w is the web width of the beam, excluding portions of the web that extend beyond the width of the column. Joint shear strength calculated in accordance with ASCE/SEI 41-17 is typically less than the value in the exception noted above. Thus, V_{nj} calculated using Equation 4-4 is generally expected to control.

4.3.4 Slab-Column Frame Strength and Integrity Requirements

The flexural strength of a slab, and the shear and moment transfer strength of slab-column connections, shall be calculated in accordance with ASCE/SEI 41-17 Section 10.4.4.3. The flexural strength of the slab, and the flexural strength of a joist system, is based on the strength of the column strip, as defined in ASCE/SEI 41-17. The shear and moment transfer strength of slab-column connections must consider the combined action of flexure, shear, and torsion in accordance with ASCE/SEI 41-17.

Where required in this methodology, slab-column joints are considered to satisfy minimum structural integrity requirements if the total area of main slab bottom bars passing through, or anchored within, the column cage, A_{sb}, is more than $2V_g/f_{ye}$, where V_g is the shear demand based on gravity loads computed in accordance with Equation 4-1, and f_{ye} is the expected strength of the slab bottom bars (Section 3.4). This is illustrated in Figure 4-1 where A_b is the area if an individual bottom bar and A_{sb} represents the total area of main slab bottom bars.

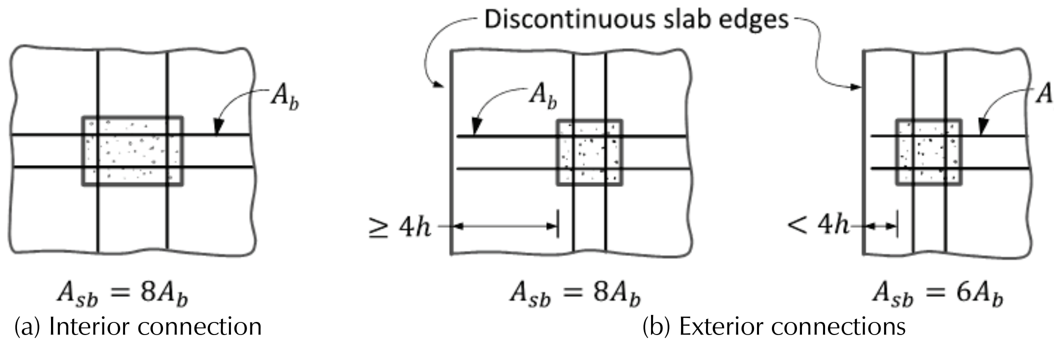

(a) Interior connection

(b) Exterior connections

Figure 4-1 Illustration of slab-column structural integrity requirements: (a) interior connection; and (b) exterior connections.

4.3.5 Concrete Wall Strength

In calculating expected shear and flexural strengths of concrete walls, expected material properties shall be used and the strength reduction factors, ϕ, should be taken as unity (i.e., $\phi = 1.0$).

4.3.5.1 Wall Shear Strength

The shear strength of a wall section shall be calculated as the expected shear strength using the procedures of ACI 318-14 Section 18.10, except that the restriction on spacing, reinforcement ratio, and number of curtains of reinforcement need not apply. If the transverse reinforcement ratio, ρ_n, is less than 0.0015, the contribution of wall reinforcement to the shear strength of the wall may be computed using $\rho_n = 0.0015$.

The shear strength of a wall shall be limited by the sliding strength at horizontal construction joints. Sliding strength shall be taken as twice the value determined in accordance with the shear friction provisions in ACI 318-14 using expected material properties, and taking the friction coefficient and strength reduction factor as unity (i.e., $\mu = \phi = 1.0$). Shear friction capacity shall be modified to account for the effects of non-conforming lap splice lengths as described below.

4.3.5.2 Wall Flexural Strength

The expected flexural strength of a wall section, M_n, is calculated in accordance with ACI 318-14 Chapter 22. The axial load for determining flexural strength shall be the expected gravity loads on the wall determined in accordance with Section 4.2.1.

For the purpose of determining the effective base shear strength and controlling building mechanism in accordance with Section 5.5, if the lap splices in the vertical reinforcement of a wall do not meet the minimum length requirements in ASCE/SEI 41-17 Section 10.3.5, the expected flexural strength shall be modified to account for a reduction in the strength of vertical reinforcement in accordance with ASCE/SEI 41-17 Section 10.3.5.

4.3.6 Infilled Frame Strength

4.3.6.1 Masonry Infill Panel Strength

Where masonry infill is present, the shear strength of a masonry infill panel, V_m, is calculated as:

$$V_m = P_{inf}^{grav}\mu + A_{w,inf}C \tag{4-5}$$

but not taken greater than:

$$f'_m t_{inf} \frac{h_{inf}}{6} n_s \tag{4-6}$$

where:

P_{inf}^{grav} = gravity load carried by the infill

μ = initial friction coefficient

$A_{w,inf}$ = horizontal cross-sectional area of an infill panel

C = cohesion, as defined in Section 3.4.3

f'_m = expected compressive strength of the masonry assembly

t_{inf} = net thickness of the masonry panel

h_{inf} = height of the masonry panel

n_s = number of struts expected to develop in the masonry panel, taken as 1 for solid panels with $L_{inf}/h_{inf} < 1.0$, and 2 otherwise

and infill panel dimensions are as defined in Figure 4-2. The horizontal cross-sectional area of an infill panel, $A_{w,inf}$, is taken as the product ($t_{inf} \times L_{inf}$) of the thickness of the infill, t_{inf}, and the length of the infill, L_{inf}. The vertical load carried by the infill, P_{inf}^{grav} , is calculated from the total expected gravity load, P_T, based on the tributary areas above the panel and story of interest, which can be estimated based on the relative stiffness of columns and infill in accordance with ASCE/SEI 41-17. In cases with wall lengths, L_{inf}, between 15 feet and 25 feet, and story heights, h_{sx}, between 10 feet and 14 feet, the vertical load carried by the infill can be estimated as $P_{inf}^{grav} = 0.5P_T$.

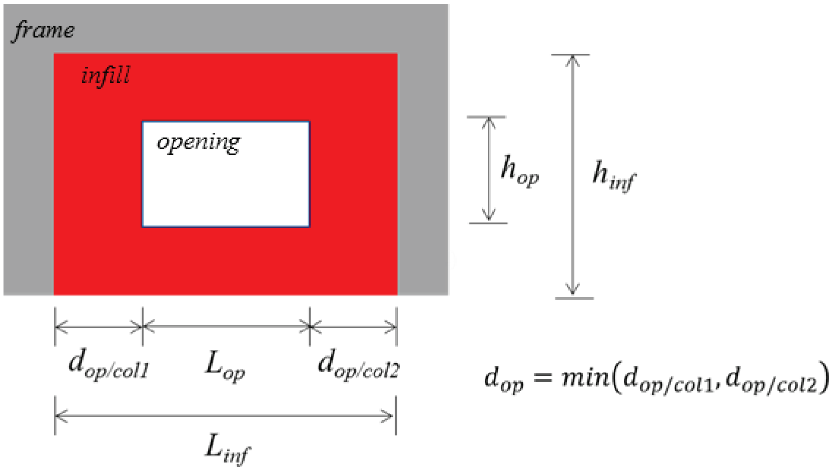

Figure 4-2 Illustration of symbols defining the geometry of masonry infill panels.

As shown in Figure 4-2, L_{inf} is the length of the infill wall, h_{inf} is the height of the infill panel, and t_{inf} is the net thickness of the panel. Wythes protruding beyond the column face are not well-confined and are ignored in the calculation of shear strength.

4.3.6.2 Infilled Bay Strength

Where masonry infill is classified as "strong" or "weak" in accordance with Section 5.3.4, the shear strength of a single, solid infilled bay, $V_{inf,solid}$, is taken as the maximum of the shear strength of the masonry infill panel in accordance with Section 4.3.6.1, and a combination of frictional resistance in the masonry plus a governing, lower value of shear strength in a column:

$$V_{inf,solid} = max\left(V_m,\ P_{inf}^{max}\mu + V_{lc}\right) \tag{4-7}$$

where:

V_m = shear strength of the masonry panel (Section 4.3.6.1)

P_{inf}^{max} = expected gravity load supported by the infill when the maximum lateral strength is reached

μ = initial friction coefficient

V_{lc} = lower governing shear strength of the weaker of the two columns bounding the infill panel of interest, taken as the lesser of V_n (Section 4.3.2.1) and V_p (Section 4.4.1) considering the role of the infill in reducing the effective height of the column

In Equation 4-7, P_{inf}^{max} is the expected gravity load supported by the infill when the maximum lateral strength is reached. Studies indicate that this value is higher than the vertical load carried by the infill, P_{inf}^{grav}, calculated in Section 4.3.6.1, and can be calculated in accordance with ASCE/SEI 41-17 Table 11-9. In cases with wall lengths, L_{inf}, between 15 feet and 25 feet, and story heights, h_{sx}, between 10 feet and 14 feet, the expected gravity load at maximum lateral strength can be taken as $P_{inf}^{max} = 0.7P_T$.

In the case of an infill panel with openings, the strength of a single, solid infilled bay shall be reduced to $V_{inf,open}$, calculated as:

$$V_{inf,open} = V_{inf,solid}\left(1 - \frac{A_{op}}{A_{inf}}\right) \tag{4-8}$$

where:

$V_{inf,solid}$ = shear strength of a single, solid infilled bay (Equation 4-7)

A_{op} = area of openings in an infill panel, in elevation, ft^2

A_{inf} = area of an infill panel, in elevation, ft^2

In cases where $A_{op}/A_{inf} > 0.6$, $V_{inf,open}$ shall be taken as 0.

4.4 Column Shear Strength Ratio

To determine the column shear strength ratio, V_p/V_n, column shear strength, V_n, is determined in accordance with Section 4.3.2.1, and the column plastic shear capacity controlled by flexure, V_p, is calculated based on the expected flexural strengths of the members framing into the joints at the top and bottom of each story.

To provide an upper bound assessment of column flexural strength in determining the column shear strength ratio, the strength of vertical reinforcement in the column shall not be reduced to account for inadequate lap splice length (Section 4.3.2.3).

4.4.1 Column Shear Capacity in a Typical Story

For columns in a typical story, the column capacity-limited (plastic) shear strength, V_p, is:

$$V_p = \frac{M_{cT} + M_{cB}}{l_u} \tag{4-9}$$

where:

M_{cT} = flexural strength at the top of the column

M_{cB} = flexural strength at the bottom of the column

l_u = clear height of the column

M_{cT} and M_{cB} are taken as the lesser of the expected flexural strength of the column section, M_n, calculated in accordance with Section 4.3.3 and the flexural strength controlled by the beams or slabs at the top or bottom of the column, respectively. The column clear height, l_u, shall account for translational or rotational restraint provided by concrete spandrel beams, partial height concrete walls, and masonry infill panels. Where the moment is controlled by the beams or slabs, l_u shall be replaced by the story height.

Alternatively, if the beams are shear-controlled, the expected flexural strength of the beam can be limited by the shear strength of the beam. Additionally, the flexural strength at the top or bottom of the column need not be taken greater than the capacity associated with the joint shear strength, taken as $V_{nj}h_b/2$, where V_{nj} is the expected shear strength of the joint determined in accordance with Equation 4-4, and h_b is the overall depth of the beam.

In T-beam construction, where slab reinforcement is in tension due to moments at the face of the joint, reinforcement located within an effective flange width determined in accordance with ACI 318-14 Section 9.2.4 should be assumed to contribute to the flexural strength of the beam.

4.4.2 Slab-Column Frames

In slab-column frames, the flexural strength at the top and bottom of the column will be limited by the expected flexural strength of the slab or the shear and moment transfer strength of slab-column connection as determined in Section 4.3.4.

Chapter 5

Structural Classification

This chapter provides rules for classifying buildings into systems of similar seismic response characteristics to enable the use of more efficient evaluation methods. This chapter also provides criteria for identifying the lowest and the highest risk buildings that are at the extreme ends of the strength and configuration ranges of these systems.

5.1 Introduction

Older concrete buildings come in many sizes, heights, and structural system types. Gravity frame systems include floors of flat slabs, shallow joists, and beams and girders supported on columns that can be round, rectangular, square, or other shape, with varying levels of confinement provided by spirals or hoops with crossties. Some gravity frame systems are explicitly designed to resist seismic forces, but all gravity framing must safely accommodate expected seismic drift demands. Concrete walls, which can resist seismic forces, are present in many older concrete buildings. A specific type of building, usually used in residential occupancies, has very few, if any, columns, with the majority of gravity loads supported by structural concrete walls.

The seismic risk presented by different types of buildings varies widely. Many buildings have limited ductility under lateral loading, particularly those governed by members failing in shear. Lateral strength also varies, and buildings with structural walls are generally stronger than buildings with frames. However, some frame systems designed for high gravity loads, such as those used in warehouse occupancies, also have relatively high strength, and frames with round columns and spiral transverse reinforcing can be quite ductile in response to earthquake shaking.

Regardless of the type of structural system, the performance of many buildings is largely influenced by the building configuration. Tall first stories, used to create lobbies or first-floor commercial spaces, are often also soft and/or weak stories that concentrate lateral displacement at that level. Other vertical irregularities, such as discontinuous walls supported on columns or girders, or columns supported on transfer girders, can be a local collapse risk that could lead to global collapse. Plan irregularities, especially in buildings with walls, induce torsional response that can amplify lateral displacement demands on frame and wall lines.

5.2 Classification of Concrete Components

5.2.1 Reinforced Concrete Columns

For the purposes of this methodology, a reinforced concrete column is a vertically oriented concrete component with an elevation aspect ratio of:

$$l_u/h_{max} \geq 2.0$$

where:

l_u = clear height of the column

h_{max} = largest cross-sectional dimension

and the section is tied with hoops, crossties, or spirals in accordance with minimum requirements for non-seismic columns.

Test data for collapse of columns used as a basis for this methodology were generally limited to cross section aspect ratios of $h_{max}/h_{min} \leq 2.5$, where h_{max} and h_{min} are the maximum and minimum cross-sectional dimensions of the component, respectively. Extrapolation of this methodology to column components with larger aspect ratios should be carefully considered for applicability by the evaluating engineer.

5.2.2 Reinforced Concrete Structural Walls

For the purposes of this methodology, vertically oriented reinforced concrete components that are not otherwise classified as columns, and that possess the following characteristics, shall be considered as structural concrete walls:

1. Thickness of at least 4 inches, or thickness at least $^{1}/_{25}$ of the distance between supporting or enclosing members.
2. Ratios of distributed longitudinal and transverse reinforcement to gross concrete area perpendicular to that reinforcement of at least 0.0015.
3. Sufficient anchorage to the floor diaphragms such that they can be considered as altering the lateral behavior of the structural system.
4. Sufficient strength to significantly impact other structural members (e.g., a spandrel that reduces the clear height of a column).

Concrete walls not meeting the requirements of this section need not be considered. Concrete walls not meeting requirements 1 and 2, above, may be considered at the option of the evaluating engineer if the effects of requirements 3 and 4 are judged to be significant.

Wall piers are vertical wall segments, typically not exceeding 8 feet in length, used as piers in pier-spandrel systems, as shorter vertical wall segments within longer walls, or located at the ends of longer walls in frame-wall or bearing wall systems.

5.3 Classification of Building Systems

Classification of buildings into structural systems of similar seismic response is necessary for implementation of the evaluation methodology. Each principal horizontal direction in a building can have a different structural system classification. Categories include frame systems (Section 5.3.1), frame-wall systems (Section 5.3.2), bearing wall systems (Section 5.3.3), and infilled frame systems (Section 5.3.4).

5.3.1 Frame Systems

Frame systems are systems composed of frames without structural walls or effective infill walls. Frame lines composing frame systems may include the following:

- Frame lines (or bays) that are designed to resist gravity loads, including beam-column systems, slab-column systems, or joist-column systems.
- Frame lines (or bays) that are designed to resist gravity plus lateral loads, regardless of the level of ductile detailing.
- Frame lines with partial-height concrete or masonry infill walls that can potentially create short column effects.

The evaluation procedure for frame systems includes Sections 5.5 to 5.9 and Chapter 6.

5.3.2 Frame-Wall Systems

Frame-wall systems are systems with both frame lines, as identified in Section 5.3.1, and structural walls, as defined in Section 5.2.2.

Pier-spandrel systems are a subset of frame-wall systems in which structural walls, usually extending around the entire building perimeter, have a regular or nearly regular set of openings that subdivide the surface of the walls into a series of vertical piers and horizontal spandrels. A pier-spandrel system, as defined in this methodology, shall have piers with typical horizontal length not less than one-third of the bay width and spandrels with typical vertical depth not less than one-third of the story height. Minor or occasional deviations from these span-to-depth ratios are permitted in pier-spandrel systems, subject to the judgment of the evaluating engineer.

Walls with openings are sometimes referred to as punched shear walls or punched wall systems. Typically, such systems feature concrete walls around the perimeter of the building with a regular pattern of window openings. Punched wall openings are usually smaller, and the walls thinner than elements in a pier-spandrel system, and punched walls would be expected to behave more like a solid wall rather than a frame. In general, it is recommended that punched walls be treated as solid walls in this methodology. If the dimensions of openings in a punched wall system approach the dimensions of a pier-spandrel system, the building should also be evaluated assuming pier-spandrel behavior, and the controlling case determined.

The evaluation procedure for frame-wall systems includes Sections 5.4 to 5.9 and Chapter 7.

5.3.3 Bearing Wall Systems

Bearing wall systems are systems configured such that the majority of gravity loads are supported on structural concrete bearing walls. Isolated columns supporting up to 25% of the gravity load in the building can be present in a bearing wall system. If columns are used to support more than 25% of the gravity load, the structure shall be classified as a frame-wall system.

The evaluation procedure for bearing wall systems includes Sections 5.4 to 5.9 and Chapter 8.

5.3.4 Infilled Frame Systems

Infilled frame systems are systems that satisfy the requirements for frames in Section 5.3.1, or frame-walls in Section 5.3.2, and also include one or more masonry infill panels confined within the beam and column framing. Classification of infill in accordance with Table 5-1 affects the strength of the infilled bay, how the infill is presumed to interact with the columns, and how the infill is considered in the evaluation methodology.

In Table 5-1, V_m is the shear strength of the masonry infill panel, as calculated in Section 4.3.6.1, A_{op} is the area of openings in an infill panel (in elevation), A_{inf} is the area of an infill panel (in elevation), and V_{lc} is the lower governing shear strength of the weaker of the two columns bounding the infill panel of interest, as calculated in Section 4.3.6.2.

To be considered in this methodology, infill panels must be tightly confined within columns on both sides, but a small gap (< 0.25 inches) between the panels and the beam above is permitted. Infill panels classified as ineffective in Table 5-1 are not considered structural infill and may be ignored.

Table 5-1 Classification of Infill

Ratio of Masonry Infill Strength to Column Strength	Infill classification	Consideration
$\frac{V_m\left(1-{}^{A_{op}}\!/_{A_{inf}}\right)}{V_{lc}} \geq 3$	Strong	Infill requires full consideration
$3 > \frac{V_m\left(1-{}^{A_{op}}\!/_{A_{inf}}\right)}{V_{lc}} \geq 1.4$	Weak	Infill requires full consideration
$\frac{V_m\left(1-{}^{A_{op}}\!/_{A_{inf}}\right)}{V_{lc}} < 1.4$	Very weak due to openings(1)	Infill not considered in strength calculations, but considered in Chapter 9 evaluation procedures
$V_m/V_{lc} < 1.4$	Ineffective	Infill not considered in strength calculations, nor for short column effects

(1) Also applies when $A_{op}/A_{inf} > 0.6$, or when $A_{op}/A_{inf} > 0.2$ and openings are within 2 feet of a column.

Buildings with infill panels that are not classified as ineffective in Table 5-1, and are not tightly confined, can be evaluated both with and without considering the effects of infill, and the building rating determined by the governing case. Infill panels that have been previously retrofitted or reinforced are outside the scope of application of the methodology for evaluation of infilled frame systems. The evaluation procedure for infilled frame systems includes Sections 5.4 to 5.9 and Chapter 9.

5.4 Wall Index and Wall Strength Index

The wall index and wall strength index are used as criteria for identifying lower seismic risk buildings that have many walls (Section 5.4.3), or identifying cases where torsion need not be considered (Section 7.6.2.1).

5.4.1 Wall Index

The effect of structural walls including wall piers on the response of the structure can be measured by the wall index, WI:

$$WI = \frac{\sum A_w}{\sum A_f} \tag{5-1}$$

where:

$\sum A_w$ = the sum of the cross-sectional area of structural walls including wall piers in the story of interest oriented in the direction under consideration

$\sum A_f$ = the total area of floors above the story under consideration

The $\sum A_w$ shall include the webs and associated boundary elements of all vertically-oriented reinforced concrete components that are classified as structural walls in accordance with Section 5.2.2. Flanges of T-, L-, and other similarly shaped walls are not counted in the direction under consideration, but are counted when considering the wall index in the perpendicular horizontal direction. Where the axis of an individual wall is not aligned with the direction under consideration, it is acceptable to use the component in the direction under consideration.

Values of the wall index must be calculated in each of two principal horizontal directions in stories identified as follows: (a) the first story of a building; (b) other stories where walls are discontinued or reduced in size going up the building; and (c) stories immediately below floors having increased floor area as compared to lower floor levels. The lowest value of the wall index calculated in any story of the building, and in either of the two principal horizontal directions, is taken as the governing value of the wall index, *WI*, for the building.

5.4.2 Wall Strength Index

The wall strength index (*WSI*) is defined as:

$$WSI = \frac{WI}{S_{a(T_e)}} \tag{5-2}$$

where:

WI = the governing value of WI from Section 5.4.1

S_a = the horizontal spectral acceleration at the site (in *g*), taken at the approximate effective structural period, T_e, determined for the direction corresponding to the governing wall index WI

For the purposes of calculating the wall strength index, the effective fundamental period of the building (in seconds) may be approximated using the following equation:

$$T_e = 0.015h_n^{0.75} \tag{5-3}$$

where h_n is the total height of the building in feet. Alternatively, the effective fundamental period may be determined using Equation 5-19, but shall not be taken less than the value given by Equation 5-3.

5.4.3 Identification of Lower Seismic Risk Buildings using the Wall Strength Index

Some frame-wall or wall systems with regular configurations can be classified as *lower seismic risk buildings* without further evaluation using the wall strength index (*WSI*). The *WSI* can be used to determine the level of seismic risk in buildings satisfying the following conditions: (a) there is no extreme torsional irregularity (as defined in this methodology); (b) there are no significant vertical irregularities (identified by extreme soft-story or weak-story irregularity as defined in ASCE/SEI 7-10 Chapter 12); and (c) there are no discontinuous walls supported on columns or beams (see Section 5.9.2).

If the above conditions are met, a frame-wall or wall structure may be classified as a *lower seismic risk building* without further evaluation if the *WSI* meets one of the following criteria:

- $WSI \geq 0.002$; or
- $WSI \geq 0.0015$ and $V_p/V_n < 0.8$ for columns comprising 50% or more of the gravity load support in the story and in the direction of the governing wall index, *WI*,

where the column shear strength ratio, V_p/V_n, is calculated in accordance with Section 4.4.

5.5 Effective Yield Strength

The effective yield strength of a structure, V_y, is defined as the base-shear strength under static lateral loading, considering expected member strengths in accordance with Chapter 4, calculated along each principal direction of the building. It is permitted to calculate the effective yield strength, V_y, using established principles of mechanics.

The nonlinear static procedure of ASCE/SEI 41-17, with a lateral force distribution in accordance with Equation 5-4, is an acceptable procedure for calculating the effective yield strength. Alternatively, it is permitted to estimate the effective yield strength based on the plastic mechanism base-shear strength, V_{p1}, using the steps outlined in Sections 5.5.1 to 5.5.5. For frame and wall systems, the mechanism procedures of Section 5.5.1 apply. For infilled frame systems, the mechanism procedures of Section 5.5.2 apply, but it is also necessary to evaluate the bare frame using Section 5.5.1. Special conditions are considered in Section 5.5.3 and 5.5.4.

5.5.1 Plastic Mechanism Base-Shear Strength for Frames and Walls

Step 1. Define the building geometry and the distribution of lateral forces as shown in Figure 5-1.

The plastic mechanism base-shear strength, V_{p1}, is calculated under static lateral loading, not including P-delta effects. The plastic mechanism base-

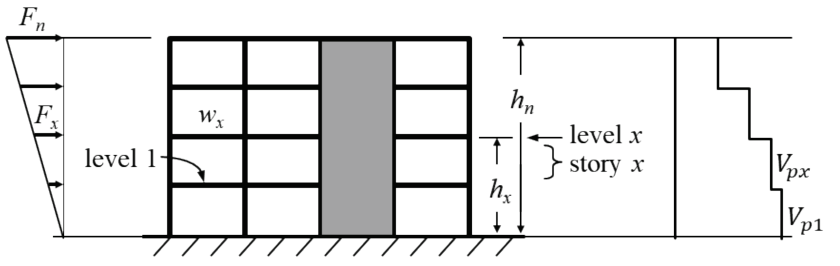

(a) Lateral forces (b) Building elevation (c) Story shears

Figure 5-1 Illustration of terms in Equation 5-4 and Equation 5-5.

shear strength, V_{p1}, is the sum of lateral forces F_x that are concentrated at each floor level x. Values at each floor level are defined by:

$$F_x = C_{vx} V_{p1} \tag{5-4}$$

where V_{p1} is a plastic mechanism base-shear strength (yet to be determined) and C_{vx} is the vertical distribution factor for story forces determined as:

$$C_{vx} = \frac{w_x h_x}{\sum_{i=1}^{n} w_i h_i} \tag{5-5}$$

where:

x = level under consideration, with level 1 designating the first level above the base

w_i and w_x = the portion of the total effective seismic weight of the structure (W) located or assigned to Level i or x

h_i and h_x = the height (ft or m) from the base to Level i or x

n = designation for the uppermost level in the main portion of the building

For the lateral loading defined by Equation 5-4, the story shear in story x (i.e., the story below level x) is related to the story shear in the first story through the following expression:

$$V_{px} = \left(\sum_{i=x}^{n} C_{vi} \right) V_{p1} \tag{5-6}$$

Step 2. Calculate the plastic mechanism base-shear strength, V_{p1}, for Mechanism 1 shown in Figure 5-2.

Mechanism 1 assumes that the building strength is controlled by the strength of structural elements in the first story. It requires calculation of the strengths of the columns and walls in the first story. The lateral strength of an individual column in the first story is the smaller of the column

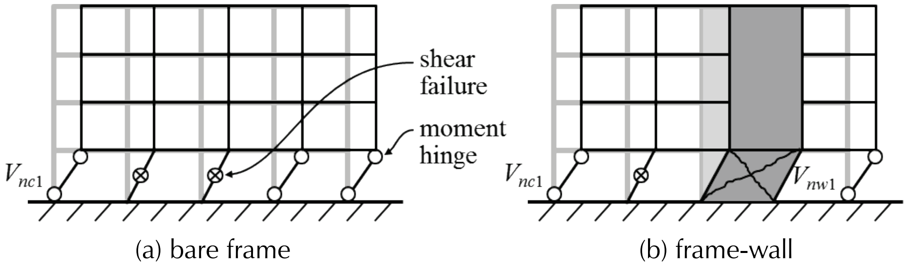

Figure 5-2 Mechanism 1 for calculation of plastic mechanism base-shear strength.

shear strength and the shear associated with development of the column flexural strength, that is:

$$V_{nc1} = \min\,[V_{nc}, \textstyle\sum M_{nc}/l_u] \tag{5-7}$$

where:

V_{nc1} = lateral strength of a column in story 1

V_{nc} = shear strength of a column in story 1, calculated in accordance with Equation 4-3

M_{nc} = flexural strength of a column, where the summation applies to the flexural strengths at the top and bottom of a column, considering the strength of the connection with the foundation where that condition applies

l_u = clear height of column in first story

The shear strength of the walls in the first story, is V_{nw1}, where:

V_{nw1} = shear strength of walls in the first story calculated in accordance with Section 4.3.5, but not exceeding the shear corresponding to development of flexural strengths at the top and bottom of the wall

The plastic mechanism base-shear strength in story 1, V_{p1}, corresponding to Mechanism 1 is:

$$V_{p1} = \textstyle\sum V_{nc1} + \sum V_{nw1} \tag{5-8}$$

where the summation applies to all the columns and walls in the first story.

Step 3. Calculate the plastic mechanism base-shear strength for Mechanism 2 shown in Figure 5-3.

Mechanism 2 assumes that the vertical elements have sufficient strength to force yielding throughout the building height. This mechanism (or mechanisms approaching this mechanism) may occur in frames with walls or in frames having columns much stronger than the beams. Mechanism 2 should be checked in frames with walls (Figure 5-3a) and in pure frames having $\sum M_{nc}/\sum M_{nb} \geq 1.5$ in typical stories within the lower half of the building height (Figure 5-3b).

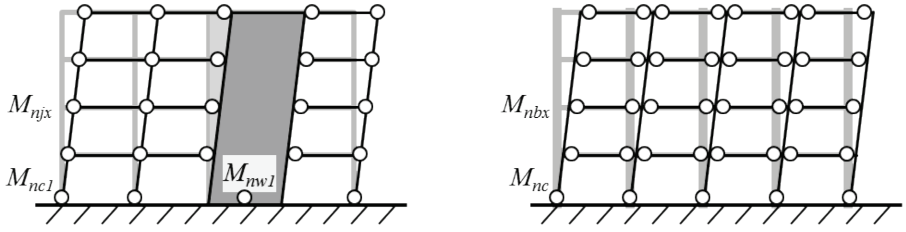

(a) frame-wall building (b) frame building

Figure 5-3 Mechanism 2 for calculation of plastic mechanism base-shear strength.

To determine the base-shear strength according to this mechanism, it is necessary to calculate the framing strengths resolved at column-footing connections, beam-column (and slab-column) connections, and beam-wall (slab-wall) connections, plus moment strengths of the walls in the first story, as follows:

M_{nc1} = flexural strength at the bottom of a column, considering the strength of the connection with the foundation where that condition applies, but not exceeding the moment corresponding to column shear failure

M_{njx} = flexural strength of beam-column, slab-column, beam-wall, and slab-wall connections (joints) at level x

M_{nw1} = flexural strength at the bottom of a wall, considering the strength of the connection with the foundation where that condition applies

At a beam-column connection, M_{njx} is the smallest moment that can be developed at the joint at level x, as limited by the column flexural strength and the beam flexural strength, that is:

$$M_{njx} = \min\left[\sum M_{nc}, \sum M_{nb}\right] \tag{5-9}$$

where:

M_{nc} = flexural strength of columns, summed above and below the beam-column joints at level x, but not exceeding the moments corresponding to column shear failure

M_{nb} = flexural strength of beams, summed on both sides of the beam-column joint in the direction of framing at level x; it is acceptable, but not required, to limit the beam moments to values corresponding to beam shear failure

In a frame building, Mechanism 2 will determine building strength only if the columns generally have strengths that exceed the strengths of the beams by a considerable margin. Therefore, it is acceptable to take $M_{njx} = \Sigma M_{nb}$ in Equation 5-9.

It is possible that the maximum moment that can be developed at a beam-column connection will be limited by the strength of the beam-column joint itself. Therefore, it is acceptable, but not required, to limit the value of M_{njx} to the value given by Equation 5-9, or to the moment corresponding to development of beam-column joint shear strength, whichever is less.

At a slab-column connection, M_{njx} is the smallest moment that can be developed at the joint, as limited by the column flexural strength and the slab-column connection strength, that is:

$$M_{njx} = \min\left[\sum M_{nc}, \sum M_{ns}\right] \tag{5-10}$$

where:

M_{nc} = flexural strength of columns, summed above and below the beam-column joints at level x, but not exceeding column moments corresponding to column shear failure

M_{ns} = moment transfer strength of the slab-column connection at level x

At a beam-wall (or slab-wall) connection, M_{njx} is the moment that can be transferred from the beam (or slab) to the wall. It is acceptable, but not required, to limit the moment that can be generated by a beam to the moment corresponding to development of beam shear strength.

Beam and column flexural strengths are calculated at faces of joints, walls, or footings. For beams and columns framing into joints or walls, it is acceptable to project the moments to the centerline of the joint or wall. This can be accomplished with reasonable accuracy by assuming that the beam (or column) moment is the negative value on one end of the beam (or column) and the positive value on the other end of the beam (or column), and then using a straight-line through these two points to extrapolate values at the centerlines of the joint or wall.

Extrapolation of moments to the centerline of members is important where vertical or horizontal members have relatively large dimensions. Because of the significant impact that large members have on pier-spandrel system response, it is required to extend pier and spandrel strengths to the joint centerlines in pier-spandrel systems, as described above.

In buildings with combinations of beam-column, slab-column, and beam-wall framing, values of M_{njx} are determined at each beam-column, slab-column, and beam-wall joint, and the results are then summed.

The plastic mechanism base-shear strength corresponding to Mechanism 2 is:

$$V_{p1} = \frac{\sum M_{nc1} + \sum M_{njx} + \sum M_{nw1}}{h_{eff}} \tag{5-11}$$

where:

M_{nc1} = flexural strength at the bottom of a column, considering the strength of the connection with the foundation where that condition applies, but not exceeding the moment corresponding to column shear failure

M_{njx} = values of M_{njx} from Equation 5-9 and 5-10, or from connections between beams and walls

M_{nw1} = flexural strength at the bottom of a wall, considering the strength of the connection with the foundation where that condition applies, calculated in accordance with Section 4.3.5

h_{eff} = effective height of the building, defined as the height from the base to the centroid of lateral forces (same as the effective height of an equivalent single-degree-of-freedom system, which may be taken as $0.7h_n$ in multistory buildings having uniform distribution of effective weight over the building height, and h_n in single-story buildings)

Step 4. Calculate the plastic mechanism base-shear strength for Mechanism 3 shown in Figure 5-4.

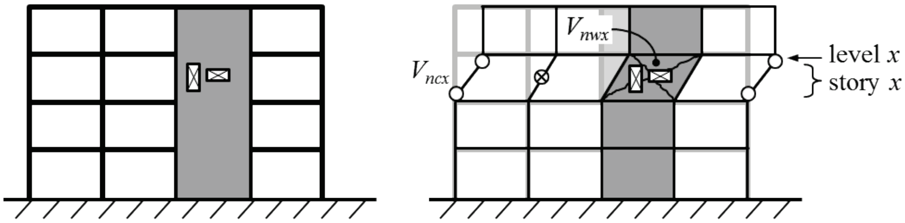

(a) vertically irregular structure

(b) Mechanism 3

Figure 5-4 Mechanism 3 for calculation of plastic mechanism base-shear strength.

Mechanism 3 applies only to buildings with an obvious strength irregularity in which one story or multiple stories have story shear strengths that are significantly reduced relative to adjacent stories. This may occur due to reduction in strength of columns, walls, or both. Mechanism 3 need only be considered where the rate of reduction in story shear strength exceeds the rate of reduction in the story shear demand (Figure 5-1) by more than 20%. Note that Mechanism 3 is similar to Mechanism 1, except the weak story is in the upper stories of a building. Therefore, the steps to determine base-shear strength for Mechanism 1 and Mechanism 3 are similar.

To determine the plastic mechanism base-shear strength corresponding to Mechanism 3, it is necessary to first identify the weak story, and then calculate the strengths of the columns and walls in the weak story. The lateral strength of an individual column in the weak story is the smaller of the column shear strength and the shear associated with development of the column moment strength, that is:

$$V_{ncx} = \min\left[V_{nc}, \sum M_{nc}/l_u\right] \tag{5-12}$$

where:

V_{ncx} = lateral strength of a column in weak story x

V_{nc} = shear strength of a column in weak story x calculated in accordance with Equation 4-3

M_{nc} = flexural strength of a column, where the summation applies to the flexural strengths at the top and bottom of the weak story x

l_u = clear height of the columns in weak story x

The shear strength of the walls in story x, is V_{nwx}, where:

V_{nwx} = shear strength of wall in weak story x calculated in accordance with Section 4.3.5, but not exceeding the shear corresponding to development of wall flexural strengths

The plastic mechanism shear strength at story x corresponding to Mechanism 3 is:

$$V_{px} = \sum V_{ncx} + \sum V_{nwx} \tag{5-13}$$

where the summation applies to all the columns and walls in the weak story x. Given the shear V_{px} at story x, the corresponding plastic mechanism base-shear strength, V_{p1}, is:

$$V_{p1} = \frac{V_{px}}{\sum_{i=x}^{n} C_{vi}} \tag{5-14}$$

where:

V_{p1} = plastic mechanism base shear strength at story 1

V_{px} = plastic mechanism shear strength at story x according to Equation 5-13

Step 5. Calculate the plastic mechanism base-shear strength for Mechanism 4 shown in Figure 5-5.

Similar to Mechanism 3, Mechanism 4 applies only to buildings with an obvious strength irregularity. In this case, the strength irregularity is associated with a significant reduction in the moment strength of columns, walls, or both. Note that Mechanism 4 is similar to Mechanism 2, except that the sidesway mechanism occurs in the upper stories of the building. Therefore, the steps to determine base-shear strength for Mechanism 2 and Mechanism 4 are similar.

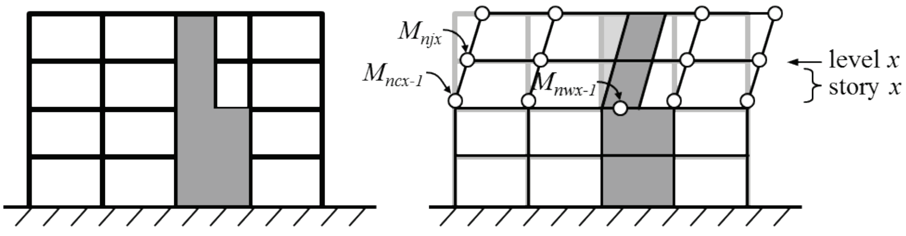

(a) vertically irregular structure (b) Mechanism 4

Figure 5-5 Mechanism 4 for calculation of plastic mechanism base-shear strength.

To determine the plastic mechanism base-shear strength corresponding to Mechanism 4, it is necessary to calculate the framing strengths of columns and walls at the level of the strength irregularity, as well as framing strengths resolved at beam-column (and slab-column), and beam-wall (slab-wall) connections. The procedures are analogous to those for Mechanism 2 and are not repeated here.

The plastic mechanism shear strength at story *x* corresponding to Mechanism 4 is:

$$V_{px} = \frac{\sum M_{ncx-1} + \sum M_{nj} + \sum M_{nwx-1}}{h^{*}_{eff}} \tag{5-15}$$

where:

M_{ncx-1} = flexural strength of a column at level $x - 1$, that is, bottom of story *x*, but not exceeding the moment corresponding to column shear failure

M_{nj} = values of moment that can be resisted at each joint, based on the limiting strength of beams, columns, and joints, similar to Mechanism 2

M_{nwx-1} = flexural strength of wall at level $x - 1$, that is, bottom of story *x*, calculated in accordance with Section 4.3.5

h^*_{eff} = height of centroid of lateral forces acting above level $x - 1$, which is the same as the centroid of the vertical distribution factors C_{vx} from level x to roof n

Given the shear V_{px} at story x, the corresponding plastic mechanism base-shear strength, V_{p1}, is:

$$V_{p1} = \frac{V_{px}}{\sum_{i=x}^{n} C_{vi}} \tag{5-16}$$

where:

V_{p1} = plastic mechanism base shear strength at story 1

V_{px} = plastic mechanism shear strength at story x according to Equation 5-15

Step 6. Calculate the plastic mechanism base-shear strength for the building as the minimum value of V_{p1} for all applicable mechanisms, as given by Equations 5-8, 5-11, 5-14, and 5-16, and use this value as the effective yield strength, V_y.

Variations in lateral force distributions during dynamic loading can result in actual yielding mechanisms that shift from one mechanism to another, so the yielding mechanisms calculated above are uncertain and not absolutely defined. In cases where Mechanism 2 controls for determination of effective yield strength, if the calculated plastic mechanism base-shear strength for Mechanism 2 is equal to or greater than three-quarters (3/4) of the calculated plastic mechanism base-shear strength for Mechanism 1, Mechanism 1 should be taken as the controlling mechanism for the purposes of identifying critical stories and calculating drift demands in Chapters 6 and 7.

5.5.2 Plastic Mechanism Base-Shear Strength for Infilled Frame Systems

The strength of an infilled frame system is a function of the strength of the infilled bays and the strength of other (reinforced concrete) components in the critical story.

Step 1. Define the building geometry and the distribution of lateral forces as shown in Figure 5-1.

Step 2. Identify the controlling mechanism by inspection. Infilled frame systems can be presumed to be controlled by Mechanism 1, unless a significant discontinuity in infill strength or configuration along the height of the building warrants consideration of Mechanism 3.

Step 3. Classify each infill bay in the building into one of four groups using Table 5-1.

Step 4. Calculate strength of all infilled bays with and without openings, in accordance with Section 4.3.6.2.

Step 5. Calculate the plastic mechanism base shear strength of the building.

The effective yield strength of an infilled frame building in each direction of loading can be taken as the sum of contributions from the infilled bays, and all reinforced concrete columns and walls in the balance of the building that are not part of infilled bays:

$$V_{px} = \sum_{i=1}^{n_{inf}} V_{inf} + \beta \sum_{i=1}^{n_c} V_{ncx} + \sum_{i=1}^{n_{wall}} V_{nw,i} \tag{5-17}$$

where:

n_{infx}, n_{infy} = number of infilled bays at the critical story in each orthogonal direction

V_{inf} = shear strength of the infilled bay, with or without openings

β = factor representing the contribution of frame elements to the total strength of an infilled frame system

n_c = number of columns in the critical story that are not adjacent to infill panels in the direction of loading, or are adjacent to infill panels classified as ineffective for calculation of strength in Table 5-1

V_{nc} = shear strength of a column, taken as the smaller of the column shear strength and the shear associated with development of the column flexural strength, as limited by the strength of the beams or slab-column connections

n_w = number of structural walls in the critical story in the direction of loading

V_{nw} = shear strength of a wall, taken as the smaller of the shear strength and the shear associated with development of the wall flexural strength

Calculations are carried out at the first story, which is assumed to be critical unless Mechanism 3 must be evaluated due to a strength or configuration discontinuity in an upper story. If Mechanism 3 controls at an upper story x, the corresponding plastic mechanism base-shear strength, V_{p1}, at the base must be calculated using Equation 5-14.

To determine the factor, β, drift ratios (in percent) at which the peak strength of the infilled bays are reached, Δ_{peak}, are estimated from Table 5-2. The factor, β, varies linearly from 0.4 to 0.9 for Δ_{peak} from 0.15% to 0.4%, and is equal to 0.9 for $\Delta_{peak} > 0.4\%$. In this determination, Δ_{peak} is the minimum of the values computed for all infilled bays at the critical story along each direction (i.e., the drift is determined by the strongest panel).

Table 5-2 Drift at which Infill is Assumed to Reach Peak Lateral Strength, Δ_{peak} (in Percent Drift Ratio)

V_p/V_n of the Weakest Column in the Infilled Bay	Δ_{peak}, Weak Infill	Δ_{peak}, Strong Infill
$V_p/V_n < 1$	$0.6 - 0.23(L_{inf}/h_{inf})$, for $(L_{inf}/h_{inf}) < 1.3$ 0.30, otherwise	$0.82 - (1/3)(L_{inf}/h_{inf})$, for $(L_{inf}/h_{inf}) < 2$ 0.15, otherwise
$V_p/V_n > 1$	0.35	

Step 6. Calculate the plastic mechanism base-shear strength for the building as the minimum value of V_{p1} for all applicable mechanisms, and use this value as the effective yield strength, V_y, for the infilled frame system.

Note that for the purposes of determining the effective fundamental period of the infilled frame system in Section 5.6.1, the plastic mechanism base-shear strength for the bare-frame system must also be determined in accordance with Section 5.5.1, ignoring the presence of the infill.

5.5.3 Plastic Mechanism Base-Shear Strength for Mezzanines and Other Configurations

Mezzanines and other framing configurations may require modifications of the basic procedures outlined in Section 5.5.1. Figure 5-6 illustrates application of Mechanisms 1 and 2 for a frame with a mezzanine.

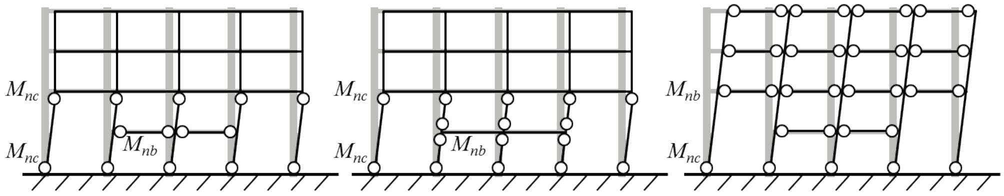

(a) Mechanism 1a (b) Mechanism 1b (c) Mechanism 2

Figure 5-6 Possible mechanisms for calculation of plastic mechanism base-shear strength of frames with mezzanines.

As discussed in Section 5.5.1, mechanisms can be controlled by flexural or shear failures in members. Not all possible mechanisms are shown.

5.5.4 Three-Dimensional Considerations

In general, cast-in-place concrete diaphragms will impose deflection compatibility for all frames aligned in a given direction. Common three-dimensional behaviors are illustrated in Figures 5-7 and 5-8.

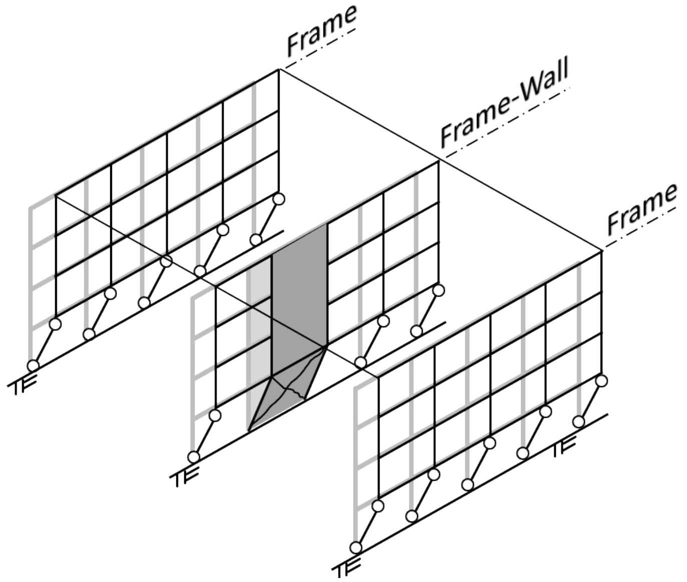

Figure 5-7 Kinematically compatible three-dimensional plastic mechanisms.

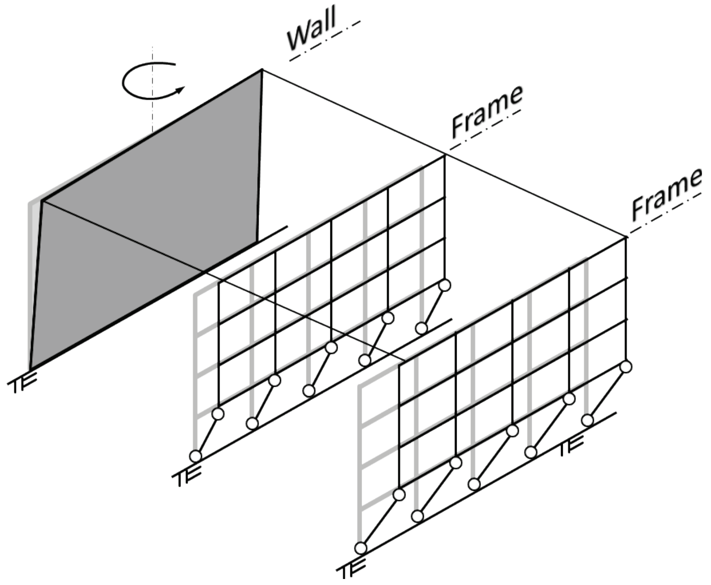

Figure 5-8 Mechanisms in buildings with extreme torsion.

In the absence of torsion, the assumed mechanism (Mechanism 1, 2, 3, or 4) should be imposed on all frame lines simultaneously. Figure 5-7 illustrates Mechanism 1 applied to three frame lines. This is repeated for each assumed mechanism, and the controlling mechanism is the one with the smallest plastic mechanism base-shear strength.

In cases with significant torsion, building response can result in different displacements and different mechanisms in different frames. Figure 5-8 illustrates the common case of a wall along one side of a building that is very strong and stiff, leading to a torsional mechanism in which other frame lines develop mechanisms per their individual strength distributions.

Although base-shear strength of such a building is difficult to define uniquely using the simplified techniques described herein, the methodology enables identification of the critical story mechanisms for individual frames.

5.5.5 Base Shear Ratio

The base shear ratio shall be taken as V_y/W, where V_y is the effective yield strength, and W is the total effective seismic weight of a structure. Values of V_y are calculated in each of two principal horizontal directions of the building.

5.6 Effective Fundamental Period

The effective fundamental periods in each of two principal horizontal directions is used to estimate the pseudo-acceleration spectral demands and spectral displacements in a building. Figure 5-9 illustrates the effective stiffness, K_e, intended for determination of fundamental period in this methodology.

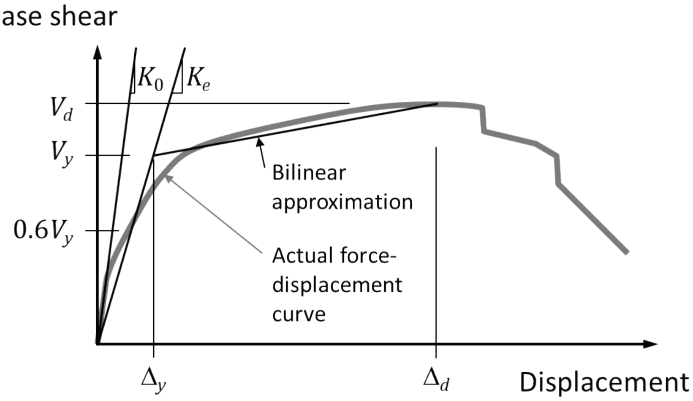

Figure 5-9 Force-displacement curve, showing the definition of effective stiffness, K_e, for calculation of the effective fundamental period (adapted from ASCE/SEI 41-17).

The effective fundamental period in this methodology is conceptually similar to the effective fundamental period defined in the Nonlinear Static Procedure of ASCE/SEI 41-17, which corresponds to an effective initial stiffness that accounts for concrete cracking and failure of more brittle elements prior to overall effective yielding of the structural system.

5.6.1 Determination of Effective Period by Formula

Frame Systems. For frame systems, the effective fundamental period, T_e, may be taken as:

$$T_e = 0.07\left(h_n\right)^{0.5}\left(\frac{V_y}{W}\right)^{-0.5} \tag{5-18}$$

For frame systems with deep spandrel beams, the period obtained by Equation 5-18 may be adjusted by the ratio (l_u/l), where l is the typical floor-to-floor column height and l_u is the typical clear height of the column.

Frame-Wall Systems. For frame-wall systems other than pier-spandrel systems, and for bearing wall systems, T_e may be taken as:

$$T_e = 0.0026\frac{h_n}{\sqrt{C_w}} \leq T_e \text{ from Equation 5-18} \tag{5-19}$$

where:

$$C_w = \frac{100}{A_{base}}\sum_{i=1}^{j}\frac{A_{wi}}{1+0.83\left(\dfrac{h_{wi}}{l_{wi}}\right)^2} \tag{5-20}$$

h_n = height from the base of the building to the highest level of the seismic force-resisting system, ft

A_{base} = area of the base of a structure, ft^2

A_{wi} = area of the web of wall i, ft^2

h_{wi} = height of wall i, ft

l_{wi} = length of wall i, ft

j = number of walls in the building effective in resisting lateral forces in the direction under consideration

Pier-Spandrel Systems. For pier-spandrel systems, T_e may be taken as:

$$T_e = 0.001\,h_n\,l_i^{0.5}\left(\frac{A_{opening}}{A_{we}}\right)^{1.5}\left(\frac{A_{base}}{A_{wp}}\right)^{0.5} \leq T_e \text{ from Equation 5-18} \tag{5-21}$$

where: $0.15 \leq \dfrac{A_{opening}}{A_{we}} \leq 0.5$

and:

l_i = typical or average bay width measured center-to-center of wall piers, ft

$A_{opening}$ = total area of openings in all pier-spandrel walls in direction under consideration, ft^2

A_{we} = total area of pier-spandrel wall, measured in elevation, including openings, in direction under consideration, ft^2

A_{wp} = total area of pier-spandrel wall, measured in plan, including openings, in direction under consideration, ft^2

Infilled Frame Systems. For infilled frame systems, the effective fundamental period, T_e may be taken as:

$$T_e = \left(1.6 - 0.6\frac{V_{p1}}{V_{p1,bare}}\right)T_{e,bare} \tag{5-22}$$

where V_{p1} and $V_{p1,bare}$ are the base shear strengths of the building calculated with infill (Section 5.5.2) and without infill (Section 5.5.1), respectively, and $T_{e,bare}$ is the effective fundamental period of the building without infill based on Equation 5-18 and $V_{p1,bare}$. In Equation 5-22, the ratio $V_{p1}/V_{p1,bare}$ shall not be taken greater than 2.0.

The effective fundamental period for frame-wall or bearing wall systems (Equation 5-19), pier-spandrel systems (Equation 5-21), or infilled frame systems (Equation 5-22) shall not be taken longer than the effective fundamental period for frame systems (Equation 5-20).

5.6.2 Determination of Effective Period by Structural Analysis

The effective fundamental period may also be determined in accordance with the Nonlinear Static Procedure in ASCE/SEI 41-17.

5.7 Global Demand-to-Capacity Ratio

The global demand-to-capacity ratio, $\mu_{strength}$, for a given direction of earthquake loading, is calculated as:

$$\mu_{strength} = \frac{S_a}{V_y / W}C_m \tag{5-23}$$

where S_a is the spectral acceleration at the effective fundamental period, T_e, V_y is the effective yield strength, and C_m is the effective mass factor determined in accordance with ASCE/SEI 41-17, as provided in Table 5-1.

Table 5-3 Values for Effective Mass Factor, C_m

No. of stories	Frame System	Wall or Frame-Wall System	Pier-Spandrel System	Infill Wall System
1-2	1.0	1.0	1.0	1.0
≥ 3	0.9	0.8	0.8	1.0

Note: C_m shall be taken as 1.0 if the fundamental period, T_e, in the direction under consideration is greater than 1.0 sec.

5.8 Identification of Lower Seismic Risk Buildings

Some buildings can be classified as *lower seismic risk buildings* without further evaluation based on the global demand-to-capacity ratio, $\mu_{strength}$.

5.8.1 Essentially Elastic Buildings

Buildings that are exceptionally strong (essentially elastic) can be classified as *lower seismic risk buildings* without further evaluation. A building is considered to be essentially elastic if the global demand-to-capacity ratio, $\mu_{strength}$, meets one of the following criteria in each of the two principal horizontal directions:

- $\mu_{strength} \leq 0.75$ in the case of frame systems with average column shear strength ratio in the critical story of $V_p/V_n > 0.6$; or
- $\mu_{strength} \leq 1.5$ in all other cases.

5.9 Identification of Exceptionally High Seismic Risk Buildings

Some buildings can be classified as *exceptionally high seismic risk buildings* without further evaluation based on the presence of certain seismic deficiencies. Correction of individual seismic deficiencies, however, should not be used as a strategy for changing the level of seismic risk determined using this methodology.

5.9.1 Exceptionally Weak Buildings

Buildings that are exceptionally weak shall be classified as *exceptionally high seismic risk buildings*. A building is considered to be exceptionally weak if the global demand-to-capacity ratio, $\mu_{strength}$, meets one of the following criteria in either of the two principal horizontal directions:

- Frame systems with $\mu_{strength} > 2.0$, and average column shear strength ratio in the critical story of $V_p/V_n > 1.5$; or
- Frame systems with $\mu_{strength} > 5.5$, and average column shear strength ratio in the critical story of $V_p/V_n < 0.6$.

Columns in the stories participating in the mechanism analysis are to be considered in computing the average shear strength ratio. In frame buildings with a combination of shear-controlled and flexure-controlled columns in the critical story, the threshold value of $\mu_{strength}$ for exceptionally weak buildings can be linearly interpolated between the values of 2.0 and 5.5, based on the average value of shear strength ratio, V_p/V_n, in the critical story, ranging from 1.5 to 0.6.

5.9.2 Discontinuous Walls Supported on Columns, Wall Piers, or Girders

Buildings with discontinuous walls supported on columns, wall piers, or girders can be further evaluated using this methodology, or classified as *exceptionally high seismic risk buildings* without further evaluation, based on the criteria in this section.

Conservatism is necessary when using simplified procedures to analyze buildings with discontinuous walls supported on columns, wall piers, or girders. Such conditions can be especially susceptible to effects of vertical acceleration and, in the case of columns, *P-M* interaction that reduces the axial capacity to well below the pure axial compressive strength, which can lead to brittle failures and loss of gravity-load-carrying ability (i.e., local collapse).

Although consideration of discontinuous walls is required in the case of concrete walls, one or more panels of discontinuous masonry infill supported on bare-frame columns may also be a concern. For masonry infill classified as strong in Table 5-1, the overturning moment generated by the discontinuous infill configuration must be estimated, and the adequacy of the supporting columns checked in accordance with Section 5.9.2.1.

5.9.2.1 Vertical Capacity Check on Columns and Wall Piers

Calculate the nominal axial force in columns and wall piers supporting discontinuous walls. In buildings not braced with shear walls in the first story in the direction under consideration, but with discontinuous walls extending above the first story, calculate the plastic base-shear strength for the frame in question for Mechanism 1. Calculate the axial force on columns and wall piers supporting discontinuous walls assuming those columns and wall piers resist the entire overturning moment for Mechanism 1, except that the moment demand need not exceed the expected flexural strength of the wall, or the moment corresponding to development of the wall shear strength, whichever is less.

In buildings braced with shear walls in the first story in the direction under consideration, calculate the axial force on columns and wall piers based on the expected flexural strength of the supported wall, or the moment corresponding to development of the wall shear strength, whichever is less. Alternatively, it is acceptable to calculate building base-shear strength in accordance with Section 5.5, and then calculate the axial force on columns and wall piers supporting discontinuous walls assuming that those columns and wall piers resist the overturning moment for the controlling mechanism in proportion to the relative resistance of the various walls in the structural system. One of the following conditions shall apply:

- Where the calculated axial force is less than the balanced axial force (which may be approximated as $0.3A_gf_{ce}'$), the columns and wall piers can be assumed capable of supporting the axial force, and can be further evaluated in accordance with procedures of Chapter 7. This condition applies regardless of column or wall pier confinement detailing.
- Where a column or wall pier is confined in accordance with ACI 318-14 (or equivalent) requirements for special moment frame columns, the column or wall pier can be assumed capable of supporting axial force up to the nominal axial strength, and the building can be further evaluated in accordance with the procedures of Chapter 7.
- Columns and wall piers not confined in accordance with ACI 318-14 requirements for special moment frame columns, with calculated axial force equal to or exceeding the balanced axial force (which may be approximated as $0.3A_gf_{ce}'$), columns shall be assumed to lose gravity-load-carrying capacity. Where the gravity loads cannot be redistributed to adjacent vertical elements, the building shall be classified as an *exceptionally high seismic risk building*. Where the gravity loads can be redistributed to adjacent vertical elements, the building rating shall be determined in accordance with this methodology, excluding consideration of the supporting columns or wall piers.

In cases were columns or wall piers are determined to be inadequate, it is recommended that the full evaluation methodology be completed to more completely identify the extent of deficiencies in the building that contribute to a *high* or *exceptionally high seismic risk* rating. Non-conforming columns or wall piers can be efficiently retrofitted (e.g., jacketed to achieve confinement equivalent of ACI 318-14 requirements) if these are the only deficiencies causing a *high* or *exceptionally high seismic risk* rating.

5.9.2.2 Girder Vertical Capacity Check

Calculate the moment and shear forces in girders supporting discontinuous walls based on the expected flexural strength of the wall, or the moment corresponding to development of wall shear strength, whichever is less. Where the girder strength exceeds the forces corresponding to the strength of the wall, the girder can be assumed capable of supporting the discontinuous wall. Where the girder strength is less than the forces corresponding to the strength of the wall, the girder shall be assumed to lose gravity-load-carrying ability. Where the gravity loads cannot be redistributed to adjacent vertical elements, the building shall be classified as an *exceptionally high seismic risk* *building*. Where the gravity loads can be redistributed to adjacent vertical elements, the building rating shall be determined in accordance with this methodology, excluding consideration of the girder.

5.10 Pounding

Consideration of pounding applies to frame, frame-wall, and infilled frame systems. Pounding between buildings requires the potential consideration of additional controlling mechanisms and critical stories, which are in addition to results from the mechanism analyses of Section 5.5. If adjacent buildings are separated by at least 1.5% of the height of the shorter building, further consideration of pounding is not required as part of this methodology.

If an adjacent building is separated from the building under consideration by less than 1.5% of the height of the shorter building, the adjacent building shall be considered an *interfering building* and considered in accordance with the requirements of this section.

5.10.1 Shorter Interfering Building

5.10.1.1 Floors Align

If the floors of the shorter interfering building align within the depth of the floor framing of the building under consideration, the story immediately above the roof of the shorter interfering building shall be designated a critical story per Mechanism 3 and evaluated in accordance with the procedures of Chapters 6, 7, and 9.

5.10.1.2 Floors Not Aligned

If the floors of the shorter interfering building do not align in accordance with Section 5.10.1.1, the story at the level of the roof of the shorter interfering building shall be designated a critical story, the exterior columns along the line of potential impact shall be given a rating of $CR = 0.7$, and the building shall be further evaluated in accordance with procedures of Chapters 6, 7, and 9.

5.10.2 Taller Interfering Building

5.10.2.1 Floors Aligned

If the floors of the taller interfering building align within the depth of the floor framing of the building under consideration, further consideration of pounding is not required as part of this methodology.

5.10.2.2 Floors Not Aligned

If the floors of the taller interfering building do not align in accordance with Section 5.10.2.1, the top story of the building under consideration shall be designated a critical story, the exterior columns along the line of potential impact shall be given a rating of $CR = 0.7$, and the building shall be further evaluated in accordance with procedures of Chapters 6, 7, and 9.

Chapter 6

Evaluation Procedure for Frame Systems

The chapter covers the evaluation of buildings classified as frame systems, as defined in Section 5.3.1.

6.1 Introduction

Evaluation of frame systems is focused on comparing drift demands with drift capacities of columns and slab-column connections, and using component demand-to-capacity ratios to define column ratings. Column ratings determine story ratings, which are used in Chapter 10 to determine the building rating.

Section 6.2 defines *critical stories* along each of two horizontal earthquake loading directions based on the results of the mechanism analyses in Section 5.5. Section 6.3 defines *critical components*, which include columns located in critical stories, as well as slab-column connections, corner beam-column connections, and discontinuous columns satisfying certain criteria. Sections 6.4 through 6.6 define the drift demands that are considered for each critical frame component. Section 6.7 defines drift capacities, and a comparison of drift demands to drift capacities in Section 6.8 establishes individual column ratings for critical components.

6.2 Identify Critical Stories

Using the controlling plastic mechanism calculated in Section 5.5 in each of the two principal framing directions, *critical stories* are defined in accordance with the following:

- Where Mechanism 1 or 2 controls the strength along a principal framing direction, the critical story in that direction is the first story above the base. Where Mechanism 2 is calculated to be the controlling mechanism, but the plastic mechanism base-shear strength for Mechanism 2 is three-quarters (3/4) or more of the plastic mechanism base-shear strength for Mechanism 1, Mechanism 1 should be taken as controlling for calculation of story drift demands (because variations in lateral force distributions during dynamic loading have a high probability of producing Mechanism 1 failures in such cases).

- Where Mechanism 3 controls the strength along a principal framing direction, the critical story in that direction is the story in which Mechanism 3 forms.
- Where Mechanism 4 controls the strength along a principal framing direction, the critical story in that direction is the lowest story in which yielding occurs in Mechanism 4.

It is possible for different plastic mechanisms to control along each of the two principal framing directions. In such cases, the critical story in one principal direction may differ from the critical story in the other principal direction.

Critical stories are also defined where adjacent buildings require pounding considerations in accordance with Section 5.10.

6.3 Identify Critical Components

Critical components are those components deemed to be most vulnerable to damage and loss of vertical load-carrying ability. Critical components are evaluated in accordance with the procedures in Sections 6.6 through 6.8.

6.3.1 Critical Columns

Columns in critical stories (defined in Section 6.2) are designated as critical components. Columns in other stories are not designated as critical, except where changes in column geometry or detailing create an increased vulnerability for column failure. In such cases, columns at other levels should also be designated as critical.

6.3.2 Critical Slab-Column Connections

In two-way slabs without beams, slab-column connections at the top of columns in critical stories are designated as critical components where the following condition applies:

- The slab moment transfer strength is less than the sum of column flexural strengths immediately above and below the slab. The slab moment transfer strength is the smaller of strengths calculated considering slab flexural strength and slab shear strength. Column flexural strength need not be taken greater than the moment corresponding to column shear failure.

Additionally, slab-column connections satisfying this condition should be designated as critical components at other levels where unusual conditions create an increased vulnerability for punching shear failure of the connection.

Such conditions typically include levels where there is a decrease in slab thickness, increase in floor loading, or significant change in slab-column connection geometry or detailing.

6.3.3 Critical Beam-Column Corner Connections

In beam-column frames, beam-column corner connections at the top of columns in critical stories are designated as critical components where both conditions (a) and (b) apply:

(a) The beam-column joint lacks transverse reinforcement.

(b) The joint shear strength calculated in accordance with Section 4.3.3 is less than the joint shear generated by the controlling mechanism.

Additionally, beam-column connections satisfying both (a) and (b) should be designated as critical components at other levels where unusual conditions create an increased vulnerability for joint shear failure. Such conditions typically include levels where there is a sudden change in the column dimensions or joint detailing.

6.3.4 Discontinuous Columns

A column is considered discontinuous at a level where there is no supporting column in the story below. A discontinuous column is designated as a critical component where both conditions (a) and (b) apply:

(a) The discontinuous columns supports loads from two or more levels.

(b) The plastic capacity of the column, V_p, calculated in accordance with Section 4.4.1, is controlled by the shear strength of the supporting beam or slab.

6.4 Calculate Global Seismic Drift Demand

Calculate the global seismic drift (displacement) demand for an equivalent single-degree-of-freedom (SDOF) system, δ_{eff}, as:

$$\delta_{eff} = C_1 C_2 S_a \frac{T_e^2}{4\pi^2} g \qquad (6\text{-}1)$$

where:

C_1 = modification factor to relate expected maximum inelastic displacement to displacement calculated for linear elastic response

C_2 = modification factor to represent the effect of pinched hysteresis shape, cyclic stiffness degradation, and strength deterioration on maximum displacement response

T_e = effective fundamental period determined in Section 5.6

S_a = spectral acceleration at period, T_e

g = acceleration of gravity

Calculate coefficient C_1 in accordance with ASCE/SEI 41-17 as:

$$C_1 = 1 + \frac{\mu_{strength} - 1}{aT_e^2} \tag{6-2}$$

where a is a site class factor equal to: 130 for Site Class A or B; 90 for Site Class C; 60 for Site Class D, E, or F; and all other terms are as previously defined. For $T_e < 0.2$ seconds, C_1 need not be taken greater than the value at $T_e = 0.2$ seconds. For $T_e \geq 1$ second, $C_1 = 1.0$.

Calculate coefficient C_2 in accordance with ASCE/SEI 41-17 as:

$$C_2 = 1 + \frac{1}{800}\left(\frac{\mu_{strength} - 1}{T_e}\right)^2 \tag{6-3}$$

where all terms are as previously defined. For $T_e > 0.7$ seconds, $C_2 = 1.0$.

Global seismic drift demands are calculated in each direction of earthquake loading.

6.5 Calculate Story Drift Demand

Calculate story drift demand, δ_x, of story x as:

$$\delta_x = \alpha_x h_{sx}\left(\frac{\delta_{eff}}{h_{eff}}\right) \leq \delta_{eff} \tag{6-4}$$

where:

α_x = coefficient to modify story drifts at story x for building configuration and strength characteristics

h_{sx} = height of story x

δ_{eff} = global drift demand of the equivalent SDOF system (Equation 6-1)

h_{eff} = effective height of the building, defined as the height from the base to the centroid of lateral forces (same as the effective height of an equivalent single-degree-of-freedom system, which may be taken as $0.7h_n$ in multistory buildings having uniform distribution of effective weight over the building height, and h_n in single-story buildings)

h_n = height from the base of the building to the highest level of the seismic force-resisting system

Story drift demands are calculated in each direction of earthquake loading.

Coefficient α modifies story drifts considering number of stories in a building, the yield mechanism, and whether the story is a critical story. Values of coefficient α for frame systems are provided in Table 6-1.

Table 6-1 Values of Coefficient α for Frame Systems

No. of Stories in the Building	Yield Mechanism(2)	Values of α(1)	
		Critical Stories	Other Stories(3)
1	(any)	1.0	(n/a)
2	1, 3	2.0	0.5
	2, 4	1.5	1.0
3-6	1, 3	2.0	$1-0.5\dfrac{x-2}{n-2}$
	2, 4	1.5	1.0
7-8	1, 3	*Linearly interpolate between the values for 6 and 9 stories*	
	2, 4	1.5	1.0
≥ 9	1, 3	2.5	1.5
	2, 4	1.5	1.0

(1) x is the story under consideration; n is the total number of stories.

(2) Where Mechanism 2 is calculated to be the controlling mechanism, but the calculated plastic mechanism base-shear strength for Mechanism 2 is three-quarters (3/4) or more of the calculated plastic mechanism base-shear strength for Mechanism 1, Mechanism 1 should be taken as the controlling mechanism for selection of α values.

(3) Values of α for "Other Stories" are generally not used, except where components in other stories are designated as critical because of increased local vulnerability, as required in Section 6.3.

6.5.1 Adjustment of Story Drift Demand for P-Delta

For frame systems, to account for the P-delta effect of gravity loads acting through lateral displacements, story drift demand, δ_x, calculated using Equation 6-4 shall be increased in accordance with Equation 6-5:

$$\delta_{x1} = \delta_x \left[\frac{1}{1 - \dfrac{W_x \delta_x}{V_{px} h_x}} \right] \tag{6-5}$$

where:

δ_{x1} = story drift demand of story x amplified for P-delta effects

δ_x = story drift demand (Equation 6-4)

W_x = gravity load, approximated as the seismic weight of the stories above level x

V_{px} = plastic mechanism shear strength at story x

h_x = height from the base of a building to level x

6.6 Calculate Drift Demands on Critical Components

6.6.1 *Adjusted Drift Demand on Critical Components*

For each critical component defined in Section 6.3, calculate the adjusted drift demand, Δ_D, as:

$$\Delta_D = A_T \gamma \delta_{x1} \tag{6-6}$$

where:

A_T = torsional amplification factor (Section 6.6.2)

γ = drift factor representing fraction of story drift affecting the critical component (Section 6.6.3)

δ_{x1} = story drift demand amplified for P-delta effects (Section 6.5.1)

6.6.2 *Torsional Amplification Factor*

Because frame systems generally include evenly distributed and proportioned frame elements and foundation conditions, inherent torsion is expected to be low. Therefore, torsion need not be considered in buildings classified as frame systems, and the torsional amplification factor, A_T, is taken as 1.0, except as noted below.

If the building under consideration possesses an unusual structural configuration that results in a torsional irregularity due to plan configuration, changes in foundation fixity, or other condition, column drifts should be amplified for torsion using the torsional amplification factor, A_T, in accordance with Section 7.6.2.

6.6.3 *Drift Factor*

The drift factor, γ, defines the fraction of story drift demand, δ_{x1}, affecting critical components. Values of drift factor, γ, for critical components are defined in the sections that follow.

6.6.3.1 Drift Factor for Columns

The column drift factor, γ, defines the portion of the story drift demand, δ_x, attributable to column deformations. Drift factors for columns are provided in Table 6-2. Values are required in critical stories for each column in each direction of earthquake loading.

In Table 6-2, the drift factor for columns depends on the ratio of the strengths of columns to the strengths of horizontal members framing into the column. This ratio is calculated for the beam-column or slab-column connection at the top of the critical story. For beam-column framing, this is represented by $\sum M_c/\sum M_b$, where $\sum M_c$ is the sum of column strengths above and below the beam-column joint, and $\sum M_b$ is the sum of the strengths of beams framing into the joint in the direction under consideration. For slab-column framing, the slab-column connection strength is substituted for the sum of the strengths of beams.

Table 6-2 Drift Factor, γ, for Columns(1)

Ratio of Column Strengths to Beam Strengths(2) $\sum M_c/\sum M_b$	Column Drift Factor γ
≤ 0.6	0.85
1	0.70
≥ 2.4	0.30

(1) For intermediate values of $\sum M_c/\sum M_b$, the drift factor, γ, may be calculated by linear interpolation or the larger value used directly.

(2) For columns below slab-column connections, substitute slab-column connection strength for the sum of the strengths of beams.

6.6.3.2 Drift Factor for Slab-Column Connections and Beam-Column Corner Connections

For slab-column connections and beam-column corner connections, the drift factor, γ, is taken as 1.0. This applies to slab-column connections of slab-column frames and to beam-column corner connections when the connections are being evaluated as critical components. It does not apply to columns of slab-column or beam-column frames. For columns, the drift factor, γ, is defined in Section 6.6.3.1.

6.7 Calculate Drift Capacity of Critical Components

6.7.1 Drift Capacity of Critical Columns

Calculate the drift capacity of critical columns as:

$$\Delta_c = l_u(\theta_c + 0.01) \quad (6\text{-}7)$$

where:

l_u = clear height of the column

θ_c = column plastic rotation capacity

Calculate column plastic rotation capacity, θ_c, in accordance with Table 6-3 for tied columns and Table 6-4 for spirally reinforced columns. Column plastic rotation capacity, θ_c, is based on the column shear strength ratio,

V_p/V_n, axial load ratio, $P/A_g f'_{ce}$, and shear reinforcement ratio, ρ_t. Except for corner columns, the axial load ratio is based on the gravity load, P_g, determined in accordance with Section 4.2. For corner columns, the axial load ratio is based on the total column axial load, $P = P_g + P_{eq}$, where P is positive in compression, and P_g and P_{eq} are determined in accordance with Section 4.2.

Tables 6-3 and 6-4 are divided between flexure-critical columns and other columns (flexure-shear or shear-critical columns). Flexure-critical columns are columns with $V_p/V_n \leq 0.6$, $\rho_t > 0.002$ and $s/d < 0.5$. Flexure-shear or shear-critical columns are defined as columns not classified as flexure-critical.

Table 6-3 Plastic Rotation Capacities for Tied Columns (1), (2), (3), (4)

Flexure-Critical Columns ($V_p/V_n \leq 0.6$, $\rho_t > 0.002$, and $s/d < 0.5$)	
For $\left(\frac{P}{A_g f'_{ce}}\right) \geq 0.1$	$\theta_c = 11.4\rho_t + 0.034 - \left(\frac{P}{A_g f'_{ce}}\right)(14\rho_t + 0.036) \geq 0.0$
For $\left(\frac{P}{A_g f'_{ce}}\right) < 0.1$	$\theta_c = 10\rho_t + 0.03 \geq 0.0$
Flexure-Shear and Shear-Critical Columns (i.e., Columns not classified as Flexure-Critical Columns)	
For $\left(\frac{P}{A_g f'_{ce}}\right) \leq 0.5$	$\theta_c = \frac{0.5}{5 + \frac{P}{0.8A_g f'_{ce}} \frac{1}{\rho_t} \frac{f'_{ce}}{f_{ye}}} - 0.01 \geq \theta_{c,\min}$ $P/A_g f'_{ce}$ should not be taken smaller than 0.1
θ_c should be reduced linearly for $\left(\frac{P}{A_g f'_{ce}}\right) > 0.5$ from its value at $\left(\frac{P}{A_g f'_{ce}}\right) = 0.5$ to zero at $\left(\frac{P}{A_g f'_{ce}}\right) = 0.7$	
$\theta_{c,\min} = 0.042 - 0.023\left(\frac{P}{A_g f'_{ce}}\right) + 0.63\rho_t - 0.023\left(\frac{V_p}{V_n}\right) \geq 0.0$ $P/A_g f'_{ce}$ should not be taken smaller than 0.1	

(1) ρ_t should not be taken greater than 0.0175 in any case, nor greater than 0.0075 when ties are not adequately anchored in the core.

(2) V_p/V_n should not be taken less than 0.2.

(3) θ_c for flexure-shear and shear-critical columns shall not exceed θ_c for a flexure-critical column with the same condition.

(4) $P = P_g$, except for corner columns where $P = P_g + P_{eq}$.

Table 6-4 Plastic Rotation Capacities for Spiral-Reinforced Columns (1), (2), (3), (4)

Flexure-Critical Columns ($V_p/V_n \le 0.6$, $\rho_t > 0.002$, and $s/d < 0.5$)	
For $\left(\frac{P}{A_g f'_{ce}}\right) \ge 0.1$	$\theta_c = 1.15\left[11.4\rho_t + 0.034 - \left(\frac{P}{A_g f'_{ce}}\right)(14\rho_t + 0.036)\right] \ge 0.0$
For $\left(\frac{P}{A_g f'_{ce}}\right) < 0.1$	$\theta_c = 1.15\left[10\rho_t + 0.03\right] \ge 0.0$
Flexure-Shear and Shear-Critical Columns (i.e., Columns not classified as Flexure-Critical Columns)	
For $\left(\frac{P}{A_g f'_{ce}}\right) \le 0.5$	$\theta_c = \frac{0.65}{5 + \frac{P}{0.8A_g f'_{ce}}\frac{1}{\rho_t}\frac{f'_{ce}}{f_{ye}}} - 0.01 \ge \theta_{c,\min}$ $P/A_g f'_{ce}$ should not be taken smaller than 0.1
θ_c should be reduced linearly for $\left(\frac{P}{A_g f'_{ce}}\right) > 0.5$ from its value at $\left(\frac{P}{A_g f'_{ce}}\right) = 0.5$ to zero at $\left(\frac{P}{A_g f'_{ce}}\right) = 0.7$	
$\theta_{c,min} = 0.06 - 0.06\left(\frac{P}{A_g f'_{ce}}\right) + 1.3\rho_t - 0.037\left(\frac{V_p}{V_n}\right) \ge 0.0$ $P/A_g f'_{ce}$ should not be taken smaller than 0.1	

(1) ρ_t should not be taken greater than 0.0175 in any case, nor greater than 0.0075 when ties are not adequately anchored in the core.

(2) V_p/V_n should not be taken less than 0.2.

(3) θ_c for flexure-shear and shear-critical columns shall not exceed θ_c for a flexure-critical column with the same condition.

(4) $P = P_g$, except for corner columns where $P = P_g + P_{eq}$.

6.7.2 Drift Capacity of Critical Slab-Column Connections

Calculate the drift capacity, Δ_c, of critical slab-column connections based on structural integrity requirements. If the reinforcement at slab-column connections satisfies the structural integrity requirements of ACI 318-14 or Section 4.3.4, the drift capacity is taken as $0.12h_{sx}$. If the structural integrity requirements are not met, the drift capacity is calculated in accordance with Table 6-5.

Table 6-5 Drift Capacity of Critical Slab-Column Connections(1)

Gravity Shear Ratio (2) V_g/V_c	Drift Capacity, Δ_c
≤ 0.1	$0.045h_{sx}$
≥ 0.6	$0.01h_{sx}$

(1) For intermediate values of gravity load, the drift capacity may be calculated using linear interpolation.

(2) The gravity shear ratio is the unfactored gravity shear, V_g, divided by the theoretical punching shear strength, without moment transfer, V_c, determined in accordance with ACI 318-14 Section 22.6.5.2.

The drift capacity in Table 6-5 is calculated for the slab at level *x*, that is, the level at the top of story *x* (see Figure 5-1 for definitions of story *x* and level *x*).

6.7.3 Drift Capacity of Critical Beam-Column Corner Connections

Calculate the drift capacity, Δ_c, of critical beam-column corner connections as:

$$\Delta_c = \left(0.1 - 0.33\frac{P}{A_g f'_{ce}}\right) h_{sx} \qquad (6\text{-}8)$$

where all terms are as previously defined. Story drift capacity, Δ_c, need not be taken less than $0.025h_{sx}$. Note that story drift capacity refers to story *x* while the drift capacity ratio is calculated for the beam-column connection at level *x*, that is, the level at the top of story *x*. See Figure 5-1 for definitions of story *x* and level *x*.

Column axial load, *P*, is calculated considering combined gravity and earthquake loading in both orthogonal directions (*X* and *Y*) as:

$$P = P_g + P_{eq,X} + P_{eq,Y} \qquad (6\text{-}9)$$

where:

P_g = axial load due to gravity, determined in accordance with Equation 4-1

P_{eq} = axial load due to earthquake overturning effects, determined in accordance with Section 4.2.2

6.8 Determine Column Ratings

Determine column ratings, *CR*, for critical columns, slab-column connections and corner beam-column connections, as the ratio of drift demand to drift capacity, Δ_D/Δ_C, in accordance with Table 6-6, for earthquake loading in each direction.

The column rating, *CR*, represents the relative likelihood that an individual column, or the slab that it supports, will lose its ability to support vertical loads under the assumed earthquake loading. Column ratings near 0.0 indicate a low likelihood of failure, while column ratings near 1.0 indicate a high likelihood of failure.

Table 6-6 Column Rating, *CR*

Drift Demand to Drift Capacity Ratio Δ_D/Δ_C	Column Rating *CR*
$\Delta_D/\Delta_C \leq 0.25$	0.0
$0.4 \geq \Delta_D/\Delta_C > 0.25$	0.1
$0.5 \geq \Delta_D/\Delta_C > 0.4$	0.2
$0.7 \geq \Delta_D/\Delta_C > 0.5$	0.3
$0.9 \geq \Delta_D/\Delta_C > 0.7$	0.4
$1.1 \geq \Delta_D/\Delta_C > 0.9$	0.5
$1.4 \geq \Delta_D/\Delta_C > 1.1$	0.6
$1.8 \geq \Delta_D/\Delta_C > 1.4$	0.7
$2.5 \geq \Delta_D/\Delta_C > 1.8$	0.8
$3.0 \geq \Delta_D/\Delta_C > 2.5$	0.9
$\Delta_D/\Delta_C > 3.0$	0.93

In beam-column frames, the column rating is determined for both:

(a) columns designated as critical components in critical stories; and

(b) columns located in the story immediately below beam-column corner connections designated as critical components.

In slab-column frames, the column rating is determined for both:

(a) columns designated as critical components in critical stories; and

(a) columns located in the story immediately below slab-column connections designated as critical components.

Figure 6-1 illustrates possible critical conditions for slab-column frames. It is possible for a column to be critical in both horizontal directions. It is also possible for the column to be critical, and for the supported beam-column corner connection or the slab-column connection to also be critical. In such cases, determine the column rating individually for all applicable conditions in either horizontal direction, and then determine the final column rating as the maximum of the individual ratings.

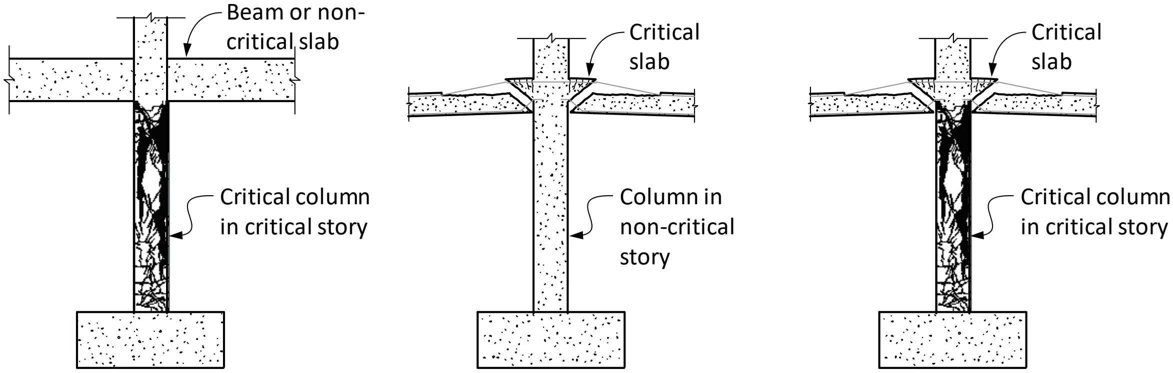
Beam or non-critical slab
Critical column in critical story
Critical slab
Column in non-critical story
Critical slab
Critical column in critical story

(a) Critical column (b) Critical slab-column connection (c) critical column and critical slab-column at same column

Figure 6-1 Illustration of possible critical conditions for a column in a slab-column frame. In (a), the column rating is equal to the rating of the critical column. In (b), the column rating is equal to the rating of the slab-column connection supported by the column. In (c) the column rating is equal to the maximum value of the ratings for the column and for the slab-column connection. A similar situation applies to beam-column corner connections.

6.8.1 Discontinuous Columns

For discontinuous columns, column ratings, *CR*, are determined as follows:

- For critical discontinuous columns supported by a beam or slab that is not a cantilever, $CR = 0.8$.
- For critical discontinuous columns supported by a cantilever beam or slab, if the demand-to-capacity ratio of the cantilever element for V_p in combination with expected vertical loads is greater than 0.7, the discontinuous column shall be assigned a column rating of 0.8, otherwise column ratings shall be determined in accordance with Section 6.8. Expected vertical loads shall be as defined in Section 4.2, considering axial loads due to overturning in addition to gravity loads.

6.9 Determine Story Ratings

The story rating is a number representing the relative likelihood that an individual story will lose its ability to support vertical loads under the assumed earthquake loading. Determine the story rating, *SR*, as:

$$SR = 1.5R_{adj} - 0.1 \tag{6-10}$$

where:

R_{adj} = the adjusted average of column ratings in the story, defined by Equation (6-11)

The story rating, SR, shall not be taken less than 0.1 nor greater than 0.9. Low values of story rating, SR, indicate a low likelihood of failure, while high values indicate a high likelihood of failure.

The adjusted average column in the story, R_{adj}, is defined as:

$$R_{adj} = R_{avg} + 0.625R_{avg}(\mathrm{COV} - 0.4) \qquad (6\text{-}11)$$

where:

$$R_{avg} = \sum_{i=1}^{n_{col}} f_{col,i} CR_i \qquad (6\text{-}12)$$

and:

R_{avg} = the weighted average column rating for all columns in the story, in which the values are weighted by the gravity load taken by each column

$f_{col,i}$ = fraction of gravity loads supported by column i in a story (note: the sum of the fraction of gravity loads supported by all columns must equal 1.0 in each story)

n_{col} = number of columns in a story

COV = the standard deviation of all the column ratings at a story divided by the weighted average column rating, R_{avg}, at that story

In Equations 6-11 and 6-12, R_{adj} shall not be taken less than R_{avg}, nor greater than $1.25R_{avg}$.

In calculating R_{avg}, every column location in a story is assigned a column rating, CR_i, determined by the highest rating for any critical column at that location, or for any supported critical beam-column corner connection or critical slab-column connection at that location, in either horizontal direction. The fraction of the gravity load taken by the column at each location, $f_{col,i}$, is used to weight the calculation of the average, regardless of whether column, slab-column connection, or beam-column connection is critical.

Chapter 7

Evaluation Procedures for Frame-Wall Systems

This chapter covers the evaluation of buildings classified as frame-wall systems, as defined in Section 5.3.2.

7.1 Introduction

The procedures for frame-wall systems parallel the procedures for bare frame systems in Chapter 6. Evaluation of frame-wall systems is focused on comparing drift demands with drift capacities of columns, slab-column connections, walls, and vertical wall segments (or wall piers). Component demand-to-capacity ratios are used to define column, wall, and wall segment ratings. Column and wall ratings are combined to determine story ratings, which are used in Chapter 10 to determine the building rating.

Section 7.2 defines *critical stories* along each of two horizontal earthquake loading directions based on the results of the mechanism analyses of Section 5.5. Section 7.3 defines *critical components*, which include columns located in critical stories, slab-column connections, corner beam-column connections, discontinuous columns satisfying certain criteria, and vertical wall segments. Sections 7.4 through 7.6 define the drift demands that are considered for each critical component. Section 7.7 defines drift capacities, and a comparison of drift demands to drift capacities in Section 7.8 establishes individual column and wall ratings for critical components.

7.2 Identify Critical Stories

Using the controlling plastic mechanism calculated in Section 5.5 in each of the two principal framing directions, *critical stories* are defined in accordance with the following:

- Where Mechanism 1 or 2 controls the strength along a principal framing direction, the critical story in that direction is the first story above the base. Where Mechanism 2 is calculated to be the controlling mechanism, but the plastic mechanism base-shear strength for Mechanism 2 is three-quarters (3/4) or more of the plastic mechanism base-shear strength for Mechanism 1, Mechanism 1 should be taken as controlling for calculation of story drift demands (because variations in lateral force distributions during dynamic loading have a high probability of producing Mechanism 1 failures in such cases).

- Where Mechanism 3 controls the strength along a principal framing direction, the critical story in that direction is the story in which Mechanism 3 forms.
- Where Mechanism 4 controls the strength along a principal framing direction, the critical story in that direction is the lowest story in which yielding occurs in Mechanism 4.

It is possible for different plastic mechanisms to control along each of the two principal framing directions. In such cases, the critical story in one principal direction may differ from the critical story in the other principal direction.

Critical stories are also defined where adjacent buildings require pounding considerations in accordance with Section 5.10.

7.3 Identify Critical Components

Critical components are those components deemed to be most vulnerable to damage and loss of vertical load-carrying ability. Critical components are evaluated in accordance with the procedures in Sections 7.6 through 7.8.

7.3.1 Critical Columns

Columns in critical stories (defined in Section 7.2) and columns below discontinuous walls are designated as critical components. Columns in other stories are not designated as critical, except where changes in column geometry or detailing create an increased vulnerability for column failure. In such cases, columns at other levels should also be designated as critical.

7.3.1.1 Critical Columns Integral with Walls

Treatment of columns that are integral with walls depends on the direction of loading, and the dimension of the column relative to the wall thickness. Columns integral with walls that have an out-of-plane dimension (parallel to the thickness of the wall web) equal to or greater than 1.5 times the thickness of the wall are designated as critical columns in the out-of-plane direction of the wall. In the in-plane direction, the columns are considered part of the wall.

Columns integral with walls that have an out-of-plane dimension less than 1.5 times the thickness of the wall are considered part of the wall in both the in-plane and out-of-plane directions of the wall.

7.3.2 Critical Walls and Vertical Wall Segments

For the purpose of evaluation, critical walls must be separated, where appropriate, into identifiable vertical wall segments. Vertical wall segments can be differentiated when there is a substantial opening (e.g., a door) separating one portion of a wall from another in a given story. Vertical wall segments in critical stories (defined in Section 7.2) are designated as critical components. Vertical wall segments in stories other than critical stories, as well as horizontal wall segments, are not designated as critical.

Critical wall segments are evaluated based on drift demands and axial demands. Seismic overturning forces shall be estimated and added to gravity loads to determine $P/A_g f'_c$ on vertical wall segments with $h_w/l_w \geq 2$ and $l_w/b_w \leq 6$ occurring at the ends of critical walls, where h_w is the clear height, l_w is the horizontal length, and b_w is the thickness of the wall segment. In other cases, tributary gravity loads can be used without seismic overturning forces.

7.3.2.1 Critical Walls with Integral Columns

Critical walls can have integral columns located at one or both ends, or within the length of the wall. Walls with integral columns are evaluated in accordance with Section 7.7.4.1.

Axial demands, $P/A_g f'_{ce}$, on critical walls with integral columns shall be calculated including the loads supported by the columns.

7.3.3 Critical Slab-Column Connections

In two-way slabs without beams, slab-column connections at the top of columns in critical stories are designated as critical components where the following condition applies:

- The slab moment transfer strength is less than the sum of column flexural strengths immediately above and below the slab. The slab moment transfer strength is the smaller of strengths calculated considering slab flexural strength and slab shear strength. Column flexural strength need not be taken greater than the moment corresponding to column shear failure.

Additionally, slab-column connections satisfying this condition should be designated as critical components at other levels where unusual conditions create an increased vulnerability for punching shear failure of the connection. Such conditions typically include levels where there is a decrease in slab thickness, increase in floor loading, or significant change in slab-column connection geometry or detailing.

7.3.4 Critical Beam-Column Corner Connections

In beam-column frames, beam-column corner connections at the top of columns in critical stories are designated as critical components where both conditions (a) and (b) apply:

(a) The beam-column joint lacks transverse reinforcement.

(b) The joint shear strength calculated in accordance with Section 4.3.3 is less than the joint shear generated by the controlling mechanism.

Additionally, beam-column connections satisfying both (a) and (b) should be designated as critical components at other levels where unusual conditions create an increased vulnerability for joint shear failure. Such conditions typically include levels where there is a sudden change in the column dimensions or joint detailing.

7.3.5 Discontinuous Columns

A column is considered discontinuous at a level where there is no supporting column in the story below. A discontinuous column is designated as a critical component where both conditions (a) and (b) apply:

(a) The discontinuous column supports loads from two or more levels.

(b) The plastic capacity of the column, V_p, calculated in accordance with Section 4.4.1, is controlled by the shear strength of the supporting beam or slab.

7.4 Calculate Global Seismic Drift Demand

Calculate the global seismic drift (displacement) demand for an equivalent single-degree-of-freedom (SDOF) system, δ_{eff}, as:

$$\delta_{eff} = C_1 C_2 S_a \frac{T_e^2}{4\pi^2} g \tag{7-1}$$

where:

C_1 = modification factor to relate expected maximum inelastic displacement to displacement calculated for linear elastic response

C_2 = modification factor to represent the effect of pinched hysteresis shape, cyclic stiffness degradation, and strength deterioration on maximum displacement response

T_e = effective fundamental period determined in Section 5.6

S_a = spectral acceleration at period, T_e

g = acceleration of gravity

Calculate coefficient C_1 in accordance with ASCE/SEI 41-17 as:

$$C_1 = 1 + \frac{\mu_{strength} - 1}{aT_e^2} \tag{7-2}$$

where a is a site class factor equal to: 130 for Site Class A or B; 90 for Site Class C; 60 for Site Class D, E, or F; and all other terms are as previously defined. For $T_e < 0.2$ seconds, C_1 need not be taken greater than the value at $T_e = 0.2$ seconds. For $T_e \geq 1$ second, $C_1 = 1.0$.

Calculate coefficient C_2 in accordance with ASCE/SEI 41-17 as:

$$C_2 = 1 + \frac{1}{800}\left(\frac{\mu_{strength} - 1}{T_e}\right)^2 \tag{7-3}$$

where all terms are as previously defined. For $T_e > 0.7$ seconds, $C_2 = 1.0$.

Global seismic drift demands are calculated in each direction of earthquake loading.

7.5 Calculate Story Drift Demand

Calculate story drift demand, δ_x, of story x as:

$$\delta_x = \alpha_x h_{sx}\left(\frac{\delta_{eff}}{h_{eff}}\right) \leq \delta_{eff} \tag{7-4}$$

where:

α_x = coefficient to modify story drifts at story x for building configuration and strength characteristics

h_{sx} = height of story x

δ_{eff} = global displacement demand of the equivalent SDOF system (Equation 7-1)

h_{eff} = effective height of the building, defined as the height from the base to the centroid of lateral forces (same as the effective height of an equivalent single-degree-of-freedom system, which may be taken as $0.7h_n$ in multistory buildings having uniform distribution of effective weight over the building height, and h_n in single-story buildings)

h_n = height from the base of the building to the highest level of the seismic force-resisting system

Story drift demands are calculated in each direction of earthquake loading.

Coefficient α modifies story drifts considering number of stories in a building, the yield mechanism, and whether the story is a critical story. Values of coefficient α for frame-wall systems are provided in Table 7-1.

Table 7-1 Values of Coefficient α for Frame-Wall Systems

No. of Stories in the Building	Yield Mechanism(1)	Values of α		
		Critical Stories	Other Stories(2)	
1	(any)	1.0	(n/a)	
2	1	1.4	0.5	
	2	1.2	1.0	
	3, 4	1.5	1.0	
≥3	1	$0.8h_{\mathit{eff}}/h_{sx}$	0.5	
	2	1.2	1.0	
	3	$0.8h_{\mathit{eff}}/h_{sx}$	0.5	
	4	1.5	*Stories below critical story*	0.5
			Stories above critical story	1.0

(1) Where Mechanism 2 is calculated to be the controlling mechanism, but the calculated plastic mechanism base-shear strength for Mechanism 2 is three-quarters (3/4) or more of the calculated plastic mechanism base-shear strength for Mechanism 1, Mechanism 1 should be taken as the controlling mechanism for selection of α values.

(2) Values of α for "Other Stories" are generally not used, except where components in other stories are designated as critical because of increased local vulnerability, as required in Section 7.3.

7.6 Calculate Drift Demands on Critical Components

7.6.1 Adjusted Drift Demand on Critical Components

For each critical component defined in Section 7.3, calculate the adjusted drift demand, Δ_D, as follows:

$$\Delta_D = A_T \gamma \delta_x \tag{7-5}$$

where:

A_T = torsional amplification factor (Section 7.6.2)

γ = drift factor representing the fraction of story drift affecting the critical component (Section 7.6.3)

δ_x = the story drift demand (Section 7.5)

7.6.2 Torsional Amplification Factor

Determine the torsional amplification, A_T, at the location of each critical component. The torsional amplification, A_T, varies linearly in plan between a value of 1.0 at the center of strength and a value of $A_{T,max}$ at the edge of the building furthest from the center of strength (i.e., the weak or flexible side of the building). For all components located on the strong or stiff side of the building (between the center of strength and the edge of the building closest to the center of strength), $A_T = 1.0$.

7.6.2.1 Calculation of the Maximum Torsional Amplification Factor

The maximum torsional amplification factor, $A_{T,max}$, is calculated in accordance with Equation 7-6, but should not be taken less than 1.0.

$$A_{T,max} = 2.75(TR) + 0.5 \tag{7-6}$$

where TR is the torsional ratio. The maximum torsional amplification factor, $A_{T,max}$, may be taken as 1.0 if the wall index, $WI < 0.0004$, or if the torsional ratio, $TR < 0.25$.

7.6.2.2 Calculation of Torsional Ratio

In Equation 7-6, TR shall be taken as the value of torsional ratio, TR_x, at the critical story, unless there is a significant torsional irregularity in another story. TR_x is the torsional ratio for story x, calculated as:

$$TR_x = \frac{T_{Dx}}{T_{Cx}} \tag{7-7}$$

where T_{Dx} is the torsion demand on story x, and T_{Cx} is the torsion capacity (strength) of story x. Torsion demand, T_{Dx}, is directional, and must be calculated for each direction of earthquake loading:

$$T_{Dx} = V_{px}e \tag{7-8}$$

where:

V_{px} = plastic shear capacity of the critical story, as calculated in Chapter 5

e = eccentricity between the center of mass and the center of strength in the direction perpendicular to the direction of earthquake loading; e may not be taken as less than 5% of L (i.e., $0.05L$), where L is the overall plan dimension perpendicular to the direction of earthquake loading

The coordinates of the center of strength, $(\bar{x}, \bar{y})$, are calculated from:

$$\bar{x} = \frac{\sum_{i=1}^{n_f} x_i V_{pfi}}{\sum_{i=1}^{n_f} V_{pfi}}, \quad \bar{y} = \frac{\sum_{i=1}^{n_f} y_i V_{pfi}}{\sum_{i=1}^{n_f} V_{pfi}} \tag{7-9}$$

where:

x, y = are the orthogonal distances from between the column or wall line of interest and an established reference point

V_{pfi} = is the plastic capacity of frame or wall line i

n_f = is the number of frame or wall lines in story x, considering all frame or wall lines that resist torsion

Torsion capacity, T_C, is calculated considering the capacity of all frame or wall lines in all orientations, and is the same regardless of the direction of loading considered:

$$T_{Cx} = \sum_{i=1}^{n_f} \left|R_{fi}\right| \left|V_{pfi}\right| \tag{7-10}$$

where R_f is the orthogonal distance between frame or wall line i and the center of strength, and all other terms are as previously defined.

7.6.2.3 Identification of Exceptionally High Seismic Risk Buildings based on the Torsional Ratio

Frame-wall systems with extreme torsion shall be classified as *exceptionally high seismic risk buildings* without further evaluation. A building is considered to have extreme torsion if the torsional ratio, $TR > 1.5$.

7.6.3 Drift Factor

The drift factor, γ, defines the fraction of story drift demand, δ_x, affecting critical components. Values of drift factor, γ, for critical components are defined in the sections that follow.

7.6.3.1 Drift Factor for Columns

The column drift factor, γ, defines the portion of the story drift demand, δ_x, attributable to deformations in critical columns. Drift factors for columns are provided in Table 7-2. Values are required in critical stories for each column in each direction of earthquake loading.

In Table 7-2, the drift factor for columns depends on the ratio of the strengths of columns to the strengths of horizontal members framing into the column. This ratio is calculated for each column at the beam-column or slab-column connection at the top of the critical story. For beam-column framing, this is represented by $\sum M_c/\sum M_b$, where $\sum M_c$ is the sum of column strengths above and below the beam-column joint and $\sum M_b$ is the sum of the strengths of beams framing into the joint in the direction under consideration. For slab-column framing, the slab-column connection strength is substituted for the sum of the strengths of beams.

Table 7-2 Drift Factor, γ, for Columns(1)

Ratio of Column Strengths to Beam Strengths(2) $\sum M_c/\sum M_b$	Column Drift Factor γ
≤ 0.6	0.85
1	0.70
≥ 2.4	0.30

(1) For intermediate values of $\sum M_c/\sum M_b$, the drift factor, γ, may be calculated by linear interpolation or the larger value used directly.

(2) For columns below slab-column connections, substitute slab-column connection strength for the sum of the strengths of beams.

7.6.3.2 Drift Factor for Slab-Column Connections and Beam-Column Corner Connections

For slab-column connections and beam-column corner connections, the drift factor, γ, is taken as 1.0. This applies to slab-column connections of slab-column frames and to beam-column corner connections when the connections are being evaluated as critical components. It does not apply to columns of slab-column or beam-column frames. For columns, the drift factor, γ, is defined in Section 7.6.3.1.

7.6.3.3 Drift Factor for Vertical Wall Segments

For critical vertical wall segments, the drift factor, γ, is taken as 1.0.

7.7 Calculate Drift Capacity of Critical Components

Calculate drift capacities of critical columns, slab-column connections, and corner beam-column connections in accordance with this section.

7.7.1 Drift Capacity of Critical Columns

Calculate the drift capacity of critical columns as:

$$\Delta_c = l_u(\theta_c + 0.01) \tag{7-11}$$

where:

l_u = clear height of the column

θ_c = column plastic rotation capacity

Calculate column plastic rotation capacity θ_c in accordance with Table 7-3 for tied columns and Table 7-4 for spiral-reinforced columns. Column plastic rotation capacity, θ_c, is based on the column shear strength ratio, V_p/V_n, axial load ratio, $P/A_g f'_{ce}$, and shear reinforcement ratio, ρ_t. Except for corner columns, the axial load ratio is based on the gravity load, P_g, determined in accordance with Section 4.2. For corner columns, the axial load ratio is based on the total column axial load, $P = P_g + P_{eq}$, where P is positive in compression, and P_g and P_{eq} are determined in accordance with Section 4.2.

Table 7-3 Plastic Rotation Capacities for Tied Columns$^{(1), (2), (3), (4)}$

Flexure-Critical Columns ($V_p/V_n \le 0.6$, $\rho_t > 0.002$, and $s/d < 0.5$)	
For $\left(\frac{P}{A_g f'_{ce}}\right) \ge 0.1$	$\theta_c = 11.4\rho_t + 0.034 - \left(\frac{P}{A_g f'_{ce}}\right)(14\rho_t + 0.036) \ge 0.0$
For $\left(\frac{P}{A_g f'_{ce}}\right) < 0.1$	$\theta_c = 10\rho_t + 0.03 \ge 0.0$
Flexure-Shear and Shear-Critical Columns (i.e., Columns not classified as Flexure-Critical Columns)	
For $\left(\frac{P}{A_g f'_{ce}}\right) \le 0.5$	$\theta_c = \dfrac{0.5}{5 + \dfrac{P}{0.8 A_g f'_{ce}} \dfrac{1}{\rho_t} \dfrac{f'_{ce}}{f_{ye}}} - 0.01 \ge \theta_{c,\min}$ $P / A_g f'_{ce}$ should not be taken smaller than 0.1
θ_c should be reduced linearly for $\left(\frac{P}{A_g f'_{ce}}\right) > 0.5$ from its value at $\left(\frac{P}{A_g f'_{ce}}\right) = 0.5$ to zero at $\left(\frac{P}{A_g f'_{ce}}\right) = 0.7$	
$\theta_{c,\min} = 0.042 - 0.023\left(\frac{P}{A_g f'_{ce}}\right) + 0.63\rho_t - 0.023\left(\frac{V_p}{V_n}\right) \ge 0.0$ $P / A_g f'_{ce}$ should not be taken smaller than 0.1	

(1) ρ_t should not be taken greater than 0.0175 in any case, nor greater than 0.0075 when ties are not adequately anchored in the core.

(2) V_p/V_n should not be taken less than 0.2.

(3) θ_c for flexure-shear and shear-critical columns shall not exceed θ_c for a flexure-critical column with the same condition.

(4) $P = P_g$, except for corner columns where $P = P_g + P_{eq}$.

Tables 7-3 and 7-4 are divided between flexure-critical columns and other columns (flexure-shear or shear-critical columns). Flexure-critical columns are columns with $V_p/V_n \le 0.6$, $\rho_t > 0.002$, and $s/d < 0.5$. Flexure-shear or shear-critical columns are defined as columns not classified as flexure-critical.

Table 7-4 Plastic Rotation Capacities for Spiral-Reinforced Columns(1), (2), (3), (4)

Flexure-Critical Columns ($V_p/V_n \leq 0.6$, $\rho_t > 0.002$, and $s/d < 0.5$)	
For $\left(\frac{P}{A_g f'_{ce}}\right) \geq 0.1$	$\theta_c = 1.15\left[11.4\rho_t + 0.034 - \left(\frac{P}{A_g f'_{ce}}\right)(14\rho_t + 0.036)\right] \geq 0.0$
For $\left(\frac{P}{A_g f'_{ce}}\right) < 0.1$	$\theta_c = 1.15[10\rho_t + 0.03] \geq 0.0$
Flexure-Shear and Shear-Critical Columns (i.e., Columns not classified as Flexure-Critical Columns)	
For $\left(\frac{P}{A_g f'_{ce}}\right) \leq 0.5$	$\theta_c = \dfrac{0.65}{5 + \dfrac{P}{0.8A_g f'_{ce}} \dfrac{1}{\rho_t} \dfrac{f'_{ce}}{f_{ye}}} - 0.01 \geq \theta_{c,\min}$ $P / A_g f'_{ce}$ should not be taken smaller than 0.1
θ_c should be reduced linearly for $\left(\frac{P}{A_g f'_{ce}}\right) > 0.5$ from its value at $\left(\frac{P}{A_g f'_{ce}}\right) = 0.5$ to zero at $\left(\frac{P}{A_g f'_{ce}}\right) = 0.7$	
$\theta_{c,min} = 0.06 - 0.06\left(\frac{P}{A_g f'_{ce}}\right) + 1.3\rho_t - 0.037\left(\frac{V_p}{V_n}\right) \geq 0.0$ $P / A_g f'_{ce}$ should not be taken smaller than 0.1	

(1) ρ_t should not be taken greater than 0.0175 in any case, nor greater than 0.0075 when ties are not adequately anchored in the core.

(2) V_p/V_n should not be taken less than 0.2.

(3) θ_c for flexure-shear and shear-critical columns shall not exceed θ_c for a flexure-critical column with the same condition.

(4) $P = P_g$, except for corner columns where $P = P_g + P_{eq}$.

7.7.2 Drift Capacity of Critical Slab-Column Connections

Calculate the drift capacity, Δ_c, of critical slab-column connections based on structural integrity requirements. If the reinforcement at slab-column connections satisfies the structural integrity requirements of ACI 318-14 or Section 4.3.4, the drift capacity is taken as $0.12h_{sx}$. If the structural integrity requirements are not met, the drift capacity is calculated in accordance with Table 7-5.

Table 7-5 Drift Capacity of Critical Slab-Column Connections(1)

Gravity Shear Ratio (2) V_g/V_c	**Drift Capacity** Δ_c
≤ 0.1	$0.045h_{sx}$
≥ 0.6	$0.01h_{sx}$

(1) For intermediate values of gravity load, the drift capacity may be calculated using linear interpolation.

(2) The gravity shear ratio is the unfactored gravity shear, V_g, divided by the theoretical punching shear strength, without moment transfer, V_c, determined in accordance with ACI 318-14 Section 22.6.5.2.

The drift capacity in Table 7-5 is calculated for the slab at level x, that is, the level at the top of story x (see Figure 5-1 for definitions of story x and level x).

7.7.3 Drift Capacity of Critical Beam-Column Corner Connections

Calculate the drift capacity Δ_c of critical beam-column corner connections as:

$$\Delta_c = \left(0.1 - 0.33\frac{P}{A_g f'_{ce}}\right) h_{sx} \tag{7-12}$$

where all terms are as previously defined. Story drift capacity, Δ_c, need not be taken less than $0.025h_{sx}$. Note that story drift capacity refers to story x while the drift capacity ratio is calculated for the beam-column connection at level x, that is, the level at the top of story x. See Figure 5-1 for definitions of story x and level x.

Column axial load, P, is calculated considering combined gravity and earthquake loading in both orthogonal directions (X and Y) as:

$$P = P_g + P_{eq,X} + P_{eq,Y} \tag{7-13}$$

where:

P_g = axial load due to gravity, determined in accordance with Equation 4-1

P_{eq} = axial load due to earthquake overturning effects, determined in accordance with Section 4.2.2

7.7.4 Drift Capacity of Critical Walls and Vertical Wall Segments

Calculate drift capacity, Δ_c, of critical walls and vertical wall segments in accordance with Table 7-6, for flexure-critical walls, and Table 7-7, for shear-critical walls. If Mechanism 2 or 4 controls, walls and vertical wall segments can be assumed to be flexure-critical. If Mechanism 1 or 3 controls, walls and vertical wall segments are generally shear-critical, except when the calculation of wall shear strength, V_{nwx}, in Chapter 5 is controlled by the shear corresponding to the development of the wall flexural strength.

In Table 7-6, l_w is the horizontal length, b_w is the thickness, and c is the neutral axis depth of the vertical wall segment. The neutral axis depth, c, can be computed from moment curvature analysis or approximated by:

$$\frac{c}{l_w} = \frac{a}{100} + b\frac{P}{A_g f'_{ce}} \tag{7-14}$$

where *a* and *b* are coefficients provided in Table 7-8. If the thickness of the wall varies over the compression zone, a weighted average value of b_w shall be used for wall thickness.

Table 7-6 Drift Capacity of Flexure-Critical Walls or Vertical Wall Segments (%)(1)

l_w/b_w (2)	c/l_w (2)											
	0.05	0.1	0.15	0.2	0.25	0.3	0.35	0.4	0.45	0.5	0.55	0.6
≤6	3.50	3.50	3.50	3.50	3.25	3.00	2.67	2.62	1.85	1.80	1.76	1.71
9	3.50	3.50	3.42	3.28	3.00	2.50	2.20	2.00	1.34	1.24	1.14	1.04
12	3.50	3.35	3.09	2.84	2.59	2.00	1.54	1.32	1.00	0.75	0.75	0.75
15	3.46	3.06	2.67	2.28	1.88	1.75	1.50	1.25	1.00	0.75	0.75	0.75
18	3.28	2.72	2.15	1.75	1.75	1.50	1.25	1.00	0.75	0.75	0.75	0.75
21	3.08	2.31	1.75	1.75	1.50	1.25	1.25	1.00	0.75	0.75	0.75	0.75
24	2.84	1.83	1.75	1.75	1.50	1.25	1.25	1.00	0.75	0.75	0.75	0.75
27	2.57	1.75	1.75	1.75	1.50	1.25	1.25	1.00	0.75	0.75	0.75	0.75
30	2.28	1.75	1.75	1.75	1.50	1.25	1.25	1.00	0.75	0.75	0.75	0.75
>35	1.75	1.75	1.75	1.75	1.50	1.25	1.25	1.00	0.75	0.75	0.75	0.75

(1) For walls with confined boundaries, drift capacity may be increased by 25%.

(2) For intermediate values, drift capacity may be calculated using linear interpolation.

Table 7-7 Drift Capacity of Shear-Critical Walls or Vertical Wall Segments(1)

$P/A_g f'_c$ (2)	Drift Capacity (%)
0.0	4.00
0.005	3.50
0.01	3.00
0.03	2.30
0.05	2.00
0.10	1.50
0.15	1.25
0.20	1.00
0.30	0.75
0.40	0.60
0.50	0.45

(1) For walls with confined boundaries, drift capacity may be increased by 50%.

(2) For intermediate values, drift capacity may be calculated using linear interpolation.

Except for vertical wall segments occurring at the ends of critical walls, as identified in Section 7.3.2, the axial load is based on the gravity load, P_g, determined in accordance with Section 4.2. For vertical wall segments at the ends of critical walls, the axial load is based on the total axial load, $P = P_g + P_{eq}$, where P is positive in compression, and P_g and P_{eq} are determined in accordance with Section 4.2.

Table 7-8 Coefficients for Calculation of Neutral Axis Depth, *c*

Cross-Section	*a*	*b*
Rectangular	10	1.2
I-shaped and Barbell	3	1.4
T-shaped, L-shaped and Half-Barbell (web in compression)	30	0.7
T-shaped, L-shaped and Half-Barbell (web in tension)	20	2.0

For walls with asymmetric cross-sections (e.g., T-shaped, L-shaped, and half-barbell configurations), the drift capacity should be evaluated in both directions of loading (i.e., flange in compression and flange in tension), and the larger value used to determine the drift capacity of the wall.

Alternatively, drift capacity (in percent) may be determined by calculation, using Equation 7-15 for flexure-critical walls and Equation 7-16 for shear-critical walls:

$$\Delta_c(\%) = 3.85 - \frac{l_w c}{30 b_w^2} - 3.5\frac{P}{A_g f'_{ce}} \geq 0.75 \qquad (7\text{-}15)$$

where $l_w c/b_w^2$ should not be taken greater than 60, and

$$\begin{aligned} \Delta_c(\%) &= 2.50 - 10\frac{P}{A_g f'_{ce}} \quad \text{for} \quad \frac{P}{A_g f'_{ce}} \leq 0.1 \\ \Delta_c(\%) &= 1.75 - 2.6\frac{P}{A_g f'_{ce}} \quad \text{for} \quad \frac{P}{A_g f'_{ce}} > 0.1 \end{aligned} \qquad (7\text{-}16)$$

7.7.4.1 Walls with Integral Columns or Boundary Elements

Where the ends of walls and vertical wall segments are confined by spirally reinforced columns or confined boundaries as defined in Table 7-9, the drift capacity may be increased by 25% for flexure-critical walls and by 50% for shear-critical walls.

Where integral concrete columns are located within the length of a wall or vertical wall segment, the drift capacity shall be determined as follows:

- For walls that are not more than 15 feet in length, with an axial load ratio of 0.30 or less, with an integral concrete column conforming to the confinement requirements in Table 7-9, located within the middle third of the wall length, the drift capacity may be taken as 4%.

- For other cases of walls with integral concrete columns, the drift capacity may be taken as the larger of:
    - the drift capacity determined for the wall or vertical wall segment, excluding consideration of the integral concrete column; or
    - the drift capacity determined for a segment of wall on either side of the column, treated as a half-barbell section, with the column assumed to be located at the compression end of the segment.

Table 7-9 Minimum Transverse Reinforcement in Integral Columns or Boundary Elements Required to be Classified as Confined

Transverse Reinforcement	Applicable Expression
$\frac{A_{sh}}{sb_c}$ for rectilinear hoops[1]	Greater of: $0.2\left(\frac{A_g}{A_{ch}}-1\right)\frac{f'_c}{f_{yt}}$ and $0.06\frac{f'_c}{f_{yt}}$
ρ_s for spiral or circular hoops	Greater of: $0.3\left(\frac{A_g}{A_{ch}}-1\right)\frac{f'_c}{f_{yt}}$ and $0.08\frac{f'_c}{f_{yt}}$

(1) To be considered for purposes of confinement, transverse reinforcement must have 135 degree hooks and spacing of no more than 8 inches.

7.8 Determine Column and Wall Ratings

Determine column ratings, *CR*, for critical columns, slab-column connections and corner beam-column connections, and determine wall ratings, *WR*, for critical walls and vertical wall segments, as the ratio of drift demand to drift capacity, Δ_D/Δ_C, in accordance with Table 7-10, for earthquake loading in each direction.

Column and wall ratings represents the relative likelihood that an individual column, supported slab, or wall will lose its ability to support vertical loads under the assumed earthquake loading. Ratings near 0.0 indicate a low likelihood of failure, while ratings near 1.0 indicate a high likelihood of failure.

In beam-column frames, the column rating is determined for both:

(a) columns designated as critical components in critical stories; and

(b) columns located in the story immediately below beam-column corner connections designated as critical components.

In slab-column frames, the column rating is determined for both:

(a) columns designated as critical components in critical stories; and

(b) columns located in the story immediately below slab-column connections designated as critical components.

Table 7-10 Column Rating, *CR*, and Wall Rating, *WR*

Drift Demand to Drift Capacity Ratio Δ_D/Δ_C	Column Rating, *CR* Wall Rating, *WR*
$\Delta_D/\Delta_C \leq 0.25$	0.0
$0.4 \geq \Delta_D/\Delta_C > 0.25$	0.1
$0.5 \geq \Delta_D/\Delta_C > 0.4$	0.2
$0.7 \geq \Delta_D/\Delta_C > 0.5$	0.3
$0.9 \geq \Delta_D/\Delta_C > 0.7$	0.4
$1.1 \geq \Delta_D/\Delta_C > 0.9$	0.5
$1.4 \geq \Delta_D/\Delta_C > 1.1$	0.6
$1.8 \geq \Delta_D/\Delta_C > 1.4$	0.7
$2.5 \geq \Delta_D/\Delta_C > 1.8$	0.8
$3.0 \geq \Delta_D/\Delta_C > 2.5$	0.9
$\Delta_D/\Delta_C > 3.0$	0.93

Figure 7-1 illustrates possible critical conditions for slab-column frames. It is possible for a column to be critical in both horizontal directions. It is also possible for the column to be critical, and for the supported beam-column corner connection or the slab-column connection to also be critical.

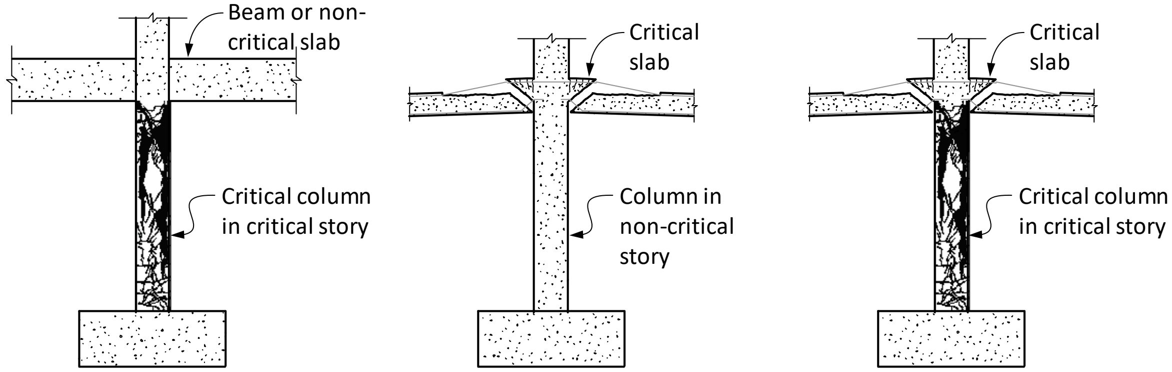
Beam or non-critical slab
Critical column in critical story
Critical slab
Column in non-critical story
Critical slab
Critical column in critical story

(a) Critical column (b) Critical slab-column connection (c) Critical column and critical slab-column at same column

Figure 7-1 Illustration of possible critical conditions for a column in a slab-column frame. In (a), the column rating is equal to the rating of the critical column. In (b), the column rating is equal to the rating of the slab-column connection supported by the column. In (c) the column rating is equal to the maximum value of the ratings for the column and for the slab-column connection. A similar situation applies to beam-column corner connections.

In such cases, determine the column rating individually for all applicable conditions in either horizontal direction, and then determine the final column rating as the maximum of the individual ratings.

7.8.1 Discontinuous Columns

For discontinuous columns, column ratings, CR, are determined as follows:

- For critical discontinuous columns supported by a beam or slab that is not a cantilever, $CR = 0.8$.
- For critical discontinuous columns supported by a cantilever beam or slab, if the demand-to-capacity ratio of the cantilever element for V_p in combination with expected vertical loads is greater than 0.7, the discontinuous column shall be assigned a column rating of 0.8, otherwise column ratings shall be determined in accordance with Section 7.8. Expected vertical loads shall be as defined in Section 4.2, considering axial loads due to overturning in addition to gravity loads.

7.9 Determine Story Ratings

The story rating is a number representing the relative likelihood that an individual story will lose its ability to support vertical loads under the assumed earthquake loading. Determine the story rating, SR, as:

$$SR = 1.5R_{adj} - 0.1 \qquad (7\text{-}17)$$

where:

R_{adj} = the adjusted average of column and wall ratings in the story, defined by Equation (7-18)

The story rating, SR, shall not be taken less than 0.1 nor greater than 0.9. Low values of story rating, SR, indicate a low likelihood of failure, while high values indicate a high likelihood of failure.

The adjusted average of column and wall ratings in the story, R_{adj}, is defined as:

$$R_{adj} = R_{avg} + 0.625R_{avg}(\mathrm{COV} - 0.4) \qquad (7\text{-}18)$$

where:

$$R_{avg} = \sum_{i=1}^{n_{col}} f_{col,i} CR_i + \sum_{j=1}^{n_{wall}} f_{wall,j} WR_j \qquad (7\text{-}19)$$

and:

R_{avg} = the weighted average rating for all columns, walls, and vertical wall segments in the story, in which the values are weighted by the gravity load taken by each column, wall, or wall segment

$f_{col,j}$ = fraction of gravity loads supported by column i

$f_{wall,j}$ = fraction of gravity loads in a story supported by wall j (note: the sum of the fraction of gravity loads supported by all columns and walls must equal 1.0 in each story)

n_{col} = number of columns in a story

n_{wall} = number of walls in a story

COV = the standard deviation of all the column and wall ratings at a story divided by the weighted average rating, R_{avg}, at that story

In Equations 7-18 and 7-19, R_{adj} shall not be taken less than R_{avg}, nor greater than $1.25R_{avg}$.

In calculating R_{avg}, every column location in a story is assigned a column rating, CR_i, and each wall and vertical wall segment in a story is assigned a wall rating, WR_j, determined by the highest rating for any critical column or wall element at that location, or for any supported critical beam-column corner connection or critical slab-column connection at that location, in either horizontal direction. The fraction of the gravity load taken by the column, $f_{col,i}$, or wall, $f_{wall,j}$, at each location is used to weight the calculation of the average.

Chapter 8

Evaluation Procedures for Bearing Wall Systems

This chapter covers the evaluation of buildings classified as bearing wall systems, as defined in Section 5.3.3.

8.1 Introduction

The procedures for bearing wall systems parallel the procedures for frame-wall systems in Chapter 7. Evaluation of bearing wall systems is focused on comparing drift demands with drift capacities of walls and vertical wall segments (or wall piers). Wall drift capacities are a function of the wall geometry, axial load ratio, and whether the wall is estimated to be flexure-critical or shear-critical. The evaluation also considers drift demands and capacities for isolated columns and slab-column connections present in bearing wall buildings. Although columns are considered in the evaluation, column performance is not expected to control global collapse, and columns that, together, support less than 10% of the gravity load in a story need not be explicitly considered in the evaluation. Wall ratings are combined with column ratings (if applicable) to determine story ratings, which are used in Chapter 10 to determine the building rating.

Section 8.2 defines *critical stories* along each of two horizontal earthquake loading directions based on the results of the mechanism analyses of Section 5.5. Section 8.3 defines *critical components*, which are vertical wall segments and columns supporting significant gravity loads. Sections 8.4 through 8.6 define the drift demands that are considered for each wall. Section 8.7 defines drift capacities, and a comparison of wall drift demands to drift capacities in Section 8.8 establishes individual wall ratings.

8.2 Identify Critical Stories

Using the controlling plastic mechanism along each of the two principal framing directions determined in Section 5.5, *critical stories* are defined in accordance with the following:

- Where Mechanism 1 or 2 controls strength along a principal framing direction, the critical story in that direction is the first story above the base. Where Mechanism 2 is calculated to be the controlling mechanism, but the plastic mechanism base-shear strength for Mechanism 2 is three-quarters (3/4) or more of the plastic mechanism base-shear strength for Mechanism 1, Mechanism 1 should be taken as controlling for calculation of story drift demands (because variations in lateral force distributions during dynamic loading have a high probability of producing Mechanism 1 failures in such cases).

- Where Mechanism 3 controls strength along a principal framing direction, the critical story in that direction is the story where Mechanism 3 forms.
- Where Mechanism 4 controls strength along a principal framing direction, the critical story in that direction is the lowest story where yielding occurs in Mechanism 4.

It is possible for different controlling plastic mechanisms to occur along each of the two principal framing directions. In such cases, the critical story for loading in one principal direction may differ from the critical story for loading in the other principal direction.

8.3 Identify Critical Components

Critical components are those components deemed to be most vulnerable to damage and loss of vertical load-carrying ability, eventually contributing to collapse. Critical components are evaluated in accordance with procedures in Section 8.7.

8.3.1 Critical Walls and Vertical Wall Segments

For the purposes of evaluation, critical walls must be separated, where appropriate, into identifiable vertical wall segments. Vertical wall segments can be differentiated when there is a substantial opening (e.g., a door) separating one portion of a wall from another in a given story. Vertical wall segments in critical stories of bearing wall buildings (defined in Section 8.2) are designated as critical components. Vertical wall segments in stories other than critical stories, as well as horizontal wall segments, are not designated as critical.

Critical wall segments are evaluated based on drift demands and axial demands. Seismic overturning forces shall be estimated and added to gravity loads to determine $P/A_g f_c'$ on vertical wall segments with $h_w/l_w \geq 2$ and $l_w/b_w \leq 6$ occurring at the ends of critical walls, where h_w is the clear height, l_w is the horizontal length, and b_w is the thickness of the wall segment. In other cases, tributary gravity loads can be used.

8.3.2 Other Critical Components

Columns in critical stories (defined in Section 8.2) and columns below discontinuous walls are designated as critical components. Where they occur, columns in other stories, columns integral with walls, slab-column connections, beam-column corner connections, and discontinuous columns and walls are identified as critical in accordance with Section 7.3.

8.4 Calculate Global Seismic Drift Demand

Calculate the global seismic drift (displacement) demand for an equivalent single-degree-of-freedom (SDOF) system, δ_{eff}, as:

$$\delta_{eff} = C_1 C_2 S_a \frac{T_e^2}{4\pi^2} g \tag{8-1}$$

where:

C_1 = modification factor to relate expected maximum inelastic displacement to displacement calculated for linear elastic response

C_2 = modification factor to represent the effect of pinched hysteresis shape, cyclic stiffness degradation, and strength deterioration on maximum displacement response

T_e = effective fundamental period determined in Section 5.6

S_a = spectral acceleration at period, T_e

g = acceleration of gravity

Calculate coefficient C_1 in accordance with ASCE/SEI 41-17 as:

$$C_1 = 1 + \frac{\mu_{strength} - 1}{a T_e^2} \tag{8-2}$$

where a is a site class factor equal to: 130 for Site Class A or B; 90 for Site Class C; 60 for Site Class D, E, or F; and all other terms are as previously defined. For $T_e < 0.2$ seconds, C_1 need not be taken greater than the value at $T_e = 0.2$ seconds. For $T_e \geq 1$ second, $C_1 = 1.0$.

Calculate coefficient C_2 in accordance with ASCE/SEI 41-17 as:

$$C_2 = 1 + \frac{1}{800}\left(\frac{\mu_{strength} - 1}{T_e}\right)^2 \tag{8-3}$$

where all terms are as previously defined. For $T_e > 0.7$ seconds, $C_2 = 1.0$.

Global seismic drift demands are calculated in each direction of earthquake loading.

8.5 Calculate Story Drift Demand

Calculate story drift demand, δ_x, of story x as:

$$\delta_x = \alpha_x h_{sx}\left(\frac{\delta_{eff}}{h_{eff}}\right) \le \delta_{eff} \tag{8-4}$$

where:

α_x = coefficient to modify story drifts at story x for building configuration and strength characteristics (Table 8-1)

h_{sx} = height of story x

δ_{eff} = global displacement demand of the equivalent SDOF system (Equation 8-1)

h_{eff} = effective height of the building, defined as the height from the base to the centroid of lateral forces (may be taken as $0.7h_n$ in multistory buildings having uniform distribution of effective weight over the building height and h_n in single-story buildings)

h_n = height from the base of the building to the highest level of the seismic force-resisting system

Table 8-1 Values of Coefficient α for Bearing Wall Systems

<table>
<tr><th rowspan="2">No. of Stories in the Building</th><th rowspan="2">Yield Mechanism[1]</th><th colspan="3">Values of α</th></tr>
<tr><th>Critical Stories</th><th colspan="2">Other Stories[2]</th></tr>
<tr><td>1</td><td>(any)</td><td>1.0</td><td colspan="2">(n/a)</td></tr>
<tr><td rowspan="3">2</td><td>1</td><td>1.4</td><td colspan="2">0.5</td></tr>
<tr><td>2</td><td>1.2</td><td colspan="2">1.0</td></tr>
<tr><td>3, 4</td><td>1.5</td><td colspan="2">1.0</td></tr>
<tr><td rowspan="5">≥3</td><td>1</td><td>$0.8h_{eff}/h_{sx}$</td><td colspan="2">0.5</td></tr>
<tr><td>2</td><td>1.2</td><td colspan="2">1.0</td></tr>
<tr><td>3</td><td>$0.8h_{eff}/h_{sx}$</td><td colspan="2">0.5</td></tr>
<tr><td rowspan="2">4</td><td rowspan="2">1.5</td><td>Stories below critical story</td><td>0.5</td></tr>
<tr><td>Stories above critical story</td><td>1.0</td></tr>
</table>

[1] Where Mechanism 2 is calculated to be the controlling mechanism, but the calculated plastic mechanism base-shear strength for Mechanism 2 is three-quarters (3/4) or more of the calculated plastic mechanism base-shear strength for Mechanism 1, Mechanism 1 should be taken as the controlling mechanism for selection of α values.

[2] Values of α for "Other Stories" are generally not used, except where components in other stories are designated as critical because of increased local vulnerability, as required in Section 8.3.

Coefficient α modifies story drifts considering number of stories in a building, the yield mechanism, and whether the story is a critical story. Table 8-1 provides values of coefficient α for bearing wall systems.

Story drift demands are calculated in each direction of earthquake loading.

8.6 Calculate Drift Demands on Critical Components

8.6.1 Adjusted Drift Demand on Critical Components

For each critical component defined in Section 8.3, calculate the adjusted drift demand, Δ_D, as:

$$\Delta_D = A_T \gamma \delta_x \tag{8-5}$$

where:

A_T = torsional amplification factor

γ = drift factor representing fraction of story drift affecting the critical component

δ_x = the story drift demand (Section 8.5)

8.6.2 Torsional Amplification Factor

Inherent torsion is expected to be low in bearing wall systems because such systems generally include well-distributed wall elements and relatively uniform foundation conditions. Therefore, torsion need not be considered in buildings classified as bearing wall systems, and the torsional amplification factor, A_T, is taken as 1.0, except as noted below.

If the building under consideration possesses an unusual structural configuration that results in a torsional irregularity due to plan configuration, changes in foundation fixity, or other condition, column drifts should be amplified for torsion using the torsional amplification factor, A_T, in accordance with Section 7.6.2.

8.6.3 Drift Factor

The drift factor, γ, defines the fraction of story drift demand, δ_x, affecting critical components. The drift factor, γ, for critical walls and vertical wall segments is taken as 1.0.

If columns and other related components (e.g., slab-column connections, beam-column connections, and discontinuous columns) are designated as critical, drift factors shall be determined in accordance with Section 7.6.3.

8.7 Calculate Drift Capacity of Critical Components

8.7.1 Drift Capacity of Critical Walls and Vertical Wall Segments

Calculate drift capacity, Δ_c, of critical walls and vertical wall segments in accordance with Table 8-2, for flexure-critical walls, and Table 8-3, for shear-critical walls. If Mechanism 2 or 4 controls, walls and vertical wall segments can be assumed to be flexure-critical. If Mechanism 1 or 3 controls, walls and vertical wall segments are generally shear-critical, except when the calculation of wall shear strength, V_{nwx}, in Chapter 5 is controlled by the shear corresponding to the development of the wall flexural strength.

Table 8-2 Drift Capacity of Flexure-Critical Walls or Vertical Wall Segments (%)(1)

	c/l_w(2)											
l_w/b_w(2)	0.05	0.1	0.15	0.2	0.25	0.3	0.35	0.4	0.45	0.5	0.55	0.6
≤6	3.50	3.50	3.50	3.50	3.25	3.00	2.67	2.62	1.85	1.80	1.76	1.71
9	3.50	3.50	3.42	3.28	3.00	2.50	2.20	2.00	1.34	1.24	1.14	1.04
12	3.50	3.35	3.09	2.84	2.59	2.00	1.54	1.32	1.00	0.75	0.75	0.75
15	3.46	3.06	2.67	2.28	1.88	1.75	1.50	1.25	1.00	0.75	0.75	0.75
18	3.28	2.72	2.15	1.75	1.75	1.50	1.25	1.00	0.75	0.75	0.75	0.75
21	3.08	2.31	1.75	1.75	1.50	1.25	1.25	1.00	0.75	0.75	0.75	0.75
24	2.84	1.83	1.75	1.75	1.50	1.25	1.25	1.00	0.75	0.75	0.75	0.75
27	2.57	1.75	1.75	1.75	1.50	1.25	1.25	1.00	0.75	0.75	0.75	0.75
30	2.28	1.75	1.75	1.75	1.50	1.25	1.25	1.00	0.75	0.75	0.75	0.75
>35	1.75	1.75	1.75	1.75	1.50	1.25	1.25	1.00	0.75	0.75	0.75	0.75

(1) For walls with confined boundaries, drift capacity may be increased by 25%.

(2) For intermediate values, drift capacity may be calculated using linear interpolation.

In Table 8-2, l_w is the horizontal length, b_w is the thickness, and c is the neutral axis depth of the vertical wall segment. The neutral axis depth, c, can be computed from moment curvature analysis or approximated by:

$$\frac{c}{l_w} = \frac{a}{100} + b\frac{P}{A_g f'_{ce}} \qquad (8\text{-}6)$$

where a and b are coefficients provided in Table 8-4. If the thickness of the wall varies over the compression zone an average value of b_w shall be used.

Except for vertical wall segments occurring at the ends of critical walls, as identified in Section 8.3.2, the axial load is based on the gravity load, P_g, determined in accordance with Section 4.2. For vertical wall segments at the ends of critical walls, the axial load is based on the total axial load, $P = P_g +$

P_{eq}, where P is positive in compression, and P_g and P_{eq} are determined in accordance with Section 4.2.

Table 8-3 Drift Capacity of Shear-Critical Walls or Vertical Wall Segments[1]

$P/A_g f'_c$ [2]	Drift Capacity (%)
0.0	4.00
0.005	3.50
0.01	3.00
0.03	2.30
0.05	2.00
0.10	1.50
0.15	1.25
0.20	1.00
0.30	0.75
0.40	0.60
0.50	0.45

[1] For walls with confined boundaries, drift capacity may be increased by 50%.

[2] For intermediate values, drift capacity may be calculated using linear interpolation.

Table 8-4 Coefficients for Calculation of Neutral Axis Depth, *c*

Cross-Section	*a*	*b*
Rectangular	10	1.2
I-shaped and Barbell	3	1.4
T-shaped, L-shaped and Half-Barbell (web in compression)	30	0.7
T-shaped, L-shaped and Half-Barbell (web in tension)	20	2.0

For walls with asymmetric cross-sections (e.g., T-shaped, L-shaped, and half-barbell configurations), the drift capacity should be evaluated in both directions of loading (i.e., flange in compression and flange in tension), and the larger value used to determine the drift capacity of the wall.

Alternatively, drift capacity (in percent) may be determined by calculation, using Equation 8-7 for flexure-critical walls and Equation 8-8 for shear-critical walls:

$$\Delta_c(\%) = 3.85 - \frac{l_w c}{30 b_w^2} - 3.5\frac{P}{A_g f'_c} \geq 0.75 \qquad (8\text{-}7)$$

where $l_w c/b_w^2$ should not be taken greater than 60, and:

$$\Delta_c(\%) = 2.50 - 10\frac{P}{A_g f'_c} \quad \text{for} \quad \frac{P}{A_g f'_c} \le 0.1$$
$$\Delta_c(\%) = 1.75 - 2.6\frac{P}{A_g f'_c} \quad \text{for} \quad \frac{P}{A_g f'_c} > 0.1 \qquad (8\text{-}8)$$

8.7.1.1 Walls with Integral Columns or Boundary Elements

Where the ends of walls and vertical wall segments are confined by spirally reinforced columns or confined boundaries as defined in Table 8-5, the drift capacity may be increased by 25% for flexure-critical walls and by 50% for shear-critical walls.

Where integral concrete columns are located within the length of a wall or vertical wall segment, the drift capacity shall be determined as follows:

- For walls that are not more than 15 feet in length, with an axial load ratio of 0.30 or less, with an integral concrete column conforming to the confinement requirements in Table 8-5, located within the middle third of the wall length, the drift capacity may be taken as 4%.
- For other cases of walls with integral concrete columns, the drift capacity may be taken as the larger of:
    - the drift capacity determined for the wall or vertical wall segment, excluding consideration of the integral concrete column; or
    - the drift capacity determined for a segment of wall on either side of the column, treated as a half-barbell section, with the column assumed to be located at the compression end of the segment.

Table 8-5 Minimum Transverse Reinforcement in Integral Columns or Boundary Elements Required to be Classified as Confined

Transverse Reinforcement	Applicable Expression
$\frac{A_{sh}}{sb_c}$ for rectilinear hoops⁽¹⁾	Greater of: $0.2\left(\frac{A_g}{A_{ch}} - 1\right)\frac{f'_c}{f_{yt}}$ and $0.06\frac{f'_c}{f_{yt}}$
ρ_s for spiral or circular hoops	Greater of: $0.3\left(\frac{A_g}{A_{ch}} - 1\right)\frac{f'_c}{f_{yt}}$ and $0.08\frac{f'_c}{f_{yt}}$

(1) To be considered for purposes of confinement, transverse reinforcement must have 135 degree hooks and spacing of no more than 8 inches.

8.7.2 Drift Capacity of Other Critical Components

If columns and other related components (e.g., slab-column connections, beam-column corner connections, and discontinuous columns) are designated as critical, drift capacities shall be determined in accordance with Section 7.7.

8.8 Determine Wall and Column Ratings

8.8.1 Determine Wall Ratings

Determine wall ratings, *WR*, for critical walls and vertical wall segments, as the ratio of drift demand to drift capacity, Δ_D/Δ_C, in accordance with Table 8-6, for earthquake loading in each direction.

Table 8-6 Wall Rating, *WR*

Drift Demand to Drift Capacity Ratio Δ_D/Δ_C	Wall Rating, *WR*
$\Delta_D/\Delta_C \le 0.25$	0.0
$0.4 \ge \Delta_D/\Delta_C > 0.25$	0.1
$0.5 \ge \Delta_D/\Delta_C > 0.4$	0.2
$0.7 \ge \Delta_D/\Delta_C > 0.5$	0.3
$0.9 \ge \Delta_D/\Delta_C > 0.7$	0.4
$1.1 \ge \Delta_D/\Delta_C > 0.9$	0.5
$1.4 \ge \Delta_D/\Delta_C > 1.1$	0.6
$1.8 \ge \Delta_D/\Delta_C > 1.4$	0.7
$2.5 \ge \Delta_D/\Delta_C > 1.8$	0.8
$3.0 \ge \Delta_D/\Delta_C > 2.5$	0.9
$\Delta_D/\Delta_C > 3.0$	0.93

8.8.2 Determine Column Ratings

If columns and other related components (e.g., slab-column connections, beam-column connections, and discontinuous columns) are designated as critical, column ratings, *CR*, shall be determined in accordance with Section 7.8.

For the purpose of calculating the story rating, *SR*, in Equation 8-9, unrated columns should be assigned a *CR* of 0.

8.9 Determine Story Ratings

The story rating is a number representing the relative likelihood that an individual story will lose its ability to support vertical loads under the assumed earthquake loading. Determine the story rating, *SR*, as:

$$SR = 1.5R_{adj} - 0.1 \tag{8-9}$$

where:

R_{adj} = the adjusted average of column and wall ratings in the story, defined by Equation 8-10

The story rating, SR, shall not be taken less than 0.1 nor greater than 0.9. Low values of story rating, SR, indicate a low likelihood of failure, while high values indicate a high likelihood of failure.

The adjusted average of column and wall ratings in the story, R_{adj}, is defined:

$$R_{adj} = R_{avg} + 0.625R_{avg}(\mathrm{COV} - 0.4) \tag{8-10}$$

where:

$$R_{avg} = \sum_{i=1}^{n_{col}} f_{col,i} CR_i + \sum_{j=1}^{n_{wall}} f_{wall,j} WR_j \tag{8-11}$$

and:

R_{avg} = the weighted average rating for all columns and walls in the story, in which the values are weighted by the gravity load taken by each column or wall at the critical story

$f_{col,i}$ = fraction of gravity loads in the critical story supported by column i

$f_{wall,j}$ = fraction of gravity loads in the story supported by wall j (note: the sum of the fraction of gravity loads supported by all columns and walls must equal 1.0 in each story)

n_{col} = number of columns in a story

n_{wall} = number of walls in a story

COV = the standard deviation of all the column and wall ratings at the critical story, divided by the weighted average rating, R_{avg}, at that story

In Equations 8-10 and 8-11, R_{adj} shall not be taken less than R_{avg}, nor greater than $1.25R_{avg}$.

In calculating R_{avg}, every column location in a story is assigned a column rating, CR_i, and each wall location in a story is assigned a wall rating, WR_j, determined by the highest rating for any critical column or wall element at that location, or for any supported critical beam-column corner connection or critical slab-column connection at that location, in either horizontal direction. The fraction of the gravity load taken by the column, $f_{col,i}$, or wall, $f_{wall,j}$, at each location is used to weight the calculations of the average.

Chapter 9

Evaluation Procedures for Infilled Frame Systems

This chapter covers the evaluation of buildings classified as infilled frame systems, as defined in Section 5.3.4.

9.1 Introduction

The procedures for infilled frame systems parallel the procedures for frame systems in Chapter 6 and frame-wall systems in Chapter 7. Infilled frame systems include masonry infill walls, referred to as *panels*, and could include reinforced concrete structural walls, referred to as *walls*. Infilled frame systems also include *infilled-frame columns*, with infill panels abutting the column on one or both sides in the direction of loading, and *bare-frame columns*, without abutting infill panels. Classification of infill in accordance with Section 5.3.4 affects the strength of the infilled bay, how the infill is presumed to interact with the columns, and how the infill is considered in the evaluation methodology.

Evaluation of infilled frame systems is focused on comparing drift demands with drift capacities of infilled-frame columns and bare-frame columns, as well as slab-column connections, walls, and vertical wall segments (or wall piers) where they exist in the building. Component demand-to-capacity ratios are used to define column, wall, and wall segment ratings. Column ratings for infilled-frame columns include consideration of the presence of infill panels assisting in the gravity load-carrying capacity of the columns. Column and wall ratings are combined to determine story ratings, which are used in Chapter 10 to determine the building rating.

Section 9.2 defines *critical stories* along each of two horizontal earthquake loading directions based on the results of the mechanism analyses of Section 5.5. Section 9.3 defines *critical components*, which include infilled-frame columns and bare-frame columns located in critical stories. Other critical components could include slab-column connections, corner beam-column connections, discontinuous columns satisfying certain criteria, walls, and vertical wall segments. Sections 9.4 through 9.6 define the drift demands that are considered for each critical component. Section 9.7 defines drift capacities, and a comparison of drift demands to drift capacities in Section 9.8 establishes individual column and wall ratings for critical components.

9.2 Identify Critical Stories

Using the controlling plastic mechanism along each of the two principal framing directions determined in Section 5.5, critical stories are defined in infilled frame systems in accordance with the following:

- Where Mechanism 1 controls the strength along a principal framing direction, the critical story in that direction is the first story above the base.
- Where Mechanism 3 controls the strength along a principal framing direction, the critical story in that direction is the story in which Mechanism 3 forms.

Infilled frame systems can be presumed to be controlled by Mechanism 1, unless a significant discontinuity in infill strength or configuration along the height, or potential out-of-plane failure, warrants consideration of Mechanism 3. It is possible for different plastic mechanisms to control along each of the two principal framing directions. In such cases, the critical story in one principal direction may differ from the critical story in the other principal direction.

Critical stories are also defined where adjacent buildings require pounding considerations in accordance with Section 5.10.

9.3 Identify Critical Components

Critical components are those components deemed to be most vulnerable to damage and loss of vertical load-carrying ability. Critical components are evaluated in accordance with the procedures in Sections 9.6 through 9.8.

9.3.1 Critical Columns in Infilled Frame Systems

Columns in critical stories of infilled frame systems (defined in Section 9.2) are designated as critical components. Critical columns in infilled frame systems include columns with infill walls abutting the column on one or both sides in the direction of loading and bare-frame columns. Infill wall panels are not considered critical components and are not rated. The effects of infill panels are considered in the rating of critical columns in Section 9.8.1.

9.3.2 Other Critical Components

Bare-frame columns below one or more panels of discontinuous masonry infill can be critical. Columns below discontinuous masonry infill classified as strong in Section 5.4.3, should be evaluated in accordance with Section 5.9.2. Where they occur, other bare-frame columns, walls and vertical wall segments, columns integral with walls, slab-column connections, beam-column corner connections, and discontinuous columns and walls are identified as critical in accordance with Section 7.3.

9.4 Calculate Global Seismic Drift Demand

Calculate the global seismic drift (displacement) demand for an equivalent single-degree-of-freedom (SDOF) system, δ_{eff}, as:

$$\delta_{eff} = C_1 C_2 S_a \frac{T_e^2}{4\pi^2} g \tag{9-1}$$

where:

C_1 = modification factor to relate expected maximum inelastic displacement to displacement calculated for linear elastic response

C_2 = modification factor to represent the effect of pinched hysteresis shape, cyclic stiffness degradation, and strength deterioration on maximum displacement response

T_e = effective fundamental period determined in Section 5.6

S_a = spectral acceleration at period, T_e

g = acceleration of gravity

Calculate coefficient C_1 in accordance with ASCE/SEI 41-17 as:

$$C_1 = 1 + \frac{\mu_{strength} - 1}{aT_e^2} \tag{9-2}$$

where a is a site class factor equal to: 130 for Site Class A or B; 90 for Site Class C; 60 for Site Class D, E, or F; and all other terms are as previously defined. For $T_e < 0.2$ seconds, C_1 need not be taken greater than the value at $T_e = 0.2$ seconds. For $T_e \geq 1$ second, $C_1 = 1.0$.

Calculate coefficient C_2 in accordance with ASCE/SEI 41-17 as:

$$C_2 = 1 + \frac{1}{800}\left(\frac{\mu_{strength} - 1}{T_e}\right)^2 \tag{9-3}$$

where all terms are as previously defined. For $T_e > 0.7$ seconds, $C_2 = 1.0$.

Global seismic drift demands are calculated in each direction of earthquake loading.

9.5 Calculate Story Drift Demand

Calculate story drift demand, δ_x, of story x as:

$$\delta_x = \alpha_x h_{sx}\left(\frac{\delta_{eff}}{h_{eff}}\right) \le \delta_{eff} \tag{9-4}$$

where:

α_x = coefficient to modify story drifts at story x for building configuration and strength characteristics

h_{sx} = height of story x

δ_{eff} = global displacement demand of the equivalent SDOF system (Equation 9-1)

h_{eff} = effective height of the building, defined as the height from the base to the centroid of lateral forces (may be taken as $0.7h_n$ in multistory buildings having uniform distribution of effective weight over the building height and h_n in single-story buildings)

h_n = height from the base of the building to the highest level of the seismic force-resisting system

Story drift demands are calculated in each direction of earthquake loading.

Coefficient α modifies story drifts considering number of stories in a building, the yield mechanism, and whether the story is a critical story. Values of coefficient α for infilled frame systems are provided in Table 9-1.

Table 9-1 Values of Coefficient α for Infilled Frame Systems

No. of Stories in the Building	Yield Mechanism	Values of α	
		Critical Stories	Other Stories[1]
1	(any)	1.0	(n/a)
≥2	1, 3	$0.8h_{eff}/h_{sx}$	0.5

[1] Values of α for "Other Stories" are generally not used, except where components in other stories are designated as critical because of increased local vulnerability, as required in Section 9.3.

9.6 Calculate Drift Demands in Critical Components

9.6.1 Adjusted Drift Demand on Critical Components

For each critical component (see Section 9.3), calculate the adjusted drift demand, Δ_D, as follows:

$$\Delta_D = A_T \gamma \delta_x \tag{9-5}$$

where:

A_T = torsional amplification factor (Section 9.6.2)

γ = fraction of story drift affecting the critical component (Section 9.6.3)

δ_x = story drift demand (Section 9.5)

9.6.2 Torsional Amplification Factor

Determine the torsional amplification, A_T, at the location of each critical component. The torsional amplification, A_T, varies linearly in plan between a value of 1.0 at the center of strength and a value of $A_{T,max}$ at the edge of the building furthest from the center of strength (i.e., the weak or flexible side of the building). For all components located on the strong or stiff side of the building (between the center of strength and the edge of the building closest to the center of strength), $A_T = 1.0$.

9.6.2.1 Calculation of Maximum Torsional Amplification Factor

The maximum torsional amplification factor, $A_{T,max}$, is calculated in accordance with Equation 7-6, but should not be taken less than 1.

$$A_{T,max} = 2.75(TR) + 0.5 \tag{9-6}$$

where TR is the torsional ratio. The maximum torsional amplification factor, $A_{T,max}$, may be taken as 1.0 if the wall index, $WI < 0.0004$, or if the torsional ratio, $TR < 0.25$.

9.6.2.2 Calculation of Torsional Ratio

In Equation 9-6, TR shall be taken as the value of torsional ratio, TR_x, at the critical story, unless there is a significant torsional irregularity in another story. TR_x is the torsional ratio for story x, calculated as:

$$TR_x = \frac{T_{Dx}}{T_{Cx}} \tag{9-7}$$

where T_{Dx} is the torsion demand on story x, and T_{Cx} is the torsion capacity (strength) of story x. Torsion demand, T_{Dx}, is directional, and must be calculated for each direction of earthquake loading:

$$T_{Dx} = V_{px}e \tag{9-8}$$

where:

V_{px} = plastic shear capacity of the critical story, as calculated in Chapter 5

e = eccentricity between the center of mass and the center of strength in the direction perpendicular to the direction of earthquake loading; e may not be taken as less than 5% of L (i.e., $0.05L$), where L is the overall plan dimension perpendicular to the direction of earthquake loading

The coordinates of the center of strength, $\left(\bar{x}, \bar{y}\right)$, are calculated from:

$$\bar{x} = \frac{\sum_{i=1}^{n_f} x_i V_{pfi}}{\sum_{i=1}^{n_f} V_{pfi}}, \quad \bar{y} = \frac{\sum_{i=1}^{n_f} y_i V_{pfi}}{\sum_{i=1}^{n_f} V_{pfi}} \tag{9-9}$$

where:

x, y = are the orthogonal distance between the frame, infilled frame, or wall line of interest and an established reference point

V_{pfi} = is the plastic capacity of frame, infilled frame, or wall line i

n_f = is the number of frame or wall lines in story x, considering all frame, infilled frame, or wall lines that resist torsion.

Torsion capacity, T_C, is calculated considering the capacity of all frame, infilled frame or wall line in all orientations, and is the same regardless of the direction of loading considered:

$$T_{Cx} = \sum_{i=1}^{n_f} \left|R_{fi}\right| \left|V_{pfi}\right| \tag{9-10}$$

where R_f is the orthogonal distance between frame, infilled frame, or wall line line i and the center of strength, and all other terms are as previously defined.

9.6.2.3 Identification of Exceptionally High Seismic Risk Buildings based on the Torsional Ratio

Infilled frame systems with extreme torsion shall be classified as *exceptionally high seismic risk buildings* without further evaluation. A building is considered to have extreme torsion if the torsional ratio, $TR > 1.5$.

9.6.3 Drift Factor

The drift factor, γ, defines the fraction of story drift demand, δ_x, affecting critical components. Values of drift factor, γ, for critical components are defined in the sections that follow.

9.6.3.1 Drift Factor for Infilled-Frame Columns

For columns with infill panels abutting the column on one or both sides in the direction of loading, $\gamma = 1.0$.

9.6.3.2 Drift Factor for Other Components

If other bare-frame columns, walls and vertical wall segments, columns integral with walls, slab-column connections, beam-column corner connections, and discontinuous columns and walls are identified as critical, drift factors shall be determined in accordance with Section 7.6.3.

The drift factor for other columns, in general, depends on the ratio of the strength of columns to the strengths of horizontal members framing into the column. For bare-frame columns in infilled frame systems, if the movement of beams framing into the column in the direction of loading is restrained by infill walls, $\gamma = 1.0$.

9.7 Calculate Drift Capacity of Critical Components

Calculate drift capacities of critical components in accordance with this section.

9.7.1 Drift Capacity of Critical Columns in Infilled Frame Systems

Calculate the drift capacity of critical columns in infilled frame systems as:

$$\Delta_c = l_{u,inf}(\theta_c + 0.01) \tag{9-11}$$

where:

$l_{u,inf}$ = effective height of column in infilled frame (Table 9-2)

θ_c = column plastic rotation capacity

Table 9-2 Effective Height of Columns in Infilled Frame Systems

Effective Height of Column	$l_{u,inf}$
Bare-frame column	l_u
Columns with abutting infill on one or both sides in the direction of loading	$l_u/2$
Partial height infills	Clear height of the column that does not have abutting infill
Columns with abutting infill with openings on one or both sides in the direction of loading	Where an opening exists within a distance of $d_{op} < h_{inf}/2$ of the column, the effective height of the column is taken as the height of the opening, h_{op}. Otherwise, use $l_u/2$.

In Table 9-2, l_u is the clear height of the column, and infill panel dimensions, d_{op}, h_{inf}, and h_{op} are as defined in Section 4.3.6.

Calculate column plastic rotation capacity θ_c in accordance with Table 9-3 for tied columns and Table 9-4 for spiral-reinforced columns. Column plastic rotation capacity, θ_c, is based on the column shear strength ratio, V_p/V_n, axial load ratio, $P/A_g f'_{ce}$, and shear reinforcement ratio, ρ_t. Except for corner columns, the axial load ratio is based on the gravity load, P_g, determined in accordance with Section 4.2. For corner columns, the axial load ratio is based on the total column axial load, $P = P_g + P_{eq}$, where P is positive in compression, and P_g and P_{eq} are determined in accordance with Section 4.2. For the purpose of calculating the plastic rotation capacity of infilled-frame columns, the infill panel is assumed to support no gravity load.

Table 9-3 Plastic Rotation Capacities for Tied Columns(1), (2), (3), (4)

Flexure-Critical Columns ($V_p/V_n \le 0.6$, $\rho_t > 0.002$, and $s/d < 0.5$)	
For $\left(\dfrac{P}{A_g f'_{ce}}\right) \ge 0.1$	$\theta_c = 11.4\rho_t + 0.034 - \left(\dfrac{P}{A_g f'_{ce}}\right)\left(14\rho_t + 0.036\right) \ge 0.0$
For $\left(\dfrac{P}{A_g f'_{ce}}\right) < 0.1$	$\theta_c = 10\rho_t + 0.03 \ge 0.0$
Flexure-Shear and Shear-Critical Columns (i.e., Columns not classified as Flexure-Critical Columns)	
For $\left(\dfrac{P}{A_g f'_{ce}}\right) \le 0.5$	$\theta_c = \dfrac{0.5}{5 + \dfrac{P}{0.8 A_g f'_{ce}} \dfrac{1}{\rho_t} \dfrac{f'_{ce}}{f_{ye}}} - 0.01 \ge \theta_{c,\min}$ $P/A_g f'_{ce}$ should not be taken smaller than 0.1
θ_c should be reduced linearly for $\left(\dfrac{P}{A_g f'_{ce}}\right) > 0.5$ from its value at $\left(\dfrac{P}{A_g f'_{ce}}\right) = 0.5$ to zero at $\left(\dfrac{P}{A_g f'_{ce}}\right) = 0.7$	
$\theta_{c,\min} = 0.042 - 0.023\left(\dfrac{P}{A_g f'_{ce}}\right) + 0.63\rho_t - 0.023\left(\dfrac{V_p}{V_n}\right) \ge 0.0$ $P/A_g f'_{ce}$ should not be taken smaller than 0.1	

(1) ρ_t should not be taken greater than 0.0175 in any case, nor greater than 0.0075 when ties are not adequately anchored in the core.

(2) V_p/V_n should not be taken less than 0.2.

(3) θ_c for flexure-shear and shear-critical columns shall not exceed θ_c for a flexure-critical column with the same condition.

(4) $P = P_g$, except for corner columns where $P = P_g + P_{eq}$.

Tables 9-3 and 9-4 are divided between flexure-critical columns and other columns (flexure-shear or shear-critical columns). Flexure-critical columns are columns with $V_p/V_n \le 0.6$, $\rho_t > 0.002$, and $s/d < 0.5$. Flexure-shear or shear-critical columns are defined as columns not classified as flexure-critical. The calculation of V_p/V_n should consider the impact of the infill in reducing the effective height of the column. The effective height of columns in infilled frame systems is provided in Table 9-2. Effective heights should be used when the infill panel is classified as "strong," "weak," or "very weak with openings" in Section 5.3.4, even if the infill panel strength is ignored in strength calculations.

Table 9-4 Plastic Rotation Capacities for Spiral-Reinforced Columns(1), (2), (3), (4)

Flexure-Critical Columns ($V_p/V_n \leq 0.6$, $\rho_t > 0.002$, and $s/d < 0.5$)	
For $\left(\frac{P}{A_g f'_{ce}}\right) \geq 0.1$	$\theta_c = 1.15\left[11.4\rho_t + 0.034 - \left(\frac{P}{A_g f'_{ce}}\right)(14\rho_t + 0.036)\right] \geq 0.0$
For $\left(\frac{P}{A_g f'_{ce}}\right) < 0.1$	$\theta_c = 1.15[10\rho_t + 0.03] \geq 0.0$
Flexure-Shear and Shear-Critical Columns (i.e., Columns not classified as Flexure-Critical Columns)	
For $\left(\frac{P}{A_g f'_{ce}}\right) \leq 0.5$	$\theta_c = \frac{0.65}{5 + \frac{P}{0.8A_g f'_{ce}} \frac{1}{\rho_t} \frac{f'_{ce}}{f_{ye}}} - 0.01 \geq \theta_{c,\min}$ $P/A_g f'_{ce}$ should not be taken smaller than 0.1
θ_c should be reduced linearly for $\left(\frac{P}{A_g f'_{ce}}\right) > 0.5$ from its value at $\left(\frac{P}{A_g f'_{ce}}\right) = 0.5$ to zero at $\left(\frac{P}{A_g f'_{ce}}\right) = 0.7$	
$\theta_{c,min} = 0.06 - 0.06\left(\frac{P}{A_g f'_{ce}}\right) + 1.3\rho_t - 0.037\left(\frac{V_p}{V_n}\right) \geq 0.0$ $P/A_g f'_{ce}$ should not be taken smaller than 0.1	

(1) ρ_t should not be taken greater than 0.0175 in any case, nor greater than 0.0075 when ties are not adequately anchored in the core.

(2) V_p/V_n should not be taken less than 0.2.

(3) θ_c for flexure-shear and shear-critical columns shall not exceed θ_c for a flexure-critical column with the same condition.

(4) $P = P_g$, except for corner columns where $P = P_g + P_{eq}$.

9.7.2 Drift Capacity of Other Critical Components

If other columns and related components (e.g., slab-column connections, beam-column corner connections, and discontinuous columns) are designated as critical, drift capacities shall be determined in accordance with Section 7.7.

9.7.3 Drift Capacity of Critical Walls and Vertical Wall Segments

If walls and wall segments are identified as critical, drift capacities shall be determined in accordance with Section 7.7.4.

9.8 Determine Column and Wall Ratings

Column and wall ratings represents the relative likelihood that an individual column, supported slab, or wall will lose its ability to support vertical loads under the assumed earthquake loading. Ratings near 0.0 indicate a low likelihood of failure, while ratings near 1.0 indicate a high likelihood of failure.

9.8.1 Determine Ratings for Columns in Infilled Frame Systems

Determine column ratings, *CR*, for critical columns in infilled frame systems, as the ratio of drift demand to drift capacity, Δ_D/Δ_C, in accordance with Table 9-5, for earthquake loading in each direction.

Table 9-5 Column Rating, *CR*

Drift Demand to Drift Capacity Ratio Δ_D/Δ_C	Column Rating, *CR*
$\Delta_D/\Delta_C \leq 0.25$	0.0
$0.4 \geq \Delta_D/\Delta_C > 0.25$	0.1
$0.5 \geq \Delta_D/\Delta_C > 0.4$	0.2
$0.7 \geq \Delta_D/\Delta_C > 0.5$	0.3
$0.9 \geq \Delta_D/\Delta_C > 0.7$	0.4
$1.1 \geq \Delta_D/\Delta_C > 0.9$	0.5
$1.4 \geq \Delta_D/\Delta_C > 1.1$	0.6
$1.8 \geq \Delta_D/\Delta_C > 1.4$	0.7
$2.5 \geq \Delta_D/\Delta_C > 1.8$	0.8
$3.0 \geq \Delta_D/\Delta_C > 2.5$	0.9
$\Delta_D/\Delta_C > 3.0$	0.93

If a column has infill panels that remain intact on both sides in the direction of loading, and there is no gap between the infill panel and the beam, the infill panels can be assumed to provide assistance in supporting gravity loads. Table 9-6 provides criteria for measuring the integrity of the infill panels based on in-plane and out-of-plane response, based on the drift at onset of residual strength, provided in Table 9-7.

Values in Table 9-6 are added to values provided in Table 9-5 to obtain a total rating for infilled-frame columns. In no case shall the total column rating, CR, including assistance provided by the infill panels, be taken less than zero.

Table 9-6 Assistance to Column Ratings Based on Infill Panel Response(1) (2)

Measure of out-of-plane response	Measure of In-Plane Response	
	$\delta < \Delta_{res}$	$\delta \geq 2\Delta_{res}$ (3)
$h_{inf}/t_{inf} < 25$	-0.3	0
$h_{inf}/t_{inf} \geq 35$	0	0

(1) Assistance is taken as 0 if there are openings within a distance of 2 feet on either side of the column in the direction of loading.

(2) For intermediate values, assistance can be calculated by linear interpolation.

(3) Δ_{res} is the drift at the onset of residual strength, provided in Table 9-7.

Table 9-7 Drift at Onset of Residual Strength, Δ_{res}, for Infilled Bays

Aspect Ratio	Weak Infill	Strong Infill(1)
$h_{inf}/L_{inf} < 1$	for column $V_p/V_n < 1$, $\Delta_{res} = 0.01h_{sx}$ for column $V_p/V_n \geq 1$, $\Delta_{res} = 0.0055h_{sx}$	$1.6\Delta_{peak}h_{sx}$
$h_{inf}/L_{inf} \geq 1$	$\Delta_{res} = 0.01h_{sx}$	

(1) Δ_{peak} is the drift at which the infill reaches peak strength, provided in Table 5-2.

9.8.2 Determine Ratings for Other Critical Components

If other columns, walls, and other related components (e.g., slab-column connections, beam-column connections, and discontinuous columns) are designated as critical, column ratings, *CR*, and wall ratings, *WR*, shall be determined in accordance with Section 7.8.

9.9 Determine Story Ratings

The story rating is a number representing the relative likelihood that an individual story will lose its ability to support vertical loads under the assumed earthquake loading. Determine the story rating, *SR*, as:

$$SR = 1.5R_{adj} - 0.1 \qquad (9\text{-}12)$$

where:

R_{adj} = the adjusted average of column and wall ratings in the story, defined by Equation (9-13)

The story rating, *SR*, shall not be taken less than 0.1 nor greater than 0.9. Low values of story rating, *SR*, indicate a low likelihood of failure, while high values indicate a high likelihood of failure.

The adjusted average of column and wall ratings in the story, R_{adj}, is defined as:

$$R_{adj} = R_{avg} + 0.625R_{avg}(\mathrm{COV} - 0.4) \qquad (9\text{-}13)$$

where:

$$R_{avg} = \sum_{i=1}^{n_{col}} f_{col,i} CR_i + \sum_{j=1}^{n_{wall}} f_{wall,j} WR_j \tag{9-14}$$

and:

R_{avg} = the weighted average rating for all columns and walls in the story, in which the values are weighted by the gravity load taken by each column or wall

$f_{col,i}$ = fraction of gravity loads supported by column i. For the purpose of weighting column ratings, infill panels are not assumed to carry gravity load, and the columns are assumed to carry all tributary gravity load

$f_{wall,j}$ = fraction of gravity loads in a story supported by wall j (note: the sum of the fraction of gravity loads supported by all columns and walls must equal 1.0 in each story)

n_{col} = number of columns in a story

n_{wall} = number of walls in a story

COV = the standard deviation of all the column and wall ratings at a story divided by the weighted average rating, R_{avg}, at that story

In Equations 9-13 and 9-14, R_{adj} shall not be taken less than R_{avg}, nor greater than $1.25R_{avg}$.

In calculating R_{avg}, every column location in a story is assigned a column rating, CR_i, and each wall location in a story is assigned a wall rating, WR_j, determined by the highest rating for any critical infilled frame column, bare-frame column, or wall element at that location, or for any supported critical beam-column corner connection or critical slab-column connection at that location, in either horizontal direction. The fraction of the gravity load taken by the column, $f_{col,i}$, or wall, $f_{wall,j}$, at each location is used to weight the calculation of the average.

Chapter 10

Determination of Building Rating

This chapter describes the determination of building ratings based on story ratings for frame, frame-wall, bearing wall, and infilled frame systems calculated in the preceding chapters. It also describes the recommended use of building ratings in ranking buildings within an inventory, and prioritizing buildings for future work.

10.1 Introduction

The building rating, *BR*, is a number between 0.1 and 0.9, inclusive, representing the relative likelihood that the building will lose its ability to support vertical loads under the assumed earthquake loading. Building ratings can be used to rank the relative risk of partial or complete collapse among buildings in an inventory of buildings. Use of building ratings in a program to reduce the seismic risk associated with older concrete buildings is described in Section 1.4.

10.2 Determine Building Rating

The building rating, *BR*, is taken as the maximum story rating, *SR*, determined in either direction, for critical stories over the height of a building. Story ratings between 0.1 and 0.9 for frame, frame-wall, bearing wall, and infill frame systems calculated in Chapters 6 through 9 are used to determine the building rating, *BR*.

10.3 Recommended Building Risk Levels

In some cases, classification of buildings in Chapter 5 results in the early identification of buildings as either *lower seismic risk buildings* or *exceptionally high seismic risk buildings* based on certain features or characteristics.

In other cases, the building rating, *BR*, is used to rank the relative risk of buildings in an inventory of buildings, and to assign buildings within three relative risk levels: *exceptionally high seismic risk buildings*, *high seismic risk buildings*, and *lower seismic risk buildings*.

10.3.1 Exceptionally High Seismic Risk Buildings

Buildings identified as *exceptionally high seismic risk buildings* in Chapter 5, or assigned a building rating, *BR*, greater than or equal to 0.7 shall be considered as a class, *exceptionally high seismic risk buildings*.

Exceptionally high seismic risk buildings are considered the highest level of relative risk and should be given the highest priority for further evaluation (or mitigation) among older concrete buildings in an inventory.

10.3.2 High Seismic Risk Buildings

Buildings assigned a building rating, *BR*, greater than 0.3 but less than 0.7 shall be considered as a class, *high seismic risk buildings*.

High seismic risk buildings should be given an intermediate priority for further evaluation (or mitigation) among older concrete buildings in an inventory.

10.3.3 Lower Seismic Risk Buildings

Buildings identified as *lower seismic risk buildings* in Chapter 5, or assigned a building rating, *BR*, less than or equal to 0.3 shall be considered as a class, *lower seismic risk buildings*.

Lower seismic risk buildings are considered the lowest level of relative risk and could include buildings of very low risk meeting conventional life safety standards. Lower seismic risk buildings should be given the lowest priority for further evaluation (or mitigation) among older concrete buildings in an inventory.

Appendix A

Development of Column Drift Capacities

A.1 Introduction

Column ratings are a critical input to the determination of story ratings and building ratings in this methodology. Column drift capacities are used in the calculation of column ratings. This appendix describes how column drift capacities, which are a combination of plastic rotation capacity and the elastic drift capacity, were determined, and how uncertainty was included in the determination of column ratings.

A.2 Column Plastic Rotation Capacity Determination

Column plastic rotation capacities, θ_c, are intended to represent the deformation at which the column is expected to lose its gravity-load bearing capacity. In all cases, drift capacities are based on experimental test data of reinforced concrete components, and intended to represent median capacities (i.e., there is a 50% chance that the true capacity is higher - or lower - than the value reported). As a result, the drift capacities may differ from those published elsewhere in cases where other publications intended to produce lower bound or conservative estimates of drift capacity.

The derivation of column plastic rotation capacities, θ_c, in this methodology differs depending on the expected failure mode of the column. For columns expected to fail in flexure, θ_c was obtained by adapting the tables provided in ASCE/SEI 41-13, *Seismic Evaluation and Retrofit of Existing Buildings* (ASCE, 2013). For flexure-shear and shear critical columns, mechanics-based equations are used, as proposed by the ACI 369 committee (Ghannoum, 2017). For both sets of equations, predictions of θ_c are intended to produce a consistent 50% probability that the observed value will exceed the predicted value, such that all values are medians. These predictions were investigated to ensure that there was no bias with respect to axial load ratio, transverse reinforcement ratio, and other column design parameters. As a result, the equations are intended to provide median values, regardless of the properties of a column.

A.2.1 Plastic Rotation Capacities for Flexure-Critical Columns

Flexure-critical columns are those with $V_p/V_n \leq 0.6$, $\rho_t > 0.002$ and $s/d < 0.5$. Equations defining column plastic rotation capacities for flexure-critical columns in this methodology were obtained by adapting the tables provided in ASCE/SEI 41-13. Values of θ_c were based on b (rather than a) values, as defined in ASCE/SEI 41-13, because this methodology is aimed at quantifying column failure, and the axial limit state is judged to occur at, or near, the time of failure. Values of θ_c in this methodology are based on the same experimental tests of rectangular columns used to develop b values in ASCE/SEI 41-13, but reported values differ in two ways: (1) they represent median values; and (2) they are equation-based rather than tabular. An adjustment for circular columns based on additional data is also proposed.

A.2.2 Plastic Rotation Capacities for Flexure-Shear and Shear-Critical Columns

Flexure-shear or shear-critical columns are defined as those columns not classified as flexure-critical. Plastic rotation capacity equations for rectangular and circular columns are based on a mechanics-based equation developed by Elwood and Moehle (2005). A mechanics-based equation was better suited for this purpose than a statistics-based equation because of the limited amount of experimental shear-critical column tests carried out to axial failure. The model is further simplified based upon recommendations in Ghannoum and Matamoros (2014) by assuming a critical shear crack angle of 65 degrees from horizontal. The provided equations are taken from Ghannoum and Matamoros (2014) and also printed in Ghannoum (2017). These equations are not used for flexure-critical columns because of the mechanics-based approach used to develop the equations, which presumes a shear or flexure-shear failure.

A.2.3 Bias in Plastic Rotation Capacity Predictions

The prediction equations for θ_c are evaluated through comparison with a database of experimental column tests. The database of column tests that was assembled for use in development of deformation capacity predictions in ASCE/SEI 41-13 was leveraged here (Ghannoum, 2017; Ghannoum and Sivaramakrishnan, 2012a and 2012b). All tests were conducted quasi-statically on columns that did not contain splice or anchorage deficiencies. In the test data, the point of axial failure was identified as either the deformation at which axial collapse was observed during the experiment, or the deformation at which the lateral strength degrades to 25% of its peak strength. A more detailed description of the experimental database is provided in Ghannoum (2017).

The relationship between the predicted values for θ_c and those observed during experimental testing (quantified as the ratio of the measured to predicted θ_c) is presented for columns other than spirally-reinforced circular columns in Figure A-1, and for spirally-reinforced circular columns in Figure A-2. Figure A-1 shows that prediction equations for columns other than spirally-reinforced circular columns are not biased with respect to axial load ratio (Figure A-1a), transverse reinforcement ratio (Figure A-1b), and column V_p/V_n (Figure A-1c). Figure A-2 indicates that prediction equations for spirally-reinforced circular columns are also not biased with respect to axial load ratio (Figure A-2a), transverse reinforcement ratio (Figure A-2b), and V_p/V_n (Figure A-2c).

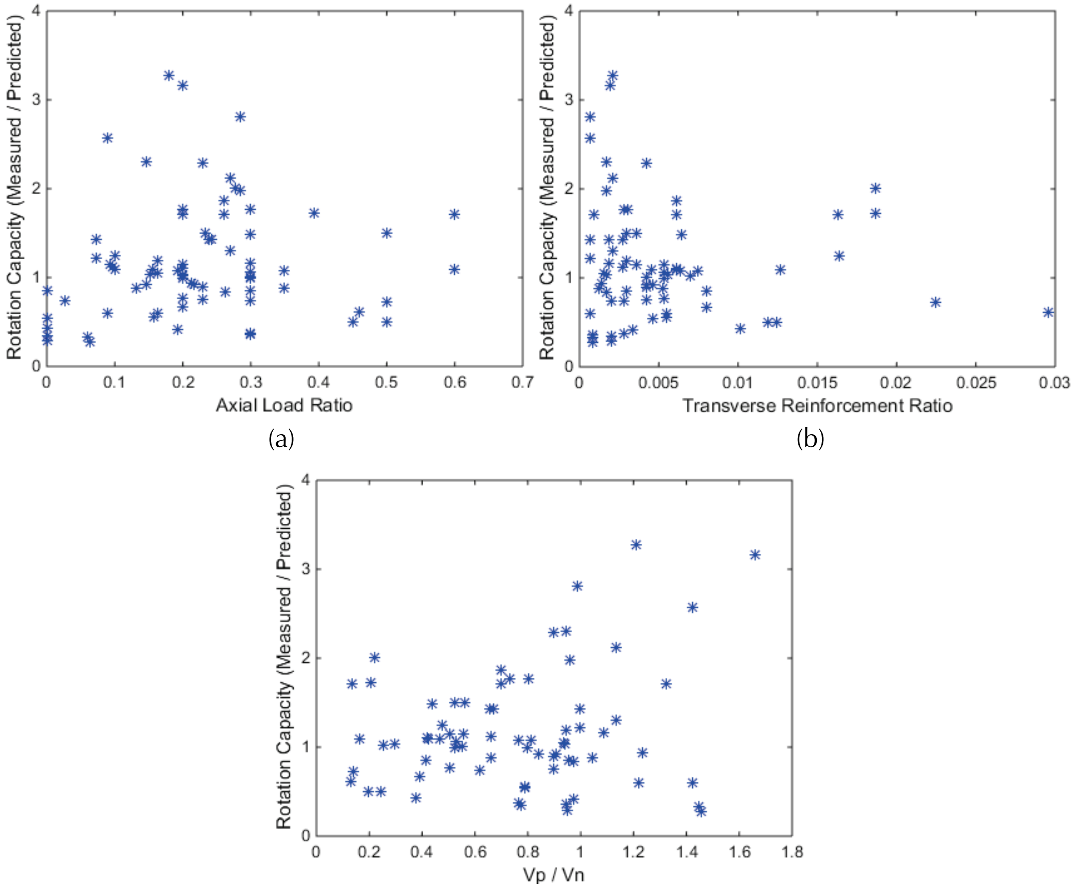

(a)

(b)

(c)

Figure A-1 Ratio of measured to predicted plastic rotation at axial failure for columns other than spirally-reinforced circular columns as a function of: (a) axial load ratio; (b) transverse reinforcement ratio; and (c) V_p/V_n.

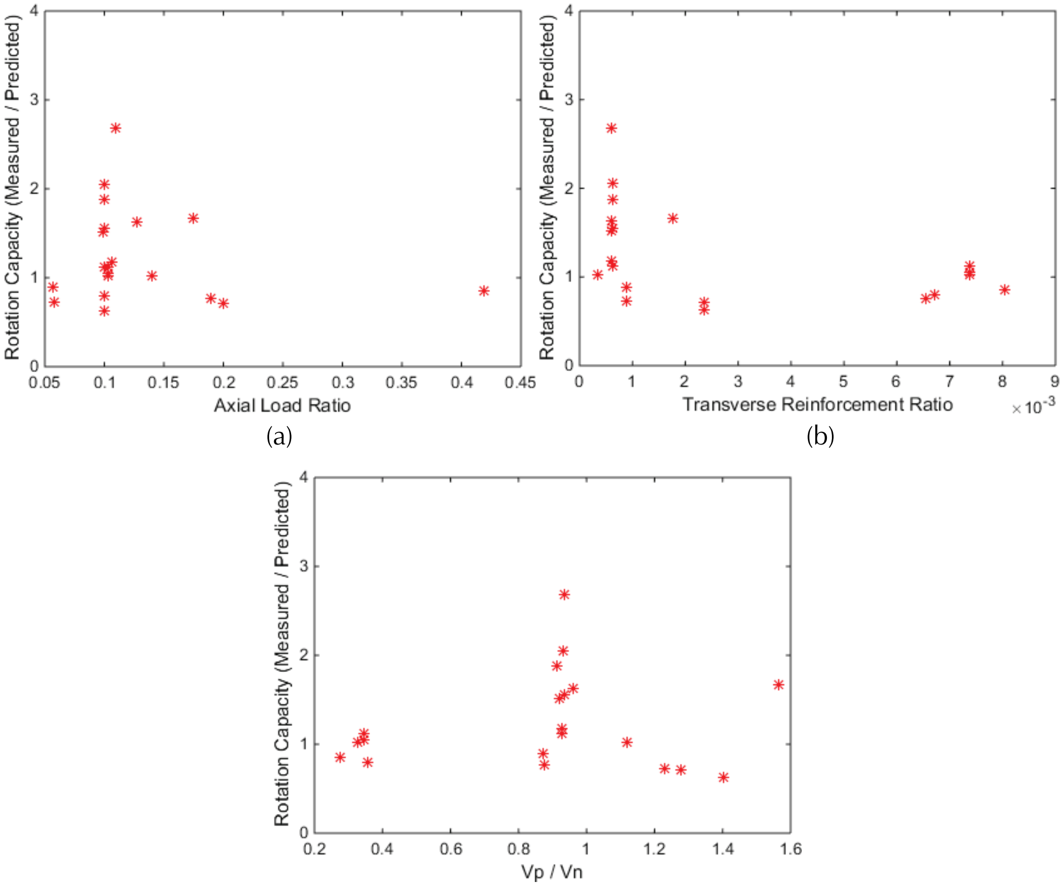

(a) (b)

(c)

Figure A-2 Ratio of measured to predicted plastic rotation at axial failure for spirally-reinforced circular columns as a function of: (a) axial load ratio; (b) transverse reinforcement ratio; and (c) V_p/V_n.

A.2.4 Comparison of Plastic Rotation Capacity Prediction Methods

The characteristics of the final deformation capacity prediction equations used in this methodology were compared against alternative methods in Figure A-3 and Figure A-4. Figure A-3 compares predicted values of plastic rotation capacity for for columns other than spirally-reinforced circular columns, and Figure A-4 compares plastic rotation capacities for spirally-reinforced circular columns.

Three different methods for prediction of plastic rotation capacity are compared in Figure A-3 and Figure A-4: (1) the plastic rotation capacity as predicted in ATC-78-3, *Seismic Evaluation of Older Concrete Frame Buildings for Collapse Potential* (ATC, 2015); (2) equations in Ghannoum (2017); and (3) the final deformation capacity prediction equations developed in ATC-78-5, *Seismic Evaluation of Older Concrete Frame, Wall, and Frame-Wall Buildings for Collapse Potential* (ATC, 2016) and used herein, labeled ATC-78-5. Tables in ATC-78-3 are based on the data used in ASCE/SEI 41-13 for both flexural and shear-critical columns, but are in tabular form rather than equation form. Prediction equations from Ghannoum (2017) have been used by ACI Committee 369 and implemented in ASCE/SEI 41-17 (which supersedes the 2013 edition of ASCE/SEI 41).

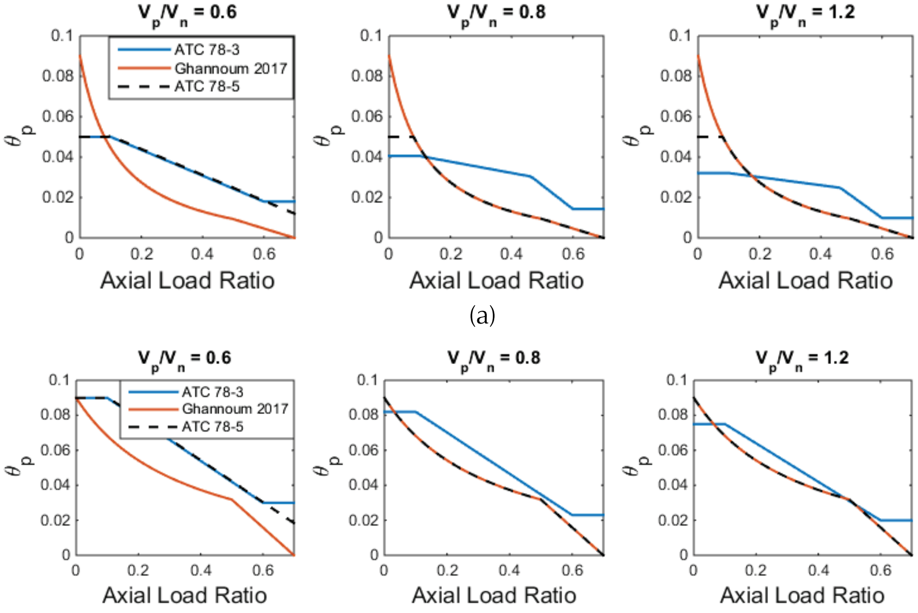

(a)

(b)

Figure A-3 Comparison of relationship between axial load ratio and plastic rotation capacity using different prediction methods for columns other than spirally-reinforced circular columns with transverse reinforcement ratio equal to: (a) 0.002; and (b) 0.006.

The form of the ATC-78-3 and Ghannoum (2017) prediction methods are quite different with respect to axial load ratio, and the form of the ATC-78-5 prediction equations is a modified combination of the two. The following observations highlight the differences between the three prediction methods:

- The ATC-78-5 prediction for θ_c follows the form of the ATC-78-3 prediction for flexure controlled columns (i.e., $V_p/V_n = 0.6$ in Figure A-3 and Figure A-4). However, the ATC-78-5 prediction decreases to zero for column axial load ratios greater than or equal to 0.7. Furthermore, the ATC-78-5 prediction is 15% larger than the ATC-78-3 prediction for flexurally controlled, spirally-reinforced, circular columns. This adjustment was made based upon new experimental test results used in the development of the ATC-78-5 method.
- For flexure-shear and shear critical columns (i.e., $V_p/V_n = 0.8$ and $V_p/V_n = 1.2$ in Figure A-3 and Figure A-4), the ATC-78-5 prediction follows the form of the Ghannoum (2017) equations. However, for columns with

low axial load ratios (< 0.1) and low transverse reinforcement ratios (0.002), the value of θ_c is limited to the value of θ_c computed for flexural controlled columns.

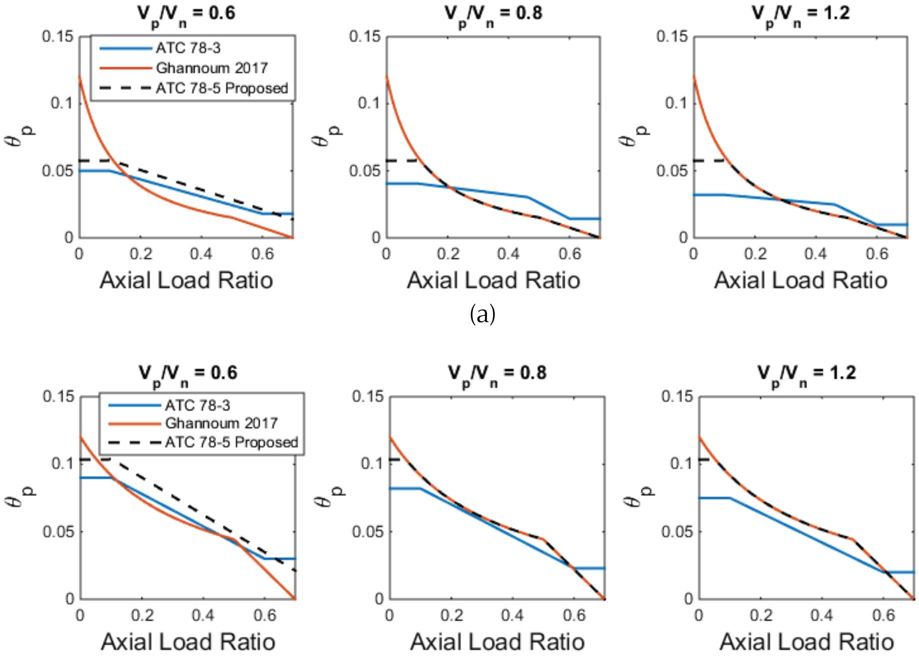

(a)

(b)

Figure A-4 Comparison of relationship between axial load ratio and plastic rotation capacity using different prediction methods for spirally-reinforced circular columns with transverse reinforcement ratio equal to: (a) 0.002; and (b) 0.006.

A.2.5 Uncertainty in Plastic Rotation Capacities

Experimental data were used to estimate uncertainty in plastic rotation capacities. Values shown in Table A-1 quantify uncertainty in the ratio of measured to predicted capacities. Values in the table range from 0.62 to 0.63.

Table A-1 Uncertainty in Predictions of Column Plastic Rotation Capacity, Obtained from Comparison with Experimental Data

Condition	$\sigma_{ln,\Delta c}$
θ_c for flexure-critical columns	0.63
θ_c for flexure-shear and shear-critical columns	0.62

Uncertainty in the plastic rotation capacity for flexure-critical columns was computed from the database of column tests used to develop the tables provided in ASCE/SEI 41-13. Uncertainty in the drift capacity prediction for flexure-shear and shear-critical columns was taken as the value reported in

Ghannoum and Matamoros (2014). On the basis of this data, the lognormal standard deviation, $\sigma_{ln,\Delta c}$, was taken to be 0.60. This value includes uncertainty in test data and in the empirical model (equation) predicting the test result, and has been incorporated in the computation of column ratings.

A.2.6 Elastic Component of Column Drift Capacity

In Section 6.7, the drift capacity of a column is computed from the plastic rotation capacity, added to an estimate of the elastic drift capacity. Equation 6-7 assumes the elastic drift capacity is 1% drift, which is a reasonable value from test data. The precise elastic capacity depends on whether or not a column fails in shear or flexure, the column stiffness, and other characteristics. For the purposes of this methodology, the 1% value was considered an adequate approximation.

A.2.7 Drift Capacity of Columns with Inadequate Lap Splices

ASCE/SEI 41-13 provides conservative estimates of the deformation capacity of columns with inadequate lap splices in longitudinal reinforcement. Columns with inadequate lap splices are classified as as flexure-critical, or flexure-shear and shear-critical based on the ratio of column shear capacity controlled by flexure to column shear capacity controlled by shear, V_p/V_n. For this purpose, the potential for lap-splices to reduce flexural strength is not considered.

Limited available test data on columns with inadequate lap splices suggest that the bond failure of a lap splice may actually increase flexibility and deformation capacity in some cases. Due to the limited and scattered nature of available data, these columns are treated the same as columns without lap splices, and the presence of lap splices is essentially ignored in determining the column drift capacity.

A.3 Slab-Column Connection Drift Capacity Determination

Drift capacities for slab-column connections were based on 85 slab-column tests conducted by various researchers and compiled by Gogus and Wallace (2015) and Aslani (2005). Thirty of these tests lacked bottom reinforcement through the column, and 55 had bottom reinforcement through the column. In these tests, punching failure of the slab-column connection was assumed to occur at the drift at which the connection lost 20% of its lateral load capacity (i.e., the drift corresponding to 80% of peak lateral load). It should be noted that this definition of drift capacity differs somewhat from the citeria used to define column drift capacity, which is based on vertical (axial) failure. A punching shear definition for slab-column connection collapse was used for the following reasons:

- Very few experimental slab-column tests were conducted to vertical failure.
- This methodology is only concerned with slab-column connections that do not satisfy minimum requirements for continuous bottom reinforcement, and vertical failure is anticipated to occur soon after punching failure.

The form of the relationship for predicting drift capacity of slab-column connections is similar to ACI 318-11, such that the drift is defined as a function of the gravity shear ratio, which represents the unfactored vertical gravity shear, V_g, divided by the theoretical punching shear strength without moment transfer, V_o. However, drift capacities are representative of median values and are, therefore, different from the values provided by ACI 318-11.

Figure A-5 compares the proposed regression to the test data, and the curve provided in ACI 318-11. The regression used in this methodology has a 49% probability of exceedance (i.e., it represents the median of test results) with a lognormal standard deviation of 0.4. The ACI 318-11 regression is more conservative, with an 89% probability of exceedance (i.e., test results are more likely to be higher than the value predicted in the regression). Figure A-6 shows that the prediction is not biased with respect to the gravity shear ratio.

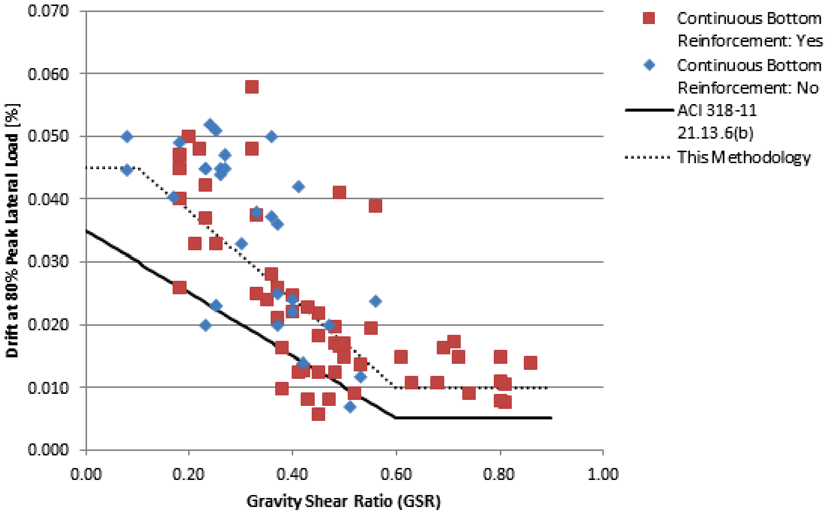

Figure A-5 Relationship between gravity shear ratio and drift capacity for slab-column connections.

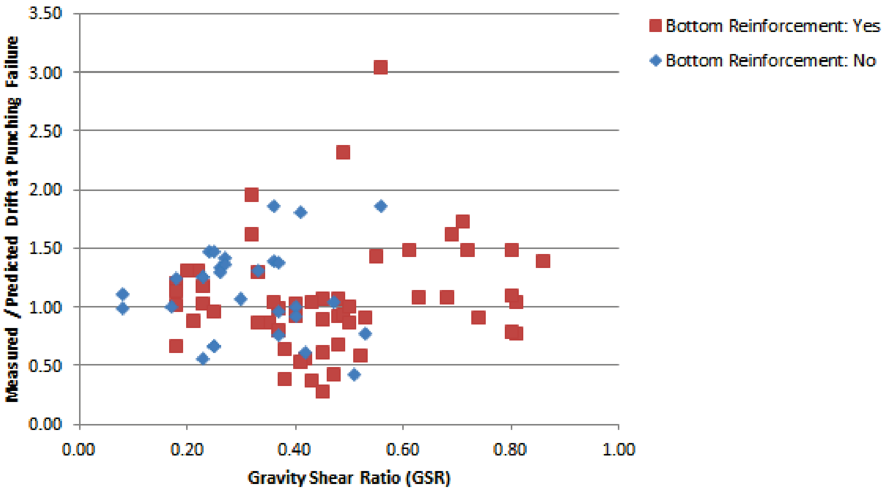

Figure A-6 Ratio of measured versus predicted drift at punching shear failure for slab-column connections with different gravity shear ratios.

This methodology assumes that punching shear failure will only occur if there is insufficient continuity (bottom) reinforcement through the connection. Where there is sufficient bottom reinforcement, a slab-column connection may punch, but it is assumed that structural integrity requirements will prevent the slab from collapsing. As a result, large drift capacities are provided for slab-column connections with sufficient bottom reinforcement.

Appendix B

Development of Method for Determining Column Ratings

B.1 Overview

A column rating represents the probability that the drift demand on a column, Δ_D, exceeds the drift capacity of the column, Δ_C. Thus, a column rating reflects the probability of column failure (under the ground motion intensity that produces that drift demand). Higher column ratings indicate that the expected performance of columns will be worse.

Drift demands and drift capacities are both assumed to be lognormally distributed. A lognormal distribution is commonly used in earthquake engineering applications. The probability that column drift demand exceeds capacity depends on the mean and standard deviations of the probability distributions for drift demand and capacity. In this methodology, uncertainty in drift demand includes record-to-record variability in drift response, as well as uncertainty in the prediction of roof and critical story drifts. Uncertainty in the drift capacity includes variability in material properties, and the predictive model for drift capacity.

A column rating should be viewed as a representation of the probability of column failure for the given level of excitation, not as the true probability of failure. As a representation of the probability of failure, column ratings are comparable between different columns in a building and between different buildings. However, due to the simplified nature of this methodology, these values should not be applied in other probabilistic analyses outside of this methodology.

B.2 Structural Reliability Methods for Computing the Column Rating

A column rating is calculated using structural reliability methods to determine the probability that a column drift demand exceeds the column drift capacity (Melchers, 1999). In the formulation that follows, it is assumed that the random variables representing drift demand and drift capacity are lognormally distributed and statistically independent (Mori and

Ellingwood, 1993). In structural reliability terms, the limit state function for this problem can be written as:

$$G = \ln\left(\tilde{\Delta}_C\right) - \ln\left(\tilde{\Delta}_D\right) \tag{B-1}$$

where:

$\tilde{\Delta}_C$ = drift capacity for the column of interest; and

$\tilde{\Delta}_D$ = drift demand for the column of interest.

"Failure" occurs when $G \leq 0$. Both $\tilde{\Delta}_C$ and $\tilde{\Delta}_D$ are random variables.

It can be shown that the reliability index, β, for this situation can be obtained from the following equation:

$$\beta = \frac{\ln\left(\dfrac{\tilde{\Delta}_C}{\tilde{\Delta}_D}\right)}{\sqrt{\sigma^2_{\ln,\Delta_C} + \sigma^2_{\ln,\Delta_D}}} \tag{B-2}$$

where:

$\tilde{\Delta}_C$ = drift capacity for the column of interest

$\tilde{\Delta}_D$ = drift demand for the column of interest

$\sigma_{\ln,\Delta_C}$ = uncertainty in the column drift capacity, taken as 0.60

$\sigma_{\ln,\Delta_D}$ = uncertainty in the column drift demand, taken as 0.60

The probability of failure, p_f, for each column can be computed from the reliability index as follows:

$$p_f = \Phi\left(-\beta\right) \tag{B-3}$$

where the operator Φ indicates the cumulative standard normal probability distribution. As a result, the column rating, *CR*, is given as:

$$CR_j = \Phi\left[-\frac{\ln\left(\dfrac{\tilde{\Delta}_C}{\tilde{\Delta}_D}\right)}{\sqrt{\sigma^2_{\ln,\Delta_C} + \sigma^2_{\ln,\Delta_D}}}\right] \tag{B-4}$$

which is the relationship that was used to develop the values shown in Table 6-4 and Table 7-4.

Appendix C

Development of Method for Determining Story Ratings

C.1 Overview

Like the column rating, the story rating represents the probability of collapse of a story, given the level ground shaking being considered. Higher story ratings indicate higher probabilities of collapse. As a representation of the probability of collapse, story ratings are comparable among stories and between buildings. However, due to the simplified nature of this methodology, these values should not be applied in other probabilistic analyses.

C.2 Probability Theory for Determining Probability of Story Collapse

Several different methods were explored to relate column failure ratings to story collapse ratings. The method used in this evaluation methodology uses probability theory to relate the probability of failure of each column at story *x* to the probability of collapse in that story. This method is employed to make up for the absence of a structural analysis model in the methodology.

The following assumptions are made in computing the probability of a story collapse:

- Story collapse is assumed to occur if at least 25% of gravity load bearing capacity in a story fails. In a frame building, for example, this corresponds to failure of columns carrying 25% of the gravity loads.
- Drift demands on all columns/walls in a story are assumed to be perfectly correlated, due to a rigid diaphragm assumption. Hence, if one column drift demand is higher than average, the other columns/walls are also expected to experience higher drift demands.
- Column/wall drift (deformation) capacities are correlated assuming the failure model shown in Figure C-1. This model captures adjacent column relationships, such that the failures of columns that are closer together are assumed to be more highly correlated (or consequential) than columns that are farther apart. The minimum level of correlation applied to the most widely-spaced columns corresponds to a correlation

coefficient of 0.20. This assumption attempts to account for progressive collapse and load redistribution probabilistically.

These correlations are used to in Monte Carlo simulations to develop story ratings based on realizations of drift demands and capacity on gravity load bearing elements that are consistent with these correlation models through multivariate random number generation. This process is described in more detail below.

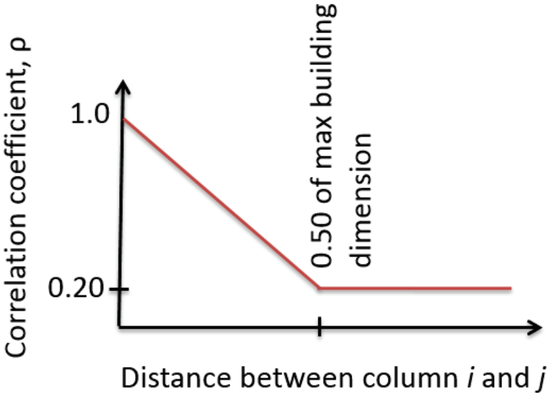

Figure C-1 Assumed model of correlation in column/wall drift capacities for failure of columns *i* and *j*, as a function of column/wall separation distance.

C.3 Development of Story Ratings

These assumptions are used to generate the story rating curve shown in Figure C-2. This curve was obtained using 10,000 Monte Carlo simulations in which random realizations of the drift demand and drift capacity of each load bearing element (column or wall) in the story were generated. These realizations were generated using a multivariate random number generator such that the assumed correlations in both demand and capacity described in Section C.2 are accounted for. An individual column or wall was identified as failed in the Monte Carlo realization if its demand exceeded its capacity. Story collapse was identified in a simulation if at least 25% of the gravity load bearing capacity in the story was identified as having failed in the simulation. The curve shown was developed for a set of buildings with different column/wall ratings, aspect ratios, and numbers of columns/walls, but there was not significant variation from building to building.

In the interest of simply representing the results shown in Figure C-3 for use in this methodology, these curves are presented as equations for linear trend lines applicable for story ratings greater than 0.1 and less than 0.9. These equations are a function of the average column/wall rating, R_{avg}, wherein the average is weighted by the fraction of gravity loads taken by each load bearing element. The fitted equations are overlaid on the curves from Figure C-2 in Figure C-3. This is the basis for Equations 6-9 and 7-14.

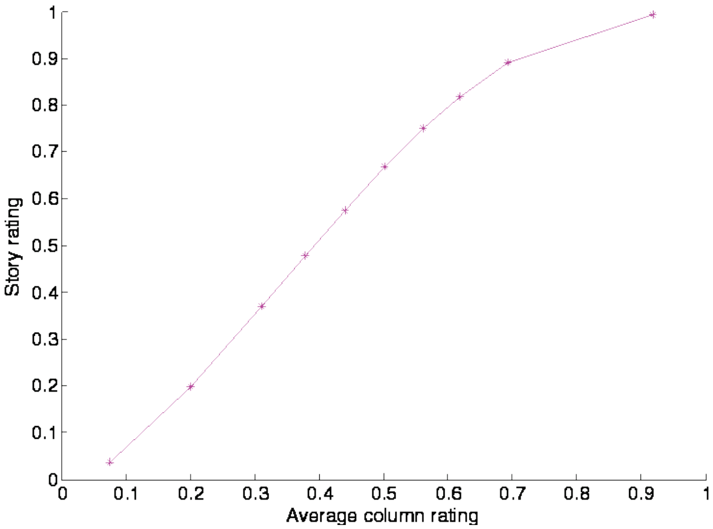

Figure C-2 Relationship between adjusted average column rating, R_{avg}, and the story rating, SR, for frame structures. The curve is the same for frame-wall and wall structures, except that the average incorporates the rating of walls through Equation 7-16.

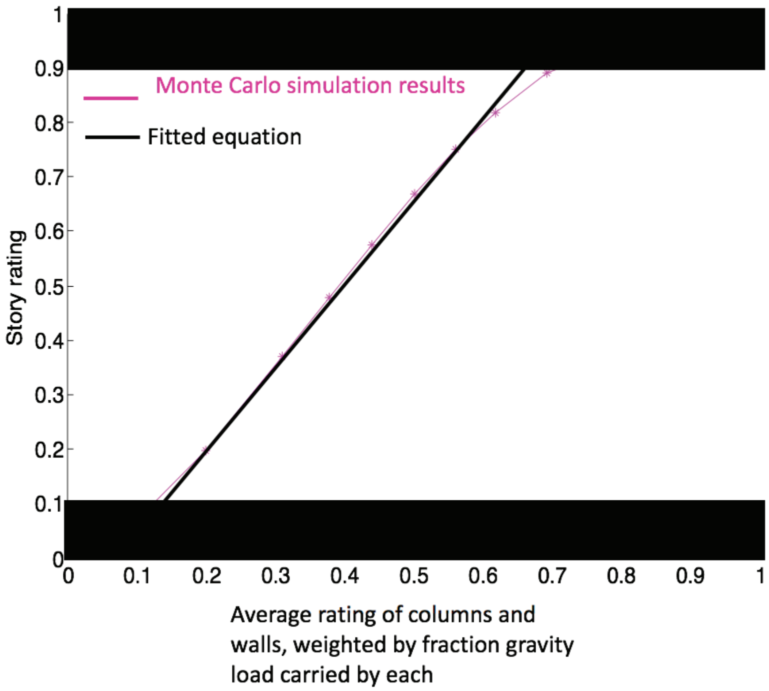

Figure C-3 Relationship between adjusted average column and wall rating, CR_{avg}, and the story rating, SR, from Monte Carlo simulation, and showing the simplified equation developed for the purpose of this methodology.

Appendix D

Wall Strength Index (WSI) Method

D.1 Overview

A significant fraction of older buildings contain walls. The seismic performance of buildings containing a large number of walls is expected to be better than the performance of pure frame buildings because of their greater overstrength. Moreover, the added stiffness provided by walls may reduce drift demands on poorly detailed columns. The following sections develop the method for quickly evaluating frame-wall and wall buildings, such that wall-dominated buildings with large number of walls are excused from having to conduct a full ATC-78 evaluation based on the so-called "Wall Strength Index". Two approaches are employed to support the development of this method based on: (1) numerical simulation; and (2) an analytical solution.

Sozen proposed the concept of a wall index (*WI*) as an indicator for building damage and collapse (Sozen, 2014). Sozen's original formulation of the *WI* is a ratio of wall to tributary floor area, and is computed at the base of the structure, not on a story-by-story basis. Additionally, Sozen proposed a column index (*CI*) which relates the cross-sectional area of all columns to the tributary floor area, arguing that it is the combination of the *WI* and *CI* that predicts a building's seismic resistance. Sozen supported these concepts using post-earthquake damage observations from five events to develop relationships between *WI*, *CI*, and damage. Contained in this dataset were buildings with *WI* that ranged from 0 to 0.0055, showing generally lower damage with higher *WI.* However, none of the five events occurred in the U.S. or in areas with construction practices similar to the U.S. In this study, Sozen's *WI* is adapted to account for the hazard level and site effects by including $S_a(T_e)$. The resulting metric, *WSI*, is used to identify frame-wall or wall buildings of lower seismic risk.

The Wall Strength Index (*WSI*) is defined as:

$$WSI = \frac{WI}{S_{a(T_{ef})}} \tag{D-1}$$

where:

WI = the governing value of WI from Section 5.4.1

S_a = the horizontal spectral acceleration at the site, taken at the approximate structural period, T_{ef}. determined for the direction corresponding to the governing wall index WI

D.2 Numerical Simulation

D.2.1 Buildings Analyzed

A set of nonlinear models of frame-wall systems is created and analyzed to establish a relationship between WSI and the collapse probability. As summarized in Table D-1, the buildings analyzed range from 2 to 6 stories in height; include frames with flexure, flexure-shear, and shear controlled columns (V_p/V_n from 0.6 to 1.2); consist of single and multiple wall systems; and have walls with varying strengths. Typical bay widths and story heights are shown in Figure D-1. Wall designs are unconfined with #4 bars at 12 inches on center, as is expected to be typical of older building; the wall lengths (l_w) and thickness (t_w) are defined in Table D-1. In total, 32 frame-wall models are analyzed, with 9 of them containing frames with flexure-controlled columns and 23 having frames with shear-critical columns. Additionally, the analyzed building set contains WI ranging from 0.0002 to 0.0040 as shown in Table D-1.

Table D-1 Frame-Wall Building Properties

Num. Stories	V_p/V_n (2)	Num. Walls	l_w (ft)	t_w (in)	WI	T_e (sec)(1)
2	1.2	1	10	10	0.0007	0.43
2	1.2	1	20	10	0.0013	0.24
2	1.2	1	30	10	0.0020	0.16
2	1.2	1	40	10	0.0027	0.12
3	1.2	1	7	10	0.0003	0.60
3	1.2	1	11	10	0.0005	0.53
3	1.2	1	20	10	0.0009	0.42
3	1.2	1	30	10	0.0013	0.27
3	1.2	1	45	10	0.0020	0.17
6	0.6	1	10	10	0.0002	1.13
6	0.6	1	20	10	0.0004	0.95
6	0.6	1	30	10	0.0007	0.89
6	0.6	1	50	10	0.0011	0.49

Table D-1 Frame-Wall Building Properties (continued)

Num. Stories	V_p/V_n[2]	Num. Walls	l_w (ft)	t_w (in)	WI	T_e (sec)[1]
6	0.6	1	60	10	0.0013	0.39
6	0.6	1	20	10	0.0004	1.20
6	0.6	1	30	10	0.0007	1.12
6	1.2	1	30	10	0.0007	0.89
6	1.2	1	40	10	0.0009	0.65
6	1.2	1	50	10	0.0011	0.50
6	1.2	1	60	10	0.0013	0.39
6	1.2	1	80	10	0.0018	0.28
6	1.2	2	30	10	0.0013	0.79
6	0.6	3	20	10	0.0013	0.65
6	0.6	5	20	10	0.0022	0.62
6	0.6	6	20	10	0.0027	0.62
2	1.2	2	20	10	0.0027	0.20
2	1.2	3	20	10	0.0040	0.19
2	1.2	3	20	10	0.0040	0.29
3	1.2	2	7	10	0.0006	0.60
3	1.2	2	11	10	0.0010	0.39
3	1.2	3	20	10	0.0027	0.36
3	1.2	4	20	10	0.0035	0.35

(1) T_e is the effective period as per Eq. 7-27 of ASCE 41-13, calculated from pushover.

(2) Ratio of column flexural to shear strength, indicating degree of shear criticality.

D.2.2 Modeling

The dynamic response of each pure frame building is modeled using distributed plasticity elements for beams and columns and elastic springs representing beam-column joints, as illustrated in Figure D-1. If the governing failure mode of a column is shear, zero length shear and axial springs are included in series with the distributed plasticity element. The response of the shear and axial springs are governed by limit state materials, with relationships defined by Elwood (2004). If walls are present, they are modeled using a distributed plasticity element and connected to the frame with a rigid link as shown in Figure D-2.

In distributed plasticity elements, the constitutive relationship of concrete fibers is described by the modified Kent and Park model (Kent and Park, 1971); steel fibers are modeled using the relation proposed by Giuffre-Menegotto-Pinto and the onset of buckling and post-bucking behavior is determined using the model proposed by Dhakal and Maekawa (2002). When the governing failure mode is flexure, a single force-based fiber element is used per flexural element and the regularized integration scheme presented by Scott and Hamutcuoglu (2008) is employed with five integration points.

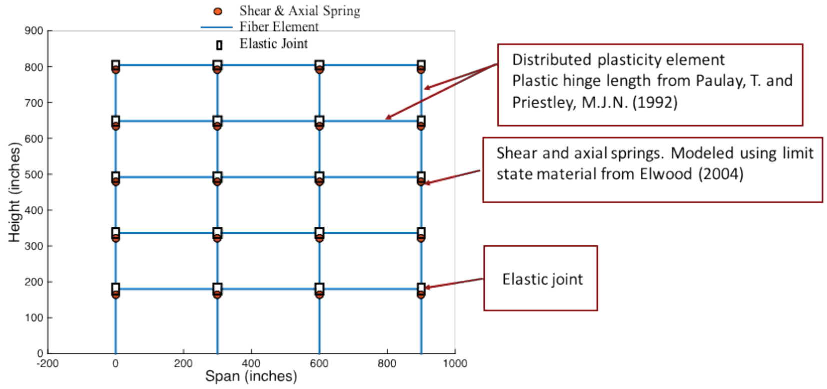
Shear & Axial Spring
Fiber Element
Elastic Joint
Height (inches)
Span (inches)
900
800
700
600
500
400
300
200
100
0
-200
0
200
400
600
800
1000

Distributed plasticity element
Plastic hinge length from Paulay, T. and Priestley, M.J.N. (1992)

Shear and axial springs. Modeled using limit state material from Elwood (2004)

Elastic joint

Figure D-1 Modeling overview for pure frame buildings.

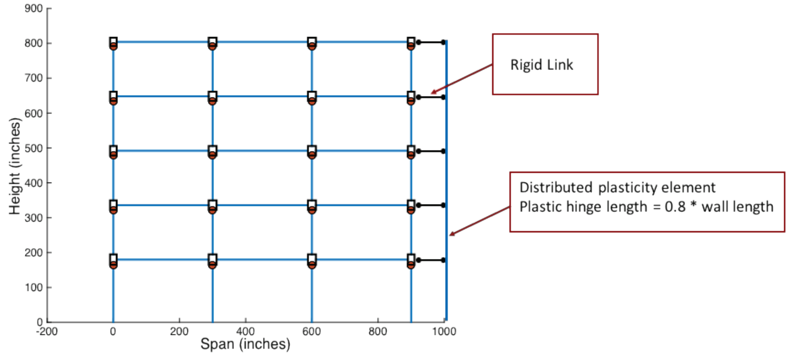
Height (inches)
Span (inches)
900
800
700
600
500
400
300
200
100
0
-200
0
200
400
600
800
1000

Rigid Link

Distributed plasticity element
Plastic hinge length = 0.8 * wall length

Figure D-2 Modeling overview for frame-wall buildings.

D.2.3 Ground Motion Selection and Scaling

The collapse capacity of each building, measured in terms of spectral acceleration, is evaluated through Incremental Dynamic Analysis or IDA (Vamvatsikos and Cornell, 2002). The FEMA P-695 far field ground motion set is used to represent the expected hazard (FEMA, 2009).

D.2.4 Collapse

Global collapse of the system is defined as occurring when the lateral resistance of any story degrades to 50% of its peak capacity. To determine this point, first, the interstory drift ratio at which any story degrades to 50% of its peak capacity is identified from pushover analysis (see Figure D-3a). This interstory drift ratio is then used to identify the collapse point during subsequent dynamic analysis. Figure D-3b plots the incipient collapse points (i.e., one step prior to collapse) for an example building during dynamic analysis. Collapse points from individual records are then used to develop the building's collapse fragility in Figure D-3c.

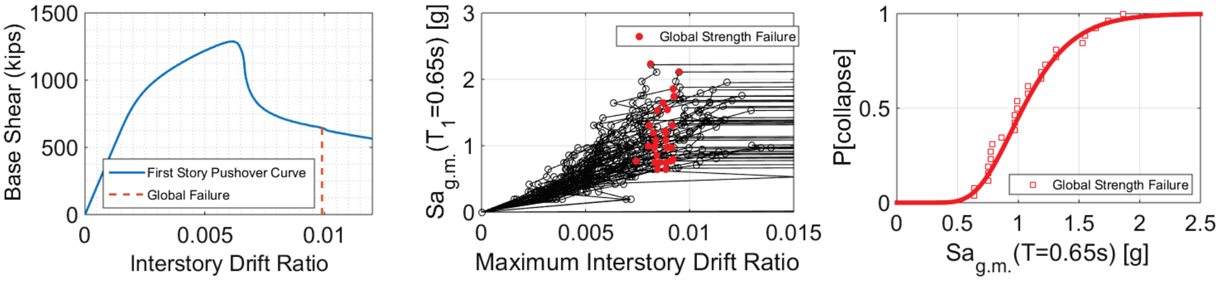

(a) (b) (c)

Figure D-3 Collapse definition for 6-story, 6-bay, frame-wall system with a single 20 ft wall and shear critical columns: showing (a) the point of global collapse identified during pushover analysis of the critical story; (b) the identification of global collapse from IDA curves; and (c) the building's collapse fragility curve.

D.2.5 Results

Buildings with many walls are expected to have low collapse probabilities. The collapse simulation results obtained for the buildings listed above were used to identify a cutoff *WSI* is selected that corresponds with an acceptably low collapse probability, on average, consistent with *Lower Seismic Risk Buildings*. Here, an acceptably low collapse probability is defined as 20%. Figure D-4 presents collapse probabilities resulting from the dynamic analysis of these buildings as a function of *WSI*. The *WSI* is defined based on the ground motion intensities and seismic hazard at the location of Davis Hall on the UC Berkeley campus. A normally distributed survival function (Kleinbaum and Klein, 2005) is used to define the form of an upper bound fit, i.e., upper bound probability of collapse for a given *WSI*. Based upon the upper bound fit, a *WSI* of greater than 0.002 is found to have a collapse probability of less than 20%, as shown by the star in Figure D-4. The buildings that govern the upper bound fit are typically frame-wall buildings that contain shear critical columns, and multiple walls with lengths of 20 feet or less. This implies that the 0.002 cutoff is conservative for buildings with fewer strong walls and flexure critical columns.

Figure D-4 presents an upper bound fit for all considered buildings. However, frame-wall buildings that contain flexural-governed columns typically have lower collapse probabilities than buildings with shear-critical columns for a given *WSI*. Based upon this observation, an upper bound fit, specific to frame-wall buildings with only flexural-critical columns is created in Figure D-5. Here, a *WSI* of 0.0015 corresponds to a collapse probability of 20%. This result signifies that wall-frame systems that contain flexurally-governed columns need fewer walls than systems with shear critical columns to produce equivalent collapse probabilities. In systems with shear critical columns, more walls are needed to reduce drift demands on poorly-detailed columns.

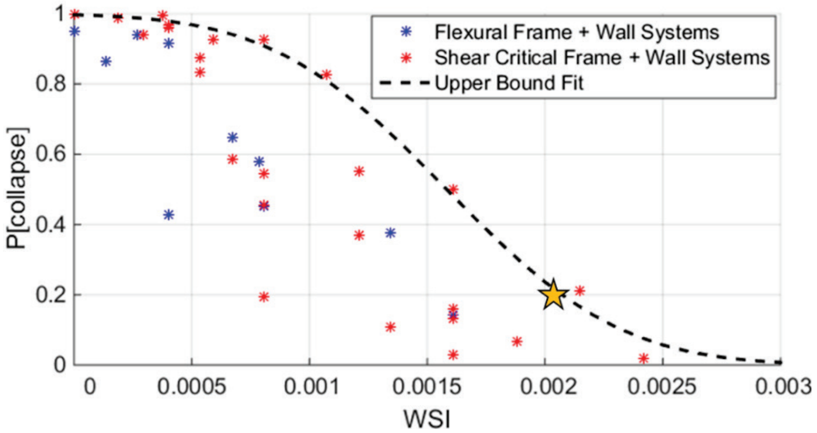

Figure D-4 Relationship between WSI and probability of collapse for 32 building models. All buildings are assumed to be located at the site of Davis Hall in UC Berkeley, CA (S_{D1} = 1.028g, S_{DS} = 1.65g) and evaluated at the design spectrum level.

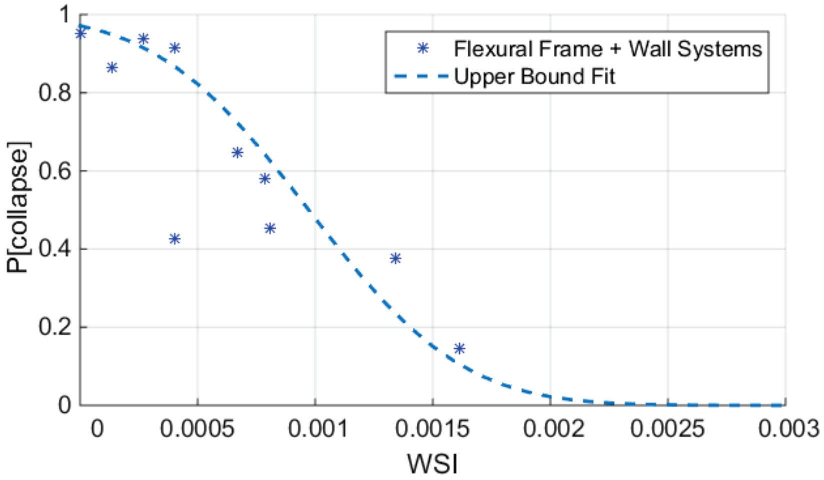

Figure D-5 Relationship between WSI and probability of collapse for wall-frame buildings with flexurally-governed columns. All buildings are assumed to be located at Davis Hall in UC Berkeley, CA (S_{D1} = 1.028g, S_{DS} = 1.65g).

Thus far, results have been presented for a single site (Davis Hall on the UC Berkeley campus). Accordingly, Figure D-6 varies the site hazard to investigate the effect of site location on the selected cutoff *WSI*. Figure D-6a presents collapse probabilities as a function of *WSI* for frame-wall buildings with shear-critical columns located at Davis Hall on the UC Berkeley campus (same site and subset of buildings from Figure D-4). Figure D-6b presents collapse probabilities for the same building set when the site hazard is taken as half the design hazard at Davis Hall. In both cases, an upper bound fit is plotted on the data. While the upper bound fit in both plots is slightly different, the *WSI* that corresponds to a collapse probability of 20% is about 0.002 in both cases. This signifies the cutoff *WSI* is relatively insensitive to the site hazard. This insensitivity is attributed to the fact that site hazard quantified in terms of $S_a(T_1)$ affects both the *WSI* and the collapse probability (the x- and y-axis in Figure D-6). Changing the site hazard in Figure D-6 alters the location of the individual data points, but the upper bound fit and cutoff *WSI* stay relatively constant.

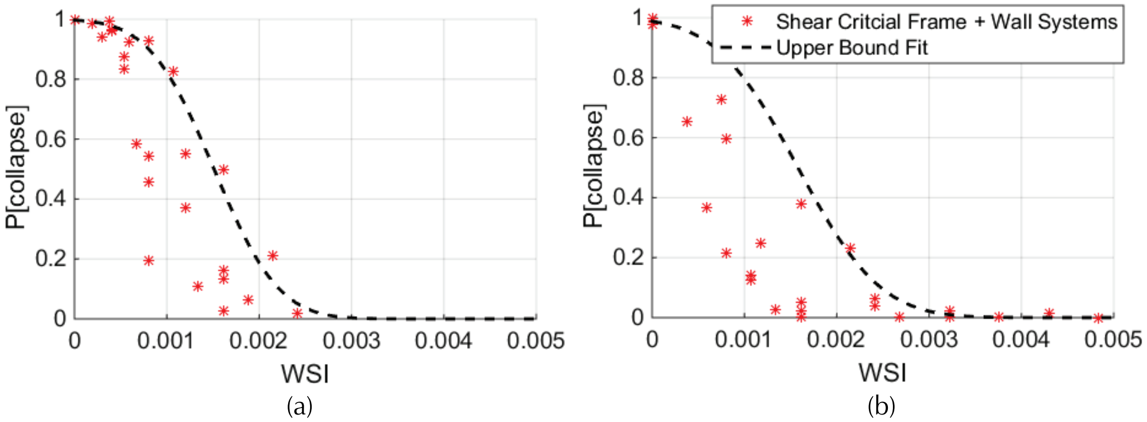

(a)

(b)

Figure D-6 Relationship between WSI and probability of collapse for wall-frame buildings with shear-controlled columns. Site hazard is taken at (a) Davis Hall in UC Berkeley, CA (S_{D1} = 1.028g, S_{DS} = 1.65g); and (b) half the hazard at Davis Hall (S_{D1} = 0.514g, S_{DS} = 0.825g).

D.3 Analytical Investigation of WSI

An alternate approach used to support the *WSI* criteria is investigated by relating the definition of the *WSI* to the shear stress check for shear walls performed during an ASCE 41-13 Tier 1 evaluation (ASCE 2013). ASCE 41-13 Tier 1 evaluations categorize buildings by their type, then evaluates significant lateral load resistance characteristics through a series of checklist items. Checklist items are intended to be conservative measures of seismic risk such that buildings that pass a Tier 1 evaluation are very likely to perform adequately during a design level event.

During a Tier 1 evaluation, the approximate shear stress in the shear walls is checked for concrete shear wall buildings. The average shear stress in a shear wall is defined in ASCE 41-13 Section 4.5.3.3 and is presented in Equation D-1:

$$v_j^{avg} = \frac{1}{M_s}\left(\frac{V_j}{A_w}\right) \qquad \text{(D-1)}$$

where, v_j^{avg} is the average shear stress in shear walls in level j, M_s is a system modification factor, V_j is the story shear at level j, and A_w is the summation of the horizontal cross-sectional area of all shear walls in the loading direction.

To satisfy life safety criteria in the Tier 1 checklist, the average shear stress in each wall must be less than the maximum of 100 psi or $2\sqrt{f_c'}$ as per ASCE 41-13 Section 16.10LS.

$$v_j^{avg} \le \max\left(100 \text{ psi}, \ 2\sqrt{f_c'}\right) \tag{D-2}$$

Substituting Equation D-2 into Equation D-1 produces Equation D-3:

$$\frac{1}{M_s}\left(\frac{V_j}{A_w}\right) \le \max\left(100 \text{ psi}, \ 2\sqrt{f_c'}\right) \tag{D-3}$$

The shear force demand can be estimated from ASCE 41-13 Section 4.5.2.1 and is shown in Equation D-4:

$$V = CS_aW \tag{D-4}$$

Here, V is the seismic base shear force, C is a coefficient to relate displacements determined from elastic analysis to expected inelastic displacements, S_a is the spectral acceleration computed at the building's fundamental period, and W is the building's effective seismic weight. If we assume each story has the same weight, the maximum shear force will occur at the first story. Substituting Equation D-4 in for V_j in Equation D-3 results in Equation D-5:

$$\frac{1}{M_s}\left(\frac{CS_aW}{A_w}\right) \le \max\left(100 \text{ psi}, \ 2\sqrt{f_c'}\right) \tag{D-5}$$

If we assume 200 lb/ft^2 (or 1.39 psi) for the dead load plus effective live load, $W = 1.39A_T$. A_T is the total of the floor areas above ground, counting all of the stories. Substituting in for W gives Equation D-6:

$$\frac{1}{M_s}\left(\frac{1.39CS_aA_T}{A_w}\right) \le \max\left(100 \text{ psi}, \ 2\sqrt{f_c'}\right) \tag{D-6}$$

The definition of *WSI*, revised to use the terminology employed in this section, is presented in Equation D-7:

$$\frac{S_aA_T}{A_w} = \frac{1}{WSI} \tag{D-7}$$

Equation D-8 is obtained by substituting Equation D-7 into Equation D-6:

$$\frac{1.39}{M_s}\left(\frac{C}{WSI}\right) \le \max\left(100 \text{ psi}, \ 2\sqrt{f_c'}\right) \tag{D-8}$$

If we then assume a concrete compressive strength of 4,000 psi:

$$\frac{1.39}{M_s}\left(\frac{C}{WSI}\right) \leq 126 \text{ psi} \tag{D-9}$$

And rearrange Equation D-9 in terms of *WSI* gives Equation D-10:

$$WSI \geq \frac{1.39}{126}\frac{C}{M_s} \tag{D-10}$$

From ASCE 41-13 Table 4-9, M_S is equal to 4 for life safety. If we assume collapse prevention is 75% of life safety, M_S is equal to 5.33, which is more in line with the goals of ATC 78.

Table D-2 WSI Required to Satisfy ASCE 41-13 Tier 1 Shear Stress Check

Num. Stories	*C* (ASCE 41-13 Table 4.8)	WSI Required
1	1.4	0.0029
2	1.2	0.0025
3	1.1	0.0023
4+	1.0	0.0021

Based upon Table D-2, the *WSI* required to satisfy the ASCE 41-13 Tier 1 shear stress check ranges from 0.0021 to 0.0029 depending on the number of stories. These results are obtained by assuming:

- equal weight per story
- seismic weight equals 200 lb/ft^2
- concrete compressive strength, $f'_c = 4000$ psi
- performance measure is collapse prevention (taken as 75% of life safety)

When compared with the required *WSI* obtained from numerical simulation (0.002), the required *WSI* in Table D-2 are slightly larger. This difference is attributed to the fact that the numerical simulations consider the effect of wall-frame interaction and the cutoff *WSI* corresponds with a collapse probability of 20%. Despite the slight differences in resulting *WSI*, the analytical solution serves to support the results obtained from numerical simulation.

D.4 Limitations

Building models used in the development of a cutoff *WSI* are regular in plan and contained walls that are continuous thorough the full building height. Therefore, additional criteria for use of the *WSI* within ATC-78 are enforced to ensure that building characteristics that may worsen seismic performance must undergo further evaluation. Additional criteria include:

- no discontinuous walls (going downward)
- no severe torsion
- no short columns

D.5 Conclusions

The collapse capacities of 32 wall-frame building models were computed through IDA. Based upon the results of this building set, a cutoff *WSI* was selected that corresponds with a collapse probability of less than 20%. For wall-frame buildings containing shear critical columns the cutoff *WSI* is 0.002 and for buildings containing flexurally-governed columns the cutoff *WSI* is 0.0015. These results are shown to be relatively independent of the site hazard and are further supported by an analytical solution that relates the cutoff *WSI* to the shear stress check for shear walls performed during an ASCE 41-13 Tier 1 evaluation.

Appendix E
Exceptionally Weak Building Criteria

E.1 Overview

Buildings that are exceptionally weak are expected to earn a high building rating, which is indicative of a relatively high probability of collapse. Here, a set of criteria is created for frame, frame-wall and wall buildings that identify exceptionally weak buildings during an early screening process. Buildings that are identified as exceptionally weak are then classified as Exceptionally High Risk (Building Rating > 0.7).

To develop the criteria for these buildings, first, a set of pure frame buildings of varying strengths was designed to the 1967 UBC. This building set has columns ranging from flexure-critical to shear-critical as shown in Table E-1. Next, flexure-critical walls with varying lengths and detailing (i.e., deformation capacities and moments of inertia) were added to the pure frame models. Properties of frame-wall buildings are presented in Table E-2. The collapse capacity of each building is then estimated through IDA and limits for exceptionally high risk weak buildings are proposed based on V_p/V_n.

Table E-1 Properties of Pure Frame Building Set

Num. Stories	Num. Bays	Median V_p/V_n	Median M_c/M_b	V_y/W	T_e (sec)[1]	Median $S_a(T_1)$ Collapse (g)
2	3	0.35	0.43	0.23	0.80	1.07
5	3	0.73	1.27	0.16	0.92	0.67
3	5	0.88	1.11	0.28	0.83	1.17
3	3	0.98	1.56	0.38	0.81	1.11
3	3	1.17	1.72	0.40	0.75	1.11
3	3	1.48	0.99	0.47	0.72	1.17
6	5	1.48	1.00	0.43	0.97	0.74

(1) T_e is the effective period as per Eq. 7-27 of ASCE 41, calculated from pushover.

Table E-2 Properties of Frame-Wall Building Set

Num. Stories	Num. Bays	Median V_p/V_n	WI	V_y/W	T_e (sec) [1]	Median $S_a(T_1)$ Collapse (g)
2	3	0.24	0.0036	0.72	0.36	1.89
3	5	0.88	0.0013	0.35	0.69	1.29
3	3	1.47	0.0024	0.55	0.58	1.67
3	3	1.28	0.0024	0.53	0.59	1.74
3	3	0.50	0.0024	0.44	0.62	1.61
3	3	0.56	0.0012	0.28	0.89	1.17
3	3	0.56	0.0024	0.42	0.61	1.47
3	3	0.97	0.0024	0.52	0.60	2.06
3	3	0.97	0.0024	0.48	0.60	1.82
5	3	0.73	0.0014	0.25	1.06	0.88
6	5	0.75	0.0006	0.17	1.28	0.88
8	3	1.28	0.0009	0.13	1.58	0.61

(1) T_e is the effective period as per Eq. 7-27 of ASCE 41, calculated from pushover.

E.2 Modeling

For an overview of the modeling techniques used evaluate each building's dynamic response, refer to Appendix D.

E.3 Ground Motion Selection and Scaling

Refer to Appendix D.

E.4 Collapse

Different collapse criteria are used depending on whether the building's columns are flexure or shear critical. For frame-wall or frame systems with shear-critical columns, collapse is taken as occurring in these analyses when 25% of columns in the story fail in shear. This collapse criterion was chosen to be consistent with earlier analyses conducted for this project, and is a proxy for loss of 25% of the gravity load bearing capacity. For frame and frame-wall buildings with flexure-critical columns, collapse is taken as the point at which the IDA curve flattens to 20% of its initial slope, i.e., sidesway (Vamvatsikos and Cornell, 2002).

E.5 Development of Criteria for Exceptionally Weak Frame Buildings

Two sources are drawn upon to develop the criteria that identifies exceptionally weak pure frame buildings: (1) nonlinear dynamic analysis results of pure frame models described above in Table E-1; and (2) Table C-10f from ATC-78-1 (ATC, 2012) which is reproduced in Table E-3, below. Table C-10f from ATC-78-1 is also based upon nonlinear dynamic analyses of RC frame buildings, however, the ATC-78-1 models used lumped plasticity elements to capture post-elastic behavior as opposed to the distributed plasticity models developed in this phase of the project and presented in Table E-1.

The collapse capacity of each pure frame building from Table E-1 is estimated through IDA. As shown in Figure E-1, there are trends in collapse capacity associated with the governing failure mode of the columns in the critical story, V_p/V_n. $\mu_{strength}$ values corresponding to a collapse probability of 0.7 are then extracted for each building. The 0.7 value is employed because it aligns conceptually with the definition of the Building Rating for Exceptionally High Risk buildings. These $\mu_{strength}$ values are then used in the development of the criteria to identify exceptionally weak pure frame buildings, as discussed below.

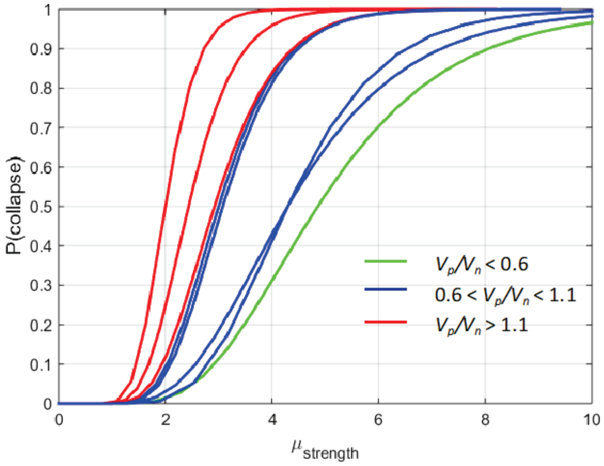

Figure E-1 Collapse fragilities for pure frame buildings from Table E-1 plotted as a function of $\mu_{strength}$.

Table C-10f from ATC-78-1 is reproduced below in Table E-3. Collapse probabilities for pure frame buildings are presented as a function of V_p/V_n and m, where $m = \mu_{strength}/C_m$. (Here, C_m is an effective mass factor dependent upon the number of stories and type of lateral load resisting system.) Combinations of V_p/V_n and m (which is converted to $\mu_{strength}$) are extracted from Table E-3 to quantify $\mu_{strength}$ associated with collapse probabilities of 0.7.

Table E-3 Table of Collapse Probabilities (from ATC-78-1) for Pure Frame Buildings

m		3	4	5	6	7	10
V_p/V_n	0.7	0.14	0.38	0.62	0.79	0.89	0.98
	0.8	0.15	0.42	0.67	0.83	0.92	0.99
	0.9	0.22	0.50	0.73	0.87	0.94	0.99
	1.0	0.30	0.60	0.80	0.91	0.96	1.00
	1.1	0.47	0.76	0.90	0.96	0.99	1.00
	1.2	0.67	0.88	0.96	0.98	0.99	1.00
	1.3	0.85	0.97	0.99	1.00	1.00	1.00

Combinations of V_p/V_n and $\mu_{strength}$ that produce collapse probabilities of 0.7 are combined from IDA analysis of the buildings in Table E-1 and Table E-3, and plotted in Figure E-2. Limiting values of $\mu_{strength}$ are defined based upon V_p/V_n such that buildings with $\mu_{strength}$ values greater than the limiting values are expected to have collapse probabilities greater than 0.7 and are classified as exceptionally weak. For pure frames with $V_p/V_n < 0.6$ in the critical story, $\mu_{strength}$ must be greater than 5.5 to be considered exceptionally weak. Pure frames with $V_p/V_n > 1.5$ must have $\mu_{strength} > 2$. Note that these criteria imply that buildings with shear-critical columns that are weak may be identified as exceptionally weak even though a frame of similar strength with flexure-critical columns is not. Linear interpolation is permitted for frames with $0.6 \leq V_p/V_n \leq 1.5$. Limiting values of V_p/V_n and $\mu_{strength}$ are shown by the solid line in Figure 2.

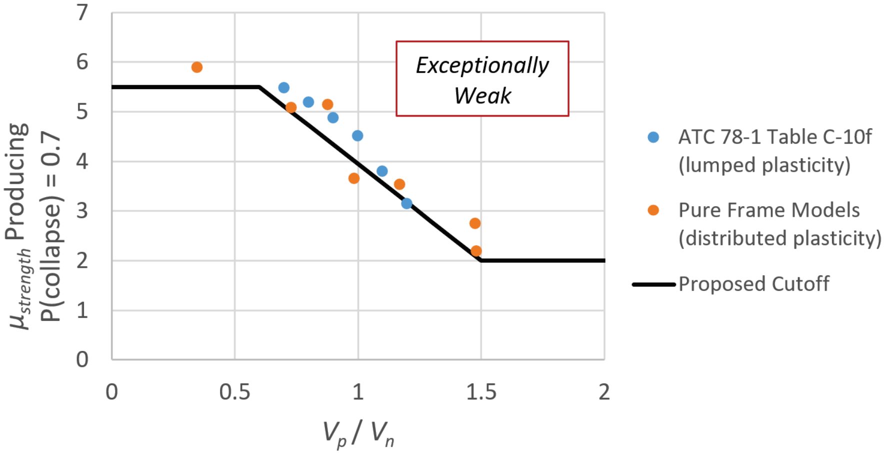

Figure E-2 Limiting values of V_p/V_n and $\mu_{strength}$ that identify exceptionally weak pure frame buildings.

E.6 Investigation of Criteria for Exceptionally Weak Frame-Wall Buildings

Collapse fragilities for the studied frame-wall buildings are plotted in Figure E-3 as a function of $S_a(T_1)$ and as a function of $\mu_{strength}$. Recall that $\mu_{strength}$ is defined as $[S_a(T_1)/(V_y/W)]C_m$. Plotting the frame-wall collapse fragilities in terms of $\mu_{strength}$ (Figure E-3b) has less scatter between buildings than collapse fragilities plotted in terms of $S_a(T_1)$ (Figure 3a), and is therefore a better predictor of collapse. Based upon this observation, $\mu_{strength}$ is chosen as the indicator used to identify exceptionally weak frame-wall buildings. As described in Section E.5, this measure is consistent with criteria used to identify exceptionally weak frame buildings.

The amount of wall present in a building relative to the total floor area, measured by the *WI*, is depicted by the color in Figure E-3. When collapse fragilities are plotted against $S_a(T_1)$ (Figure E-3a), the results show an increasing probability of collapse with decreasing *WI* (i.e., decreasing contribution of walls to the structural response). Interestingly, when plotted as a function of $\mu_{strength}$ (Figure E-3b), buildings with large *WI* have larger collapse probabilities for a given $\mu_{strength}$ value than buildings with small *WI*.

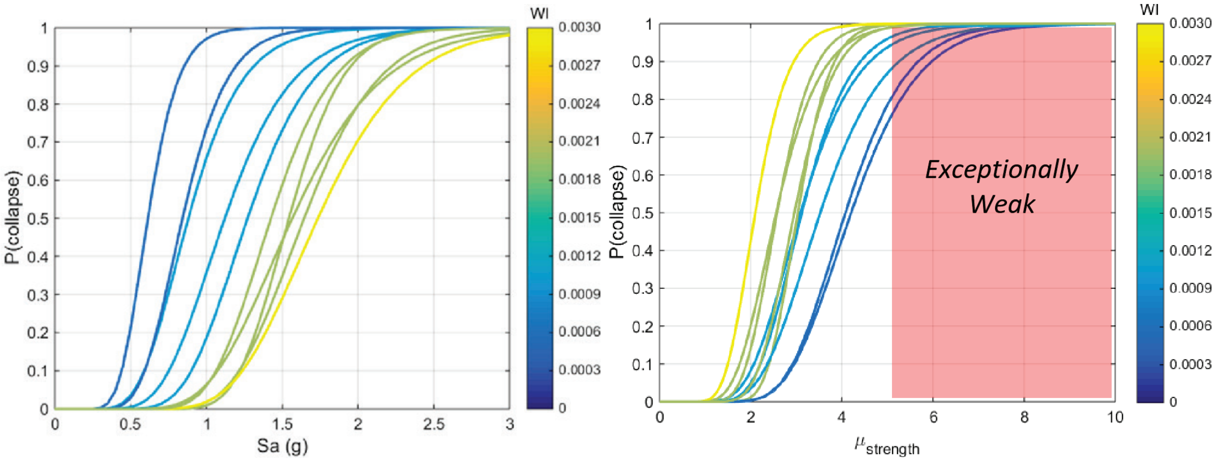

(a) (b)

Figure E-3 Collapse fragilities for frame-wall buildings plotted as a function of: (a) spectral acceleration at each building's fundamental period, shown in Table E-2; and (b) $\mu_{strength}$.

Figure E-4 explores the reason collapse fragilities for buildings with large *WI* values appear more vulnerable than buildings with small *WI* values when plotted against $\mu_{strength}$. As expected, the addition of structural walls to a building with a fixed floor plan increases the building strength, or V_y/W, (Figure E-4a), and increases the collapse resistance of the building (Figure E-4b) due to the additional strength provided by the walls. However, the addition of structural walls to a system increases V_y/W more rapidly than the collapse resistance of the building is increased, as shown in Figure E-4c. As a result, in Figure E-3b, the collapse fragilities of buildings with large *WI* values to plot on the left of buildings with small *WI* values. Therefore, the *WI* trends are counteracted by the use of the imperfect demand-to-capacity ratio of $\mu_{strength}$.

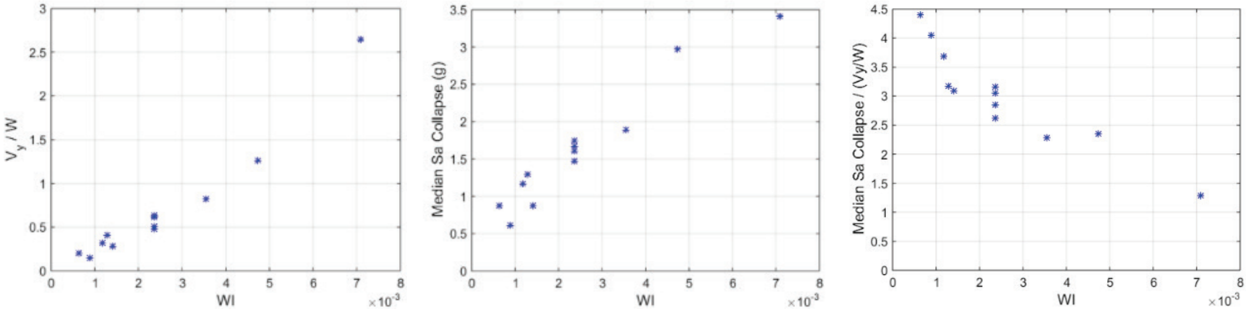

(a) (b) (c)

Figure E-4 Relationship between *WI* and: (a) V_y/W; (b) median collapse $S_a(T_1)$; and (c) the ratio of median collapse $S_a(T_1)$ to V_y/W.

As a result of the trends observed in Figure E-3b and the desire to use $\mu_{strength}$ as an indicator for exceptionally weak buildings, the limiting value identifying exceptionally weak buildings was selected based upon frame-wall models with small *WI* values. This simplification was deemed appropriate because buildings with many walls (high *WI*) will perform better than buildings with fewer walls (Figure E-3a) and are unlikely to be exceptionally weak. $\mu_{strength}$ of 5.5 corresponds with a collapse probability of 0.7 for buildings with *WSI* from 0.0003 to 0.0006. Therefore, $\mu_{strength}$ of 5.5 was used as a criterion for identifying exceptionally weak frame-wall buildings, as shown in Figure E-3b.

Unfortunately, trial evaluations on real, or realistic, test-case frame-wall buildings with varying amounts of concrete walls present in the buildings, did not show a good correlation between *WI* values and the building ratings resulting from a full application of the methodology. As a result, the wall index, *WI*, did not prove to be a reliable indicator of performance, and use of *WI* values to identify *exceptionally high seismic risk buildings* was abandoned.

Appendix F

Beam-Column Joints

F.1 Introduction

The behavior of beam-column connections in older-type construction has been widely studied (Moehle, 2014). Of particular interest are:

- Performance of connections with discontinuous beam bottom longitudinal reinforcement
- Strength of joints in beam-column connections without joint transverse reinforcement
- Effect of joint eccentricity on joint and column behavior
- Axial failure of beam-column connections

Each of these topics is reviewed in the following text.

F.2 Performance of Connections with Discontinuous Beam Bottom Longitudinal Reinforcement

Many older buildings have discontinuous beam bottom reinforcement that extends a short distance into the beam-column joint. A typical extension was 6 inches (the minimum permitted by the then-current ACI building codes). Short embedments of this type are insufficient to develop full strength of the embedded bars. However, the embedded bars are well confined by the surrounding concrete, so they are unlikely to cause a brittle splitting failure. For this reason, it is reasonable to calculate the bar stress capacity of the embedded bar in accordance with the provisions of ASCE 41-13, to apply this stress to calculate the moment strength of the beam for loading that puts the embedded bars in tension. This reduced moment strength usually can be sustained through relatively large rotations.

Figure F-1 plots measured strengths for interior beam-column joints without transverse reinforcement, both with and without continuous beam bottom longitudinal reinforcement. Cracking strength is notably affected by axial load, whereas ultimate strength is less affected by axial load. Reduced strength associated with discontinuous beam bottom longitudinal reinforcement is apparent.

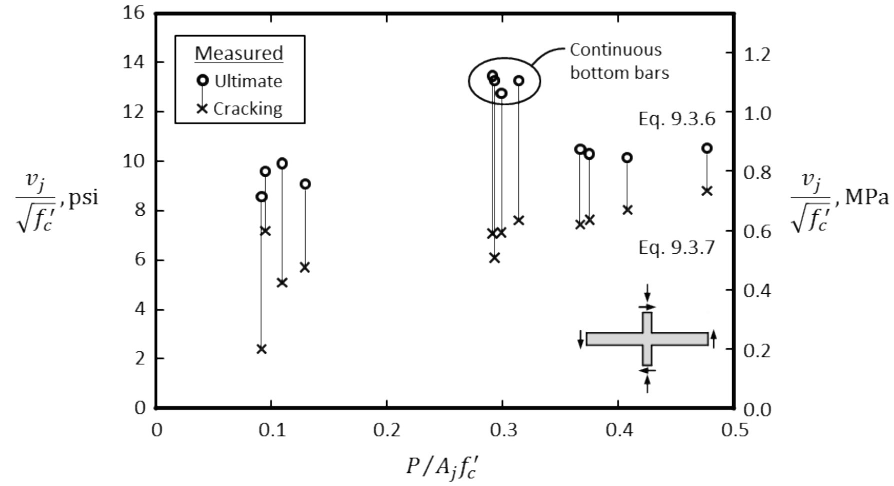

Figure F-1 Shear strength of unreinforced interior joints. Test specimens with continuous beam bottom bars are noted. All other test specimens have discontinuous bottom bars embedded in the joint. (Data from Pessiki et al., 1990, and Beres et al., 1992, after Moehle, 2014.)

F.3 Strength of Joints in Beam-Column Connections without Joint Transverse Reinforcement

Figure F-1 presents data for edge connections load parallel to the edge. Measured joint shear strength is at least $10\sqrt{f'_c}A_j$ (psi), with higher strengths noted for connections with continuous longitudinal reinforcement. These joints had aspect ratio $h_b/h_c \sim 1$.

Figure F-2 compares measured and calculated strengths for exterior connections with columns continuous through the joint, loaded perpendicular to the edge, including corner connections. Calculated strength is based on the ASCE 41 expression, that is, $V_n = 6\lambda\sqrt{f'_c}A_j$. In the tests, the joints failed without significant inelastic flexural response in the beams or columns. The comparison suggests (a) ASCE 41 calculated strengths are conservative; and (b) joint strength is a function of joint aspect ratio h_b/h_c.

The data from Figures F-1 and F-2 suggest an alternative form of joint shear strength could provide improved correlation between measured and calculated strengths. One suggested shear strength expression is:

$$V_n = 10\lambda\sqrt{\frac{h_c}{h_b}}\sqrt{f'_c}\ \text{(psi)}$$

where:

$$h_c/h_b \le 1.0$$

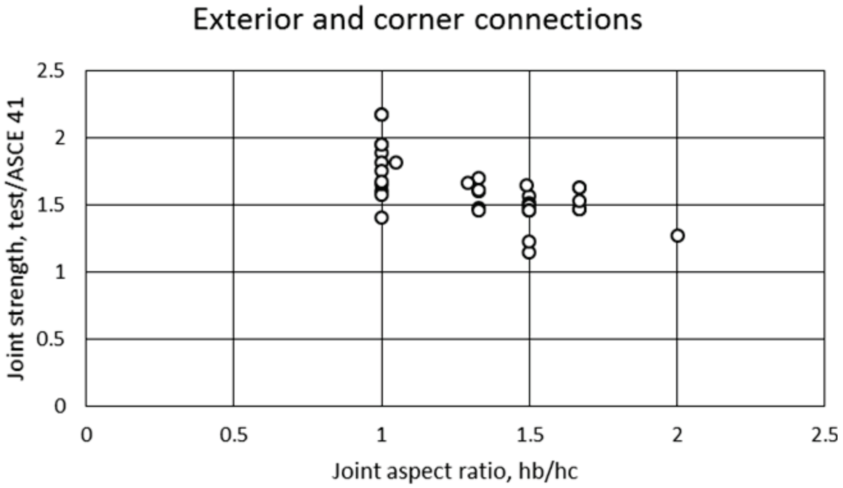

Figure F-2 Measured and calculated strengths for exterior joints loaded perpendicular to the edge, including corner joints. Data are for joints failing in shear without significant inelastic flexural deformation in adjacent beams or columns (data after Hassan, 2011).

Figure F-3 compares measured and calculated results, using the same test data shown in Figure F-2, and using the revised expression to calculate shear strength. Overall correlation is improved considerably.

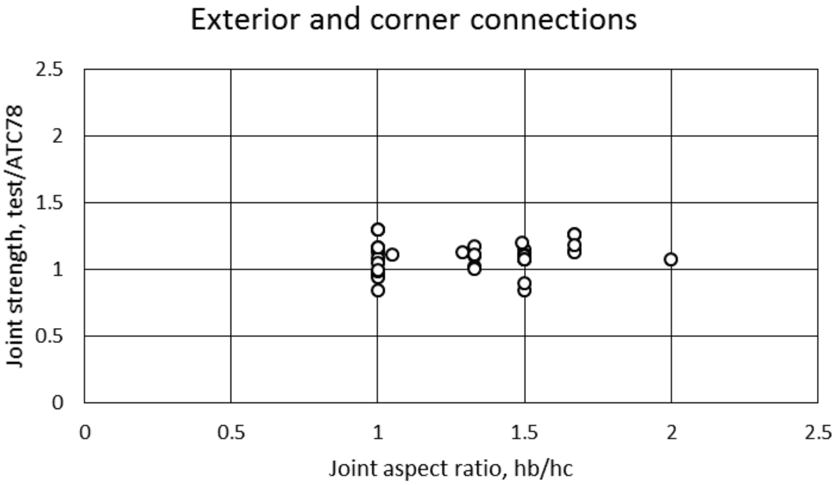

Figure F-3 Measured and calculated strengths for exterior joints loaded perpendicular to the edge, including corner joints. Data are for joints failing in shear without significant inelastic flexural deformation in adjacent beams or columns (data after Hassan, 2011).

F.4 Effect of Joint Eccentricity on Joint and Column Behavior

Several researchers have studied behavior of eccentric beam-column joints, that is, joints for which centerlines of beams and columns framing into the joint are eccentric. LaFave et al. (2005) provide a summary of the principal findings.

Force transfer at an eccentric beam-column joint is complicated by the misalignment of the framing members. Figure F-4(a) depicts the local force transfer mechanism. The diagonal struts forming within the joint depth are oriented in opposite directions on opposite sides of the joint, suggesting the occurrence of joint torsion, which could reduce joint strength. The localization of force transfer at the intersection between the beam and column results in localization of joint damage [Figure F-4(b)], which also could justify reduced joint strength for eccentric connections. Some writers have also identified the possibility of column torsion, and have suggested that this column torsion could reduce column shear strength due to the superposition of shear stresses from shear and torsion. This effect appears to be ameliorated by the presence of a floor slab, which can resist any torsional moments through in-plane bending of the diaphragm (Figure F-4(c)). Physical evidence of column damage due to induced torsion is limited, and does not appear to justify consideration in a rapid evaluation method, if at all.

LaFave et al. (2005) recommend including the effect of joint eccentricity by defining the joint area $A_j = h_c(b_c + b_w)/2$. None of the joints reviewed by LaFave et al. had beams extending outside the plan of the column. Therefore, it is recommended that b_w not exceed the width of the beam web that is contained within the outline of the column dimensions.

Available test data do not show significant reduction in deformation capacity of eccentric beam-column joints compared with otherwise equivalent concentric joints.

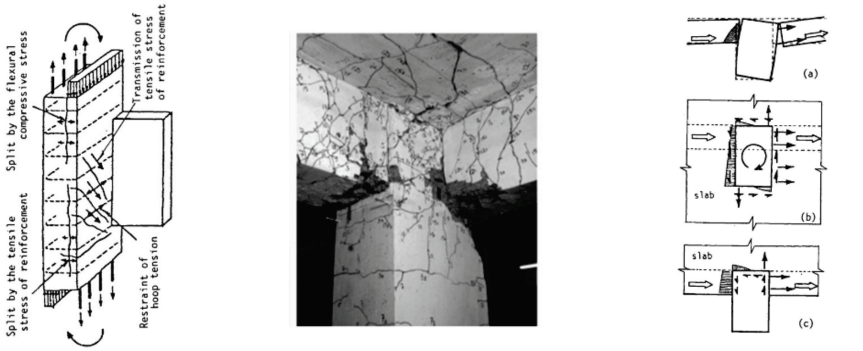
Split by the flexural compressive stress
Transmission of tensile stress of reinforcement
Split by the tensile stress of reinforcement
Restraint of hoop tension
(a)
slab
(b)
slab
(c)

Joh, Goto, Shibata, ACI SP 123
(a) Force transfer

Canbolat and Wight, ACI, 2008
(b) Localized damage

Joh, Goto, Shibata, ACI SP 123
(c) Slab reduces the effect

Figure F-4 Force transfer at eccentric beam-column connections.

F.5 Axial Failure of Beam-Column Connections

Several buildings that collapsed in past earthquakes have shown evidence of severe joint damage. On the other hand, physical evidence of building collapses having been triggered by joint failures is less clear. Laboratory studies also have not provided convincing proof that building collapse can be triggered by joint failure. One of the reasons for absence of evidence may be that laboratory tests may not be subjecting beam-column connections to sufficiently severe loadings because of limitations in testing equipment capabilities.

In one study, Hassan (2011) subjected a series of corner beam-column joints to severe lateral and axial loading histories. The joints eventually showed signs of axial shortening through the joint at late stages of testing, although sudden axial failure was never obtained. Hassan also collected laboratory test data from tests conducted by other researchers, delineating, for final loading stages, those tests that showed signs of axial shortening within the joint and those that did not. Figure F-5 plots the results. The bilinear relation divides those connections showing axial shortening from those not showing axial shortening. According to Hassan, connections falling below the bilinear relation can be considered safe from axial collapse, while those falling above the relation might be suspected of triggering axial collapse.

At the time of this writing, the writers are not aware of any test data providing physical evidence that axial failure can be triggered by failure of edge or interior connections.

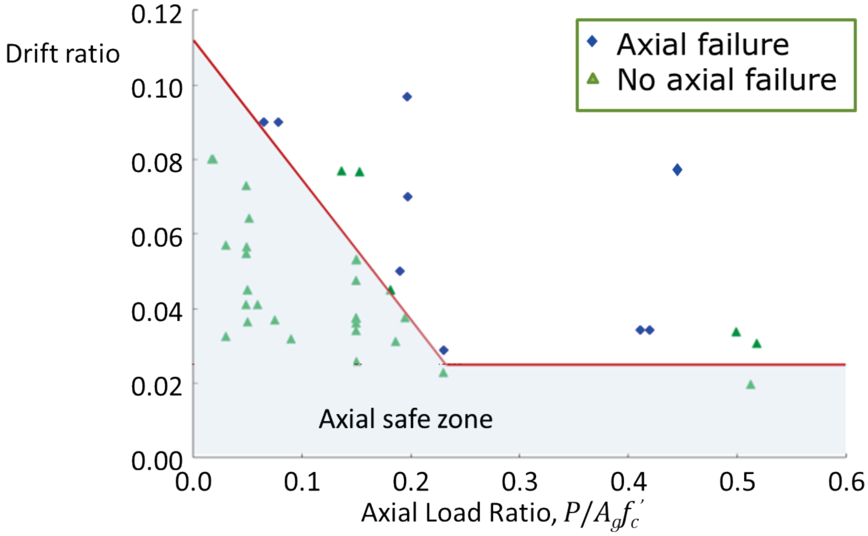

Figure F-5 Maximum observed drift ratios and axial load ratios of corner beam-column connections (after Hassan, 2011).

Appendix G

Effective Fundamental Period

ASCE/SEI 7 and ASCE/SEI 41 present equations for fundamental period of frame buildings as a function of either height or number of stories. These equations are useful for identifying a conservative set of lateral forces for strength design, as emphasized in ASCE/SEI 7 and the linear methods of ASCE/SEI 41. The methodology presented in this report places more emphasis on estimation of lateral drifts rather than forces. Furthermore, it is intended to be applied to individual buildings whose strength may vary widely from the minimum base-shear strength required by ASCE/SEI 7. Given these different objectives, it was desirable to develop alternative period equations.

G.1 Frame Buildings

As a starting point, an analytical study was undertaken to identify the effect of building strength and height on building period (Renouard, 2014). A series of four-, eight-, and 12-story tall frame buildings with uniform rectangular plans were designed for gravity loads plus a set of lateral loads having an inverted triangular pattern. Building heights were 46 feet, 90 feet, and 134 feet respectively. Target building base-shear strengths were $0.05W$, $0.10W$, $0.15W$, and $0.25W$, where W corresponds to the building weight.

Each building was assumed to have two perimeter moment-resisting frames in each direction designed to resist all the earthquake forces. This assumption allowed for simplified analysis models in which the buildings were modeled as two-dimensional frames, with each perimeter frame providing half the required lateral resistance. Each frame included six bays. Furthermore, the buildings were assumed to have symmetric plans so that the building response to lateral forces included minimal plan torsion.

Each building was designed using an algorithm that sized the columns for target longitudinal reinforcement ratios of 0.01, 0.015, 0.018, 0.02, 0.025, or 0.03. Beam sizes were varied to obtain typical reinforcement ratios. The following parameters were used to better emulate actual construction and ease member size selection:

- Column and beam sizes were changed every two stories.
- Column size was limited to no smaller than 12″ × 12″.

- Beam depth-to-width ratio was limited to no greater than 1.4.

All building models were analyzed using the following nominal material properties:

- Reinforced Concrete Strength, $f_c' = 3000$ psi
- Steel Reinforcement Grade 60, $f_y = 60$ ksi
- Reinforced Concrete modulus of elasticity, $E_c = 3122$ ksi
- Steel Reinforcement modulus of elasticity, $E_s = 29000$ ksi

The building models were further idealized as two-dimensional fishbone models (Luco et al., 2003). This simplified model lumps column and beam stiffnesses by condensing all the columns of a story into one column and all the beams into one rotational beam spring. This method allows for a simplified building model with a greatly reduced number of degrees of freedom. Figure G-1 depicts the planar frame and fishbone idealizations for a four-story building.

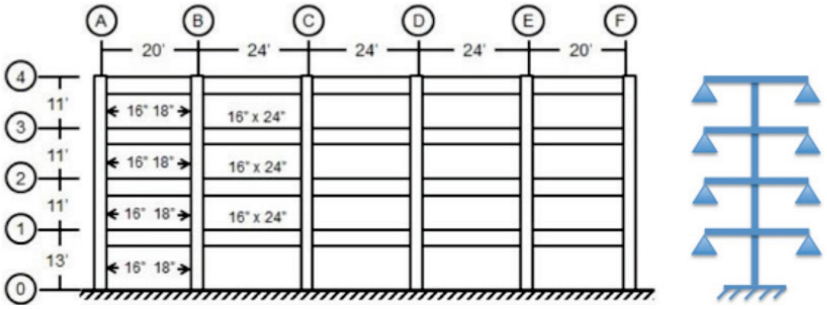

Figure G-1 Example planar frame and fishbone idealizations of a four-story building.

The analytical models consist of line elements representing the flexibilities of beams and columns rigidly connected to zero-length joints. Flexibilities considered flexural, shear, and axial forces. Each element has flexural stiffness properties calculated from the member cross section, using the effective moment of inertia as proposed by Elwood and Eberhard (2009), which considered the effect of reinforcement slip from beam-column joints. It was assumed the beams were cast monolithic with the slabs. Therefore, the moment of inertia of the beams with slabs was assumed to be equal to twice the moment of inertia of the beams if there was no slab. The structures were assumed to have fixed base foundations.

Figure G-2 depicts the calculated results for all buildings studied. Values of percent strength refer to the V_{base}/W ratios of the buildings considered. As expected, period increases with increasing height and decreases with increasing strength. The target column longitudinal reinforcement ratio has some effect on period, but the effect is less important than other variables.

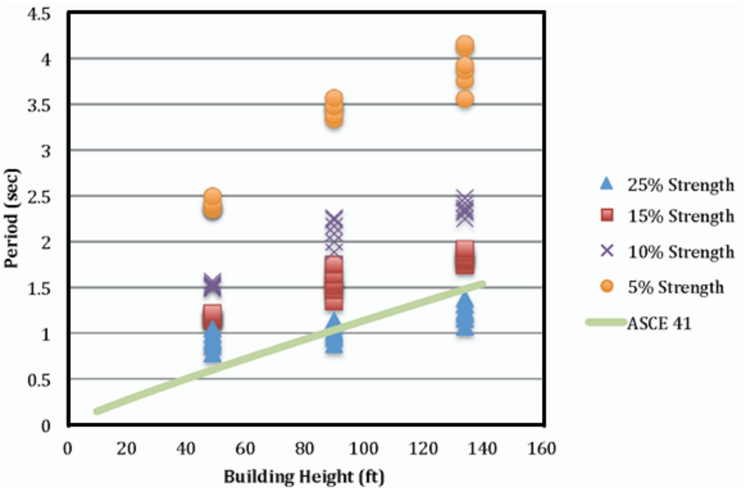

Figure G-2 Calculated periods for all buildings studied.

ASCE/SEI 41 uses the following expression to approximate the fundamental period of a concrete frame:

$$T = 0.018 h_n^{0.9} \tag{G-1}$$

where h_n = height to the roof level n in feet. This expression is plotted in Figure G-2. It provides nearly a lower bound to the calculated data, as might be expected for an equation intended to produce a conservative (high) set of lateral forces.

An approximation to the calculated results is given by:

$$T = 0.07\sqrt{h_n}\frac{1}{\sqrt{\left(V_y/W\right)}} \tag{G-2}$$

where V_y = base-shear strength. Figure G-3 plots results of Equation G-2. Figure G-3 also plots data reported by Goel and Chopra (1997). Note that the data of Goel and Chopra are for responses to moderate ground motions and likely do not include data for response into the inelastic range.

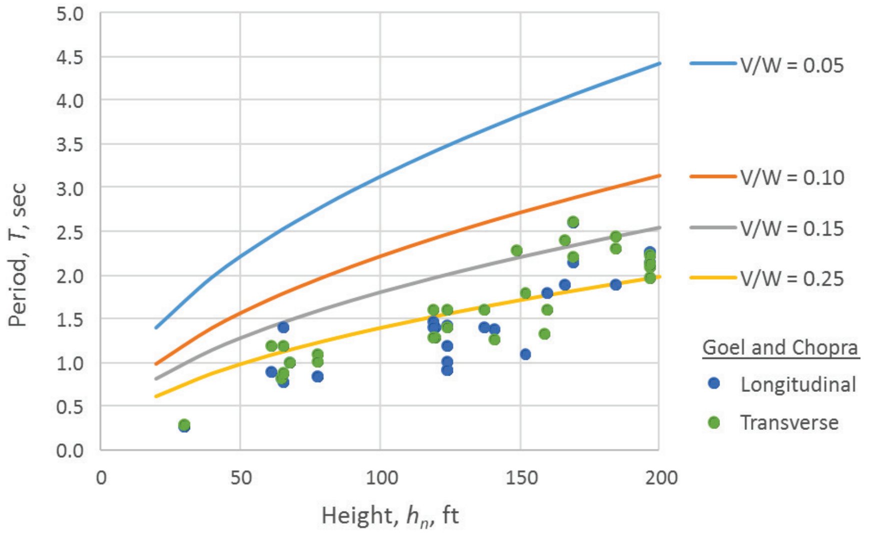

Figure G-3 Comparison of calculated periods.

G.2 Frames with Deep Spandrels

Frames with deep spandrel beams will have reduced fundamental periods relative to typical frames because deep spandrels are stiffer than typical beams and deep spandrels reduce the effective length of the columns. The effect on overall building period will depend on the fraction of frames in the building that have deep spandrel beams.

To estimate the effect of deep spandrel beams on building period, it was first assumed that the stiffness of a frame is inversely proportional to the cube of the column height. Consequently, the stiffness of a frame with deep spandrel beams would be approximately $(l / l_u)^3$ times that of a bare frame, where l is the floor-to-floor column height and l_u is the clear height of the column. A small parameter study was carried out in which the fraction of spandrel frames was varied from one-half to one-third of the total number of frames. Relative stiffnesses of the combined frame and deep spandrel systems were calculated, and period was assumed to vary inversely with the square root of the system stiffness. From this study, it was observed that the period of the building with deep spandrels was approximately (l_u / l) times the period of the same building without deep spandrels.

G.3 Pier-Spandrel Systems

An analytical study was undertaken to investigate the effect of geometry of a building with pier-spandrel system on its vibration period. Important geometry parameters include the building height, dimensions of deep spandrels and piers, and the ratio of wall thickness to the floor dimension transverse to direction of vibration. It was assumed that minimum reinforcement was present, so this was not considered a major variable. A series of four-, eight-, and twelve-story tall archetype pier-spandrel wall buildings with uniform rectangular plans was developed based on actual buildings with large openings in shear walls. The typical story height was 12 feet, resulting in building height, h_n, of 48 feet, 96 feet, and 144 feet, respectively. The seismic mass of the building was determined from the combination of ($DL + 0.25LL$), where DL was taken as 200 psf and LL was 40 psf for typical office use.

This type of building typically has perimeter walls extending full length of the building on all building sides. Therefore, two-dimensional simplified analytical models of pier-spandrel systems were developed in the computer software ETABS (Computers and Structures, Inc.) with the assumption that each perimeter system provides half the required lateral resistance with no resistance provided by interior framing. Additionally, the building plans were assumed to be symmetric such that the effects of torsion on the building response were negligible. Results of a two-dimensional model were compared with results from a full three-dimensional archetype including interior frames to demonstrate that the two-dimensional idealization produced calculated period within a few percent of the calculated period for the complete three-dimensional building.

The building models were further idealized as single-bay models (Luco et al., 2003). Figure G-4 displays the planar pier-spandrel wall system and the model idealization for a four-story building. Figure G-5 illustrates the definition of the main variables considered in the parametric study.

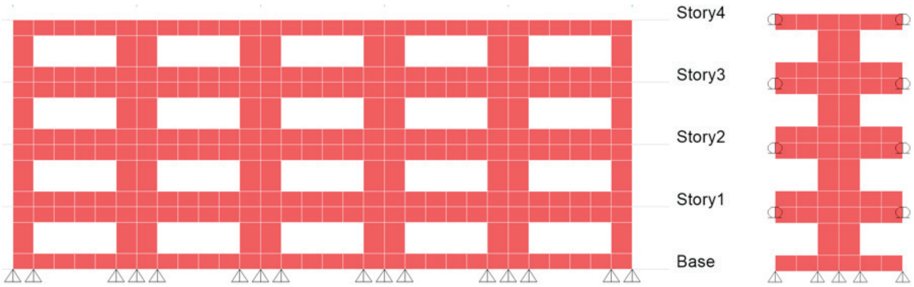

Figure G-4 Example of pier-spandrel system and model idealizations of a four-story building.

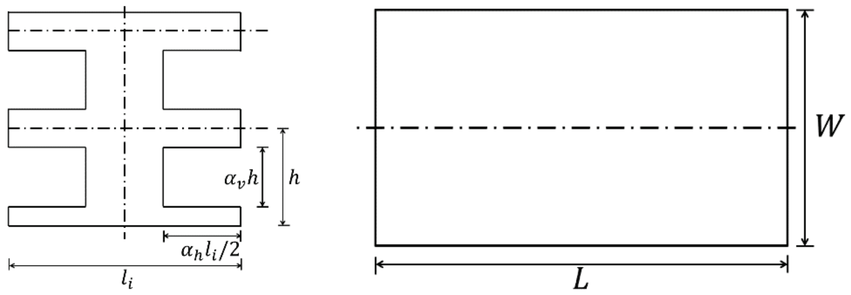

(a) (b)

Figure G-5 Illustration of variables and constants in the parametric study: (a) Elevation view; (b) Typical floor plan view.

For each single-bay model representing an archetype building with certain height, a_v and a_h were varied between 0.4 to 0.8 while the bay width, l_i, was varied from 18 feet to 30 feet. The seismic mass imposed on each level of the simplified model was calculated as the load combination ($DL + 0.25LL$) multiplied by the bay width in the direction of vibration and half the building dimension in the transverse direction, W. Story height h = 12 feet, floor plan dimension W = 120 feet, wall thickness t = 12 inches, concrete compressive strength f_c' = 5,000 psi, elastic modulus of concrete E_c = 4,030 ksi, and DL = 200 psf and LL = 40 psf were kept constant for all single-bay models.

Piers, spandrels, and joint panels are modeled by thin-shell element with flexural and shear stiffnesses of $0.5E_cI_g$ and $0.3E_cA_g$, respectively. The flexural stiffness is in accordance with ASCE 41 and reflects a reduction in stiffness associated with cracking. The shear stiffness is reduced to three-quarters of the shear stiffness in ASCE 41 to reflect the effect of modest shear cracking on effective period—the reduction factor was established after discussion with a sample of practicing engineers who have analyzed these buildings by ASCE 41, review of test data, and judgment of the authors. The structures were assumed to be fixed to the base foundations.

Figure G-6 presents the calculated periods for all building models studied on the y-axis. Key variables were identified and organized in an algebraic form that would facilitate implementation in the present methodology, and a nonlinear regression analysis was carried out to minimize the sum of squared error to determine the final form of an equation that best fit the calculated periods. The results given by the resulting equation are shown on the x-axis. The coefficient of determination (R-squared) was 0.9332.

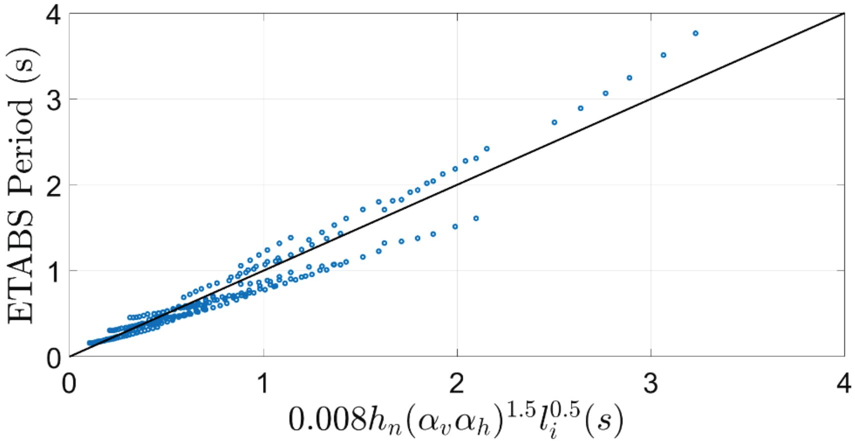

Figure G-6 Comparison of calculated periods.

As the gross moment of inertia $I_g = td^3/12$ and gross area $A_g = td$ of the cross section are linear functions of the wall thickness, t, the global stiffness of the analytical models is known to be linearly proportional to the wall thickness. The seismic mass of the building can be assumed to be approximately linearly proportional to the floor plan dimension, W, such that the seismic mass of a typical floor can be expressed by $(DL + 0.25LL)WL$. Given that vibration period generally has the form $T_e = \sqrt{M / K}$, it is evident that the period is proportional to $\sqrt{W / t}$. With W and t normalized by 120 feet and 1 foot, respectively, and L already incorporated in analytical models by the bay width, l_i, the period equation derived from nonlinear regression analysis shown in Figure G-6 can be extended to apply to other buildings of different floor dimensions and wall thickness:

$$T_e = 0.008h_n(a_v a_h)^{1.5} l_i^{0.5} \sqrt{\frac{W/120}{t/1}} \tag{G-3}$$

Resulting in the final form of the period equation:

$$T_e = 0.001h_n \left(\frac{A_{opening}}{A_{we}}\right)^{1.5} \left(l_i \frac{A_{base}}{A_{wp}}\right)^{0.5} \tag{G-4}$$

$$\text{for } 0.15 \le \left(\frac{A_{opening}}{A_{we}}\right) \le 0.5$$

where:

h_n = height of building (ft)

$A_{opening}$ = total area of openings in all pier-spandrel walls in direction of vibration (ft^2)

A_{we} = total area of all pier-spandrel walls, measured in elevation, including openings, in direction under consideration (ft^2)

l_i = typical or average bay width measured center-to-center of wall piers, (ft)

A_{base} = WL = typical floor plan area (ft^2)

A_{wp} = total area of pier-spandrel wall, measured in plan, including openings, in direction under consideration, = $2tL$ assuming two walls of thickness t and length L in each direction, (ft^2)

$\alpha_v\alpha_h$ = A_{base}/A_{wp} can be shown on average from elevation view of walls

The limits on ($A_{opening}/A_{we}$) are based in part on the limits of the variables considered in this study and in part to prevent use of the equation for buildings whose large openings result in the building being more like a frame system than a pier-spandrel system.

G.4 Wall and Frame-Wall Buildings

Vibration periods of wall buildings are affected by building height, base-shear strength, and wall aspect ratio. Goel and Chopra (1998) present data and an analytical study of vibration periods of wall buildings that provides the starting point for developing a period equation suitable for use in this methodology.

The Goel and Chopra (1998) approach incorporates the assumptions of full-height, fixed-based walls with rectangular cross sections and with flexibility contributions from shear and flexure, resulting in a theoretical expression for vibration period. The expression was adjusted to better match measured periods from wall buildings shaken by earthquakes, leading to the following equations as a lower-bound estimate of period:

$$T = 0.0019 h_n \frac{1}{\sqrt{C_w}} \tag{G-5a}$$

$$C_w = \frac{100}{A_B} \sum_{i=1}^{x} \left(\frac{h_n}{h_i}\right)^2 \frac{A_i}{\left[1 + 0.83\left(\frac{h_i}{l_{wi}}\right)^2\right]} \tag{G-5b}$$

where:

A_B = area of base of structure, ft^2

A_i = web area of shear wall i in ft^2

l_{wi} = length of shear wall i in ft

h_i = height of shear wall i in ft

x = number of shear walls in the building effective in resisting lateral forces in the direction under consideration

The form of Equation G-5 is based on Goel and Chopra (1998), but is taken from ASCE/SEI 7, which adopted the formula as one method for estimating vibration period of a wall building.

In this methodology, Equation G-5 is further modified by increasing the coefficient from 0.019 to 0.026 to obtain a period more representative of a heavily cracked wall. Note that Goel and Chopra (1998) identified the coefficient 0.026 as an upper bound to the measured wall periods from their database. Additionally, it is assumed that ratio $h_n/h_i = 1$.

Results of Equations G-2 and G-5 were compared for a small sample of typical building geometries to verify that, for a given height and base-shear strength, the calculated period of wall buildings is less than the calculated strength of frame buildings.

For the purposes of determining the wall strength index in Chapter 5, a simpler alternative equation for buildings with walls is provided.

$$T_e = 0.015 h_n^{0.75} \tag{G-6}$$

Equation G-6 is only to be used for determination of the wall strength index. It is similar in form to that provided in ASCE/SEI 41, and was found to result in an approximate period that was close to effective periods estimate from pushover analyses for a set of frame-wall building models used in other studies (e.g., wall strength index studies presented in Appendix D).

Appendix H

Development of Procedures to Estimate Story Drift Demands

H.1 Introduction

In this methodology, the collapse potential of an existing reinforced concrete building is estimated by comparison of the story drift demands and story drift capacities of critical structural components. The procedure to estimate story drift demands in each principal framing direction is summarized as follows:

- Estimate the effective fundamental vibration period of the building, T_e, along a principal framing direction.
- Determine the equivalent single-degree-of-freedom (SDOF) drift demand δ_{eff} at an elevation h_{eff} that corresponds to the effective modal height of the fundamental vibration mode of the building, using a response spectrum representing the seismic hazard.
- Given the drift demand at the effective height and the building configuration, estimate the distribution of story drift demands, δ_i, over the building height based on the building configuration and strength distribution.

Appendix G describes the development of equations to estimate the effective fundamental period, T_e. Section H.2 describes studies to evaluate the method used to calculate the SDOF drift demand δ_{eff}. The balance of this appendix describes studies to explore methods to estimate story drift demands.

H.2 Studies of the SDOF Drift Demand

H.2.1 Basic Procedure to Calculate SDOF Drift Demand

The equivalent SDOF displacement at the effective modal height is determined using a procedure mirroring the target displacement approach of ASCE 41. Specifically, the displacement, δ_{eff}, is calculated as follows:

$$\delta_{eff} = C_0 C_1 C_2 S_a \frac{T_e^2}{4\pi^2} g \qquad \text{(H-1)}$$

where, C_0, C_1, and C_2 are coefficients from ASCE 41, S_a is the response spectrum pseudo acceleration at period T_e, and g is the acceleration of gravity. In Equation H-1, the quantity $S_a(T_e^2/4\pi^2)g$ is the spectral displacement, S_d, at period T_e. Coefficients C_0, C_1, and C_2 modify the spectral displacement to estimate the roof displacement considering the effects of several modeling and nonlinear behavioral factors.

Coefficient C_0 is a modification factor to relate spectral displacement of an equivalent single-degree-of-freedom (SDOF) system to the displacement at the effective height of the building multi-degree-of-freedom (MDOF) system. Values of C_0 were found to range from 0.9 to 1.1 for typical buildings. Given the small variability of C_0, this term was set equal to 1.0 and dropped from the equation in the methodology.

Values of h_{eff} were calculated for typical multi-story frame or frame-wall buildings. It was found that a value of $0.7h_n$ is a close approximation of the actual value of h_{eff}, except $h_{eff} = 1$ for one-story buildings.

Coefficient C_1 and C_2 are adopted directly from ASCE 41.

H.2.2 Comparison with Results of Nonlinear Response History Analyses

To check the accuracy of Equation H-1, incremental dynamic analyses were carried out on a series of 4, 6, 8, and 12-story frames designed to be representative of older concrete buildings. Figure H-1 illustrates the configuration of an exterior frame. Interior frames were designed as gravity-only frames. The frames included columns whose failure mode was controlled by either inelastic flexure or by shear and axial failure. The frames were proportioned to have resistance in proportion with demands from an inverted triangular lateral loading, except weak stories were introduced into some of the frames for the purposes of this study. See Galanis and Moehle (2015) for additional details.

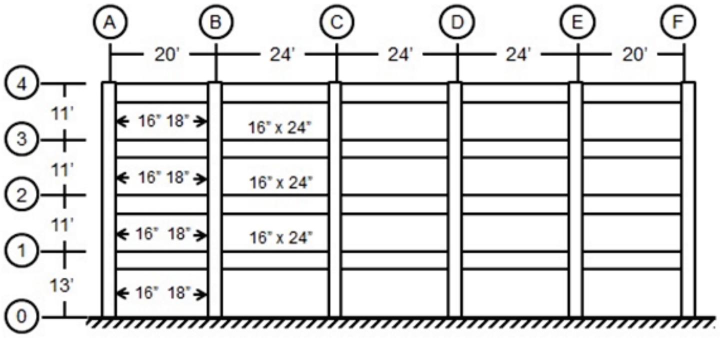

Figure H-1 Schematic elevation of the simulated 4-story frames.

The study confirmed that cyclic degradation does not appreciably affect the predictive accuracy of Equation H-1 for buildings having vibration periods exceeding 1.0 second. Furthermore, the study showed that Equation H-1 is more accurate for buildings with damage distributed over height of the building and less accurate for buildings with a weak story leading to concentrated damage. Some results of the study are summarized in the following paragraphs.

Table H-1 presents the coefficients C_0, C_1, and C_2 employed in Equation H-1 for the studied frame buildings.

Table H-1 Coefficients C_0, C_1, and C_2 of the Studied Buildings

Parameter	4-Story	6-Story	8-Story	12-Story
Period T_e (sec)	1.14	1.38	1.62	1.95
C_0	1.09	1.05	1.11	0.94
C_1	1.00	1.00	1.00	1.00
C_2	1.00	1.00	1.00	1.00

Table H-2 presents the mean ratios of displacements of the 6-story idealized building from the inelastic dynamic analyses and those obtained from Equation H-1, all reported at the effective modal height, h_{eff}. In Table H-2, $\sum M_c/\sum M_b$ refers to the ratio of the sum of column nominal moment strengths to the sum of beam nominal moment strengths at each beam-column joint, and V_p/V_n refers to the ratio of column plastic shear demand (determined as twice the nominal moment strength M_n divided by the column clear height l_u) divided by the column nominal shear strength calculated in accordance with ASCE 41 with cyclic strength degradation factor $k = 1$. Similar results were found for the 4, 8, and 12-story frames.

Table H-2 Average Ratio of (Maximum Displacement at Effective Modal Height of Non-Linear Analysis) / (Estimated Displacement at Effective Modal Height) for Different V_p/V_n and M_c/M_b Ratios of the 6-Story Idealized Building

	V_p/V_n			
$\Sigma M_c/\Sigma M_b$	0.6	0.8	1.0	1.2
0.6	0.79	0.81	0.90	1.00
0.8	0.79	0.81	0.89	1.00
1.0	0.79	0.81	0.88	0.98
1.2	0.85	0.80	0.81	0.91
1.4	1.03	0.90	0.85	0.83
1.6	1.18	1.03	0.94	0.87
1.8	1.30	1.15	1.02	0.95

It was of interest to establish whether building lateral strength would affect the accuracy of displacement calculations. The preferred method to carry out this investigation would be to design several buildings with different lateral strengths and observe the effect on displacement estimation. For the present study, however, an alternative approach was used that made use of readily available data. Specifically, a building frame was subjected to ground motions scaled to progressively increasing intensity, and the displacements obtained from nonlinear dynamic analysis for each scaling factor were compared with the results of Equation H-1. The process was repeated for each of 44 different earthquake ground motions from FEMA P-695 (FEMA, 2009). The results are presented as a function of the effective demand to capacity ratio, $\mu_{strength}$, defined as $\mu_{strength} = S_aW/\ V_y$, where V_y equals the base shear strength calculated from nonlinear static analysis under lateral loads distributed in an inverted triangular pattern. Figure H-2 presents a sample of the results.

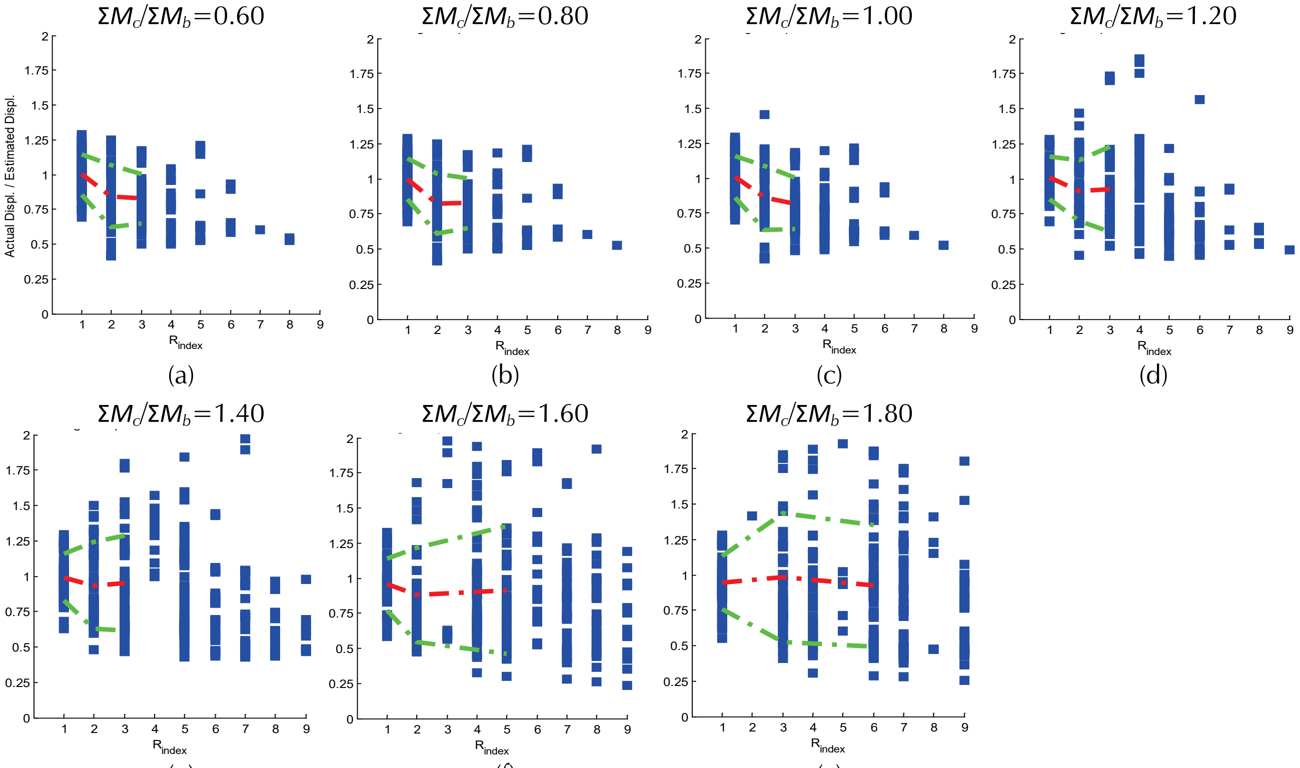

(a) (b) (c) (d)

(e) (f) (g)

Figure H-2 Ratio of (maximum displacement at effective modal height of non-linear analysis) / (estimated displacement at effective modal height) for different $\mu_{strength}$ values.

Each plotted point in Figure H-2 corresponds to a single earthquake ground motion at a particular scaling factor. The actual value of $\mu_{strength}$ in each case is truncated to an integer value for plotting (the integer values are designated R_{index} in Figure H-2). The red broken curve represents the mean of the results, and the green broken curves represent mean plus and minus one standard deviation of the results. The results indicate that, for most of the cases, Equation H-1 provides a conservative estimate of the expected maximum displacement at the effective modal height. The accuracy of the displacement estimation improves as the ratio of column to beam strengths increases.

H.3 Studies of the Story Drift Demand

H.3.1 Basic Procedure to Calculate Story Drift Demand

The basic procedure to calculate story drift demand is to use the assign a fraction of the total SDOF drift δ_{eff} to various stories based on the configuration and strength characteristics of the building, that is, story drift demand, δ_x, of story x is defined as:

$$\delta_x = \alpha_x h_{sx} \left(\frac{\delta_{eff}}{h_{eff}} \right) \leq \delta_{eff} \qquad \text{(H-2)}$$

where:

α_x = coefficient to modify story drifts at story x for building configuration and strength characteristics, and

h_{sx} = height of story x

Values of α_x are determined based on: (a) results of inelastic analyses of numerical models of multi-story buildings; and (b) judgment of the project team. The remainder of this section presents representative findings from the inelastic analyses.

H.3.2 Bare Frames

The values of coefficient α were explored for a series of uniform planar 4- to 12-story frames having nearly equal story height in every story, designed to have strength closely matching the demands associated with a load combination comprising: (a) gravity load; and (b) lateral load equal to $0.1W$ distributed in an inverted triangular load pattern. They were subjected to a series of 44 far-field ground motions with scaling factors gradually increased until collapse was obtained. Collapse was defined as either side-sway collapse when the maximum story drift ratio exceeded 10% or vertical collapse when more than 50% of the columns of a story failed from shear-induced axial load failure. Values of α were mined for a ground motion scaling factor slightly less than the factor required to achieve collapse.

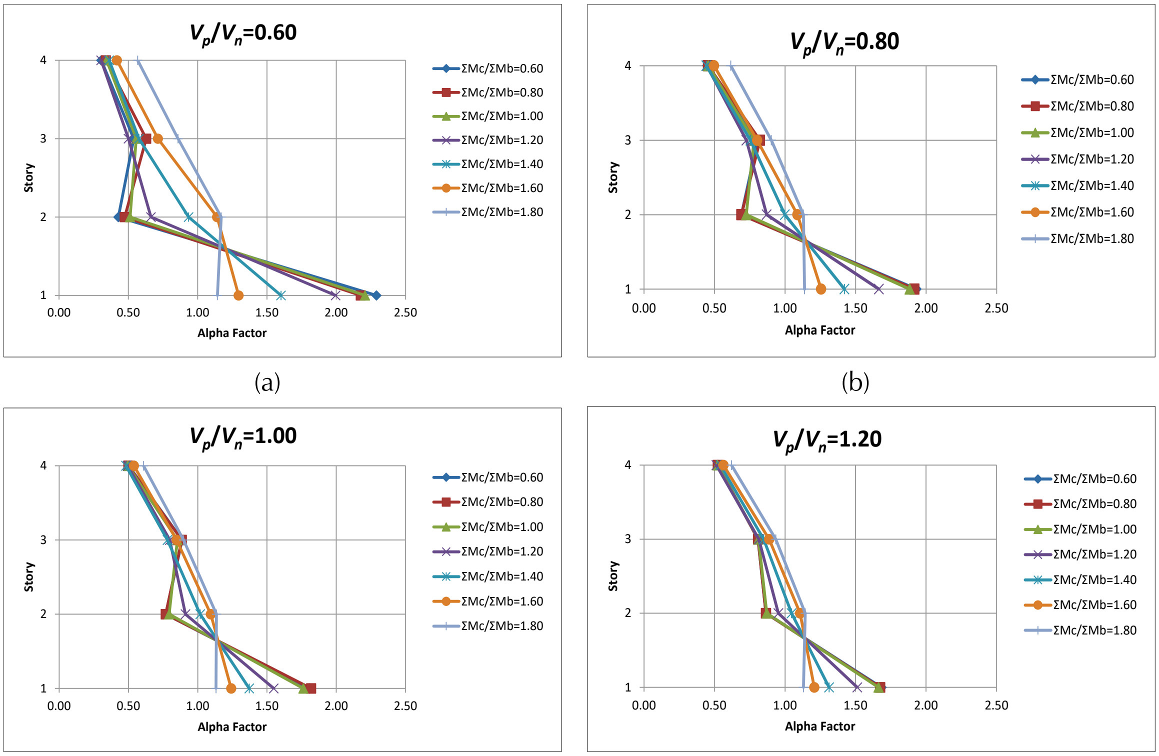

(a) (b)

(c) (d)

Figure H-3 Alpha factor story profiles for different variations of the 4-story idealized building.

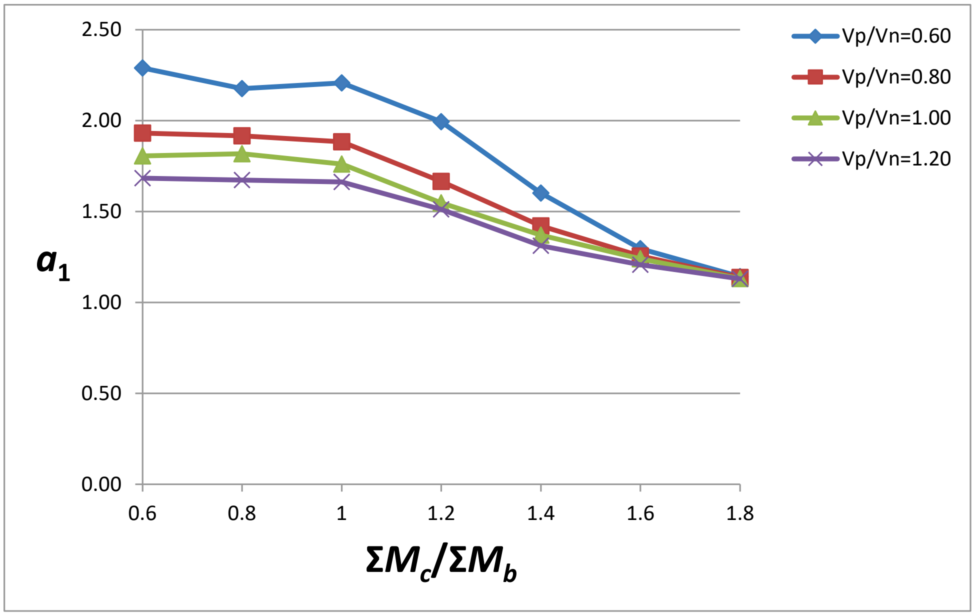

Figure H-4 Alpha factor mean value at 1st story for different variations of the 4-story idealized building.

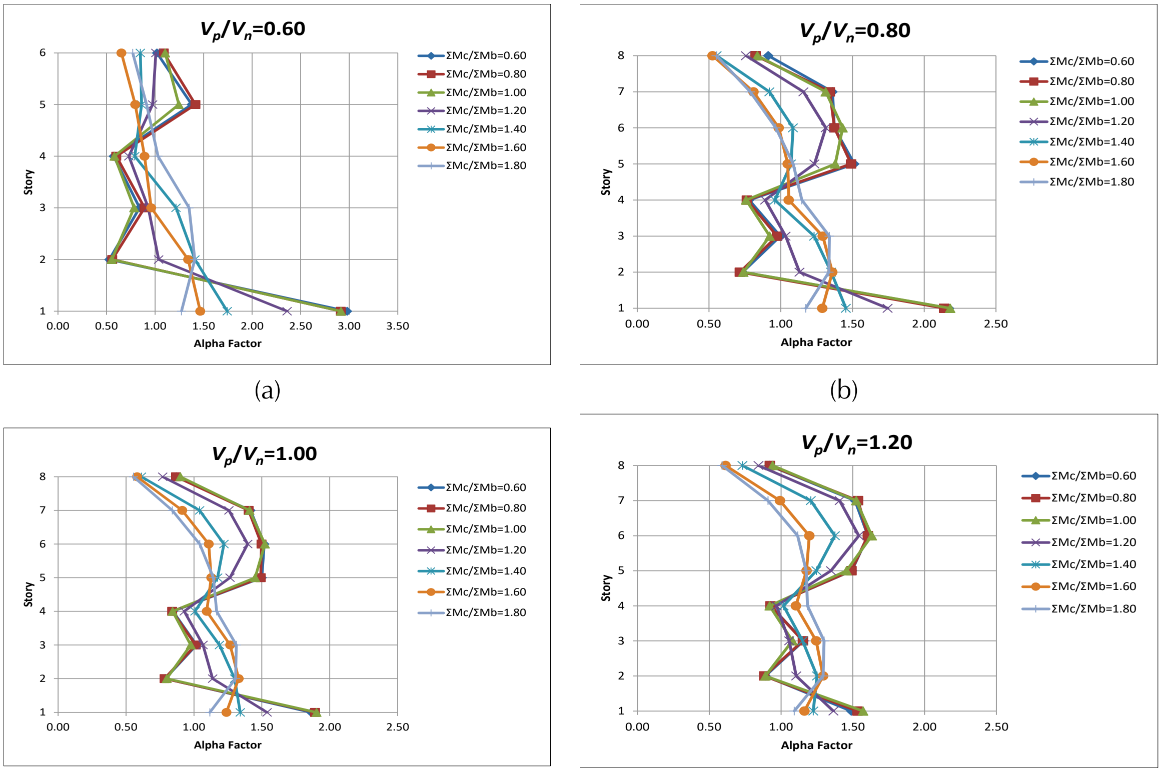

(a) (b)

(c) (d)

Figure H-5 Alpha factor story profiles for different variations of the 8-story idealized building.

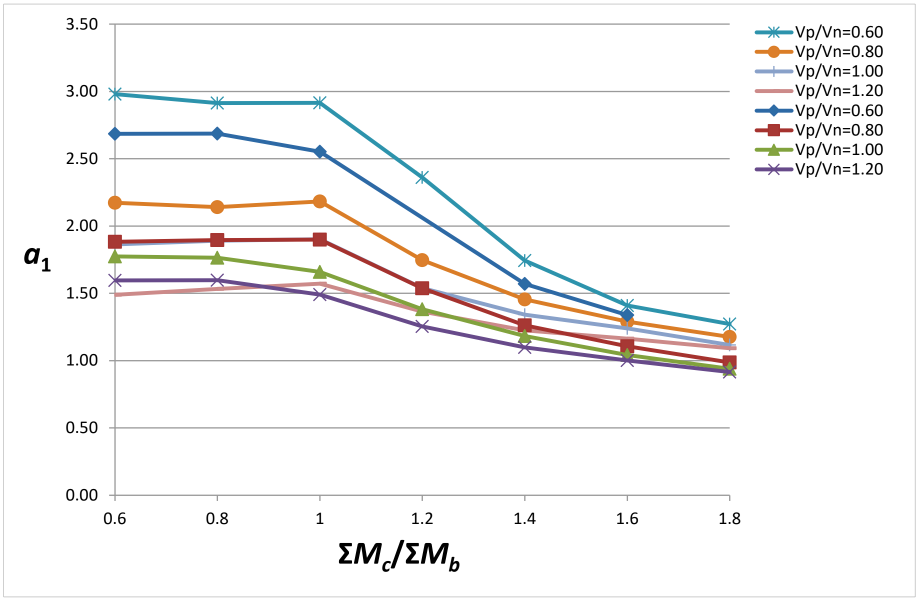

Figure H-6 Alpha factor mean value at 1st story for different variations of the 8-story idealized building.

For taller frames, failures for some ground motions occur in the first story while failures for different ground motions occur in upper stories. The latter failures occur due to apparent higher-mode effects. Because failure can occur in one of several stories, the mean drift ratio for any story ends up being dominated by several collapse realizations in which collapse occurs in other stories. Thus, although the alpha value correctly represents the mean, it does not provide a good indication of the story drift for those realizations in which collapse occurs in that story. To better understand this behavior, values of α were recalculated for each story considering only those cases in which that story was the one that collapsed. The mean values for α are provided in Table H-3.

Table H-3 Mean Values for α Factor for the 1st Story only for a 6-story Idealized Building with Critical 1st Story

	V_p/V_n			
$\Sigma M_c/\Sigma M_b$	0.6	0.8	1	1.2
0.8	2.56	2.04	1.91	1.93
1.2	2.16	1.53	1.55	1.69
1.8	1.75	1.61	1.46	1.34

Values of α were also explored for frames with weak stories at the first level or at other levels. For example, the 6-story building described previously was modified by increasing the strength of all the stories except the critical story by 50%. Two cases where explored. In the first case the critical story was located in the 1st story of the building, while in the second case the critical story was located in the 4th story.

For the frame with the critical first story, most of the inelastic deformation was concentrated in the first story for all combinations of variables, with results similar to those reported previously. For the frame with a critical fourth story, most of the inelastic deformation was concentrated in the fourth story (Figures H-7 through H-9).

Studies were also carried out to explore effects of inadequate lap length for column longitudinal reinforcement and light transverse reinforcement. Damage at such locations is likely to result in rapid loss of moment resistance at the location of the lap splice.

To study this behavior, a strength-degrading plastic hinge was introduced at assumed locations of lap splices in the model buildings. The inadequate lap splicing conditions were modeled according to the experimental results provided by Melek and Wallace (2004). The backbone rotational behavior of the plastic hinge modeling the inadequate lap splicing conditions is shown in Figure H-10.

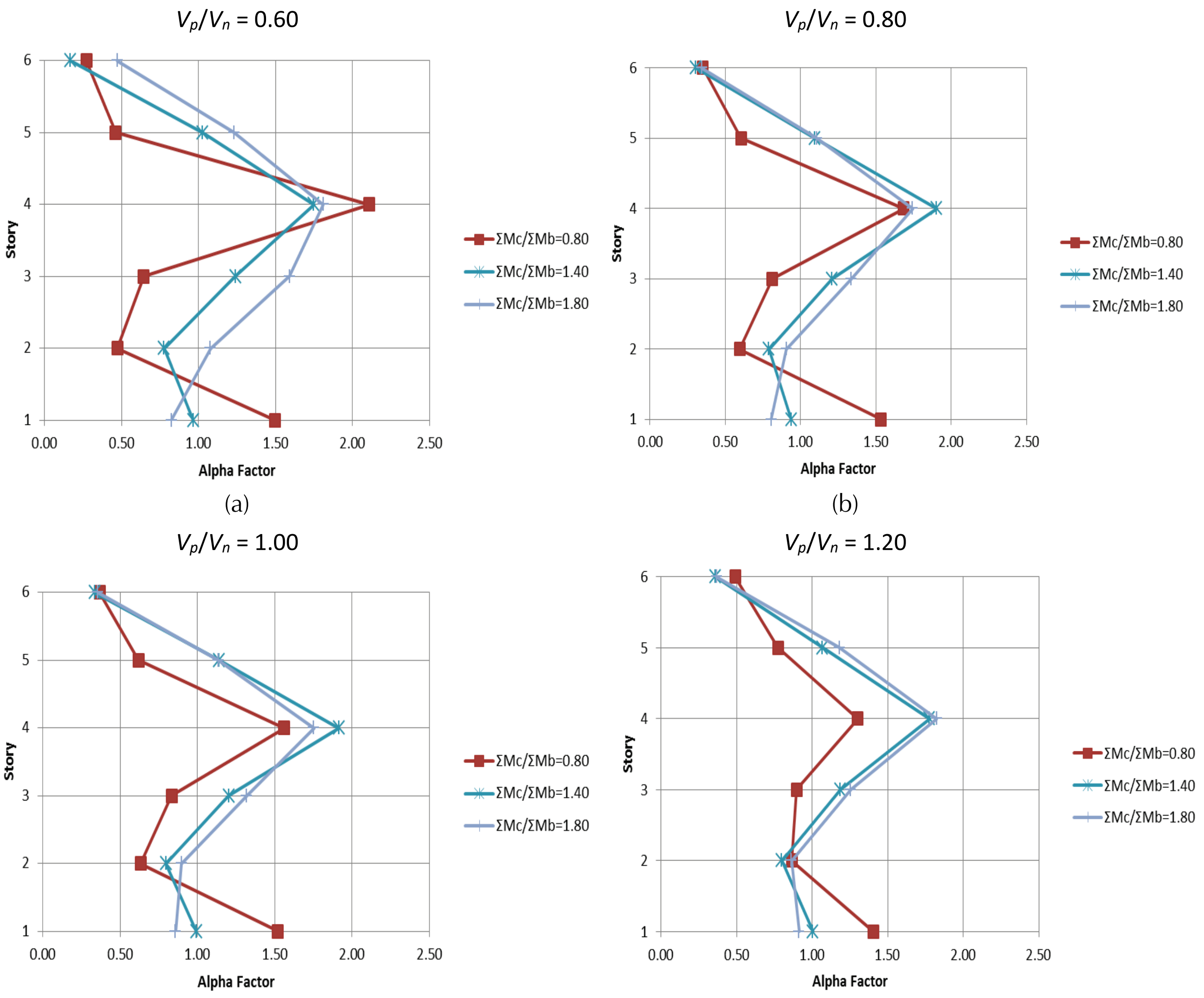

(a) (b) (c) (d)

Figure H-7 Alpha factor story profiles for different variations of the 6-story idealized building with a critical 4th story.

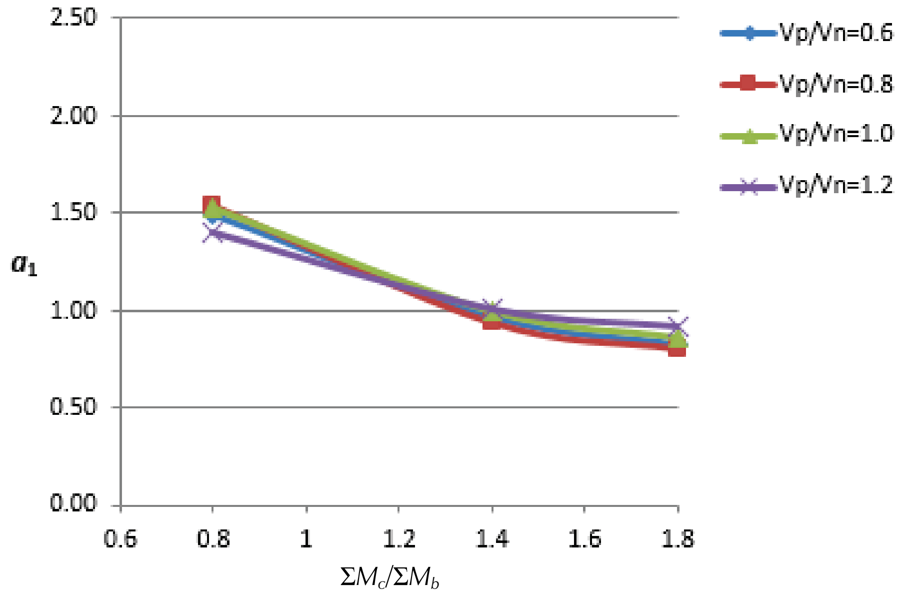

Figure H-8 Alpha factor mean value at 1st story for different variations of the 6-story idealized building with a critical 4th story.

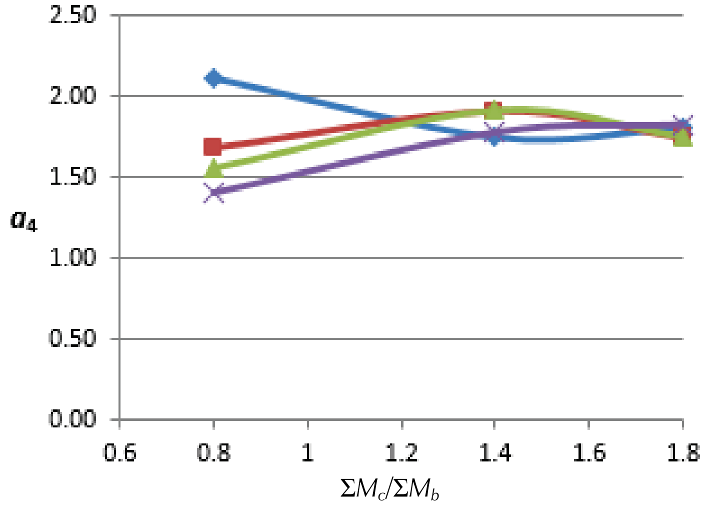

Figure H-9 Alpha factor mean value at 4th story for different variations of the 6-story idealized building with a critical 4th story.

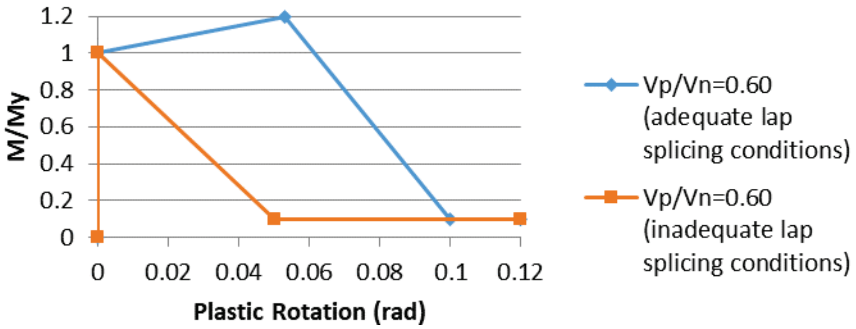

Figure H-10 Zero-length plastic hinge rotational behavior for adequate and inadequate lap splicing conditions.

Nonlinear dynamic analyses were conducted on model frames with flexure-critical columns ($V_p/V_n = 0.6$) including lap splices. Frames with different $\Sigma M_c/\Sigma M_b$ ranging from 0.8 to 1.6 were investigated. Figures H-11 through H-13 illustrate representative results for the case of lap splices introduced into the bottom of the 1st and 4th stories of the 8-story frame. The results demonstrate that, for the case of buildings with a tendency to form weak stories (that is, $\Sigma M_c/\Sigma M_b \leq 1.20$), the lap-splice has minimal effect. On the other hand, for cases where the building has a tendency for a more uniform drift profile (that is, $\Sigma M_c/\Sigma M_b > 1.20$) the lap splice magnifies the drift in the story containing the lap splice.

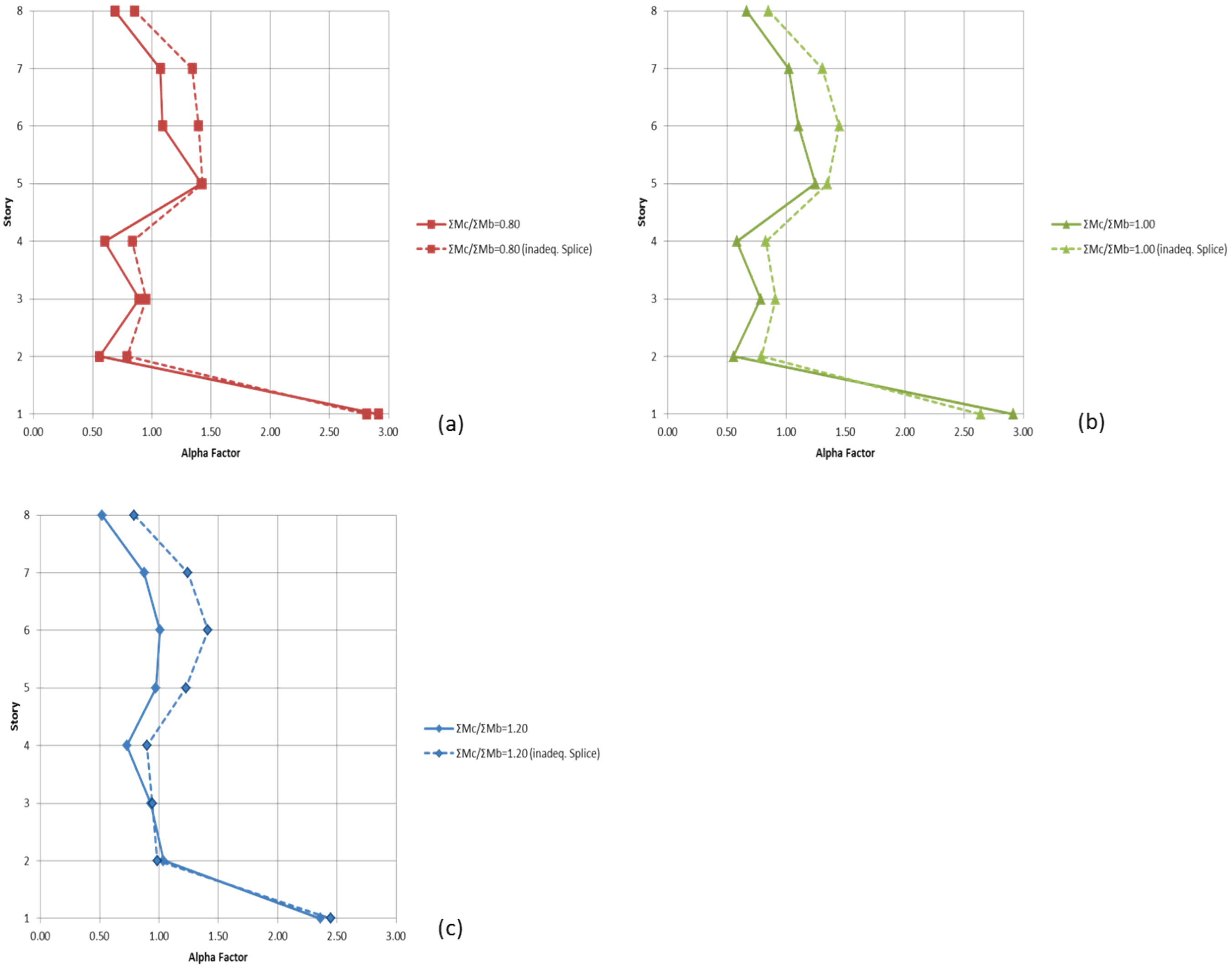

Figure H-11 Alpha factor story profiles for different variations of the 8-story building with and without inadequate lap-splicing conditions. ($V_p/V_n = 0.6$ in the above building variations)

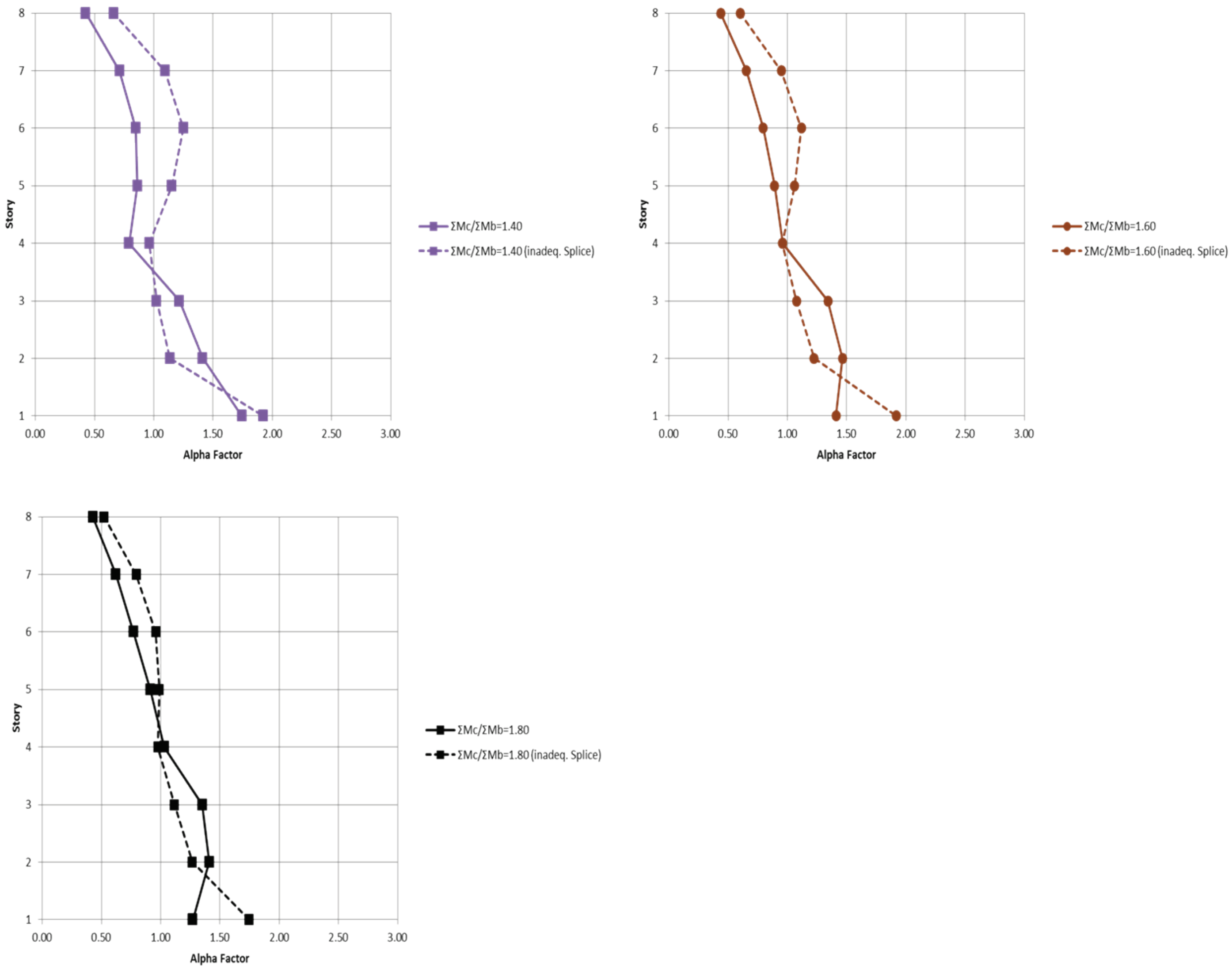

Figure H-12 Alpha factor story profiles for different variations of the 8-story building with and without inadequate lap-splicing conditions. (V_p/V_n = 0.6 in the above building variations.)

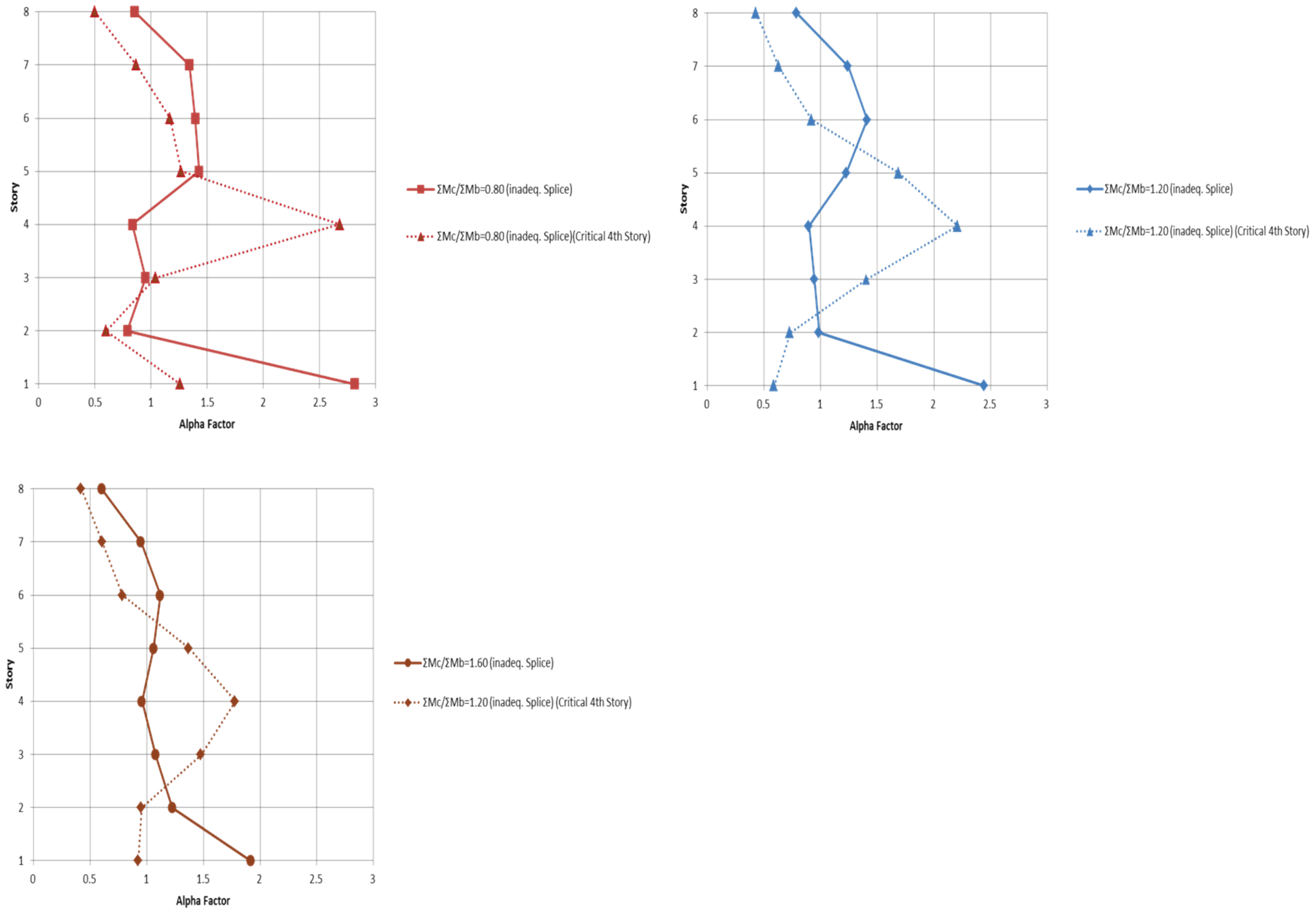

Figure H-13 Alpha factor story profiles for different variations of the 8-story building with inadequate lap-splicing conditions at the 1st and 4th critical story. (V_p/V_n = 0.6 in the above building variations)

The main observations are as follows:

- Very little amplification occurs where $V_p/V_n > 1.0$. This is apparently because only limited yielding of the column longitudinal reinforcement occurs in this case, such that the lap splices seldom fail.
- Relatively little amplification occurs for the case of $\Sigma M_c/\Sigma M_b \leq 1.2$, whereas greater amplification occurs for $\Sigma M_c/\Sigma M_b > 1.2$. Apparently, the former case corresponds to a case for which a weak story is already formed because of the weak columns, such that further reduction in strength due to splice failure does not significantly exacerbate the story failure. For the latter case, the presence of the lap splice results in reduced moment strength at one end of the column if the column yields, which tends to produce a weak-story condition. However, because the columns are stronger than the beams, the extent of column yielding is reduced, such that the amplification factor again is not much affected.

H.3.3 Frames and Walls

Several studies of frame-wall structures were carried out. Most of the analyses were inelastic static (pushover) analyses. Results were spot checked using inelastic dynamic analyses, with the conclusion that the static analyses adequately represented the key behaviors of interest. Only the static analysis results are shown here.

H.3.3.1 Case 1: Frame Plus One Continuous Wall

The values of coefficient α were explored for several 4- and 8-story frame-wall planar structures. Inelastic response in walls was restricted to inelastic flexure. Section H.2.2 introduced the archetype structure used for analysis of bare frames, also considered here. Additionally, to evaluate the sensitivity of values of coefficient α under variations in frame detailing, two other modifications of archetype frames were considered: modified frame 1 (cross section of first story beams assigned for all beams) and modified frame 2 (cross section of top story beams assigned for all beams). Analyzed cases included a frame plus one continuous rectangular wall, as presented in Figure H-14. Figure H-15 shows the typical wall cross section.

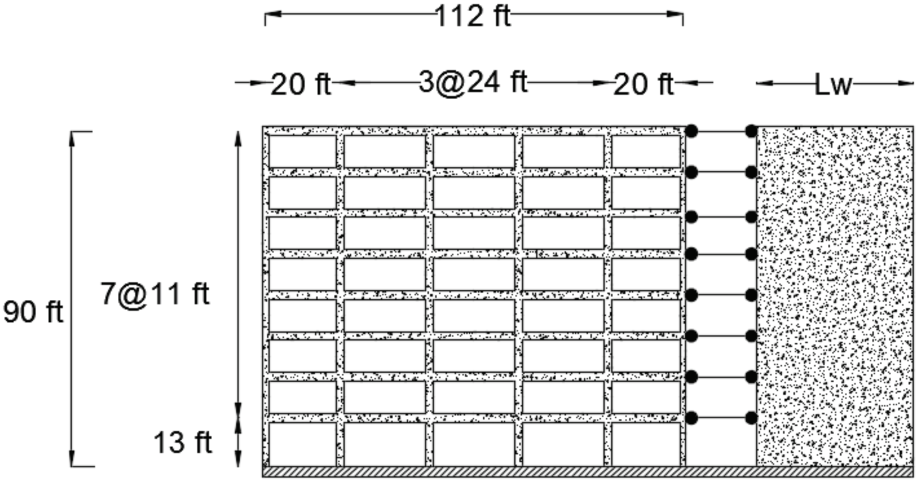

Figure H-14 Schematic elevation view of the simulated 8-story frame plus one rectangular wall.

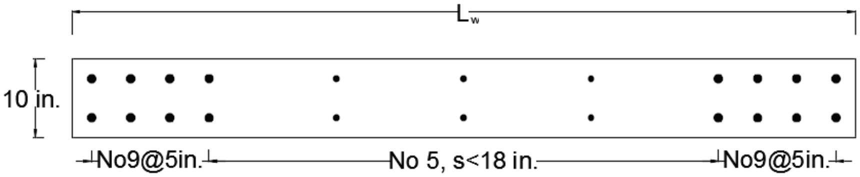

Figure H-15 Typical wall cross section.

Several values of wall length L_w were considered to evaluate the influence of the wall stiffness and strength on values of coefficient α. Beam gravity loads were those applied for analysis of bare frames. In walls, a constant gravity force was applied at each story to obtain an axial force demand at the base of $0.1f'_c A_g$, where A_g is the wall cross-sectional area.

The values of coefficient α were estimated for each case from nonlinear static analysis considering an inverted triangular force pattern, increased until collapse was obtained. Tables H-4 to H-6 present the values of coefficient α for 4-story frame-wall structures, where the parameter *index* is the ratio between the wall area and the total floor tributary area of the analyzed structure.

Table H-4 Values of Coefficient α Estimated from Pushover Analysis for a 4-Story Archetype Frame Plus One Continuous Wall

	Archetype Frame + Wall								
	Wall Length L_w (in.)								
	50	60	70	80	125	225	250	275	300
	Index = A_g / A_{floor}								
Story	0.0004	0.0004	0.0005	0.0006	0.0009	0.0016	0.0018	0.0019	0.0021
1	1.0	1.0	0.9	1.0	0.9	1.0	1.0	1.0	1.0
2	1.1	1.0	1.0	1.0	1.0	1.0	1.0	1.0	1.0
3	1.0	1.0	1.0	1.0	1.0	1.0	1.0	1.0	1.0
4	0.9	1.0	1.0	1.0	1.0	1.0	1.0	1.0	1.0

Table H-5 Values of Coefficient α Estimated from Pushover Analysis for a 4-Story Modified Frame I Plus One Continuous Wall

	Modified Frame I + Wall								
	Wall Length L_w (in.)								
	50	60	70	80	125	225	250	275	300
	Index = A_g / A_{floor}								
Story	0.0004	0.0004	0.0005	0.0006	0.0009	0.0016	0.0018	0.0019	0.0021
1	1.0	1.0	1.0	1.0	1.0	1.0	1.0	1.0	1.0
2	1.1	1.1	1.0	1.0	1.0	1.0	1.0	1.0	1.0
3	1.0	1.0	1.0	1.0	1.0	1.0	1.0	1.0	1.0
4	0.9	1.0	1.0	1.0	1.0	1.0	1.0	1.0	1.0

Table H-6 Values of Coefficient α Estimated from Pushover Analysis for a 4-Story Modified Frame 2 Plus One Continuous Wall

	Modified Frame II + Wall								
	Wall Length L_w (in.)								
	50	60	70	80	125	225	250	275	300
	Index = A_g / A_{floor}								
Story	0.0004	0.0004	0.0005	0.0006	0.0009	0.0016	0.0018	0.0019	0.0021
1	1.0	0.9	0.9	0.9	0.9	0.9	1.0	1.0	1.0
2	1.1	1.1	1.0	1.0	1.0	1.0	1.0	1.0	1.0
3	1.0	1.0	1.0	1.0	1.0	1.0	1.0	1.0	1.0
4	0.9	1.0	1.0	1.0	1.0	1.0	1.0	1.0	1.0

Figure H-16 presents a comparison between the collapse mechanism of a 4-story bare frame and the same frame with an added 50 in. wall.

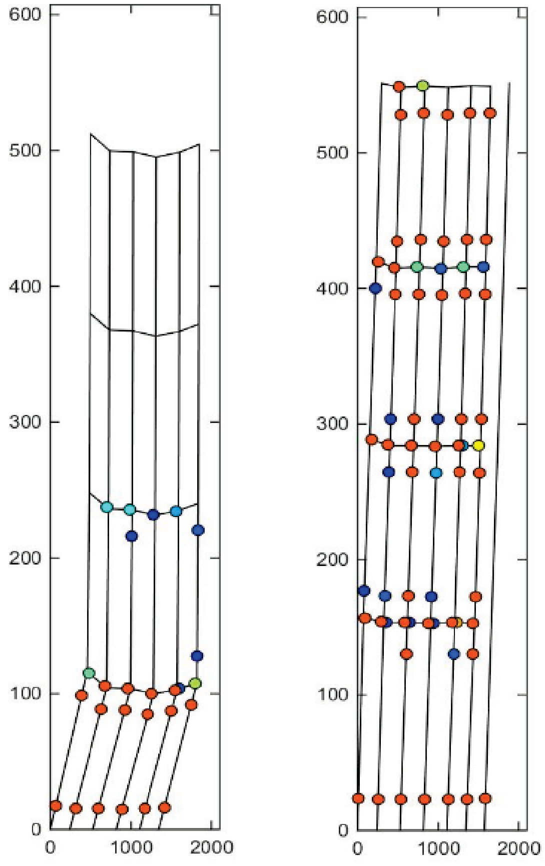

(a) (b)

Figure H-16 Collapse mechanism for a 4-story structure: (a) bare frame; (b) frame plus 50 in. wall.

Data presented in Tables H-4 to H-6 and Figure H-16 suggest that the presence of a short wall suffices to completely change the frame collapse mechanism, preventing soft story from occurring, and obtaining story drift ratios nearly equal to the roof drift ratio at all stories.

Tables H-7 to H-9 present the values of coefficient α for 8-story frame-wall structures.

Table H-7 Values of Coefficient α Estimated from Pushover Analysis for an 8-Story Archetype Frame Plus One Continuous Wall

	Archetype Frame + Wall									
	Wall Length L_w (in.)									
	50	60	70	90	100	125	175	225	275	300
	Index = A_g / A_{floor}									
Story	0.0002	0.0002	0.0002	0.0003	0.0004	0.0004	0.0006	0.0008	0.0010	0.0011
1	0.7	0.8	0.7	0.8	0.8	0.8	0.8	0.8	0.9	0.9
2	1.2	1.1	1.0	0.9	0.9	0.9	0.9	0.9	0.9	1.0
3	1.3	1.2	1.1	1.0	1.0	1.0	1.0	1.0	1.0	1.0
4	1.3	1.2	1.1	1.1	1.1	1.1	1.0	1.0	1.0	1.0
5	1.2	1.2	1.1	1.1	1.1	1.1	1.1	1.1	1.0	1.0
6	1.1	1.0	1.1	1.1	1.1	1.1	1.1	1.1	1.1	1.0
7	0.8	0.9	1.0	1.0	1.1	1.1	1.1	1.1	1.1	1.0
8	0.6	0.7	0.9	1.0	1.0	1.1	1.1	1.1	1.1	1.0

Table H-8 Values of Coefficient α Estimated from Pushover Analysis for an 8-Story Modified Frame I Plus One Continuous Wall

	Modified Frame I + Wall									
	Wall Length L_w (in.)									
	50.0	60.0	70.0	90.0	100.0	125.0	175.0	225.0	275.0	300.0
	Index = A_g / A_{floor}									
Story	0.0002	0.0002	0.0002	0.0003	0.0004	0.0004	0.0006	0.0008	0.0010	0.0011
1	1.1	1.1	1.0	0.8	0.8	0.8	0.8	0.9	0.9	0.9
2	1.5	1.3	1.2	1.0	1.0	1.0	0.9	0.9	1.0	1.0
3	1.6	1.4	1.3	1.1	1.1	1.0	1.0	1.0	1.0	1.0
4	1.3	1.3	1.2	1.1	1.1	1.1	1.0	1.0	1.0	1.0
5	1.0	1.1	1.1	1.1	1.1	1.1	1.0	1.0	1.0	1.0
6	0.7	0.8	0.9	1.0	1.0	1.1	1.1	1.1	1.0	1.0
7	0.4	0.5	0.7	0.9	1.0	1.0	1.0	1.1	1.0	1.0
8	0.3	0.4	0.6	0.9	1.0	1.0	1.0	1.1	1.0	1.0

Table H-9 **Values of Coefficient α Estimated from Pushover Analysis for an 8-Story Modified Frame II Plus One Continuous Wall**

	Modified Frame II + Wall									
	Wall Length L_w (in.)									
	50.0	60.0	70.0	90.0	100.0	125.0	175.0	225.0	275.0	300.0
	Index = A_g / A_{floor}									
Story	0.0002	0.0002	0.0002	0.0003	0.0004	0.0004	0.0006	0.0008	0.0010	0.0011
1	1.2	0.9	1.0	0.9	0.9	0.9	0.9	0.9	0.9	0.9
2	1.5	1.3	1.2	1.1	1.0	1.0	1.0	1.0	1.0	1.0
3	1.5	1.4	1.2	1.1	1.1	1.0	1.0	1.0	1.0	1.0
4	1.4	1.4	1.2	1.1	1.1	1.0	1.0	1.0	1.0	1.0
5	1.1	1.1	1.1	1.1	1.0	1.0	1.0	1.0	1.0	1.0
6	0.7	0.8	0.9	1.0	1.0	1.0	1.0	1.0	1.0	1.0
7	0.4	0.6	0.8	0.9	1.0	1.0	1.0	1.0	1.0	1.0
8	0.3	0.4	0.7	0.9	0.9	1.0	1.0	1.0	1.0	1.0

According to Tables H-7 to H-9, 8-story frames require a wall longer than 50 inches in length to obtain all values of coefficient α close to 1.

H.3.3.2 Case 2: Frame Plus Two Continuous Walls

For this case, the values of coefficient α were determined for several 4- and 8-story frame-wall planar structures, considering only the archetype frame plus two rectangular, flexure-controlled continuous walls. Figure H-17 shows a schematic elevation view of one of the analyzed structures. Considering cases including only walls with equal cross section, previously presented in Figure H-15. As before, constant gravity forces are applied at each story to obtain an axial force demand of $0.1f_c'A_g$ at the base of each wall, and the distributed gravity loads in beams are those used before for the analysis of bare frames.

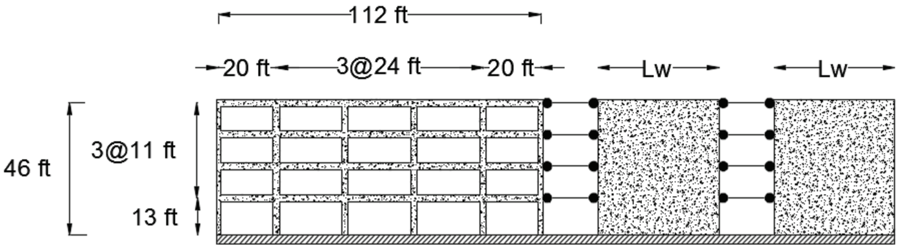

Figure H-17 Schematic elevation view of the simulated 4-story frame plus two rectangular walls.

Only a few cases are presented here to demonstrate that two short walls, 50 in. length, suffice to obtain all values of coefficient α equal to 1. Tables H-10 and H-11 present the calculated values from nonlinear static analysis.

Table H-10 **Values of Coefficient α Estimated from Pushover Analysis for a 4-Story Archetype Plus Two Continuous Walls**

	Archetype Frame + 2 Continuous Walls		
	Wall Length L_w (in.)		
Story	50	60	70
1	0.9	1.0	1.0
2	1.0	1.0	1.0
3	1.0	1.0	1.0
4	1.0	1.0	1.0

Table H-11 **Values of Coefficient α Estimated from Pushover Analysis for an 8-Story Archetype Plus Two Continuous Walls**

	Archetype Frame + 2 Continuous Walls		
	Wall Length L_w (in.)		
Story	50	60	70
1	1.0	1.0	1.0
2	1.1	1.0	1.0
3	1.1	1.0	1.0
4	1.0	1.0	1.0
5	1.0	1.0	1.0
6	1.0	1.0	1.0
7	0.9	1.0	1.0
8	0.9	1.0	1.0

H.3.4 Frames with Walls Discontinuous in the First Story

This section presents the values of coefficient α for several 4- and 8-story frame-wall planar structures, considering the archetype frame plus two walls of equal cross section. One of the walls is continuous and the other one is discontinuous in the first story, where two non-ductile columns (18×18 in. cross section with 1% longitudinal steel ratio) support it. Figure H-18 presents and schematic elevation view of one of these cases.

Regarding gravity loads, the beams and the continuous wall are treated as in the previous sections. For the discontinuous wall, a constant gravity force is applied at each story to obtain an axial force demand at each of the supporting columns of $0.15 f'_c A_g$, where A_g is the column area.

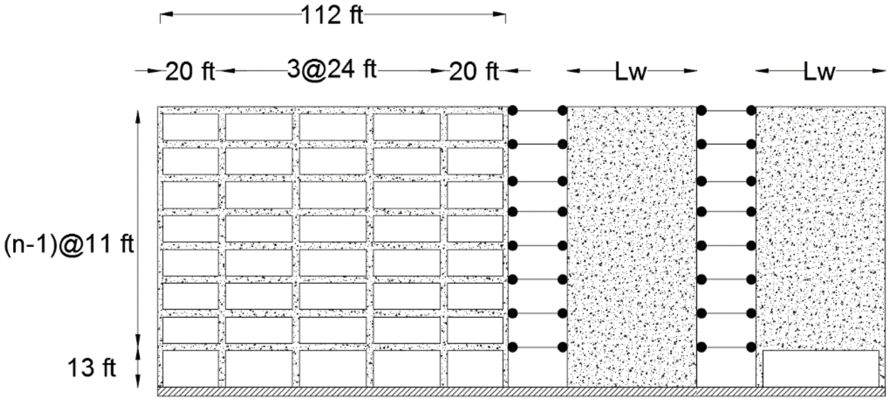

Figure H-18 Schematic elevation view of the simulated 8-story frame plus two rectangular walls, one discontinuous in the first story.

Tables H-12 and H-13 present the values of coefficient α calculated for these cases.

Table H-12 Values of Coefficient *α* Estimated from Pushover Analysis for a 4-Story Archetype Plus One Continuous Wall and One Discontinuous Wall in the First Story

Story	Archetype Frame + Continuous Wall + Discontinuous Wall					
	Wall Length L_w (in.)					
	50	60	70	80	90	100
1	1.0	1.0	1.0	1.0	1.0	1.0
2	1.0	1.0	1.0	1.0	1.0	1.0
3	1.0	1.0	1.0	1.0	1.0	1.0
4	1.0	1.0	1.0	1.0	1.0	1.0

Table H-13 Values of Coefficient *α* Estimated from Pushover Analysis for an 8-Story Archetype Plus One Continuous Wall and One Discontinuous Wall in the First Story

Story	Archetype Frame + Continuous Wall + Discontinuous Wall					
	Wall Length L_w (in.)					
	50	60	70	80	90	100
1	1.0	1.0	1.0	1.0	1.0	1.0
2	1.0	1.0	1.0	1.0	1.0	1.0
3	1.0	1.0	1.0	1.0	1.0	1.0
4	1.0	1.0	1.0	1.0	1.0	1.0
5	1.0	1.0	1.0	1.0	1.0	1.0
6	1.0	1.0	1.0	1.0	1.0	1.0
7	1.0	1.0	1.0	1.0	1.0	1.0
8	1.0	1.0	1.0	1.0	1.0	1.0

For this case two 50 in. walls suffice to obtain a collapse mechanism with constant story drift ratio equal to the roof drift ratio. However, when one of the walls is discontinuous and supported by two nonductile columns, collapse is driven by capacity loss in the column below the discontinuous walls that is being compressed by lateral loading. Figure H-19 presents one of these cases (4-story frame plus two 50 in. walls), where one of the supported columns experienced sudden strength loss at roof drift ratio of 2.5%.

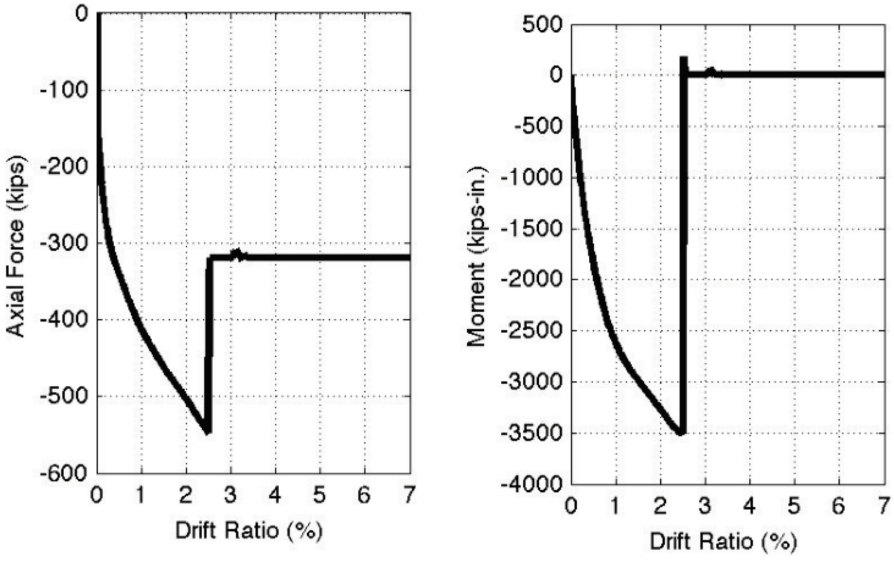

(a) (b)

Figure H-19 8-story frame plus two 50 in. walls building, one discontinuous and supported by discontinuous columns: (a) axial force versus drift ratio; (b) bending moment versus drift ratio.

Analyses also included cases where the discontinuous wall was supported by two columns detailed to result in ductile axial force-displacement behavior, as might be anticipated in a column with modern details or a column that has been retrofitted by external jacketing. These cases showed a considerable improvement in the structural performance of these columns, as presented in Figure H-20, where the sudden strength loss is not observed.

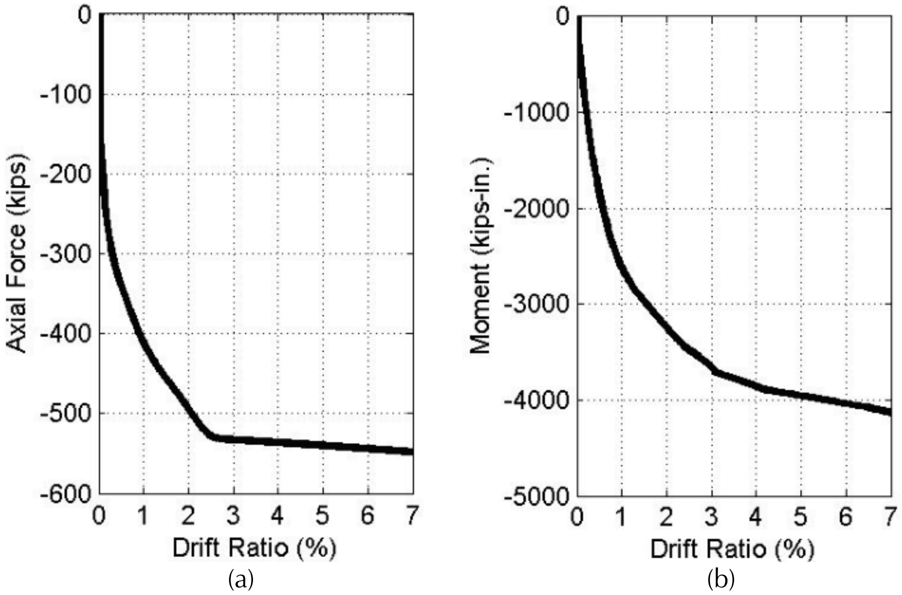

Figure H-20 8-story frame plus two 50 in. walls building, one discontinuous and supported by ductile columns: (a) axial force versus drift ratio; (b) bending moment versus drift ratio.

H.3.5 Frames with Walls Discontinuous in Upper Stories

In this section, values of coefficient α are calculated for frame-wall structures that comprise the archetype frame plus two walls of equal cross section, where one of the walls is discontinuous in an upper story. Different cases are studied to evaluate the sensitivity of values of coefficient α under several structural configurations. Both walls have an axial force demand due to gravity load of $0.1f'_cA_g$ at the base. Gravity forces in beams are those described in previous sections.

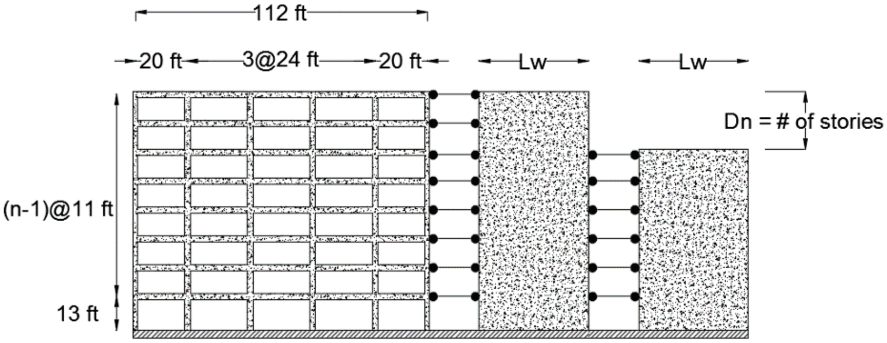

Figure H-21 Schematic elevation view of the simulated 8-story frame plus two rectangular walls, one discontinuous in upper story.

Tables H-14 to H-23 present the values of coefficient α calculated for these cases.

Table H-14 Values of Coefficient α Estimated from Pushover Analysis for a 4-Story Archetype Plus One Continuous Wall and One Wall That Ends in the Third Story

	Archetype Frame + Continuous Wall + Discontinuous Wall							
	Wall Length L_w (in.) $D_n = 1$							
Story	**50**	**60**	**70**	**80**	**90**	**100**	**150**	**200**
1	1.0	1.0	1.0	1.0	1.0	1.0	1.0	0.8
2	1.0	1.0	1.0	1.0	1.0	1.0	1.0	1.1
3	1.0	1.0	1.0	1.0	1.0	1.0	1.0	1.1
4	1.0	1.0	1.0	1.0	1.0	1.0	1.0	1.1

Table H-15 Values of Coefficient α Estimated from Pushover Analysis for a 4-Story Archetype Plus One Continuous Wall and One Wall That Ends in the Second Story

	Archetype Frame + Continuous Wall + Discontinuous Wall							
	Wall Length L_w (in.) $D_n = 2$							
Story	**50**	**60**	**70**	**80**	**90**	**100**	**150**	**200**
1	1.0	1.0	1.0	1.0	1.0	1.0	0.9	0.8
2	1.0	1.0	1.0	1.0	1.0	1.0	1.0	1.1
3	1.0	1.0	1.0	1.0	1.0	1.0	1.0	1.1
4	1.0	1.0	1.0	1.0	1.0	1.0	1.0	1.1

Table H-16 Values of Coefficient α Estimated from Pushover Analysis for a 4-Story Archetype Plus One Continuous Wall and One Wall That Ends in the First Story

	Archetype Frame + Continuous Wall + Discontinuous Wall							
	Wall Length L_w (in.) $D_n = 3$							
Story	**50**	**60**	**70**	**80**	**90**	**100**	**150**	**200**
1	1.0	0.9	0.8	0.8	0.5	0.4	0.3	0.3
2	1.0	1.0	1.1	1.1	1.2	1.2	1.2	1.2
3	1.0	1.0	1.1	1.1	1.2	1.2	1.3	1.3
4	1.0	1.0	1.1	1.1	1.2	1.3	1.3	1.3

Table H-17 **Values of Coefficient α Estimated from Pushover Analysis for an 8-Story Archetype Plus One Continuous Wall and One Wall That Ends in the Seventh Story**

Story	Archetype Frame + Continuous Wall + Discontinuous Wall Wall Length L_w (in.) $D_n = 1$ 70	80	90	100
1	0.8	0.9	0.9	0.9
2	1.0	1.0	1.0	1.0
3	1.0	1.0	1.0	1.0
4	1.0	1.0	1.0	1.0
5	1.1	1.1	1.0	1.0
6	1.1	1.1	1.0	1.0
7	1.0	1.0	1.0	1.0
8	1.0	1.0	1.0	1.0

Table H-18 **Values of Coefficient α Estimated from Pushover Analysis for an 8-Story Archetype Plus One Continuous Wall and One Wall That Ends in the Sixth Story**

Story	Archetype Frame + Continuous Wall + Discontinuous Wall Wall Length L_w (in.) $D_n = 2$ 70	80	90	100
1	0.9	0.9	0.9	0.7
2	1.0	1.0	1.0	0.8
3	1.0	1.0	1.0	1.0
4	1.0	1.0	1.0	1.1
5	1.0	1.0	1.0	1.1
6	1.0	1.0	1.0	1.1
7	1.0	1.0	1.0	1.1
8	1.0	1.0	1.0	1.1

Table H-19 Values of Coefficient α Estimated from Pushover Analysis for an 8-Story Archetype Plus One Continuous Wall and one Wall That Ends in the Fifth Story

	Archetype Frame + Continuous Wall + Discontinuous Wall			
	Wall Length L_w (in.) D_n = 3			
Story	70	80	90	100
1	0.6	0.9	0.9	0.8
2	0.8	1.0	1.0	1.0
3	1.0	1.0	1.0	1.0
4	1.1	1.0	1.0	1.0
5	1.1	1.0	1.0	1.0
6	1.2	1.0	1.0	1.0
7	1.2	1.0	1.0	1.0
8	1.1	1.0	1.0	1.0

Table H-20 Values of Coefficient α Estimated from Pushover Analysis for an 8-Story Archetype Plus One Continuous Wall and One Wall That Ends in the Fourth Story

	Archetype Frame + Continuous Wall + Discontinuous Wall			
	Wall Length L_w (in.) D_n = 4			
Story	70	80	90	100
1	0.8	0.9	0.9	0.8
2	0.9	1.0	1.0	1.0
3	1.0	1.0	1.0	1.0
4	1.0	1.0	1.0	1.0
5	1.1	1.0	1.1	1.0
6	1.1	1.0	1.1	1.0
7	1.0	1.0	1.1	1.0
8	1.0	1.0	1.0	1.0

Table H-21 Values of Coefficient α Estimated from Pushover Analysis for an 8-Story Archetype Plus One Continuous Wall and One Wall That Ends in the Third Story

	Archetype Frame + Continuous Wall + Discontinuous Wall			
	Wall Length L_w (in.) D_n = 5			
Story	70	80	90	100
1	0.3	0.7	0.9	0.8
2	0.6	0.9	1.0	1.0
3	0.8	1.0	1.0	1.0
4	1.1	1.0	1.0	1.0
5	1.3	1.1	1.0	1.1
6	1.4	1.1	1.0	1.1
7	1.3	1.1	1.0	1.0
8	1.2	1.1	1.0	1.0

Table H-22 Values of Coefficient α Estimated from Pushover Analysis for an 8-Story Archetype Plus One Continuous Wall and One Wall That Ends in the Second Story

	Archetype Frame + Continuous Wall + Discontinuous Wall			
	Wall Length L_w (in.) D_n = 6			
Story	70	80	90	100
1	0.0	0.1	0.1	0.1
2	0.1	0.1	0.2	0.1
3	1.1	1.1	1.1	1.1
4	1.4	1.4	1.3	1.4
5	1.4	1.4	1.4	1.4
6	1.4	1.4	1.4	1.4
7	1.4	1.4	1.4	1.4
8	1.3	1.4	1.4	1.4

Table H-23 Values of Coefficient α Estimated from Pushover Analysis for an 8-Story Archetype Plus One Continuous Wall and One Wall That Ends in the First Story

Story	Archetype Frame + Continuous Wall + Discontinuous Wall			
	Wall Length L_w (in.) D_n = 7			
	70	80	90	100
1	0.0	0.2	0.0	0.0
2	0.6	0.8	0.7	0.8
3	1.3	1.1	1.2	1.2
4	1.3	1.2	1.2	1.2
5	1.3	1.3	1.2	1.2
6	1.3	1.3	1.2	1.2
7	1.2	1.2	1.2	1.2
8	1.2	1.2	1.2	1.2

These limited analyses show that, for the studied 4-story building, ending the discontinuous wall in the second story or above did not have an appreciable effect in the values of coefficient α. However, when the discontinuous wall ended in the first story, for 90 in. wall or longer, the collapse mechanism changed and it occurred above the first story. For 8-story buildings, similar behavior was clear for discontinuous walls ending in the second story or below, for 70 in. walls or above.

The results obtained from the static inelastic analyses were compared with results from the mechanism analysis of Chapter 5. For this limited set of archetypes, the mechanism analysis was able to identify the inelastic yielding mechanism of the archetype.

H.3.6 Buildings with Shear-Critical Walls

Modeling of shear critical walls is a task of ongoing investigation due to the complexities involved in adequately reproducing axial/flexural shear interactions. In this section, a simple approach is used to study the impact of shear critical walls that are coupled to frames, in which an elastic-perfectly plastic shear spring is connected in series with the beam-column flexural element representing the wall at a given critical story (Figure H-22). As shown in Figure H-22c, the horizontal drift at a given story has two components, a flexural deformation, δ_f, and a shear deformation, d_v. In this setup, a coupled shear/flexure response is only possible for strain-hardening behavior at the constitutive level of each component.

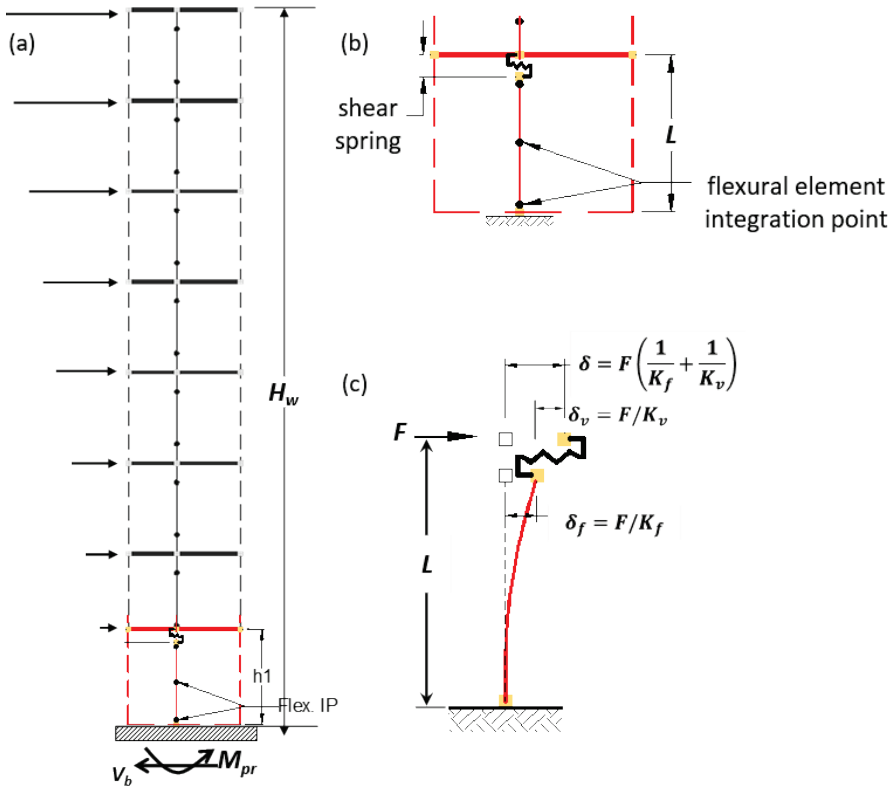
(a)
(b)
shear spring
L
flexural element integration point
(c)
$\delta = F\left(\frac{1}{K_f} + \frac{1}{K_v}\right)$
$\delta_v = F/K_v$
F
$\delta_f = F/K_f$
L
H_w
h1
Flex. IP
V_b
M_{pr}

Figure H-22 Schematic elevation view of an 8-story wall with a shear critical story. (b) model of shear frame plus two rectangular walls, one discontinuous in upper story.

This model can also be thought of as a set of two springs in series as presented in Figure H-23a. For an elastoplastic response (Figure H-23b), in which the shear spring capacity is smaller than the associated shear capacity for flexural yielding, all the plastic demand will be concentrated in the shear spring.

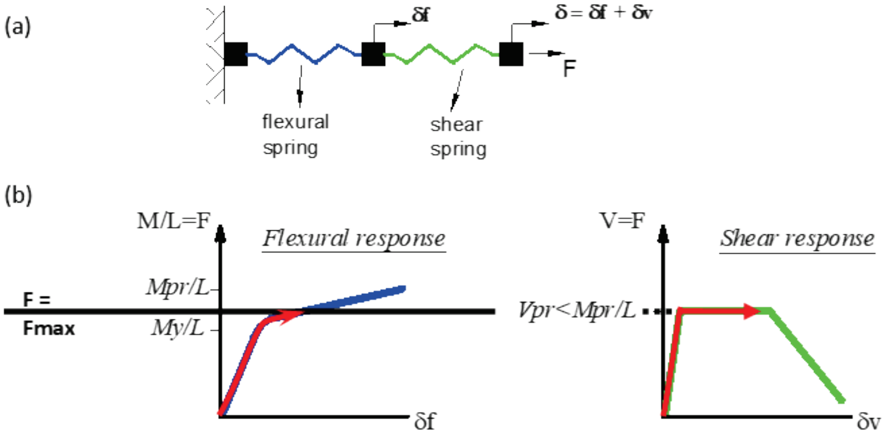
(a)
δf
δ = δf + δv
F
flexural spring
shear spring
(b)
M/L=F
Flexural response
Mpr/L
F = Fmax
My/L
δf
V=F
Shear response
Vpr<Mpr/L
δv

Figure H-23 (a) Two-spring in series model. (b) Response of each individual component representing flexure and shear.

The setup used to model shear critical stories in this study is based on the description presented above with a shear spring whose capping strength is given by ACI 318 provisions.

H.3.6.1 Static Response: Pushover Analyses

Figure H-22a shows an isolated cantilever wall, with a shear critical section at the base. Under an inverted triangular static load pattern, the minimum shear strength ($V_{sp,min}$) at the base to guarantee flexural failure is given by Equation H-3:

$$V_{spt,min} > (3/2)\, M_{pr}/H_w \tag{H-3}$$

where M_{pr} is the expected flexural strength at the base and H_w is the height of the wall. For a uniform (rectangular) pattern of lateral loading, the minimum required shear strength increases to:

$$V_{spr,min} > 2M_{pr}/H_w \tag{H-4}$$

Figures H-24 to H-26 describe the response of a frame-wall system with a wall having a shear critical cross-section at the first story. In each figure, plot (a) shows the building roof drift versus the base shear (pushover curve) along with a point of interest marked with a square, plot (b) shows the displaced shape along with the plastic hinges formed at the noted point, plot (c) shows the story drift ratio (SDR) and the displaced shape at the noted point, figure (d) shows the alpha values of the building (in red) at the noted point along with the theoretical alpha distribution for a cantilever wall at yielding, (e1) shows the base reaction of each component of the frame-wall system, (e2) the moment-curvature relationship at the base of the wall, and (e3) shows the demand on the shear spring.

The only difference among the models is the strength of the shear spring at the first story. Variable V_{ns} defines the provided shear strength of the wall at the critical section. Provided shear strength ratio, $V_{ns}/V_{spr,min}$, are 1.5, 1.1 and 0.5 for buildings in Figure H-24 trough to Figure H-26, respectively. It is worth noting that this strength is defined for an isolated cantilever wall. The three cases of study defined are: (i) *building with a strong spring (BSS)*, where the shear spring expected to remain linear (Figure H-24); (ii) *building with adequate shear strength (BAS)*, where the shear spring strength is 10% larger than the demand required to yield it under a rectangular load pattern in an isolated cantilever wall (Figure H-25); and (iii) *building with a weak shear spring (BWS)*, where the wall is expected to fail in shear prior reaching its flexural strength (Figure H-26).

Response of the shear spring in the BSS model is linear (Figure H-24e3). The alpha value for the building is close to 1.0, reminding that the wall is stiff (e.g., L_w = 200 in.) and strong enough as to command the response of the whole structure. The first story alpha value of the building is smaller than 1.0, following the trend of the theoretical closed-form solution of a cantilever wall at yielding.

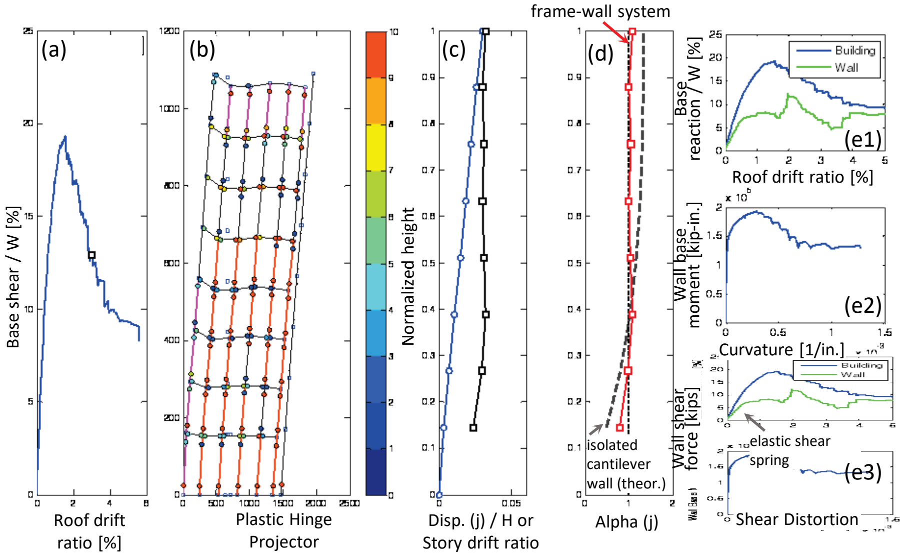

Figure H-24 Response of the 8-story archetype frame-wall structure for wall length L_w = 200 in. with a shear critical section at the wall base. Simulation for a strong spring $V_{ns}/V_{spr,min}$ = 1.5 (BSS model).

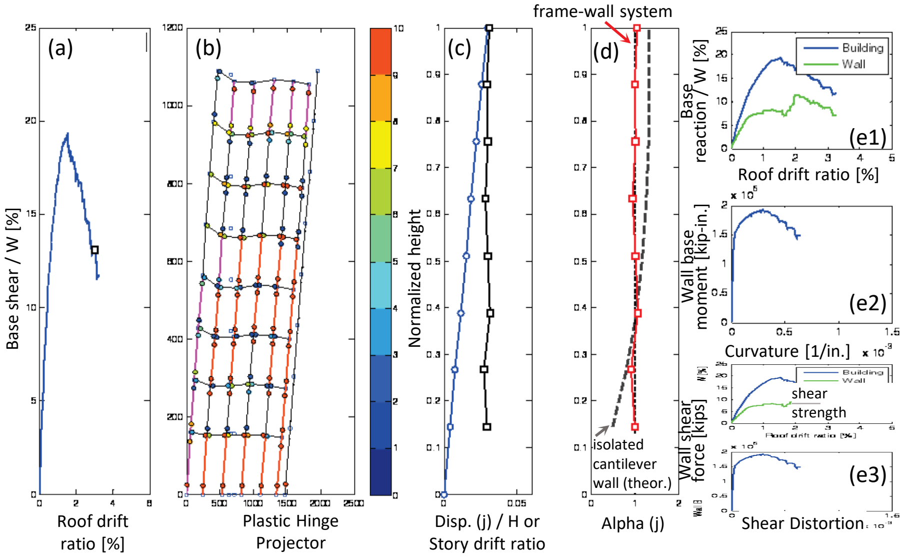

Figure H-25 Response of the 8-story archetype frame-wall structure for wall length L_w = 200 in. with a shear critical section at the wall base. Simulation for $V_{ns}/V_{spr,min}$ = 1.1 (BAS model).

For the BAS model, it is observed that although the shear spring strength ratio is larger than 1.0, the wall shear spring yields (Figure H-25e3), implying that coupling of the wall and the frame may result in an arm of the resultant forces along the wall that is closer to the base, shorter than that of a triangular or a rectangular load pattern (e.g., $(2/3)H_w$ or $(1/2)H_w$, respectively). This increase in the shear force distribution along the wall height is likely to be more pronounced under dynamic loading due to apparent higher-mode effects. Figure H-25c shows that alpha values for the BAS model are still close to 1.0, but it is already developing drift demand concentration at the shear critical story.

The BWS model shows an apparent concentration of drift at the first story. Flexural strength at the base of the wall is not developed, and the force demand is concentrated in the weak shear spring (Figures H-26e2 and H-26e3). Figure H-26b shows a soft 1st -story forming, with alpha values reaching 2.0 at that location.

Although BWS model results are expected, behavior of the BSS, and the BAS model need to be analyzed in the dynamic domain to account for apparent higher mode effect that are likely to increase the shear demand along the height of the wall, and may trigger shear failures not observable under pushover analyses.

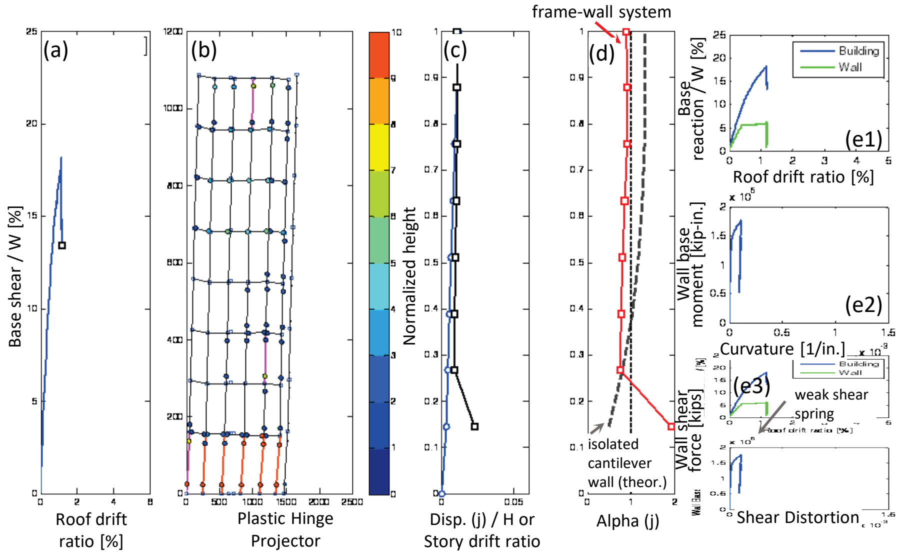

Figure H-26 Response of the 8-story archetype frame-wall structure for wall length L_w = 200 in. with a shear critical section at the wall base. Simulation for a weak spring $V_{ns}/V_{spr,min}$ = 0.5 (BWS model).

H.3.6.1 Dynamic Response

In this section, the wall-frame systems described above are studied under dynamic loading. It is of special interest to evaluate the likelihood of shear failure in buildings with stronger shear springs. Building models BSS, BAS, and BWS are evaluated under three sets of ground motions of increasing intensity: low hazard set (LH); intermediate hazard set (IH); and high hazard set (HH) (Figure H-27).

Figure H-28 shows the response of the building whose wall behavior is dominated by the shear spring (BWS model in Figure H-26). Given the fragile nature of the wall at the first story, responses shown only include those associated to the lower demand set of ground motions (e.g., LH set). Alpha values are separated according to the mode of failure observed into flexure or shear. The low shear strength of the wall commands the response in the dynamic space as well, by failing 97% of the times in shear. Responses for higher demands are similar.

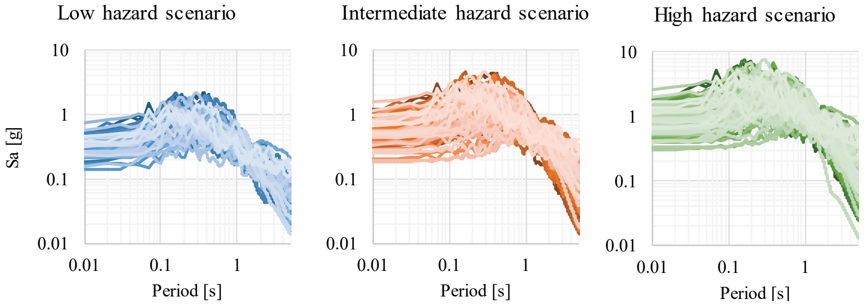

Figure H-27 Earthquake scenarios for shear critical models evaluation.

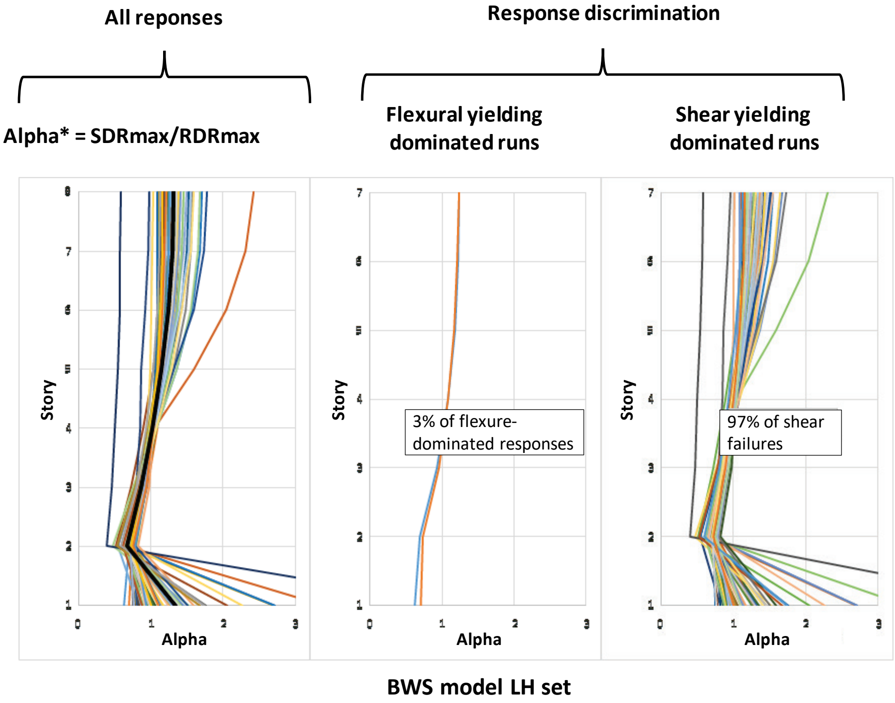

Figure H-28 Dynamic response of the BWS model under the LH set.

Figure H-29 through H-31 show the response of the building whose wall has “adequate” shear strength (BAS model in Figure H-27). Responses shown include the three levels of demand described before. In Figure H-29 it is observed that the response is dominated by flexure (58% of the times) for LH set, although plastic excitation of the shear spring is also apparent (42% of the runs). For higher intensity demand such as that of the IH and the HH sets, the plastic shear demand is observed in 67% and 86% of the analyses, respectively.

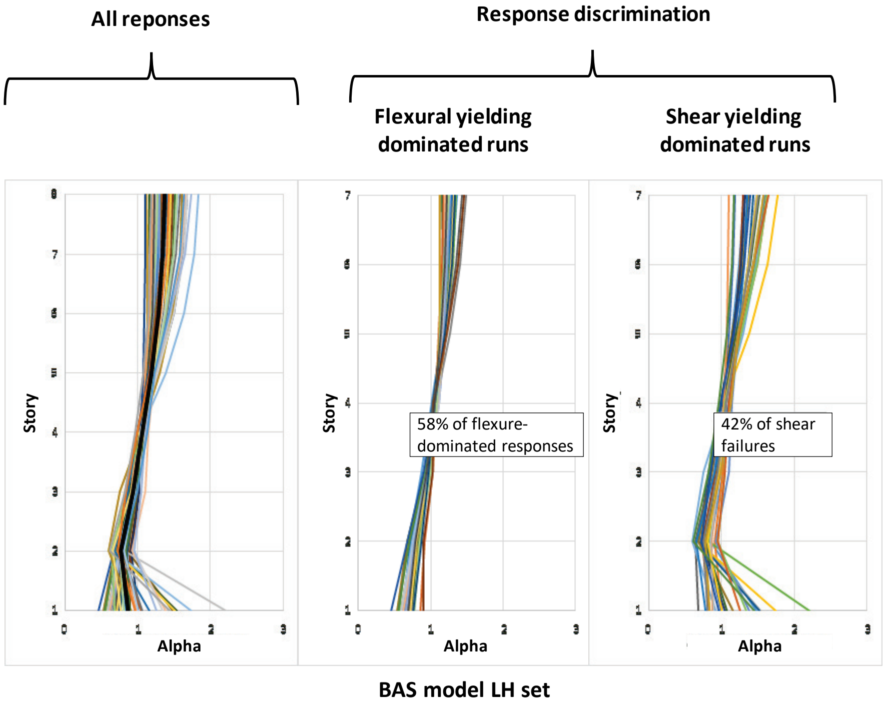

Figure H-29 Dynamic response of the BAS model under the LH set.

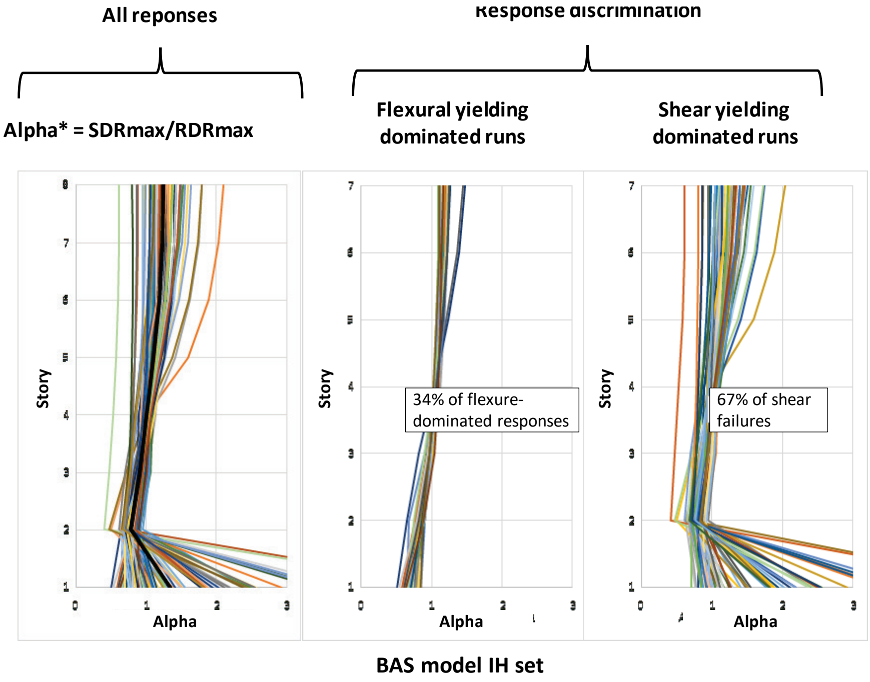

Figure H-30 Dynamic response of the BAS model under the IH set.

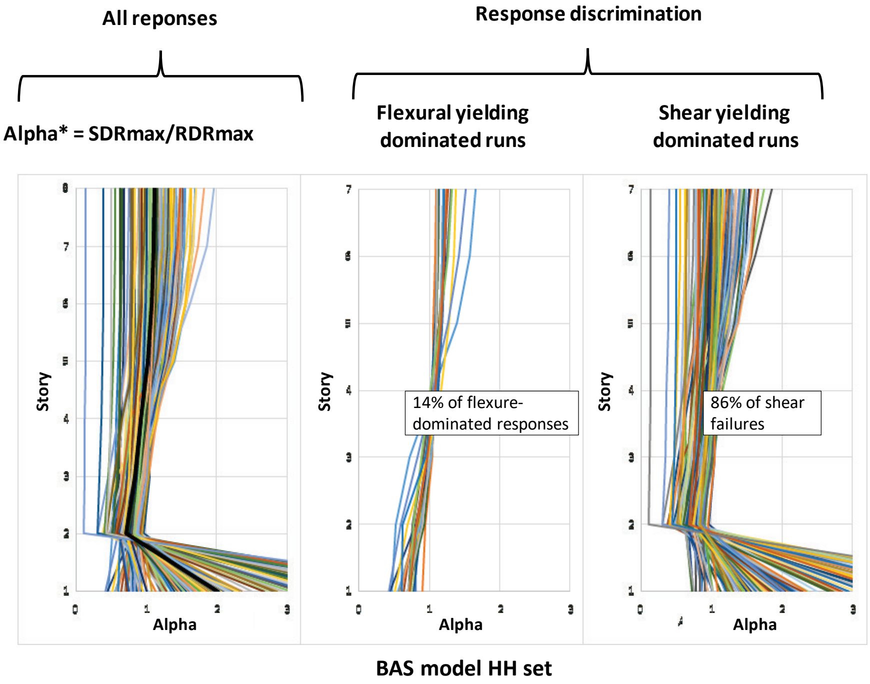

Figure H-31 Dynamic response of the BAS model under the HH set.

Figure H-32 through 34 show the response of the building with a shear-competent wall. Although its shear strength is 50% larger than the demand required to fail the wall in flexure (under uniform loading), the BSS model also exhibits plastic demand on the shear spring, even at lower levels of demand. For this model, the proportion of shear failures is lower than that of the BAS model, but still fails 30 to 50% of the times in shear.

Result from the dynamic analyses allow concluding that coupling of the wall with the framing system, along with shear amplification due to apparent higher mode effects may negatively impact the response of a frame-wall building. In the cases presented, the wall is of sufficient length to control the response and result initially in values of α approximately equal to 1.0, but if shear failure occurs, then most of the subsequent displacement occurs in the story where shear failure occurs. This is, of course, an outcome of the relatively simple model being used for shear.

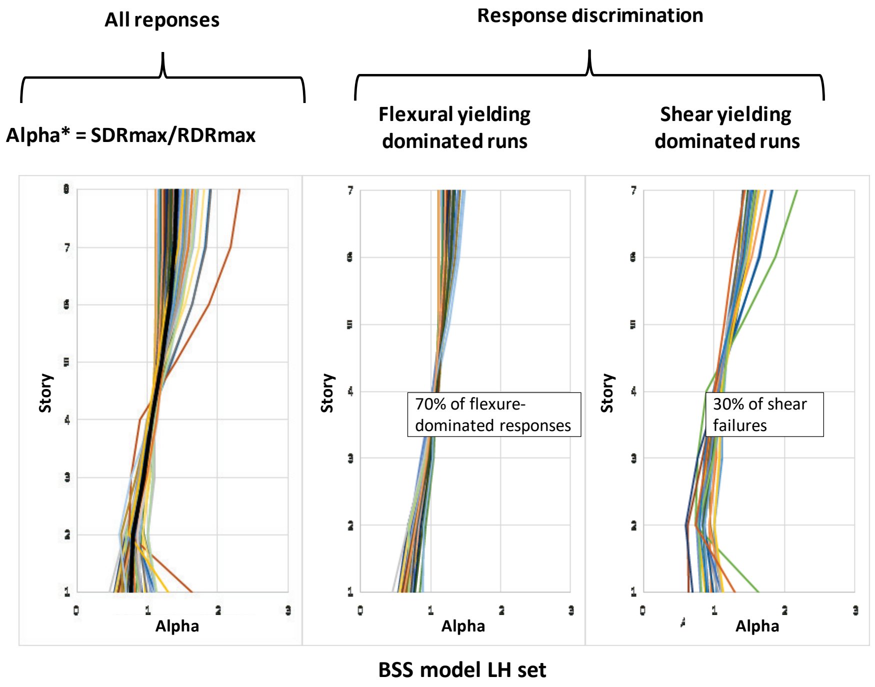

Figure H-32 Dynamic response of the BSS model under the LH set.

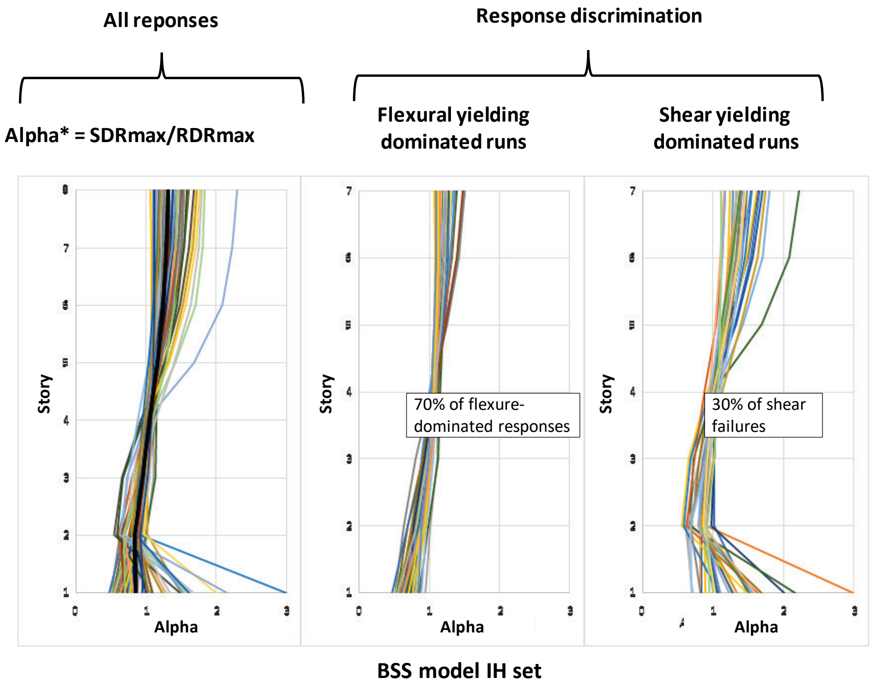

Figure H-33 Dynamic response of the BSS model under the IH set.

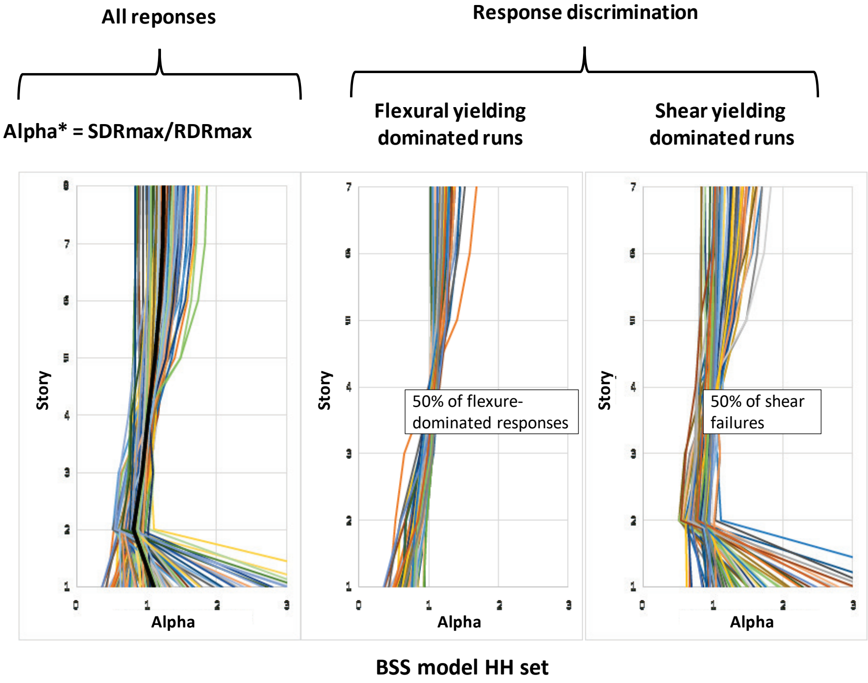

Figure H-34 Dynamic response of the BSS model under the HH set.

To explore the impact in overall building response of shear critical walls with a weak section upstairs, three models where constructed with the same shear spring strengths as described above, but locating the shear critical section at the third story. Responses of these structures are presented in Figure H-32 for the three set of ground motions of various intensities. In this setup, the distinction between flexural- or shear-dominated responses is more difficult to assess, therefore, all responses are combined in each case. Nevertheless, the median response helps understand the influence of the shear strength in the global behavior of the buildings. For example, the building with the strong spring (BSS model) is not affected much by the presence of a shear weakness upstairs. On the other hand, the BWS model is highly influenced by the weak capacity at all level of seismic demand, showing displacement demand concentration at the third story. Response of the building with adequate strength (BAS model) shows some impact of the shear plastic deformation for higher levels of demand, but median alpha values are still close to 1.0 at the third story.

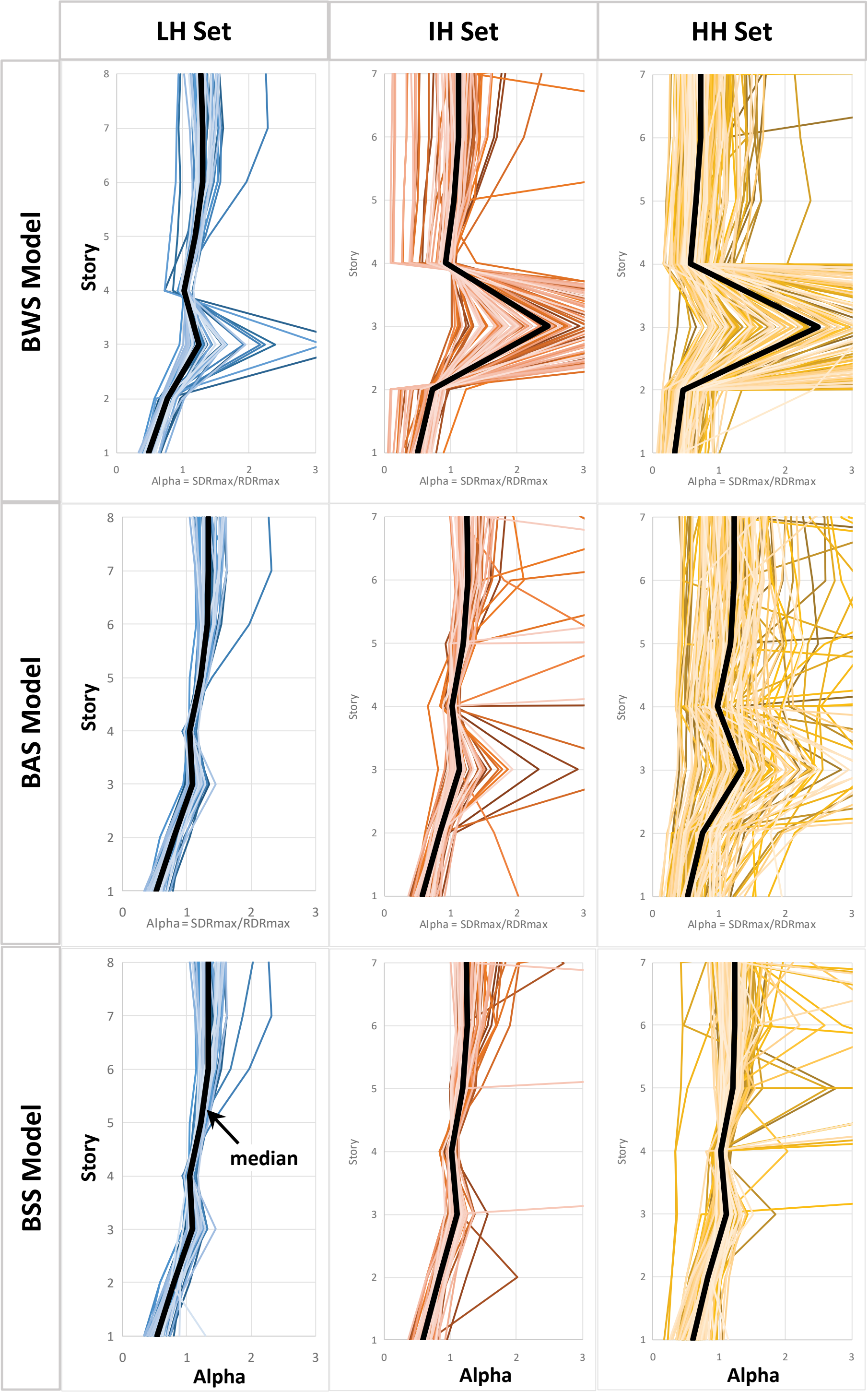

Figure H-35 Dynamic response of the BWS, BAS and the BSS models under the LH, IH, and HH sets.

Appendix I

Torsion Studies

I.1 Introduction

The perception that torsion problems are a significant contributor to collapse risk has been shaped by building collapses in past earthquakes, such as the CTV building in Christchurch, New Zealand in 2011, as well as a large number of other cases observed in New Zealand and other earthquakes over the past several decades (Canterbury Earthquakes Royal Commission, 2012). The goal of the studies conducted herein is to avoid excessive conservatism in identification of buildings with torsion problems, while quantifying the potentially negative impact of torsion, when present, on the collapse risk evaluation for the purposes of this methodology.

The studies described in this appendix aim to quantify the displacement amplification experienced by columns and walls in torsionally irregular buildings. This amplification is included in the evaluation procedures of columns and walls in Chapters 7 and 8. In addition, the studies identify the following conditions: (1) when torsion is negligible and is not expected to significantly influence collapse risk; and (2) when torsion is so significant such that the building can be classified as Exceptionally High Risk (so-called "Extreme Torsion").

Torsional irregularity is quantified using the Torsional Ratio (*TR*), which is a strength-based assessment of the ratio of torsional demand to capacity. The Torsional Ratio is used to predict a displacement amplification factor for frame-wall buildings (Chapter 7) and, occasionally, for bearing wall buildings (Chapter 8). It is also used, together with information about building strength, to identify buildings that have Extreme Torsion. The Wall Index (defined in Appendix D) is also used to identify cases where torsion can be neglected. Torsional effects are neglected entirely for pure frame structures (Chapter 6), since these buildings are unlikely to have a configuration that would induce enough torsion to change the collapse risk.

The study presented in this appendix builds on torsion studies presented in earlier versions of this document. Together, the results are used to develop the procedures outlined in this document.

I.2 Identify Critical Stories

The severity of torsion is quantified by the torsional ratio, *TR*, at the critical story. In this methodology, *TR* is defined as the torsional demand, T_D, of the critical story, *x,* divided by the torsional capacity, T_C, of the critical story:

$$TR = \frac{T_{Dx}}{T_{Cx}} \tag{I-1}$$

Torsional demand, T_D, is directional, and must be calculated for each direction of earthquake loading:

$$T_{Dx} = V_{px}e \tag{I-2}$$

where:

V_{px} = plastic shear capacity of the critical story;

e = eccentricity between the center of mass and the center of strength in the direction perpendicular to the direction of earthquake loading; *e* may not be taken as less than 5% of the overall plan dimension perpendicular to the direction of earthquake loading (i.e., 0.05*L*);

L = maximum plan dimension perpendicular to the direction of earthquake loading.

The center of rotation is taken as the center of strength. The coordinates of the center of strength, $\left(\bar{x}, \bar{y}\right)$, are calculated in each direction as the summation of the products of frame/wall line location and frame/wall strengths, divided by the summation of frame/wall strengths, as shown in Figure I-1:

$$\bar{x} = \frac{\sum_{i=1}^{n_f} x_i V_{pfi}}{\sum_{i=1}^{n_f} V_{pfi}}, \quad \bar{y} = \frac{\sum_{i=1}^{n_f} y_i V_{pfi}}{\sum_{i=1}^{n_f} V_{pfi}} \tag{I-3}$$

Figure I-1 is an illustration of dimensions to be used in computing the center of strength. Geometries are shown for only one frame, but the process needs to be repeated for all of the frames and wall lines as suggested by the summation in Equation I-3. The example uses the bottom left corner as the reference point for computing frame locations. Note that accidental torsion is not considered in this computation, except that *e* has a minimum value.

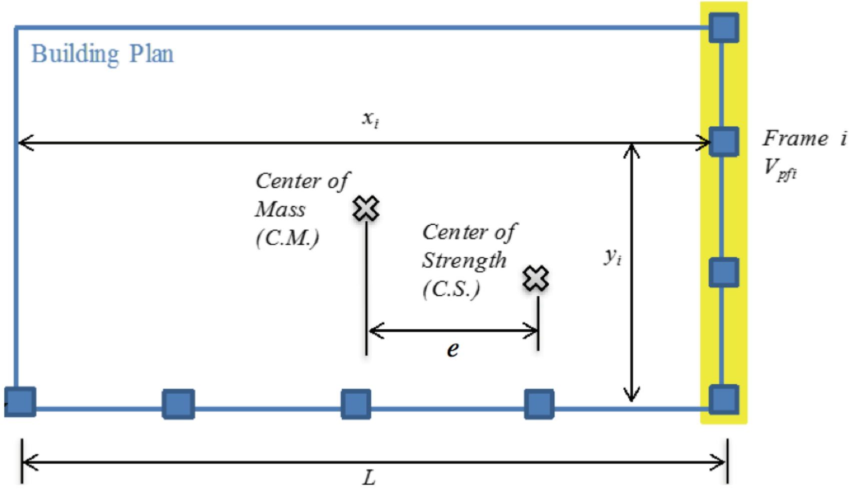

Figure I-1 Illustration of the calculation of the center of strength for an example frame line, using the bottom left corner as the reference location; this computation would be repeated for each frame/wall line in the structure.

Torsional capacity, T_C, is calculated considering the capacity of frame/wall lines in all orientations, and thus is the same regardless of the direction of loading considered:

$$T_{Cx} = \sum_{i=1}^{n_f} |R_{fi}||V_{pfi}| \tag{I-4}$$

where:

R_{fi} = is the orthogonal distance between the frame/wall line i and the center of strength (as shown in Figure I-2);

V_{pfi} = is the plastic capacity of frame/wall line i; and

n_f = is the number of frame/wall lines in story x, considering all those that resist torsion, regardless of orientation

Figure I-2 illustrates the torsional capacity computation, considering a building with two frame lines in orthogonal directions. These calculations would be repeated for all of the frame/wall lines in a building.

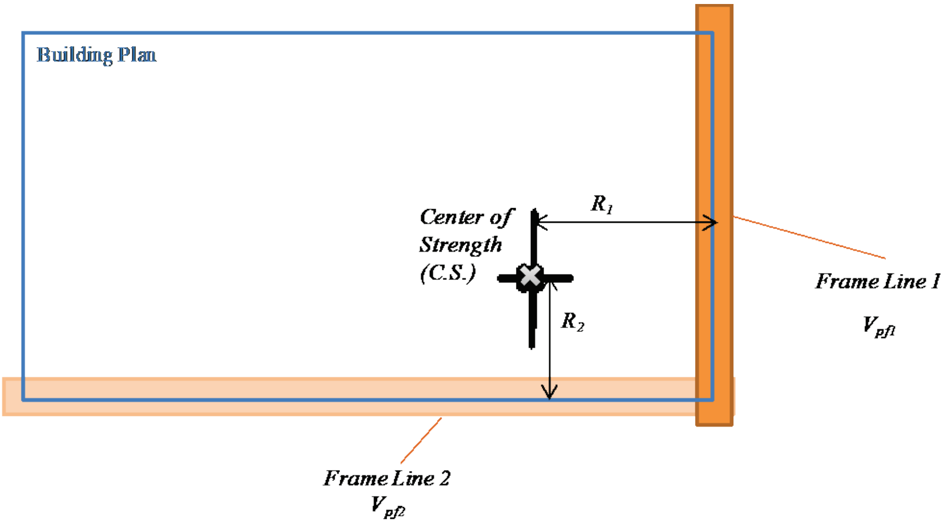

Figure I-2 Illustration of the calculation of torsional capacity.

I.3 Simulation of Collapse of Torsionally-Sensitive Buildings

The procedures developed here to account for buildings with torsional irregularities are based on nonlinear dynamic simulation of collapse of torsionally-irregular buildings. This section discusses the buildings analyzed and the simulation models employed.

I.3.1 Buildings Analyzed

The torsion assessment is based on variations of a real structure that have varying degrees of torsional irregularity. The 8-story real structure that provides the basis for these archetypes experienced larger than design seismic loading in the 2011 Christchurch NZ earthquake, and was designed using pre-1974 ACI design codes (Marcilla et al., 2017). The structure experienced significant damage, and reconnaissance studies (Canterbury Earthquakes Royal Commission, 2012; Marcilla et al., 2017) found that torsion was a contributor to this damage. In this study, the configuration of this building was varied systematically investigate the influence of torsion on collapse risk.

The study investigates 15 8-story buildings with the same floor plan, as shown in Figure I-3. The structures vary in terms of the location and length of the added reinforced concrete wall, such that they range from a symmetric pure frame building, to a building with extreme torsion behavior due to a large eccentrically placed wall. Each wall building with an eccentric wall has a comparison symmetric case with the same length wall placed at the center of the plan (i.e., a comparison case of equivalent lateral strength).

Story heights of 10 ft. are consistent throughout the height of the structure. All columns are 18 in. square with eight #6 rebar placed symmetrically. Tie spacing is 6 in. over the height of the columns. All beams are 8 in. by 30 in. and have two #7 rebar placed at the top and two at the bottom. These designs differ somewhat from the original structure and ensure that the structures have a M_c/M_b ratio of 0.85 at every location, indicating that moment failure will occur in the columns before the beams. All columns in the modeled building have a V_p/V_n ratio of 0.63, indicating the expected failure mode is flexure. (Although shear critical columns are not directly considered in this study, the columns fail flexurally in are brittle manner, such that flexural degradation occurs at low drifts and the columns are expected to experience a rapid reduction of post peak strength not dissimilar from a shear failure.)

Wall designs vary from model to model. Shorter walls are 8 in. thick with #8 rebar spaced at 8 in. on center in both the vertical and horizontal directions. Larger walls (Case D and beyond) are 12 in. thick and have additional rows of #8 longitudinal reinforcing bars over a length of 0.15L at each end of the wall. The walls are assumed not to have clearly defined boundary elements.

Figure I-3 summarizes the characteristic of the cases analyzed, including the Wall Index (*WI*) from Equation 5-1, and Torsional Ratio (*TR*) from Equation 7-7. The period (T_x) represents the period in the *x* (shaking) direction, obtained from eigenvalue analysis of the building model. Since the periods vary slightly between the torsional and the symmetric cases, the mean value, considering both the torsional and the symmetric buildings, is reported.

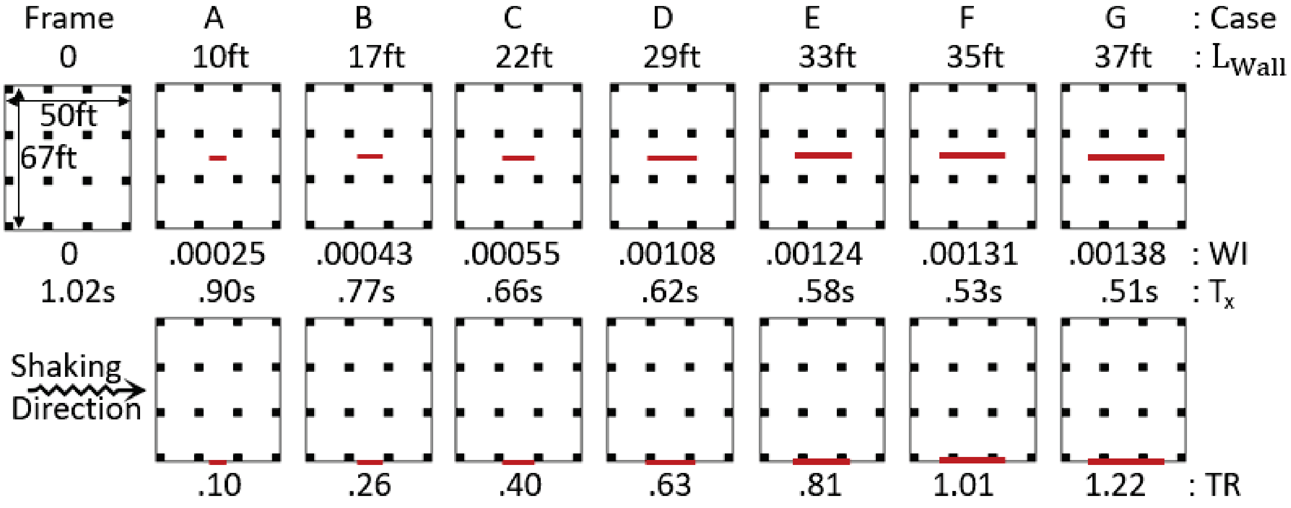

Figure I-3 Buildings analyzed in torsional study, showing variation in Torsional Ratio due the length of the walls. Each irregular case has a corresponding symmetric case. All properties are the same in the symmetric and torsional cases, except for the location of the wall and the Torsional Ratio.

I.3.2 Modeling

The building is modeled in three dimensions as shown in Figure I-4. Column, beam and wall elements are modeled with force-based distributed plasticity fiber elements. In the fiber elements, the concrete fibers are assigned the Kent-Scott-Park stress strain model, assuming no tensile strength (Kent and Park, 1971). The steel material is defined in tension in as a tri-linear curve that follows modeling recommendations in FEMA P-695 (NIST, 2010c), as shown in Figure I-5, considering strain hardening and steel fracture. The backbone of the steel model in compression considers buckling in both columns and walls, which depends on the tie spacing. The parameters for the buckling model follow the Dhakal model, which is based on experimental results and finite element models of buckling of reinforcing bars (Dhakal and Maekawa, 2002). The length of the plastic hinge is determined from recommendations by Paulay and Priestley (1992), and is used to define the location of the integration points and weighting scheme such that the response is regularized (i.e., not dependent on the number of elements). Regularization is consistent with the discussion in Appendix L.

Floor diaphragms are modeled as rigid by the use of nodal constraints, and the base is fixed. Beam-column joints are not explicitly modeled. The models assume 2% Raleigh damping at the 1st and 3rd mode periods. Each element definition utilized a P-delta geometric transformation.

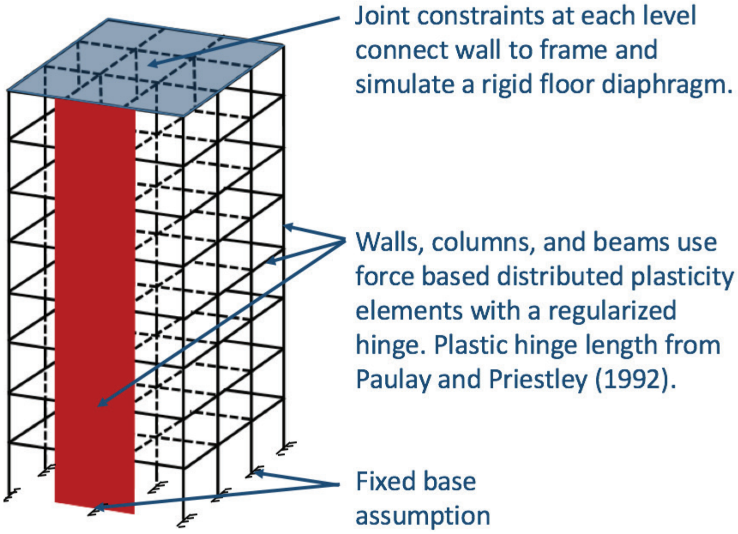
Joint constraints at each level connect wall to frame and simulate a rigid floor diaphragm.
Walls, columns, and beams use force based distributed plasticity elements with a regularized hinge. Plastic hinge length from Paulay and Priestley (1992).
Fixed base assumption

Figure I-4 Diagram of 3D models used for torsional simulation.

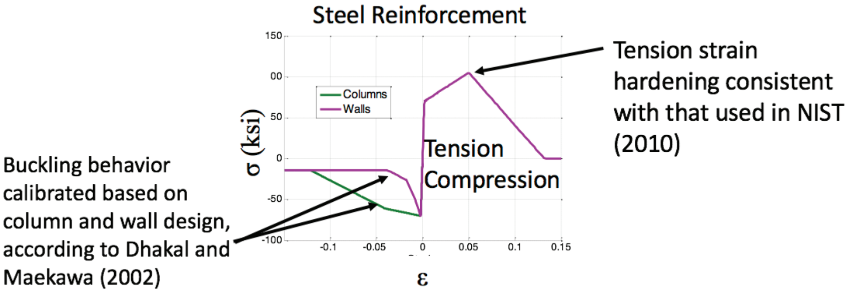

Tension strain hardening consistent with that used in NIST (2010)

Buckling behavior calibrated based on column and wall design, according to Dhakal and Maekawa (2002)

Figure I-5 Steel material behavior used in fiber models.

I.3.3 Analysis Procedures

Each building is excited in the in-plane direction of the walls. Shaking in the analysis is considered in only one dimension for consistency with this methodology's procedures which analyze buildings separately in each orthogonal direction. The analysis uses both horizontal recordings of the 22 far-field pairs of ground motions defined in the FEMA P-695 document (FEMA, 2009), for a total of 44 individual analyses.

Each building is assessed using incremental dynamic analysis, in which the ground motions are scaled until collapse occurs. Ground motions are scaled by the spectral acceleration of the first-mode period of the building.

For this study, collapse is defined as occurring when displacement demand on at least 25% of the columns has reached or exceeded 1% story drift. This drift is not constant over the plan of the building, due to torsion. The force displacement curves in Figure I-6 show how a collapse criteria of 1% drift was determined from initial sensitivity studies. This figure shows the force displacement response of two columns (with the locations shown on the figure). These responses indicate that these flexurally-dominated columns experience a dramatic loss in capacity around 1% drift, such that the column is not contributing significantly to the lateral capacity of the building beyond that point.

Incremental dynamic analysis was carried out for each of the buildings illustrated in Figure I-3.

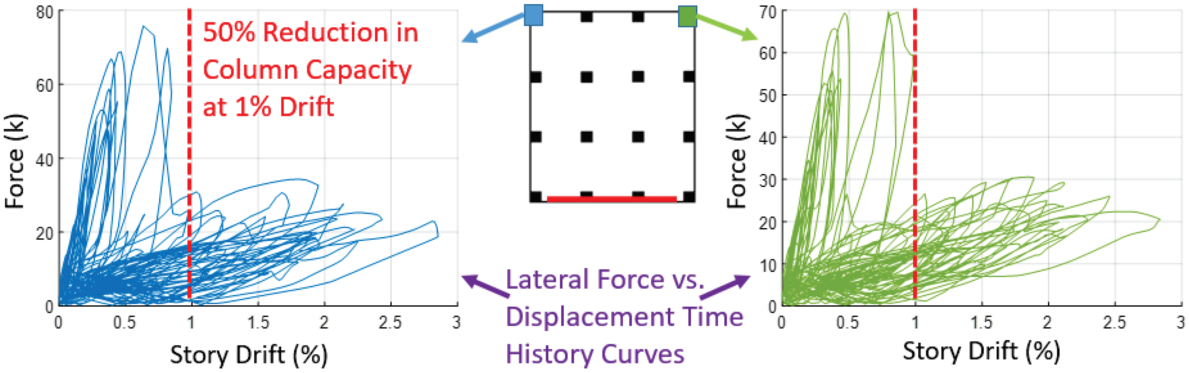

Figure I-6 Response of columns in a torsionally-irregular building model, showing how the 1% story drift collapse definition was determined.

I.3.4 Detailed Results for Selected Buildings

Figure I-7 and I-8 provide the pushover and incremental dynamic analysis results for Case E. The pushover shows the disaggregated wall and frame strengths, and the total system strength. For Case E, the wall is somewhat stronger than the frame systems, and the failure of the columns is controlling the post-peak response. This behavior is consistent with most of the other cases examined. However, for cases where the wall strength is much greater than the strength of the frame and the building is symmetric, then building failure is dependent on wall failure.

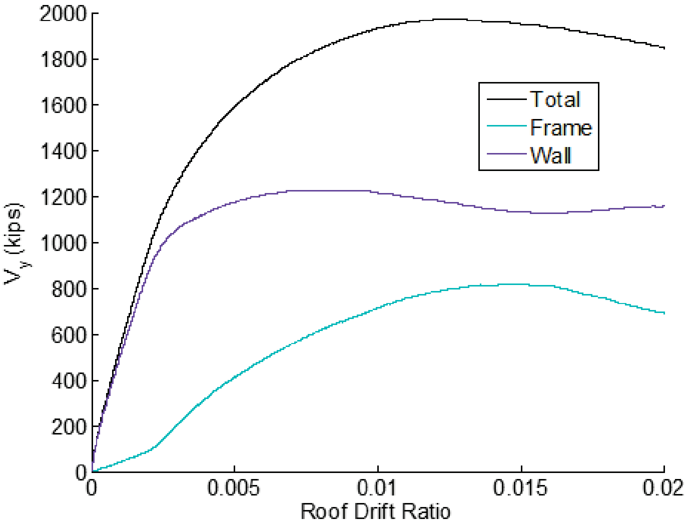

Figure I-7 Pushover results for case E, deaggregated to show contributions from frame and wall lines.

Figure I-8 provides an example of the dynamic analysis results that are used to develop the recommendations in this appendix. These results show that symmetric cases are generally able to withstand larger ground motion intensities (spectral accelerations) before reaching collapse than the torsional buildings. For Case E, the median collapse capacity at a period of 0.66 s is

2.3g for the symmetric building, which is 30% larger than the median collapse capacity for the torsional building.

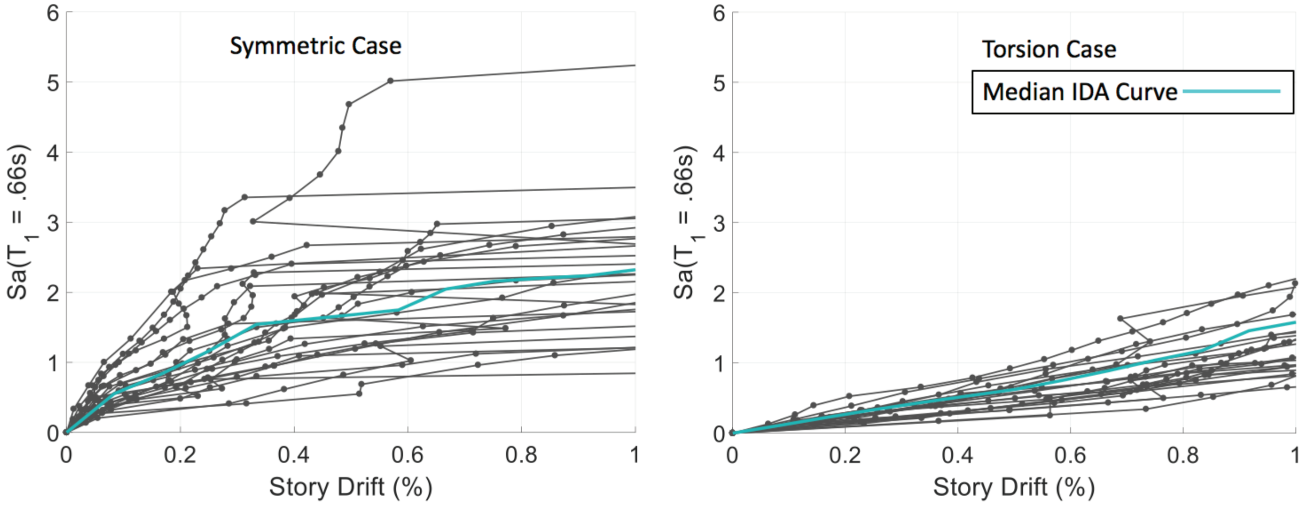

Figure I-8 Incremental dynamic analysis results for Case E, showing response of the building with the symmetrically-placed wall and the asymmetrically-placed wall, and the lower collapse capacity of the torsionally-irregular building.

I.3.5 Normalization of Results for Comparison between Buildings

Figure I-9 summarizes the median collapse capacities for all the buildings analyzed. For the purposes of this comparison, we recalculate the spectral accelerations such that all values are reported at the same period.

Figure I-9 shows that, for Cases A-C, there is negligible difference in the collapse resistance of the torsional and symmetric cases; for Cases E-G there is an increasing difference in behavior between the torsional and symmetric cases, with the torsionally-irregular buildings indicating lower collapse resistance.

Figure I-10 examines the collapse results for the torsional buildings (bottom row in Figure I-3). For this purpose, the collapse capacity of each building is normalized by the strength of the building, i.e., $\mu_{Strength}$, permitting comparison across buildings with different wall lengths and, accordingly different lateral strengths; the x-axis is represented as the torsional ratio. Each set of points connected by a dashed line represents a different percentile on the collapse fragility curve. The normalized median collapse points are shown in turquoise. The points corresponding to the 30th and 70th percentiles are also highlighted to clarify later discussions.

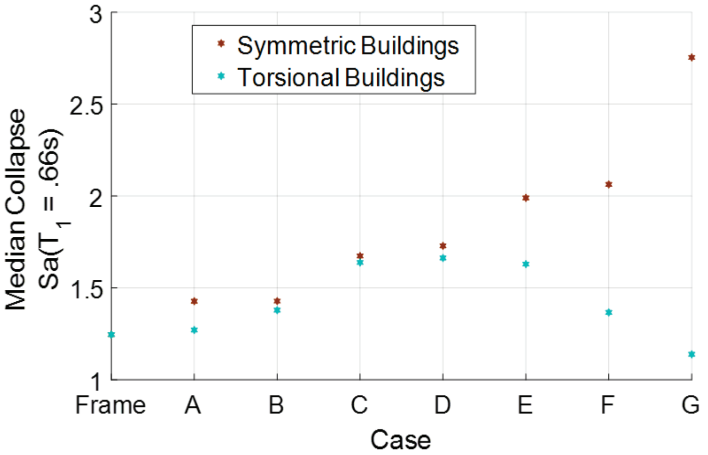

Figure I-9 Median collapse capacities of all the building cases analyzed in this study. Refer to Figure I-3 for a diagram of each case.

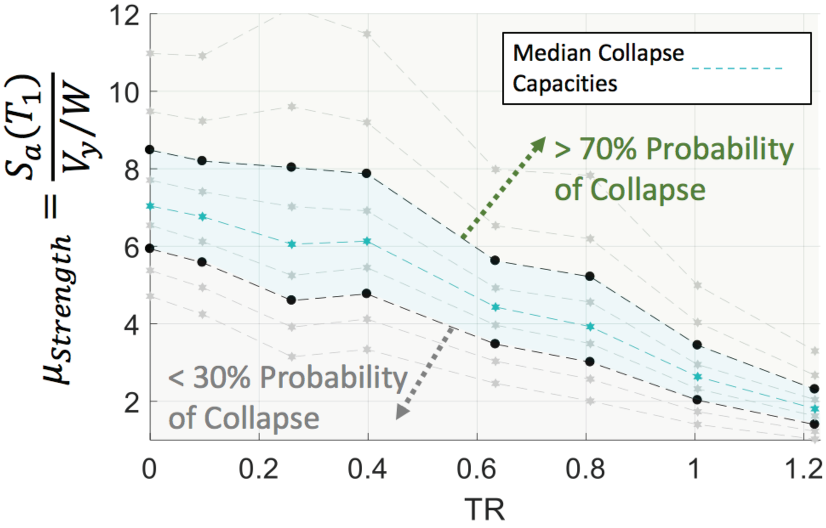

Figure I-10 Collapse fragility for the torsionally-irregular buildings shown in Figure I-3, plotted in terms of $\mu_{Strength}$.

I.4 Extreme Torsion

The Extreme Torsion provision identifies those buildings that have torsion that is so significant the building is classified as *Exceptionally High Seismic Risk* without more detailed calculation.

Extreme torsion is defined as those buildings that are found to have more than 70% probability of collapse in the dynamic simulations of building response, according to the results plotted in Figure I-10 and repeated in Figure I-11. We focus on that region of the plot where torsion has a significant influence on collapse (i.e., $TR > 0.8$). Buildings with $TR = 0.8$ and $\mu_{Strength} > 5$ have a simulated collapse probability greater than 0.70. As TR increases beyond 0.8, indicating even greater torsional irregularity, the

$\mu_{Strength}$ required to cause collapse is smaller (i.e., smaller excitation relative to base shear strength will cause collapse). For $TR > 1$, the torsional amplification factor, A_T, is not well defined, and any building with this TR, regardless of strength is judged to have a high collapse probability. This "collapse prone" region is shown in Figure I-11 and labeled as Extreme Torsion. These buildings are judged to be *Exceptionally High Seismic Risk*.

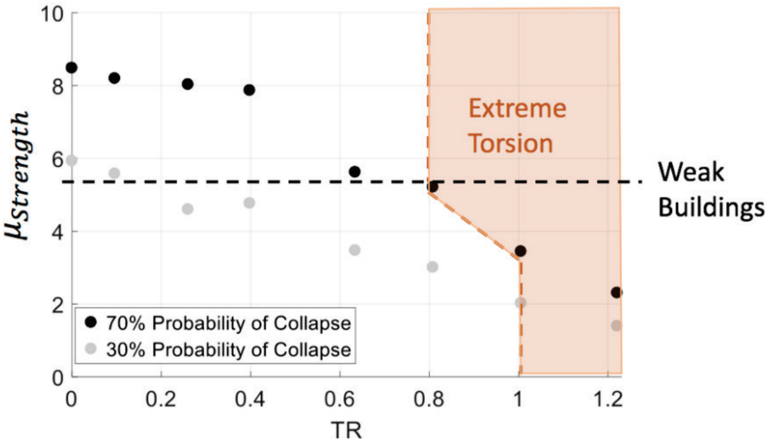

Figure I-11 Buildings that are define to have "Extreme Torsion" are shown in the shaded area, identifying cases that may exceed 70% collapse probability. The "weak building line" defines when $\mu_{Strength} > 5.5$, which indicates buildings that are *Exceptionally High Risk* due to being exceptionally weak (Appendix E).

I.5 Neglecting Torsion

In frame-wall buildings, even those that have some torsional irregularity, torsion may not significantly influence response. For these buildings, the analyst may neglect the torsional amplification factor in computation of drift demands on columns due to the small expected effect of torsion on building risk. This section describes the results used to identify those buildings for which torsion is not significant.

To define those situations in which we can neglect torsion we return to Cases A-C, where the difference in collapse capacity between symmetric and torsional cases is shown to be negligible, as plotted in Figure I-9 and Figure I-12. These results identify the region ($TR < 0.4$) for which torsion is not expected to be significant.

Note that the *TR* limit illustrated in Figure I-12 is effective at identifying cases where torsion does not significantly influence collapse risk, but the calculation of *TR* is cumbersome. Figure I-13 is the same as Figure I-12, except the x-axis has been replaced by the wall index (*WI*). Figure I-14 shows that buildings with $WI < 0.006$ are not expected to have significant enough torsion effects to warrant detailed analysis of torsional amplification of drift demands on columns. We note that the *WI* is the same regardless of where the walls are found in the building. This analysis suggests that a frame-wall building with *WI* < 0.006, regardless of how the walls are configured, does not have sufficient torsional irregularity to substantially alter the collapse outcome. Like the frame buildings, these frame-wall buildings with relatively small amounts of walls are not expected to be vulnerable to torsion.

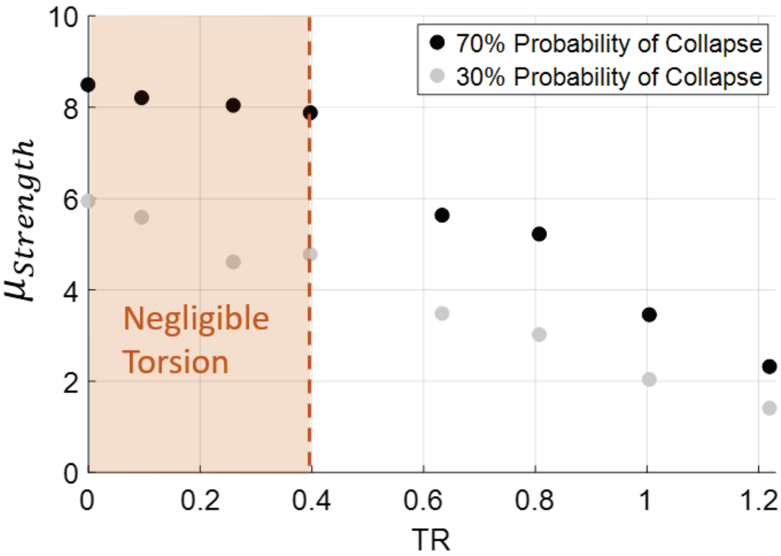

Figure I-12 Buildings for which torsional effects can be neglected are shown in the shaded area as a function of the torsional ratio. Buildings that fall in the shaded area were shown to have negligible difference in behavior between symmetric and torsional models.

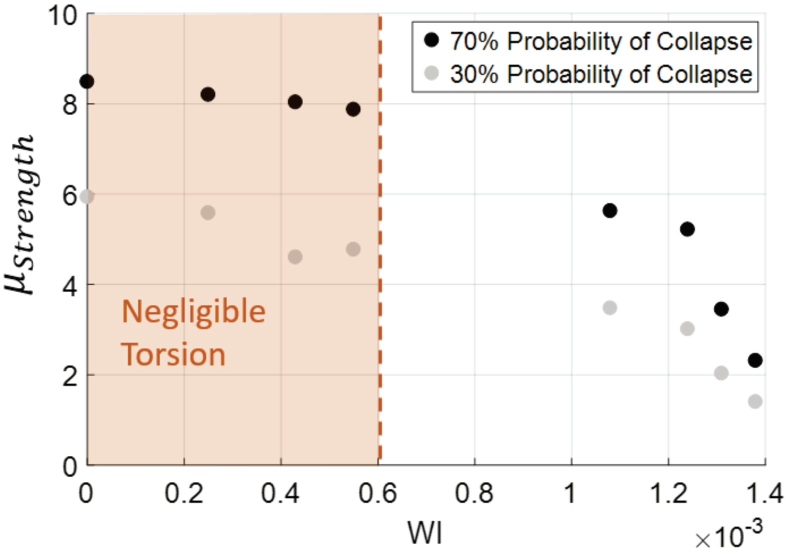

Figure I-13 Buildings for which torsional effects can be neglected are shown in the shaded area as a function of the wall index. Buildings that fall in the shaded area were shown to have negligible difference in behavior between symmetric and torsional models.

I.6 Torsional Amplification

I.6.1 Torsional Amplification Overview

All other frame-wall and wall buildings will require a full torsional analysis. Buildings for which the torsional analysis is needed are defined by Figure I-14.

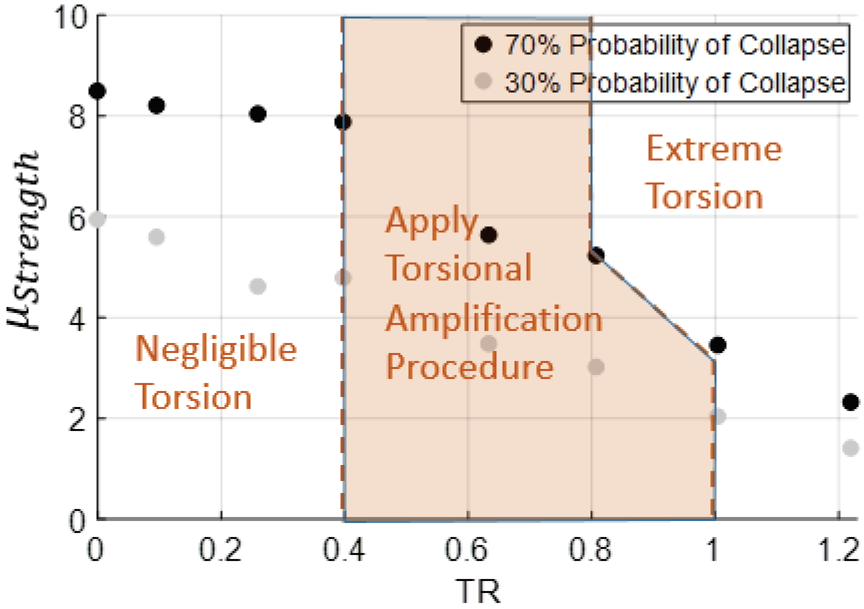

Figure I-14 Buildings that are required to undergo a full torsional analysis are defined by the shaded area.

I.6.2 Extraction of Torsional Amplification from Analytical Models

Buildings that qualify for torsional analysis require that the displacement demand on columns are amplified beyond the story displacement demand to account for torsion. To obtain the displacement amplification from the analysis, Equation I-5 is used.

$$A_{T,max} = \frac{max\left(\delta_{Edge}\right)}{max\left(\delta_{Story}\right)} \tag{I-5}$$

Here, $max(\delta_{Edge})$ is the maximum displacement experienced at the edge of the building in the time history analysis. $max(\delta_{Story})$ is the maximum displacement experienced at the center of strength. This calculation is illustrated in Figure I-15. Torsional amplification values are computed for each ground motion at each scale level considered in the dynamic analysis.

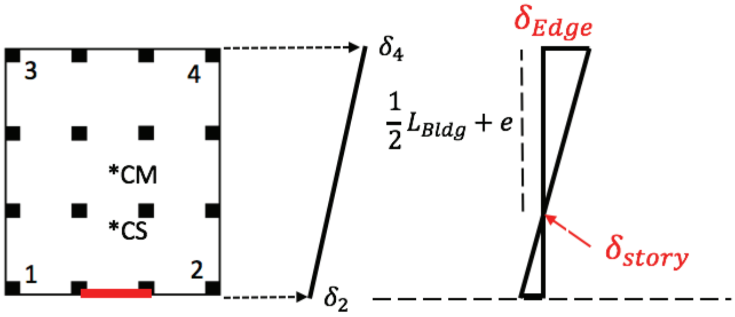
3
4
*CM
*CS
1
2
δ_4
δ_2
δ_{Edge}
$\frac{1}{2}L_{Bldg} + e$
δ_{story}

Figure I-15 Column drift amplification due to torsion is the multiplier required to convert story drift to edge drift.

The accuracy of the torsional amplification factor being extracted from the models depends on *e*, the distance between the center of mass and the center of strength. Here, we compare hand calculated estimates of *e* to the *e* extracted from the model result, and compared to results obtained by analysis of simple 3D portal frame (Figure I-16).

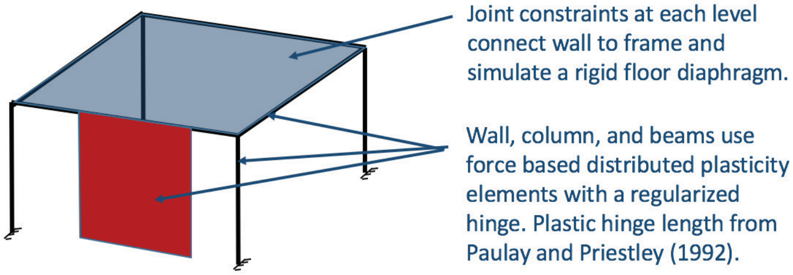
Joint constraints at each level connect wall to frame and simulate a rigid floor diaphragm.
Wall, column, and beams use force based distributed plasticity elements with a regularized hinge. Plastic hinge length from Paulay and Priestley (1992).

Figure I-16 3D portal frame used to examine estimates of e.

Figure I-17 illustrates the difference in *e* when hand calculated using either center of stiffness (Equation I-7) or strengths from mechanism calculations (Equation I-6), compared to *e* extracted from the pushover of a simplified 3D portal frame analytical model. At small lateral load levels, the building rotates about its center of stiffness. However, as the load level increases and the building response becomes nonlinear, the system begins to rotate about the center of strength from the hand calculations. Since we are trying to determine the nonlinear performance of a building just before collapse, then using a strength based eccentricity is an appropriate choice. The strengths used are determined from mechanism analysis.

$$\overline{y} = \frac{\Sigma y_i V_{pfi}}{\Sigma V_{pfi}} \tag{I-6}$$

$$\overline{y} = \frac{\Sigma y_i K_{pfi}}{\Sigma K_{pfi}} \tag{I-7}$$

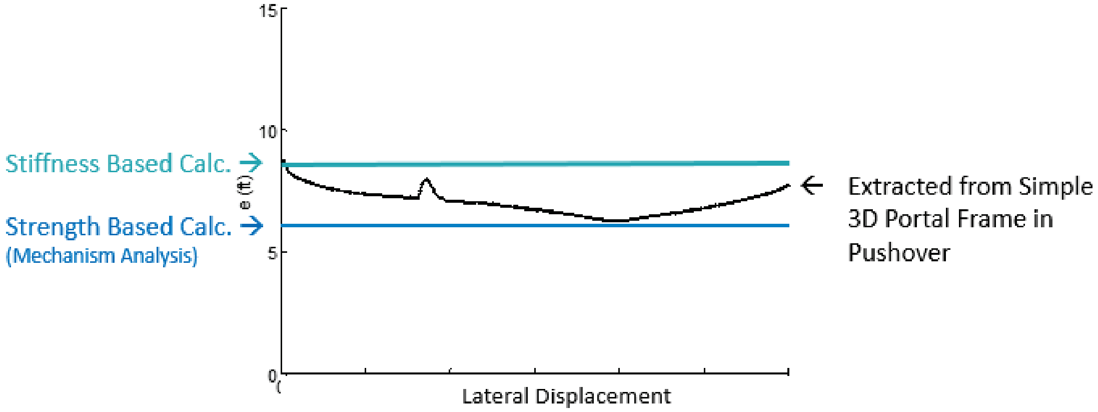

Figure I-17 Difference between stiffness based eccentricity and strength based eccentricity compared to eccentricity extracted from a model 3D portal frame with a wall on one side.

I.6.3 Torsional Amplification Results

The median torsional amplification values obtained from the models at the scale level corresponding to "collapse" are shown in Figure I-18, and are compared to the torsional amplification equation proposed in this document (Equation 7-6 and I-8). For $TR < 1$ the equation for torsional amplification factor fits the data well. However, for buildings with a $TR > 1$, the equation may under predict the drift demand; these buildings are defined as having Extreme Torsion. Buildings with $TR > 0.4$ do not require torsional amplification to be used in analysis.

$$A_{T,max} = e^{TR} \tag{I-8}$$

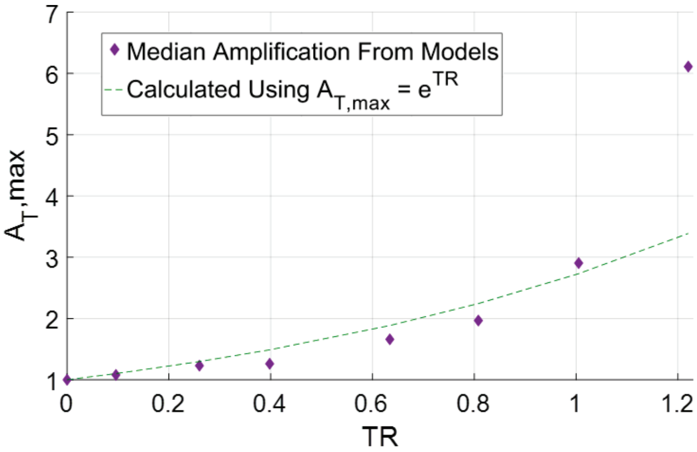

Figure I-18 Torsional amplification curve. $A_{T,max}$ defines the drift amplification on the edge of the building relative to the drift demand at the center of strength.

I.6.4 Torsional Amplification Calculations in Each Column

After the torsional amplification is determined, the torsional amplification of the drift at each column is determined by geometry (and as illustrated in Figure I-19). At the edge farthest away from the center of strength of the building (i.e., the weak or flexible side of the building), the amplification is equal to the maximum amplification. At the center of strength, the amplification is 0, and it varies linearly in plan to the maximum value. On the side of the building closest to the center of strength (strong or stiff side), the amplification is taken as 1.0, as shown in Figure I-20.

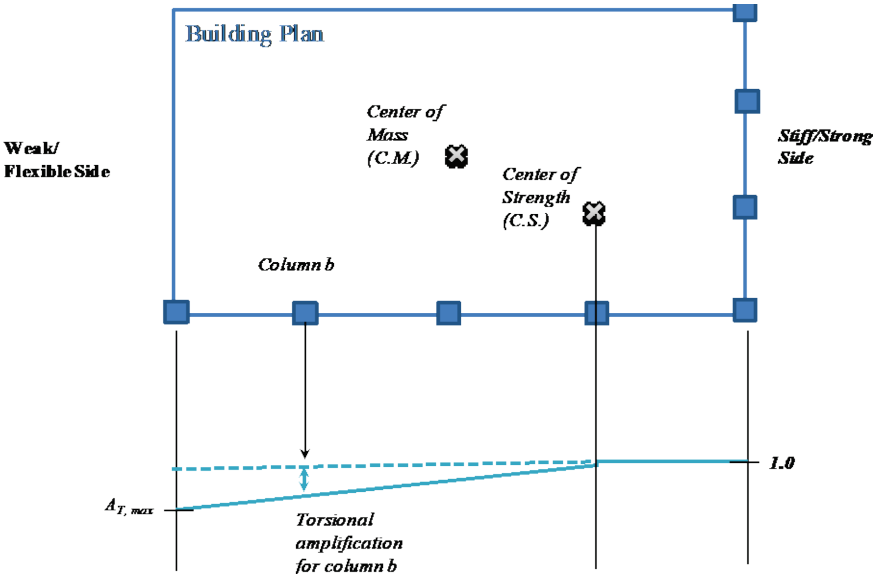

Figure I-19 Illustration of torsional amplifications computed for earthquake loading in the N-S direction. The amplification in each column depends on the location of the column.

I.7 Comparison of Results to Other Torsion Studies

Figure I-20 compares the collapse capacities obtained from this study to analysis of torsionally-critical buildings conducted for the ATC-123 Project by DeBock (2017). As we did here, DeBock (2017) simulates building with an array of torsional layouts ranging from symmetric to highly torsional. The differences are that here we examine non-ductile pre-1980 concrete building behavior, while the DeBock (2017) buildings are representative code compliant ductile structures. To model these structures, DeBock (2017) represented the lateral resisting system of code compliant systems with two frame lines acting in each horizontal direction at various locations, modeled with hysteretic springs capturing the response of each line of resistance at each story. Two subsets of the buildings from DeBock (2017) study are included for comparison here: those low-rise buildings that are code compliant and those low-rise buildings that are code compliant and designed to have proportional strength and stiffness. We compare to the low-rise buildings because they have periods close to the buildings considered in this study.

The DeBock (2017) results are superimposed on the results from this study in Figure I-20, reporting the median collapse capacities on the collapse fragility results obtained in this study. In most cases, the median collapse capacities (normalized by strength) fall between the 30th and 70th percentile curves from the results of this study, showing relatively good agreement. At high torsional levels, the DeBock (2017) results have relatively higher collapse capacities, due to the additional design requirements in modern seismic codes when torsional irregularities are significant (DeBock et al., 2014).

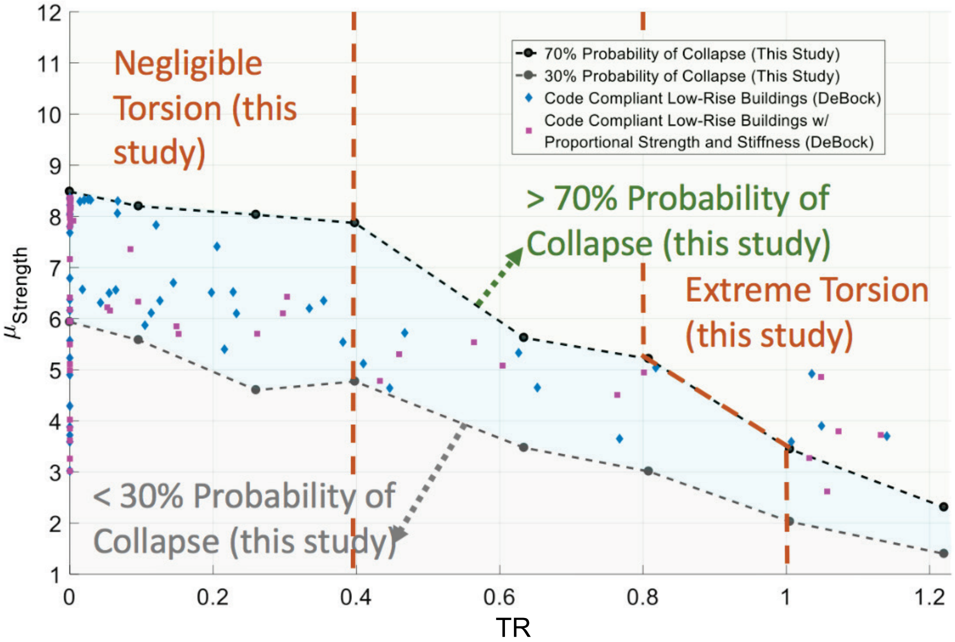

Figure I-20 Collapse capacities from buildings analyzed by DeBock (2017), compared to the results of this study.

Appendix J
Determination of Drift Factors

J.1 Overview

In this methodology, the fraction of the story drift that is taken by the critical component is denoted γ. For example, during seismic excitation, the story drift demand in a frame structure is resisted by beams and columns. During elastic (or near elastic) response, the drift demand is distributed between beams and columns in proportion to their relative stiffnesses. During nonlinear response, drift tends to concentrate in the components of the building that have yielded (or experienced some other physical damage that leads to a significant reduction in component stiffness and degradation of response). γ quantifies this drift concentration in particular components.

This appendix shows how the values of γ were determined for cases where columns are critical (J.2), where slab-column or beam corner connections are critical (J.3), and where walls or wall segments are critical (J.4).

J.2 Drift Factor for Critical Columns

J.2.1 Buildings Analyzed

For frame and frame-wall buildings the values of γ were obtained from dynamic analysis of models of six-story reinforced concrete frame buildings, subjected to a suite of 44 ground motions. The flexural and shear properties of the columns in the buildings were varied between models to obtain a broad data set capable of capturing the values of γ for buildings with varying characteristics.

J.2.2 Results

If the building is responding in the nonlinear range, the portion of the drift taken by the column, γ, depends on the relative strength of the columns and the beams framing into a joint (or relative strength of columns and slab-column connection framing into a joint). This is because the drift tends to concentrate in the weaker element. To extract values of γ from the nonlinear models, the portion of drift taken by the columns was read from lumped-plasticity, nonlinear springs which were present at beam and column ends in the nonlinear models. The maximum ratio of column drift to total story drift was taken from the analysis in which the ground motion was scaled to a spectral acceleration value corresponding to incipient collapse. Results were then averaged over all of the ground motions to obtain the values shown in Figure J-1. In Figure J-1, each point represents the results obtained from analysis of a 6-story building with a uniform ratio of column to beam strength at every joint, and a uniform ratio of column shear capacity to flexural capacity in every column. The portion of drift taken by the column during nonlinear response depends on both the ratio of column to beam strength, $\Sigma M_c/\Sigma M_b$, and the ratio of column shear capacity controlled by flexure to column shear capacity controlled by shear, V_p/V_n.

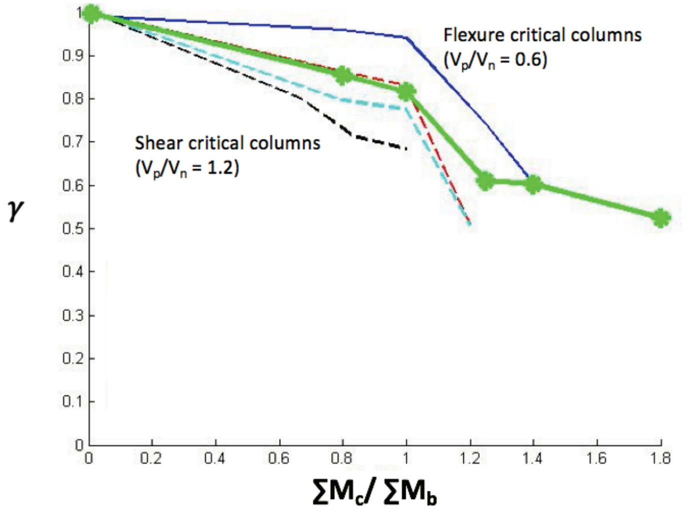

Figure J-1 Portion of drift taken by the column, γ, during nonlinear response from incremental dynamic analysis of selected 6-story buildings.

To simplify the calculation of γ in the nonlinear range, the value of γ was taken to be linear with respect to relative strength of the columns and the beams framing into a joint. This relationship is shown in Figure J-2. Note that for $\Sigma M_c/\Sigma M_b$ greater than 1.4, γ should be taken as 0.6. Limited analyses were conducted for larger $\Sigma M_c/\Sigma M_b$ ratios.

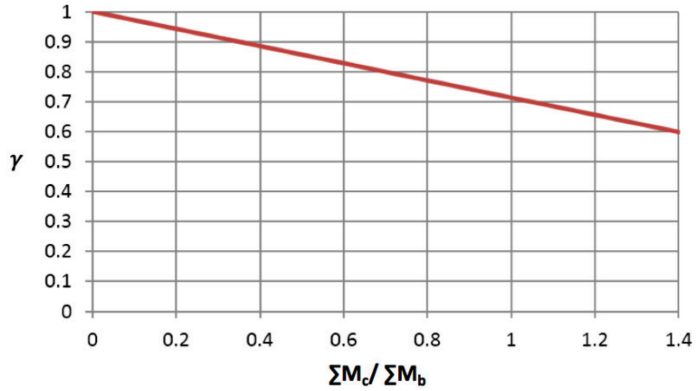

Figure J-2 Portion of drift taken by the column, γ, assuming a linear relationship with $\Sigma M_c/\Sigma M_b$.

Failure to consider γ is conservative because it assumes all of the drift is taken by the column.

J.3 Drift Factor for Critical Slab-Column Connections and Beam-Column Corner Connections

If the slab-column connection is found to be the critical component, γ, will be taken as 1.0. This is because the drift capacities for connections are based on the entire connection subassembly, considering the deformation of the slab/beam, connection, and column. Therefore, there is no need to separate the drift attributable to these different components.

J.4 Drift Factor for Critical Wall and Wall Segments

In frame-wall and wall buildings, the story drift is the same as the drift in the wall. For this reason, for critical walls and wall segments, the drift factor, γ, is taken as 1.0.

Appendix K

Archetype Building Analysis Methods

K.1 Introduction

This Appendix presents the methods considered for analysis of archetype structures including bare frames and frame plus walls combinations. The included methods are: nonlinear static analysis, incremental dynamic analysis, dynamic analysis for hazard consistent ground motions, and 3-dimensional dynamic analysis for torsion studies.

K.2 Nonlinear Static Analysis

Nonlinear static analyses (pushover) were performed in structural systems composed of one frame plus different wall configurations to identify the influence of the walls in the building strength, the plastic collapse mechanism, and the story drift demands at collapse. The structures were subjected to an inverted triangular load pattern. For studies of the effect of wall shear strength on building response, some of the nonlinear static analyses were conducted using lateral forces that were uniformly distributed over height. Selected results from the analyzed cases are presented in Appendix H.

The software OpenSees was used as analysis platform. It was not possible to obtain a unique set of parameters for nonlinear analysis that provides the best results for all structures. Therefore, all the cases were analyzed several times under different parameters (tolerances, controlled horizontal DOF, nonlinear analysis algorithm, and others). Nonlinear analysis algorithms included Newton, Modified Newton and Krylov-Newton. Detailed description of nonlinear fiber models considered in this study can be found in appendix L. Analysis results were post-processed in the software MATLAB.

K.3 Incremental Dynamic Analysis

Incremental dynamic analyses (Vamvatsikos and Cornell, 2002) were employed to assess the collapse potential of shear- and flexure-dominated bare frames models and for the analysis of selected frame-wall structures. This analysis methodology uses a set of seed ground motions which are scaled progressively to perform response history analyses of the structural model under consideration. For each scaling factor, each ground motion has an associated intensity measure (IM) value and a corresponding peak structural response of interest, referred to as an engineering demand parameter (EDP). The ground motion scaling factor is incremented until a response threshold is surpassed for each ground motion. At the end of the analysis process, each EDP of interest is associated to a distribution of IM values. Figure K-1 shows an example of the IDA results, along with the estimation of two points of the corresponding fragility curve of certain EDP level. The process consists of counting the proportion of IM realizations of ground motion that result in the EDP level under consideration. A lognormal distribution is usually fitted to the empirical probability function estimated (Baked, 2015).

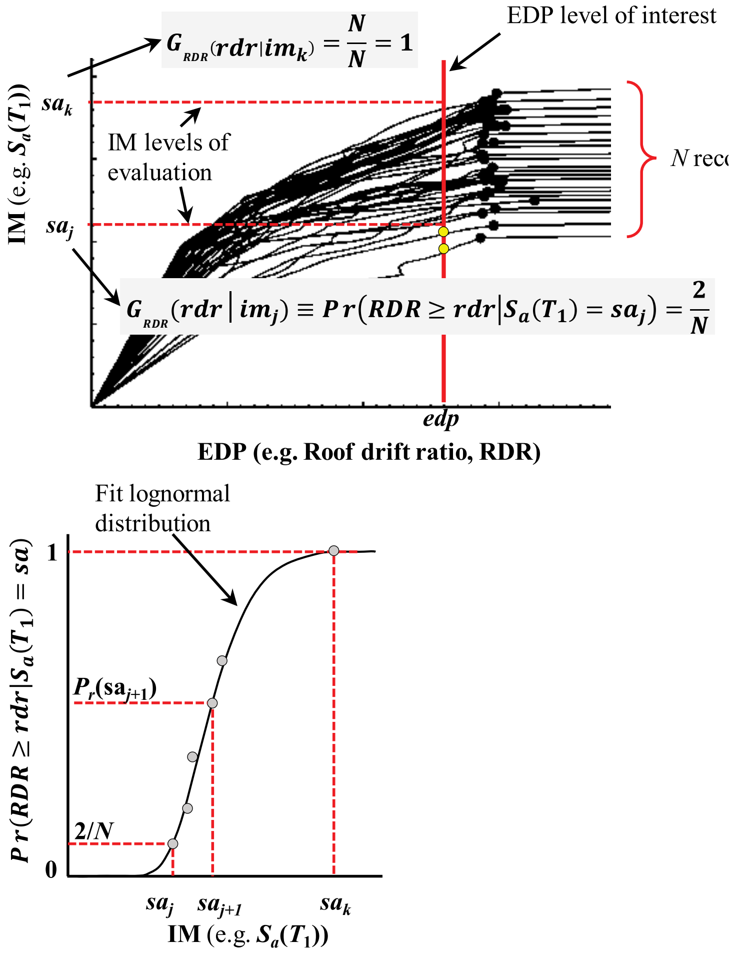

Figure K-1 IDA results and corresponding fragility curve estimation (adapted from Haindl et al., 2015).

Collapse was defined for the smallest input motion required to achieve either one of the following two limit states: (1) maximum story drift ratio exceeding 10% of story-height; or (2) shear or axial failure in more than 50%

of the columns in any story. A suite of 22 pairs of far-field ground motions was selected, for a total of 44 ground motions. The output of the analysis is the relation between the spectral acceleration (at the first-mode period T_1 of the building) and maximum story drift ratio for a given ground motion record.

Figure K-2 shows a typical output from an IDA analysis of a single building model. Each line in the figure represents the response of the building model to a single ground motion record scaled to increasing intensity. Note that the curves begin to flatten out at maximum story drift ratio of approximately 0.03 to 0.04, suggesting that the structure becomes unstable at around this story drift ratio. The collapse risk of each building model was obtained from statistics on the IDA results. In this study, collapse performance was evaluated using the probability of collapse as a function of the ground motion intensity level, defined in terms of $S_a(T_1)$. The collapse probabilities in terms of $S_a(T_1)$ were assumed to be log-normally distributed. Figure K-3 shows collapse fragility relations.

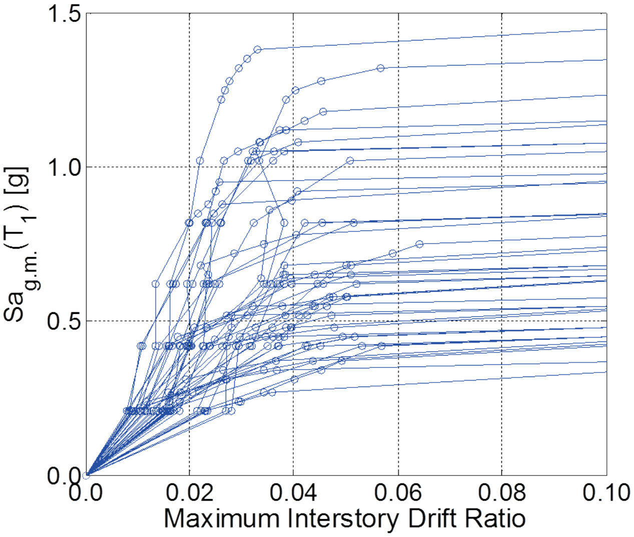

Figure K-2 Incremental Dynamic Analysis (IDA) curves for an 8-story modern code design building model ($V_u/V_n = 0.6$, $\Sigma M_{nc}/\ \Sigma M_{nb} = 1.2$).

In incremental dynamic analysis a single-record provides a single measure of how collapse occurs for that one ground motion record. To measure the variability in the dynamic response, multiple IDA analyses are done using different ground motions. After the IDA procedure has been completed for each seed ground motion, post-processing of the results is required to develop the fragility curve of the specified model. A first step is to established the empirical cumulative distribution function (CDF) of probability of collapse as a function of ground motion intensity. Then, a lognormal distribution is fit to the collapse data points. The lognormal collapse fragility is defined by two parameters, which are the logarithmic mean (μ_{ln}) and the standard deviation (σ_{ln}). This study considered only the record-to-record collapse (aleatory) uncertainty. Modeling (epistemic) uncertainties were not considered. Also, the effect of spectral shape of the considered ground motions in the estimation of the probability of collapse was not considered.

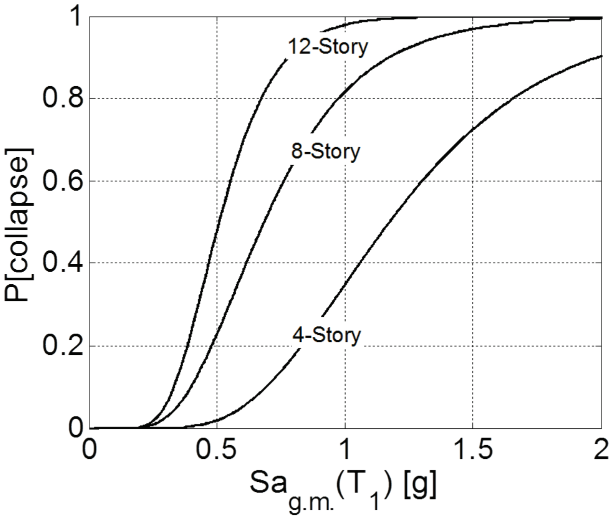

Figure K-3 Collapse fragility functions for the "modern code design" building models (V_u/V_n = 0.6, $\Sigma M_{nc}/\Sigma M_{nb}$ = 1.2).

K.4 Dynamic Analyses with Hazard-Consistent Ground Motions

Some studies of frame-wall structures used dynamic analyses with hazard-consistent ground motions. Hazard consistency in ground motion selection allows assigning rates of occurrence to each time series used in nonlinear dynamic analyses. Assigned rates are defined based on spectral shape and intensity. Under the assumption that structural responses have the same rate of occurrence as the uniform excitation that generate them, a hazard-consistent set of ground motions allows estimating the risk of engineering demand parameters (EDP) of interest. Figure K-4 shows data for a set of ground motions selected based on the Conditional Scenario Spectra (CSS) Methodology (Arteta and Abrahamson, 2017) for a site of high seismicity in the West Coast of the United States.

The CSS is a set of ground motions with assigned rate of occurrence that represents the hazard at a site over a period of 100,000 years. The selection procedure for the CSS is based on targeting several Conditional Mean Spectra (CMS) (Baker, 2011) with corresponding variability at increasing return periods. These CMSs are anchored at a given period to Uniform

Hazard Spectra (UHS) that are estimated from the hazard curves at a site, which are typically estimated by means of a Probabilistic Seismic Hazard Analysis (PSHA). This ensures that the selected ground motions have the proper spectral shape at all intensities of selection, thus allowing recovery of the hazard according to Equation K-1:

$$v(S_a(T) > z) = \sum_{i=1}^{\#\,recordings} Rate_{CS,i} H\left(S_{a,i}\left(T\right) - z\right) \tag{K-1}$$

where $S_{a,i}(T)$ is the spectral acceleration of the i^{th} recording, z is a test level, H is the Heaviside function (for example, $H(x) = 1$ for $x > 0$ and $H(x) = 0$ for $x \leq 0$); and $Rate_{CS,i}$ is the assigned rate of occurrence to each ground motion.

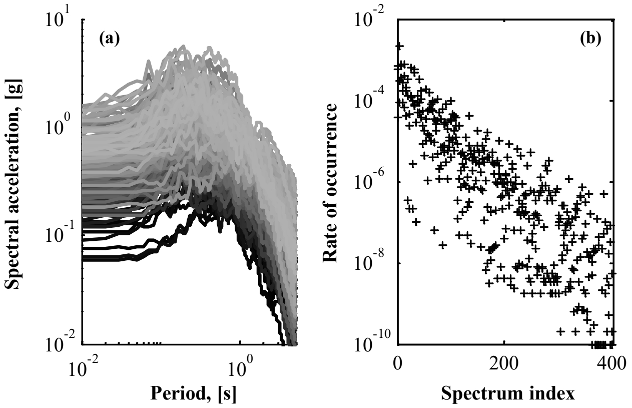

Figure K-4 Scenario spectra: (a) 402 scenario spectra (5% damped); (b) assigned rate of occurrence for each spectrum of the CSS (after Arteta and Abrahamson, 2017).

Figure K-5 compares the hazard recovered from the CSS with target hazard curves (estimated in a PSHA) of a site in a high seismicity site. The target and recovered hazard curves are shown for hazard levels from 10^{-2} to 10^{-5} at three different periods.

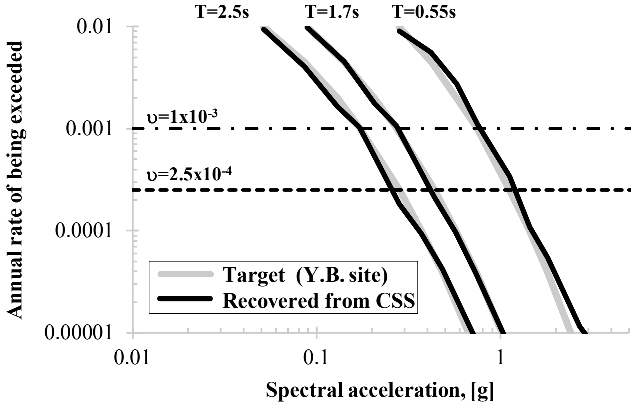

Figure K-5 Hazard curves at different periods recovered with the CSS set.

The risk of response parameters of interest, such as story drift ratio (SDR) or roof drift ratio (RDR), can be readily estimated using Equation K-2, which has the same functional form as Equation K-1:

$$\lambda(edp) \equiv \nu(EDP > d) = \sum_{i=1}^{\#recordings} Rate_{CS,i} H(EDP - d) \qquad \text{(K-2)}$$

where $\nu_{EDP}(EDP > d)$ is the annual frequency with which demand level d is exceeded, and, as before, $H(EDP - d)$ is either 1 or 0, per the Heaviside function H, depending on whether the EDP from time series i exceeds level d.

The seismic behavior of frame-wall systems was assessed using the Conditional Scenario Spectra methodology. To illustrate the type of data available after analyzing structural systems with the CSS, Figure K-6 shows the response of two 8-story reinforced concrete building models, one whose lateral load resisting system comprises a bare frame, and the other having in addition a competent flexural wall. Figure K-6a compares the response of the pushover curves of the structures, showing an apparent improved response of the frame-wall system with respect to the bare frame. Figure K-6b shows maximum roof drift ratio versus rate of occurrence relationships.

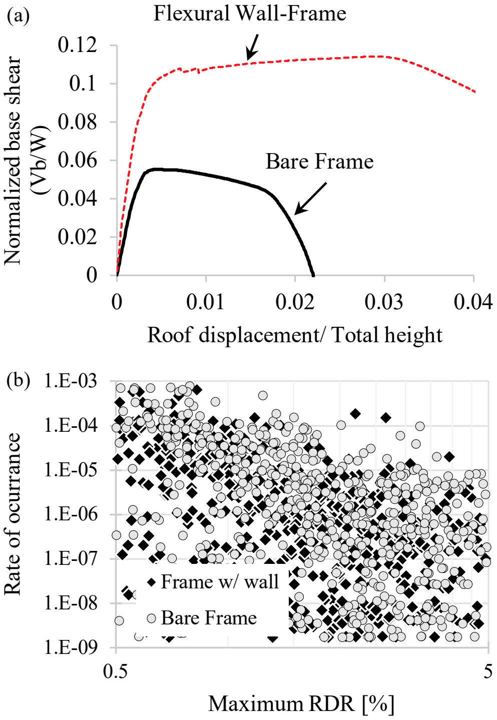

Figure K-6 Static and dynamic response of two 8-story buildings: (a) pushover curves; (b) maximum roof drift ratio versus rate of occurrence.

Reduction of the data in Figure K-6b through Equation K-2 allows estimating the annual rate of exceedance of any EDP of interest. Figure K-7 shows risk curves for the maximum roof drift ratio of the aforementioned structures. A feature of the graph worth noting feature is that it offers an objective platform to compare system performances at various levels of return periods. In the example shown, the wall-frame system shows an apparent (measurable) improved behavior with respect to the bare frame system at any return period over 75 years.

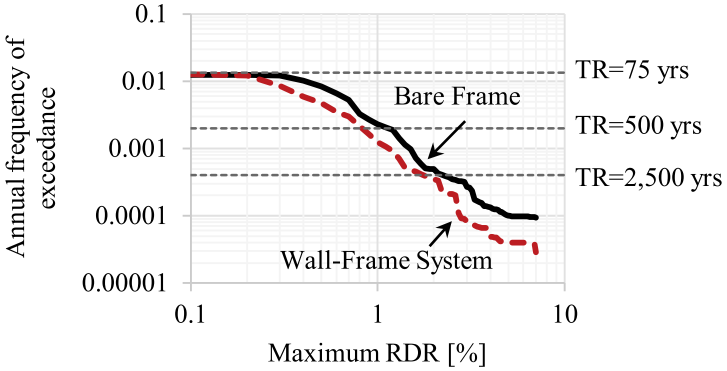

Figure K-7 Risk curves of maximum roof drift ratio for two 8-story buildings.

Because of the broad range of intensities covered, the CSS is an adequate set to study building behavior in the elastic and the inelastic range of response. This allows construction of fragility curves, with the advantage that the spectral accelerations used as predictor are also hazard-consistent. Figure K-8a shows a scatter plot of spectral acceleration at the fundamental period, $S_a(T_1)$, versus maximum roof drift ratio for the bare frame system described above. The data are organized by S_a, and probabilities of exceeding certain demand levels can be estimated (Figure K-8b). Typically, a lognormal cumulative density function is fitted to the empirical data. Fragility curves also allow comparing building responses at different levels of demand (Figure K-8c).

The same data presented above, can also be analyzed to estimate dynamic alpha values at various levels of seismic demand. Figure K-9 shows the transition of alphas values from those of an archetype bare-frame 4-story building (Figure K-9a) to those of frame-wall structures with walls of increasing length (e.g., L_w = 50 in. and L_w = 80 in., Figures K-9b and K-9c, respectively). It is observed that as the walls grow in length, the mean alpha distributions tend to one.

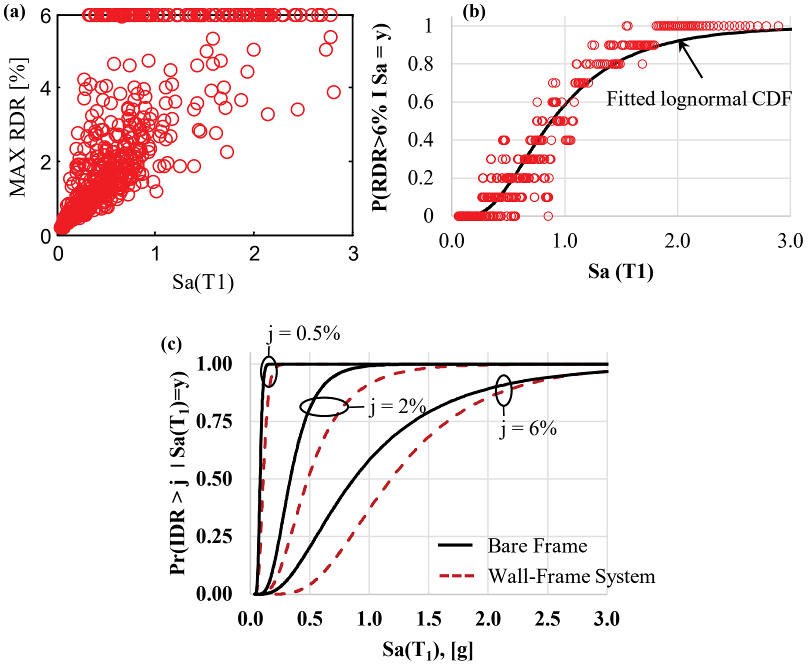

Figure K-8 Fragility curves construction: (a) scatter plot of raw data; (b) fragility curve construction; (c) fragilities comparison.

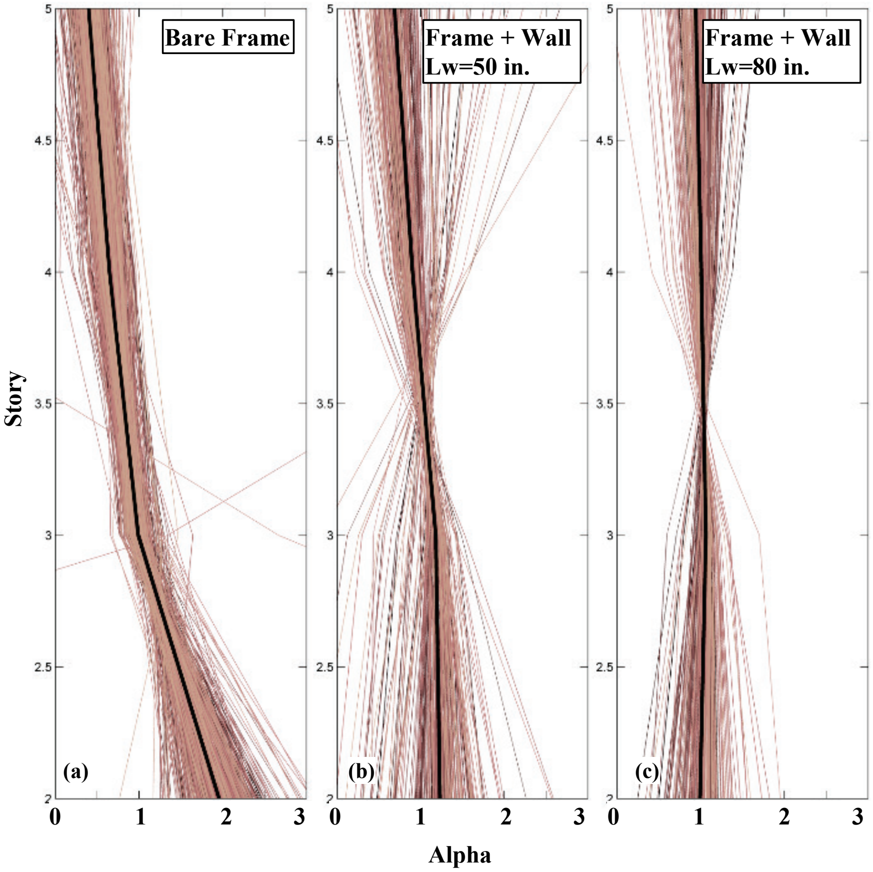

Figure K-9 Dynamic alphas, 4-story building: (a) bare frame archetype; (b) frame coupled to a wall with L_w = 50 in.; (c) frame coupled to a wall with L_w = 80 in.

Figures K-10 shows the transition of alphas values from those of an archetype bare-frame 8-story building (Figures K-10a) to those of frame-wall structures with walls of increasing length (e.g., L_w = 50 in. and L_w = 100 in., Figures K-10b and K-10c, respectively). It is observed how the alpha values transition from a distribution with large concentrations in the bare frame (due to a weak story upstairs) to a more uniform distribution with alpha values close to one and smaller for a frame-wall system with a wall of length L_w = 100 in.

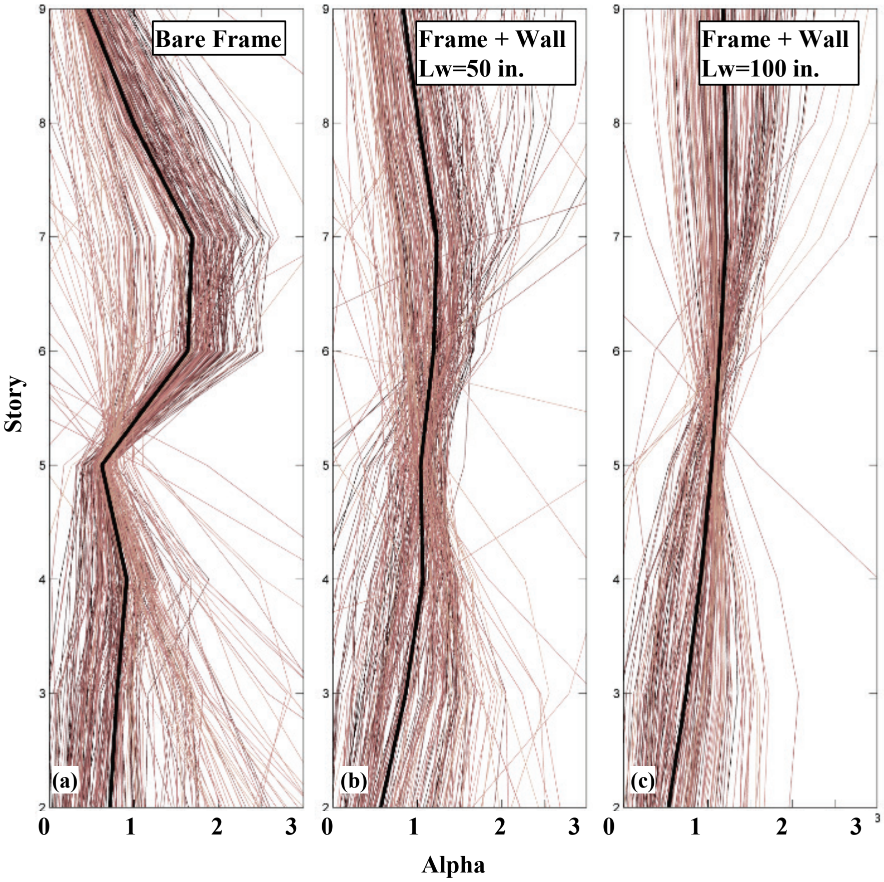

Figure K-10 Dynamic alphas, 8-story building: (a) bare frame archetype; (b) frame coupled to a wall with L_w = 50 in.; (c) frame coupled to a wall with L_w = 100 in.

K.5 Dynamic Analyses for Torsion Studies

Incremental dynamic analyses were employed for the torsion studies. However, for the torsion studies, models were three-dimensional. In this study, seismic excitation was applied to the 3D models in only one horizontal direction at a time. This decision was made for consistency with the ATC-78 methodology, which looks at response in the two orientations of the building separately before combining to obtain a building rating. The IDA thus proceeds as described above using the same 22 pairs of far-field ground motions, with each ground motion applied separately for a total of 44 separate analyses.

In the torsion studies, collapse was defined as occurring when displacement demand on at least 25% of the columns reached or exceeded 1% story drift. The columns used in that study were brittle, and this collapse state corresponded to the loss of shear capacity, and likely gravity-load bearing capacity, of an entire frame line. More details and illustrations are provided in Appendix I.

Appendix L

Frame and Wall Modeling Procedures

L.1 Introduction

This Appendix describes modeling procedures for gravity and seismic analyses of bare frames and frame-wall combinations.

L.2 Bare Frames Models

Buildings were modeled using two-dimensional structural frames. Thus, biaxial interaction associated with simultaneous loading in two plan directions was not represented. The mathematical model is an assemblage of line beam-column elements, representative of the stiffness of beams and columns, connected to beam-column joints and to fixed supports at the base. To approximate flexibilities of beam-column joints, the joints were modeled as rigid, with dimensions equal to $d/2$, where d is the effective depth of the connected beam and column. Diaphragms were modeled as rigid in their plane. P-Delta formulation was employed to account for non-linear geometry effects. For dynamic analyses, Rayleigh damping was employed, with parameters adjusted to achieve 2% of critical damping at the initial first- and third-mode periods.

Buildings with different ratios of shear demand to shear capacity, V_u/V_n, were modeled. Thus, failure of structural components could be initiated due to either flexure or shear. It was assumed that shear failure does not dominate member failure where $V_u/V_n < 0.7$. Thus, only flexural failure was modeled for this case. Where $V_u/V_n \geq 0.7$, the possibility of having shear failure or shear induced axial failure was also considered by explicitly modeling nonlinearities associated with flexural, shear, and axial failure (Galanis and Moehle, 2015).

A concentrated plasticity approach was used to model both beams and columns. By this approach, the plasticity of the elements is represented by a nonlinear rotational spring with hysteretic rules assigned at the ends of a linear elastic beam-column element, with effective (cracked) stiffness properties. For those cases where shear and axial failure was likely, horizontal and vertical springs were also connected in series with the linear elastic element.

L.2.1 Building with Flexure-Controlled Columns

For the cases where $V_u/V_n < 0.7$, non-linear flexural response was modeled using the concentrated plasticity approach, where a flexural linear-elastic member is connected to two plastic hinges at the ends (Figure L-1).

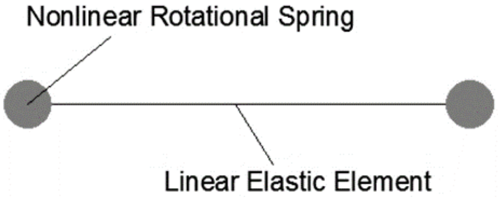
Nonlinear Rotational Spring
Linear Elastic Element

Figure L-1 Beam column element with concentrated flexural plasticity at the ends (after Galanis and Moehle, 2015).

The inelastic rotational spring response follows the Clough model, using hysteresis implemented in OpenSees by Ibarra et al. (2005), This model uses a post-peak negative slope to model strain-softening behavior associated with degradation of the flexural resisting mechanism. The model also incorporates cyclic strength degradation (Figure L-2).

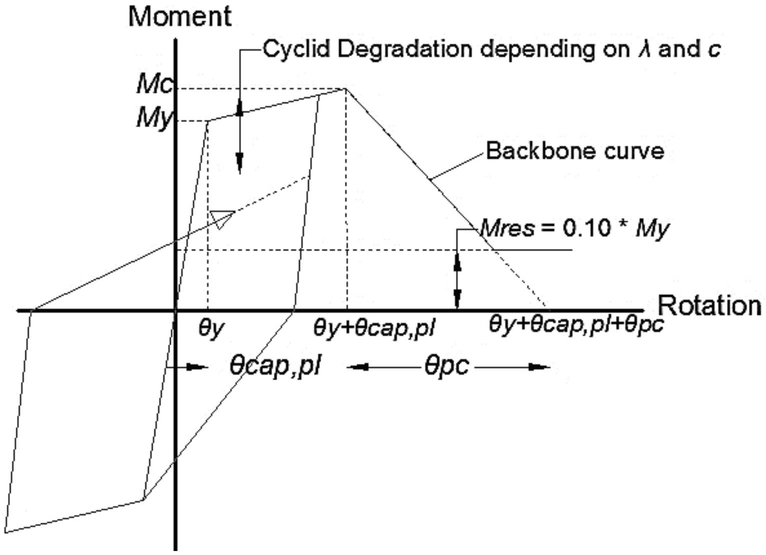
Moment
Cyclid Degradation depending on λ and c
Mc
My
Backbone curve
Mres = 0.10 * My
Rotation
θy
θy+θcap,pl
θy+θcap,pl+θpc
θcap,pl
θpc

Figure L-2 Backbone and cyclic response rule of the rotational spring representative of the flexural plastic hinge region (after Galanis and Moehle, 2015).

Seven parameters are required to control the response of the beam-column element: $[M_y, M_c/M_y, \theta_{cap,pl}, \theta_{pc}, \lambda, c]$; where M_y is the nominal moment strength according to ACI 318-11 (2011) provisions; ratio M_c/M_y was assumed to be equal to 1.2. The values of λ, c, $\theta_{cap,pl}$ and θ_{pc} were estimated using the equation in Haselton et al. (2007) but re-calibrated to exclude the cases for which shear or flexure-shear failure were reported.

L.2.2 Building with Shear-Critical Columns

For the cases where $V_u/V_n > 0.7$, shear failure may occur, possibly followed by axial failure. The Elwood and Moehle (2008) model introduced to simulate this behavior was adopted here. Flexural response is modeled using a lumped plasticity model, similar to the model used for flexure-controlled behavior. Two additional springs are added at the top of each column member to model shear and axial failure (Figure L-3).

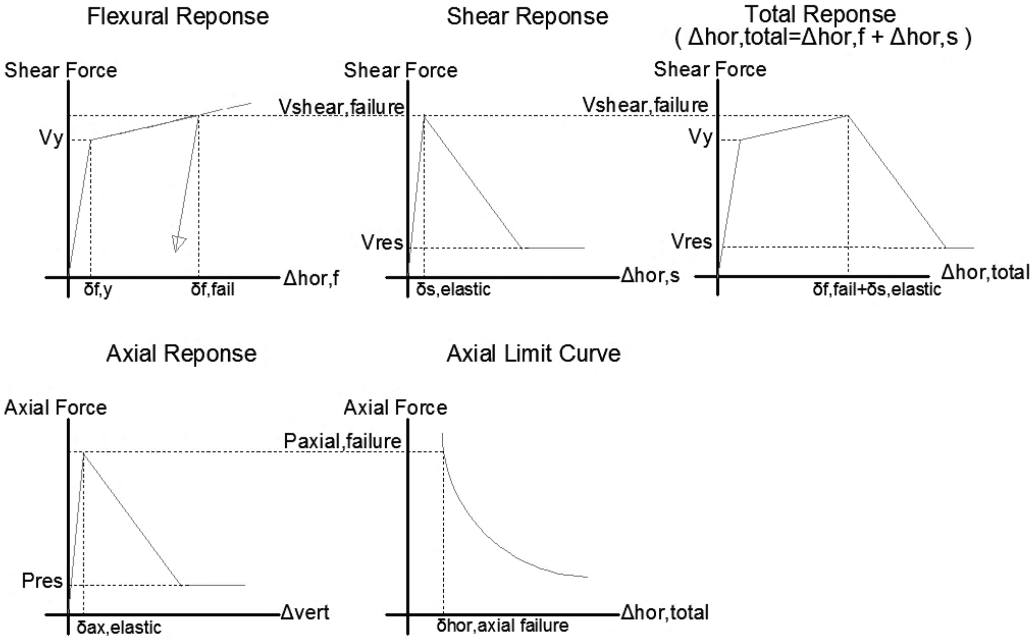
Flexural Reponse
Shear Reponse
Total Reponse
(Δhor,total=Δhor,f + Δhor,s)
Shear Force
Vy
δf,y
δf,fail
Δhor,f
Shear Force
Vshear,failure
Vres
δs,elastic
Δhor,s
Shear Force
Vshear,failure
Vy
Vres
δf,fail+δs,elastic
Δhor,total
Axial Reponse
Axial Limit Curve
Axial Force
Paxial,failure
Pres
δax,elastic
Δvert
Axial Force
δhor,axial failure
Δhor,total

Figure L-3 Limit state shear-axial-spring material introduced (after Galanis and Moehle, 2015).

The shear spring is linearly-elastic until the shear failure strength. For larger drifts, the post-peak response of the shear spring follows a linear softening. The onset of shear failure is defined as a function of the story drift ratio of the column. In its original definition, the model was restricted so that shear failure only occurs after flexural yielding. For this work, the model was updated such that shear failure could be initiated prior to flexural yielding.

L.3 Modeling Criteria of Frame-Wall Systems

In older construction, reinforced concrete walls were sometimes added for lateral resistance but they were also added as stair case enclosures, as firewalls, and/or as partitions. Consequently, the configuration, location, and reinforcement are not always ideal for lateral force resistance. These walls can resist a significant portion of the overall story shear because of their inherent lateral stiffness and strength. Additionally, interaction with structural frames may result in moment demand distribution along the height of the wall that may produce yielding at multiple elevations. It is necessary to use models that enable development of these varied yielding mechanisms. This section presents the modeling approach selected to simulate walls interacting with older frames.

L.3.1 Frame-Wall Definition

To study the response of a shear wall in a frame-wall system, a lightly reinforced concrete wall is coupled to a ductile frame using rigid links. Figure L-4 presents the 8-story structure, which comprises a 4-bay ductile frame, braced by a 260 in. wall.

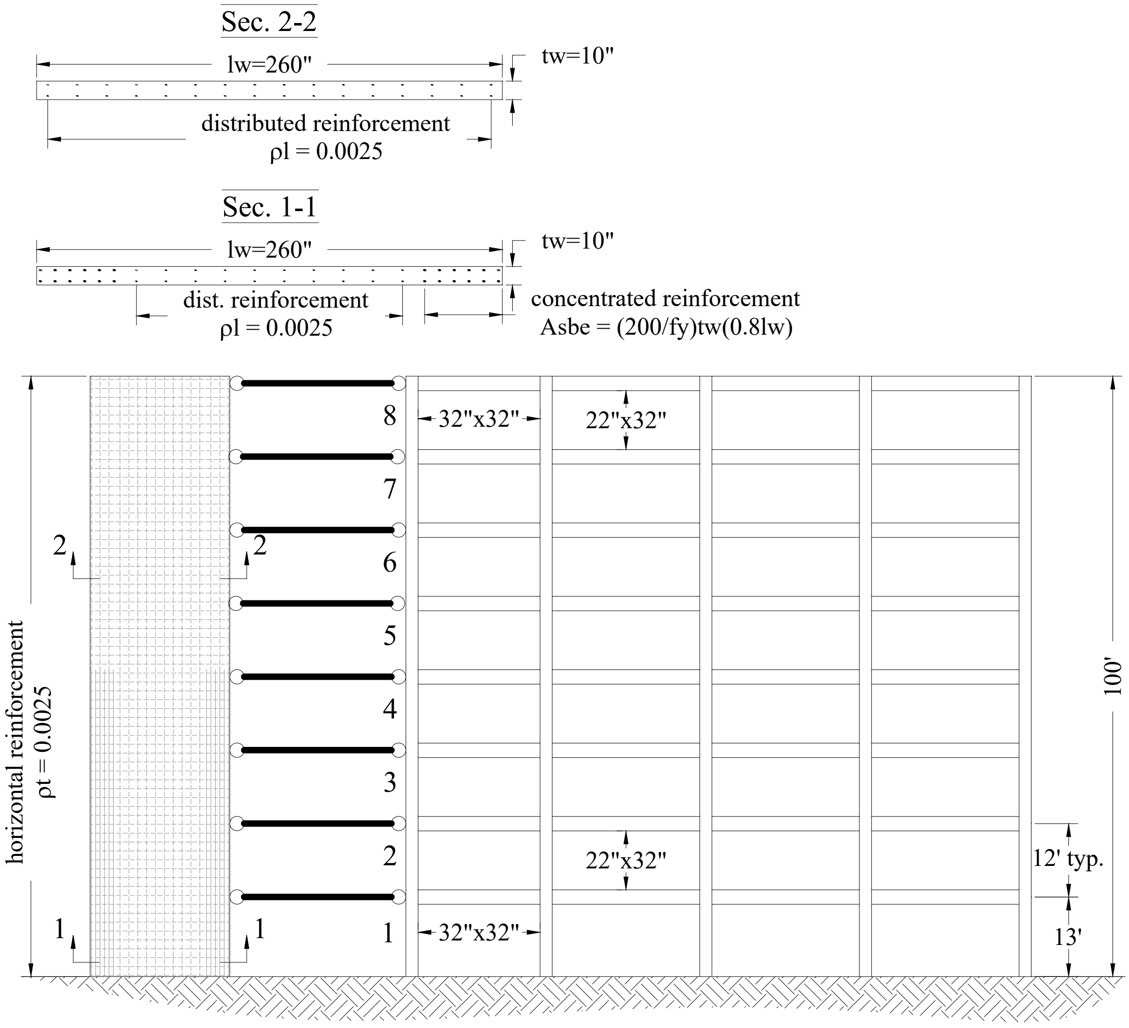
Sec. 2-2
lw=260"
tw=10"
distributed reinforcement
ρl = 0.0025
Sec. 1-1
lw=260"
tw=10"
dist. reinforcement
ρl = 0.0025
concentrated reinforcement
Asbe = (200/fy)tw(0.8lw)
8
7
6
5
4
3
2
1
32"x32"
22"x32"
22"x32"
32"x32"
2
2
1
1
horizontal reinforcement
ρt = 0.0025
100'
12' typ.
13'

Figure L-4 Elevation and wall reinforcement detailing of the frame-wall structure used for this study.

For the frame, concrete is assumed normal weight (γ_c = 150 lb/ft^3) with nominal strength f_c' = 6 ksi and reinforcing steel with nominal yielding strength of f_y = 60 ksi. Columns are 32 × 32 in. with longitudinal steel ratios (total area of steel to gross area ratio) ρ_{min} = 1.00% and transverse steel ratio with A_v / bs > 0.87%, where A_v is the total area of transverse reinforcement within distance s of two adjacent layers and b is the core dimension of column. Beams are 22 × 32 in. with longitudinal steel ratios (area of tension reinforcement divided by web width and effective depth) ranging from ρ = 0.39 to 0.54% and transverse steel ratios A_v / b_s > 0.63%. Given the adequate framing detailing, shear failure is not expected in the frame; therefore, shear in beams and columns is modeled as elastic. The shear wall was detailed following recommendation of (ACI Committee-318, 1977) with longitudinal and transverse reinforcement ratio of 0.25%. Additionally, the bottom half of the wall has boundary reinforcement with area $A_{s,be}$ = (200 / f_y) t_w (0.8l_w), where f_y = 60 ksi, t_w = 10 in. is the thickness of the wall and l_w = 260 in. is its length. The concrete of the wall is normal weight with f_c' = 4.5 ksi and it is assumed that no confinement is provided by the transverse reinforcing steel. The axial load at the base of the wall is assumed to be $0.1 A_g f_c'$ and decreases proportionally to the height.

L.3.2 Wall Modeling Approach for Frame-Wall Systems

Force-based nonlinear beam-column elements with concentrated plasticity at the ends were used to model all structural elements of the frame (Scott and Fenves, 2006). This modeling technique allows selecting the span of plasticity spread by allowing the selection of a plastic hinge length. Fiber sections assigned to the plastic hinge regions simulate material nonlinearities while accounting for moment-axial load interaction.

Distributed plasticity formulation offers a flexible platform for modeling structural walls because the location of the critical section cannot be predicted prior to the analysis. Three main formulations of distributed plasticity elements are: the force-based, the displacement-based, and the mixed formulation (Scott and Hamutçuoğlu, 2008). In this study, we selected the force-based nonlinear beam-column element with distributed plasticity (Spacone et al., 1996).

Computational implementation of the force-based elements requires selection of a numerical integration method. Three quadrate (or integration) rules were considered in this study: (i) *Gauss-Lobatto*; (ii) *Gauss-Legendre*; and (iii) *Gauss-Radau*.

To test the impact of different quadrature rules in the response of the force-based element, a cantilever wall with the geometry, material characteristics, and reinforcement layout of that in Figure L-4 was programmed in OpenSees. Figure L-5 shows the geometry of the mathematical model. The centerline of the element representing the wall coincides with the centroid of the cross section and does not migrate with the neutral axis location. Concrete was modeled as unconfined using the stress-strain relationship proposed in Kent and Park (1971) as modified by Scott et al. (1982) to include the tensile behavior of concrete. The hysteretic behavior of concrete under stress reversal was modeled according to Mohd Yassin (1994), including gradual degradation of stiffness under unloading and reloading in compression (Spacone et al., 1996). The longitudinal reinforcing steel stress-strain behavior was assumed to be bilinear with isotropic strain hardening (Filippou et al., 1983) but modeled with a hysteretic material as implemented by Scott and Filippou in OpenSees.

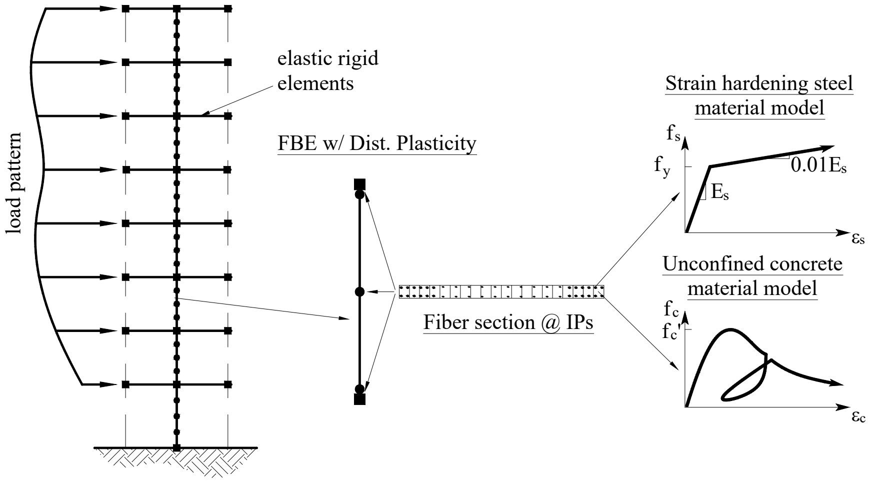

Figure L-5 Nonlinear force-based element with distributed plasticity formulation for the wall.

A physical interpretation often given to the weights of the quadrature rules used in the formulation of distributed plasticity elements is related to the spread of plasticity within the element. For softening behavior, it is expected that the inelastic demand over the element concentrates on a single integration point. In flexure, this results in high curvature demand at the section level, which results in a reduced total deformation capacity of the element. To test the impact of this behavior, three wall models were constructed using the Gauss-Lobatto integration rules (i.e., with integration points at the ends of the element) with increasing number of integration points: $N_p = 3$, 4 and 5 (models *GLo3*, *GLo4* and *GLo5*). It was of interest to test if the reduced length (weights) of the external integration point impacted the behavior of the wall at a global and at a section level. A fourth wall model was also constructed by mixing the Gauss-Radau integration rule with 2 integration points for the first story and Gauss-Legendre rule with 3 integration points for the rest of the elements (model *GRa2GLe3*). The ideas behind this integration point scheme are: (i) using the quadrature rule with the largest weight at the end of the first story element allows representing the spread of plasticity at the critical section (base) over a larger, more meaningful length (approximately $0.15lw$), while still maintaining accuracy; (ii) using a more accurate integration rule, such as the Gauss-Legendre, for the rest of the wall element, where integration points at the ends of each story are not necessary, allows reducing the total number of integration points, hence the running cost.

Pushover analyses were conducted over the aforementioned models using two different load patterns of lateral force: an inverted triangular load pattern with horizontal forces proportional to the height of each floor and a similar triangular load pattern with a reversed force at the roof. The latter pattern simulates interaction with the framing system, and generates large moment demand in the sections above the wall midheight.

Figures L-6 through L-9 show the pushover curves under the triangular load pattern. Two critical sections are observed along the height of the wall: one at the base and another at the moment capacity discontinuity above the fourth story. The pushover curve shape is similar for all models but the onset of softening occurs at lower roof drift ratios for lower values of the weight of the first integration point. Four instances in the force-displacement relation of the wall are isolated to study the moment and curvature demand distribution along its length: (i) cracking capacity (red markers); (ii) first yield (green markers); (iii) onset of concrete crushing (cyan markers); and (iv) 3.5% roof drift ratio (blue markers). Moments and curvature values depicted were obtained at each integration point along the height of the wall and are plotted at the relative distance within each element according to the selected integration rule.

Moment distribution along the height of the wall is similar for all models. The curvature figures show that all the models are able to spread the plasticity above the critical integration point (i.e., above the first IP in the first and fifth story). Curvature distribution along the height of the wall is similar for all models while the wall remains elastic. Inelastic curvature demand follows a parabolic shape within the first story element (which contains the critical section). Elements with larger number of IPs model this distribution in a smoother manner. The downside to this is that, for larger roof displacements, much of the inelastic curvature demand is concentrated within the first IP which has a smaller associated physical length (weight).

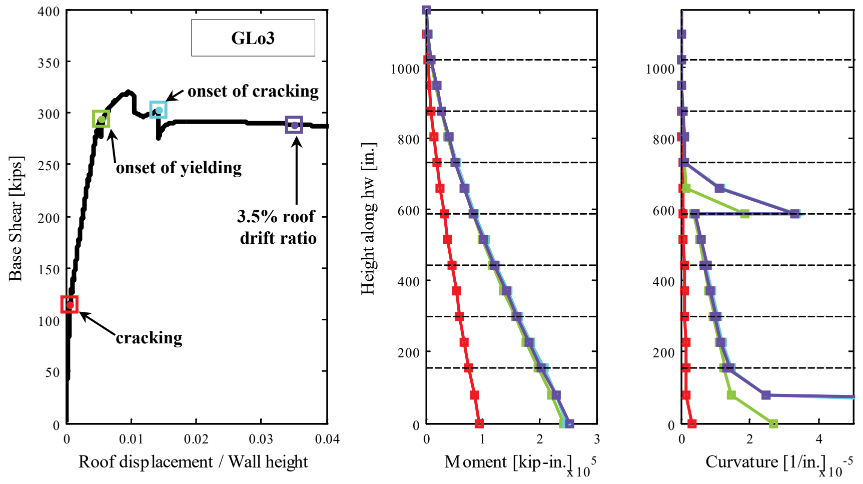

Figure L-6 Wall response under triangular load pattern for Gauss-Lobatto rule with three integration points.

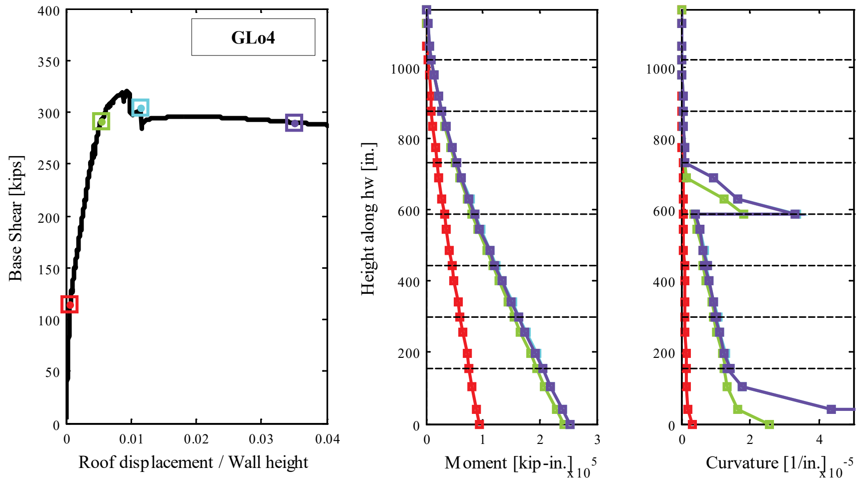

Figure L-7 Wall response under triangular load pattern for Gauss-Lobatto rule with four integration points.

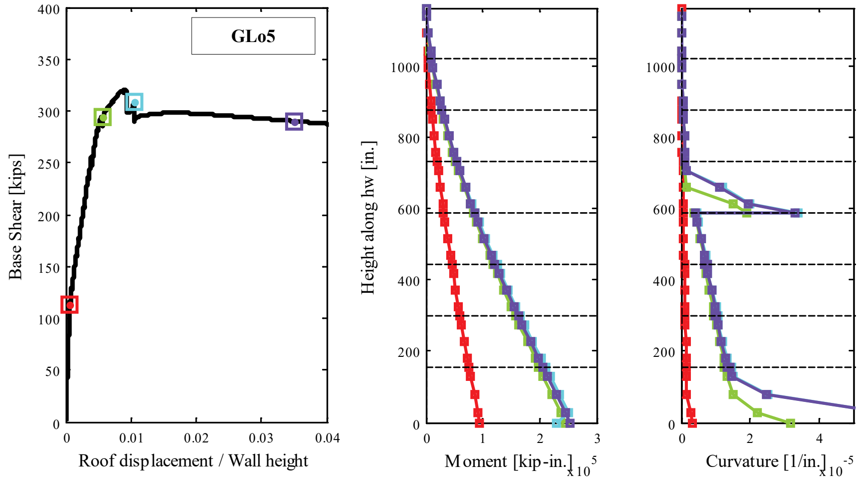

Figure L-8 Wall response under triangular load pattern for Gauss-Lobatto rule with five integration points.

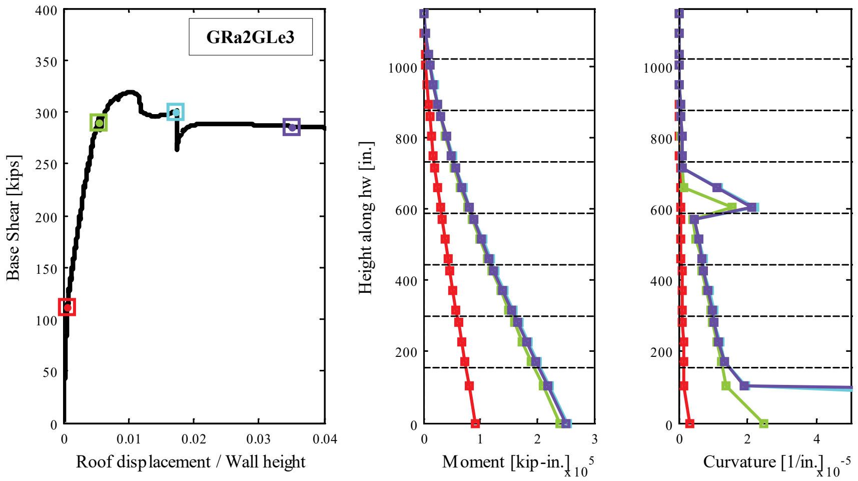

Figure L-9 Wall response under triangular load pattern for Gauss-Radaue rule with two integration points in the first story and three Gauss-Legendre integration points upstairs.

Figure L-10 shows the pushover curves under the triangular load pattern with a load reversal at the roof level for the GRa2GLe3 model. Curvatures shown are for two levels of magnification and show that the model is able to model curvature sign change within the length of a single element and the parabolic nature of the curvature distribution given the moment distribution along the element length.

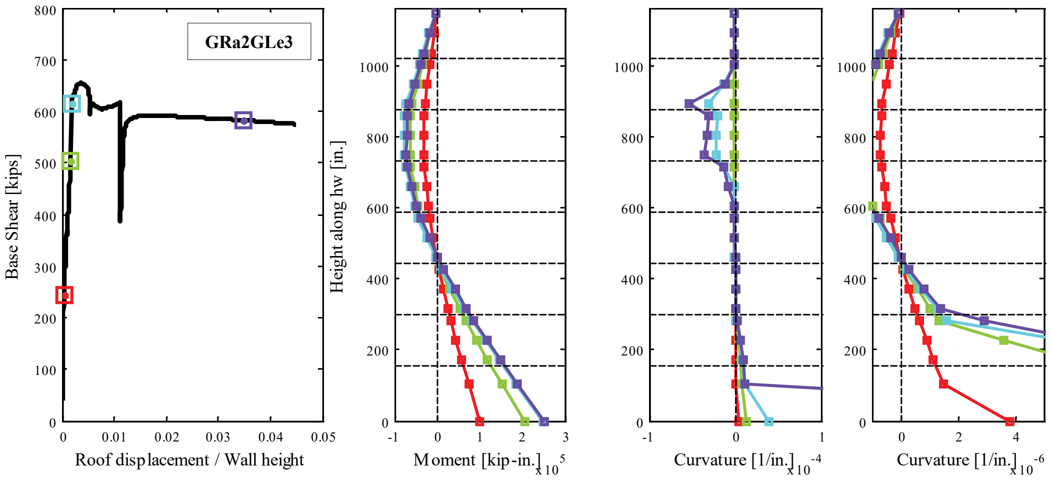

Figure L-10 Wall response under triangular load pattern with a reversed load at the roof for Gauss-Radaue rule with 2IPs at the first story, and 3 Gauss-Legendre IPs upstairs.

Figure L-11a shows the roof drift ratio at which the first three states of response (e.g., cracking, yielding, and crushing) occurred for each model. Figure L-19b shows, in logarithmic space, the curvature demand at the first IP of the wall for different levels of roof drift ratio. This is normalized by the curvature at the onset of yielding, obtained from a moment-curvature analysis of the critical section, under the axial load at the base. The moment-curvature ductility demand relation of the section at the base is presented in Figure L-11c. The curvature ductility demand is defined as the curvature divided by the yielding curvature.

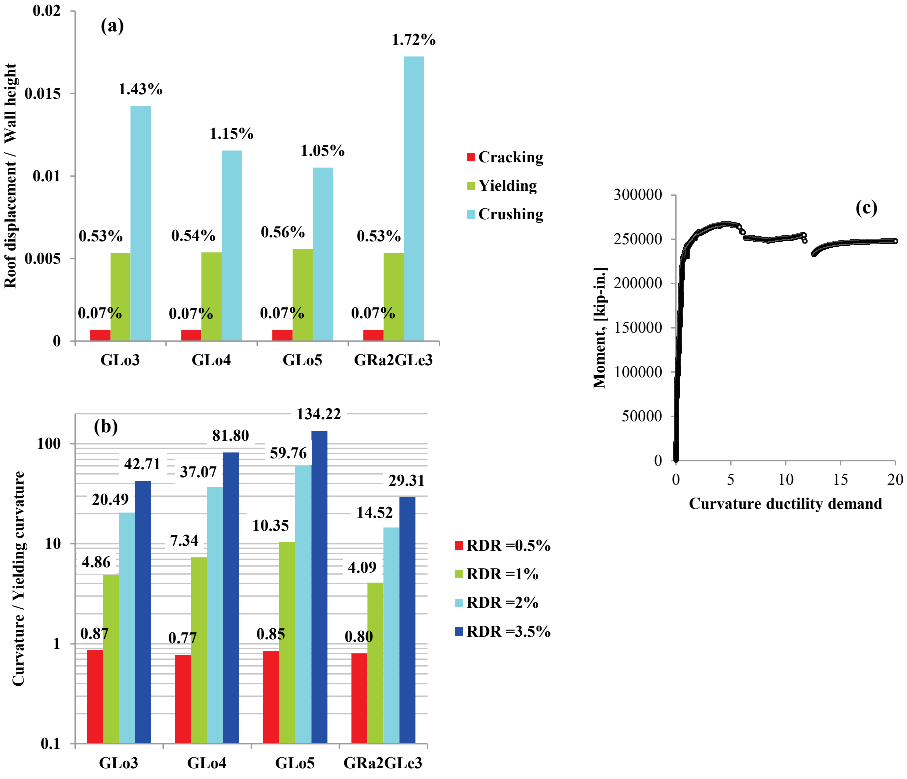

Figure L-11 Normalized curvature demand at the first integration point (critical section at the base) for the inverted triangular load pattern.

It is concluded that after the onset of yielding, the limitation of displacement capacity for larger numbers of IP is apparent. The onset of crushing produces differences in roof drift capacity as large as 60% (GRa2GLe3 vs GLo5). This is supported by the fact that even for very low levels of roof drift ratio (e.g., 0.5%) the curvature demand at the critical section can differ by a factor as large as 2.5 (GLo5/GRa2GLe3) among the models. For larger roof drift ratios (e.g., 3.5%), this ratio doubles. The moment-curvature relation shows that the wall has limited ductility capacity, and some integration rules might produce demands at the critical section past meaningless physical values. This can be solved with material regularization, to account for the size of the integration points. This requires additional effort to estimate fracture energy of the constitutive models and is outside the scope of this report.

In view of the preceding, and to keep local demands within tolerable values, the integration scheme used for the ATC-78 project to model walls is the GRa2GLe3, which has the lowest number of integration points along the wall length, hence requiring shorter computation times, yet maintaining adequate accuracy for the numerical integration of deformations and the stiffness matrix at the element level.

L.3.3 Frame Modeling Approach for Frame-Wall Systems

The modeling approach of frame-wall systems mainly focused on identifying how walls of different characteristics modified the global response of the coupled system. Therefore, the framing portion of the model followed a simpler approach than that described above in Section L.2.

Force-based nonlinear beam-column elements with concentrated plasticity at the ends were used to model all structural elements (Scott and Fanver, 2006), without modeling shear failure or shear-induced axial failure. Fiber sections assigned to the plastic hinge regions simulate material nonlinearities while accounting for moment-axial load interaction. For nonlinear dynamic analyses, mass and stiffness-proportional Rayleigh damping was used to simulate the energy dissipation characteristics of the building that is not accounted for by the nonlinear behavior of the structural elements. The Rayleigh damping coefficients were established to achieve a damping ratio of $\zeta = 2.5\%$ at periods corresponding to the first and third translational vibration modes of the linear model. Calculated periods for the nonlinear models were obtained after applying the vertical load, such that some initial service level cracking is accounted for. P-Delta effects were accounted for in the formulation of the columns.

Appendix M
Column Shear Strength

M.1 Column Shear Strength Equation

The column shear strength equations adopted in this methodology are based on the equations specified in ASCE/SEI 41, except for the way widely spaced shear reinforcement is considered. ASCE/SEI 41 defines transverse reinforcement to be 100% effective in contributing to the shear strength term V_s for spacing-to-effective-depth ratios $s/d \leq 0.75$, to be 0% effective for $s/d \geq 1.0$, with effectiveness linearly interpolated between these limits. In contrast, this methodology considers transverse reinforcement to be fully effective for any spacing.

The shear strength expression in this methodology was adopted after a review of the original data set that served as a basis for the ASCE/SEI 41 expression (Sezen and Moehle, 2004). Figure M-1 plots the results. Solid circles correspond to strength ratios V_{test}/V_n based on this methodology (identified as ATC-78 in the figure), while open circles correspond to strength ratios V_{test}/V_n based on ASCE/SEI 41. The data points plot atop one another for $s/d \leq 0.75$, and begin to diverge for $s/d \geq 0.75$. The data suggest that the expression in this methodology remains suitably conservative for wider hoop spacing.

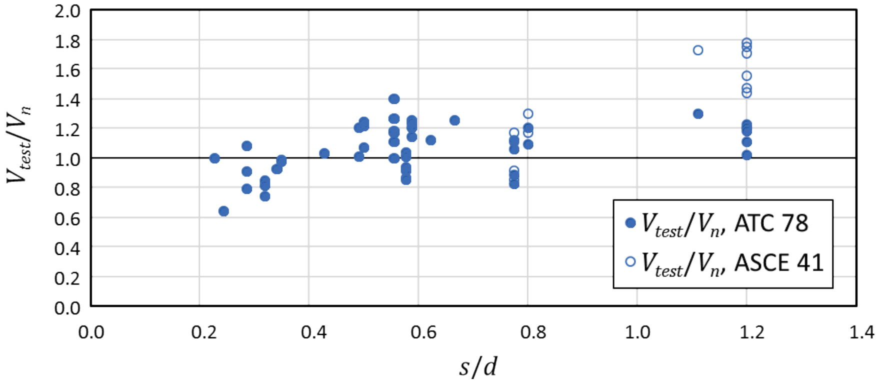

Figure M-1 Column shear strength (data from Sezen and Moehle, 2004).

Older building codes permitted tie spacing as large as the greatest of: (a) 16 times the longitudinal bar diameter; (b) 48 times the tie bar diameter; and (c) the least dimension of the column. Consequently, tie spacing sometimes approached the column gross cross-sectional dimension, which exceeds effective depth d. The shear strength expression in this methodology is intended to permit the engineer to count on that reinforcement in calculating V_s.

Appendix N

Development of Wall Drift Capacities

N.1 Introduction

In this methodology, wall drift capacities at axial failure are used to compute the wall ratings, which are then used to compute story and building ratings. This appendix first presents an approach to determine the expected failure mode for reinforced concrete (RC) structural walls, i.e., whether a wall is flexure- or shear-controlled, and it then describes the details of the development of drift capacities at axial failure for both flexure- and shear-controlled walls. The drift capacities are based on wall test data filtered from a database of more than 1000 wall tests (i.e., UCLA-RCWalls) developed by Abdullah and Wallace (2018a). The drift capacities given in this appendix are at axial failure, unless noted otherwise.

N.2 Expected Wall Behavior and Failure Mode

For the purpose of deriving the wall drift capacities, it is important to distinguish between flexure-controlled (slender) walls and shear-controlled walls/piers (low-rise squat walls/piers), as they have different lateral load resisting mechanisms and thus different behavior expectations. Currently, unlike RC column, there is no consensus approach to quantitatively define flexure- and shear-controlled walls. ASCE/SEI 41-17 Section C10.7.1 defines slender and squat walls as walls with aspect ratio (h_w/l_w) > 3.0 and < 1.5, respectively. Walls with intermediate aspect ratios are defined as flexure-shear-controlled walls. ACI 318-14 defines slender walls as walls with $h_w/l_w > 2.0$. However, as well be shown in the next paragraph, shear-flexure strength ratio ($V_{n,ACI}/V_{@Mn}$) is a better indicator of the expected wall behavior and failure mode than aspect ratio (or shear span ratio). Therefore, a different approach was used in this methodology, which is based on shear and flexural strength ratio. This approach is similar to that used for columns in this methodology and in ASCE/SEI 41-17.

A recently developed database (known as UCLA-RCWalls) by Abdullah and Wallace (2018a) that contains detailed information and test results from more than 1000 wall tests reported in literature was used to define the criterion for distinguishing flexure- and shear-controlled walls. The database includes the reported failure modes of the wall tests. When recording the failure modes in the database, the authors made sure that the reported failure mode in the reference documents matches the observed behavior and damage.

The database was filtered to obtain a dataset of 990 walls with flexure, shear, or flexure-shear failure modes. Walls with failure modes due to insufficient lap-splices or anchorages of longitudinal reinforcement were not included. The results are presented in Figure N-1, where $V_{n,ACI}$ is the nominal wall shear strength computed from ACI 318-14 Equation 18.10.4.1 using tested material strengths, $V_{@Mn}$ is the shear strength associated with the development of wall nominal flexural strength (M_n) at concrete compressive strain of 0.003 using sectional analysis and tested material strengths, and V_{Test} is the peak base shear obtained during the test. From this figure, it is clear that all shear-controlled walls (i.e., walls failed in diagonal tension or compression) have shear-flexure strength ratio $V_{n,ACI}/V_{@Mn} < 1.0$, and most flexure-controlled walls have $V_{n,ACI}/V_{@Mn} \geq 1.0$. Walls that fail in shear sliding at the base mainly have $V_{n,ACI}/V_{@Mn} \geq 1.0$ because shear friction strength should be used instead of ACI 318-14 Equation 18.10.4.1 to compute nominal shear strength, V_n. Walls with failure modes reported as flexure-shear (i.e., yielded in flexure but failed in shear) are mainly scattered between $0.5 < V_{n,ACI}/V_{@Mn} < 1.5$. Therefore, in this methodology, walls with $V_{n,ACI}/V_{@Mn} < 1.0$ are classified as shear-controlled walls, and walls with $V_{n,ACI}/V_{@Mn} \geq 1.0$ are classified as flexure-controlled walls.

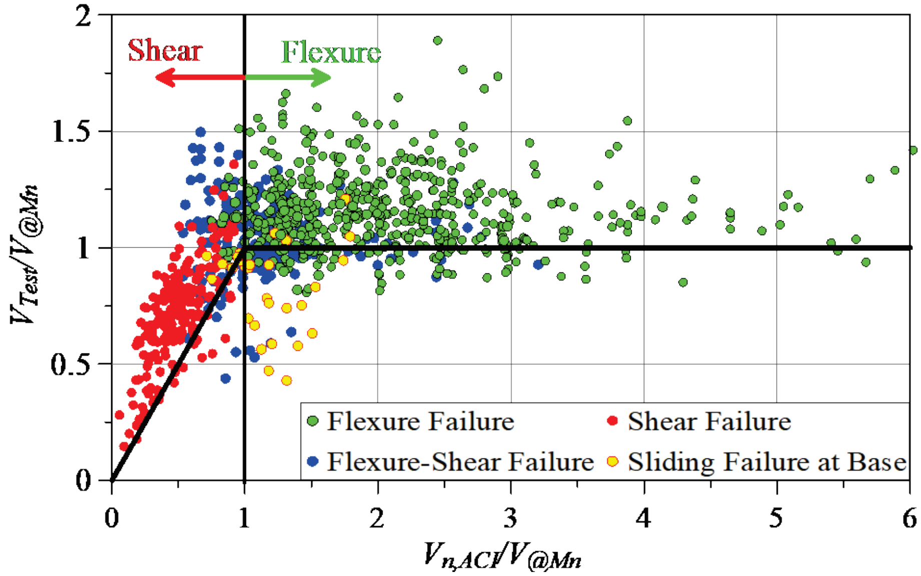

Figure N-1 Definition of flexure-controlled and shear-controlled walls based on results from a dataset of 990 wall tests.

N.3 Drift Capacity of Poorly Detailed Flexure-Controlled Walls

The UCLA-RCWalls database was used to obtain a dataset of poorly detailed walls in which deformation at axial failure is reported or complete loss of lateral strength was observed due to out-of-plane instability or concrete crushing in both the boundary zones and the web. A reduced dataset of 80 wall tests was identified that satisfied the following requirements:

- Walls exhibiting flexure failure mode, i.e., $V_{n,ACI} / V_{@Mn} \geq 1.0$
- Walls tested under quasi-static, reversed cyclic loading
- Walls with one or two curtains of web vertical and horizontal reinforcement
- Walls with ratio of provided-to-required (per ACI 318-14 Section 18.10.6.4) area of boundary transverse reinforcement, $A_{sh,provided}/A_{sh,required} \leq 0.7$, or ratio of vertical spacing of boundary transverse reinforcement to minimum diameter of longitudinal boundary reinforcement, $s/d_b \geq 8.0$.

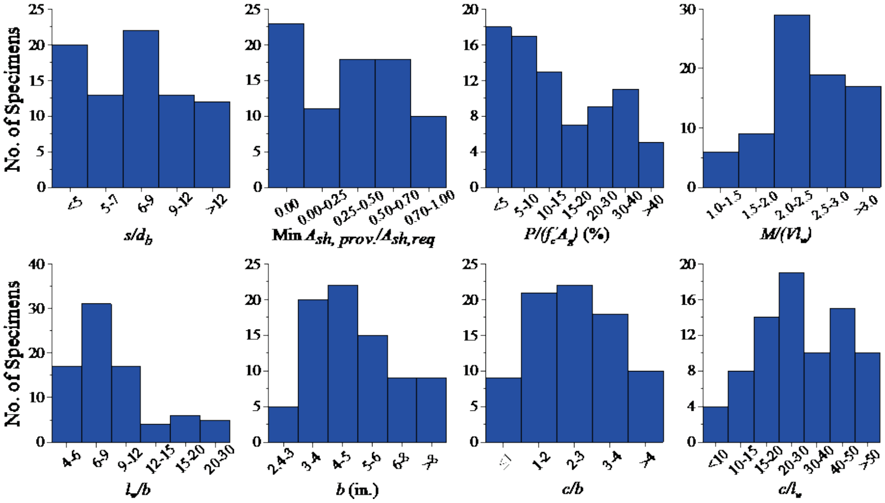

Figure N-2 Histograms of the reduced dataset of 80 flexure-controlled walls.

Histograms for various dataset parameters for the 80 wall tests are shown in Figure N-2, where $\left(P / A_g f_c'\right)$ is the sustained axial load used during the test normalized by concrete compressive strength $\left(f_c'\right)$ and gross concrete area (A_g), and $M/(Vl_w)$ is the ratio of base moment-to-base shear normalized by wall length (l_w), b is the width of compression zone, and c is the depth of neutral axis corresponding to concrete compressive strain of 0.003. Since this methodology is applied to older buildings constructed prior to development of modern building codes (i.e., pre-1971), wall tests that do not satisfy the design and detailing requirements of ACI 318-14 for special structural walls are used to develop the drift capacities.

Abdullah and Wallace (2018b) studied the drift capacity of flexure-controlled walls with special boundary elements at 20% lateral strength loss and found that wall drift capacity correlates well with a slenderness parameter $\lambda_b = l_w c/b^2$, which is the product of the ratio of wall neutral axis depth-to-width of the compression zone, c/b, and the ratio of the wall length-to-width of the compression zone, l_w/b. This slenderness parameter considers the impact of concrete and reinforcement material strengths, axial load, wall cross-section geometry, and quantities and distributions of longitudinal reinforcement at the wall boundaries and in the web.

After studying the reduced dataset shown in Figure N-2, it was found that $\lambda_b = l_w c/b^2$ also correlates well with wall drift capacity at loss of axial load carrying capacity. Although the axial load is included in the λ_b parameter through depth of neutral axis, c, it was found that the level of axial load has a significant impact on post-strength loss deformation capacity. Figure N-3 shows the variation of drift capacity at axial collapse as a function of λ_b and $P / A_g f'_c$. Application of linear regression analyses for the dataset of 80 tests, including the variables that significantly impact lateral drift capacity (i.e., λ_b and $P / A_g f'_c$), resulted in the following predictive equation for drift capacity (DC) at axial failure:

$$DC(\%) = 3.85 - \frac{\lambda_b}{30} - 3.5\frac{P}{A_g f'_c} \geq 0.75\% \tag{N-1}$$

where $\lambda_b = l_w c/b^2$ should not be taken more than 60. Results from Figure N-3 and Equation N-1 are presented in a tabular format in Figure N-4.

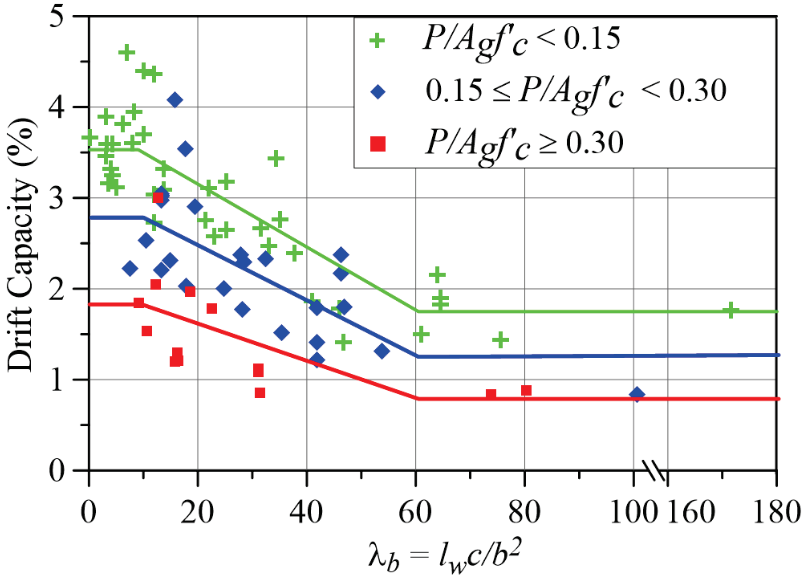

Figure N-3 Variation of drift capacity at axial failure as a function of λ_b and $P / A_g f'_c$.

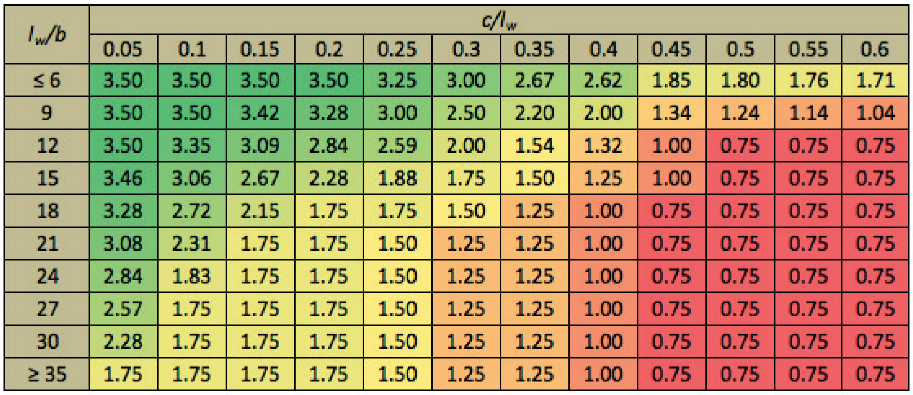

l_w/b	c/l_w											
	0.05	0.1	0.15	0.2	0.25	0.3	0.35	0.4	0.45	0.5	0.55	0.6
≤ 6	3.50	3.50	3.50	3.50	3.25	3.00	2.67	2.62	1.85	1.80	1.76	1.71
9	3.50	3.50	3.42	3.28	3.00	2.50	2.20	2.00	1.34	1.24	1.14	1.04
12	3.50	3.35	3.09	2.84	2.59	2.00	1.54	1.32	1.00	0.75	0.75	0.75
15	3.46	3.06	2.67	2.28	1.88	1.75	1.50	1.25	1.00	0.75	0.75	0.75
18	3.28	2.72	2.15	1.75	1.75	1.50	1.25	1.00	0.75	0.75	0.75	0.75
21	3.08	2.31	1.75	1.75	1.50	1.25	1.25	1.00	0.75	0.75	0.75	0.75
24	2.84	1.83	1.75	1.75	1.50	1.25	1.25	1.00	0.75	0.75	0.75	0.75
27	2.57	1.75	1.75	1.75	1.50	1.25	1.25	1.00	0.75	0.75	0.75	0.75
30	2.28	1.75	1.75	1.75	1.50	1.25	1.25	1.00	0.75	0.75	0.75	0.75
≥ 35	1.75	1.75	1.75	1.75	1.50	1.25	1.25	1.00	0.75	0.75	0.75	0.75

Figure N-4 Drift capacity at axial failure for poorly detailed flexure-controlled walls. Drift capacity values in this figure should be multiplied by a factor of 1.25 for flexure-controlled walls with spirally reinforced boundary columns (see Section N.7.1).

Figure N-5 presents a comparison of predicted drift capacities from Equation N-1 and Figure N-4 with experimentally obtained drift capacities at axial failure from the dataset of 80 wall tests, with a mean of 1.02 to 1.03 and coefficient of variation (COV) of 0.20 to 0.23.

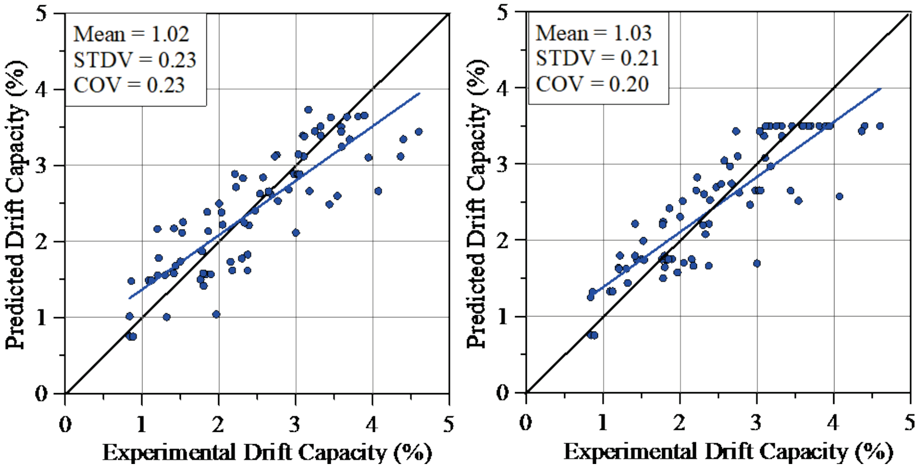

(a) Equation N-1

(b) Figure N-5

Figure N-5 Comparison of predicted drift capacities from Equation N-1 and Figure N-4 with experimentally obtained drift capacities.

In Figure N-4 and Equation N-1, the depth of neutral axis, c, can be computed from sectional analysis of the wall using the expected material properties and the sustained gravity load. Alternatively, Equation N-2 can be used to compute an approximate c (Abdullah and Wallace, 2018c), which is derived based on data from 696 walls in the UCLA-RCWalls database with $P / A_g f_c' > 0$ and different cross-sectional shapes.

$$\frac{c}{l_w} = k_1 + k_2 \frac{P}{A_g f_c'} \tag{N-2}$$

where values of k_1 and k_2 are obtained from Table N-1. Figure N-6 compares the depth of neutral axis computed from Equation N-2 with that computed from detailed sectional analysis using as-tested material properties.

Table N-1 Neutral Axis Depth (*c*) Parameters Used in Equation N-2

Wall Cross-Section Shape	k_1	k_2	Mean	COV
Rectangular	0.10	1.2	1.04	0.17
Barbell	0.03	1.4	1.05	0.27
T-, L-shaped, and flanged; flange in compression	0.03	0.7	1.00	0.30
T-, L-shaped, and half-barbell; web in compression	0.20	2.0	1.01	0.24

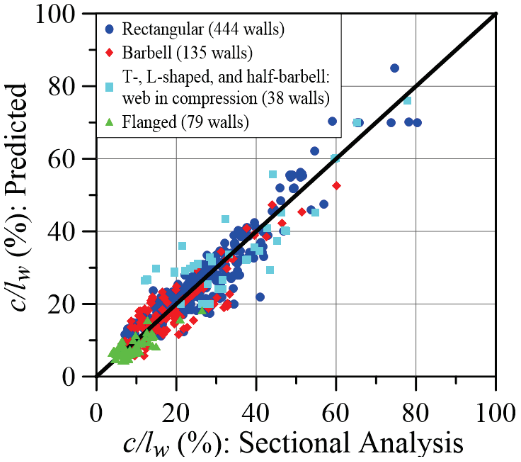

Figure N-6 Comparison of neutral axis depth, *c*, computed from Equation N-2 with that from detailed sectional analysis.

N.4 Drift Capacity of Shear-Controlled Walls/Piers

As noted previously, shear-controlled walls are defined as walls with shear-flexure strength ratio $V_{n,ACI}/V_{@Mn} < 1.0$. The limited available literature was reviewed to identify parameters that primarily control drift capacity at axial failure. Wallace et al. (2008) developed an axial collapse model for lightly reinforced wall piers under axial load based on a shear-friction model. They found that in addition to axial load, the amount of wall web reinforcement provided had a significant impact on drift capacity at axial failure. Looi et al. (2017) showed that drift capacity of heavy reinforced squat walls is primarily a function of axial load ratio.

Similar to flexure-controlled walls/piers, the UCLA-RCWalls database was filtered to obtain shear-controlled wall tests for which the deformation at loss of axial load-carrying capacity is reported, which resulted in a subset of 33 wall tests.

Drift Capacities of the wall tests are plotted against $P / A_g f'$ in Figure N-7 for two levels of provided minimum wall web reinforcement ratio (i.e., the least of the vertical and horizontal reinforcement ratio). From this figure, it is clear that axial load has a significant impact on drift capacity, and that there is only a moderate trend for wall web reinforcement ratio, which could be due to limited data for walls with web reinforcement ratios < 0.0025. Therefore, the impact of web reinforcement ratio was ignored herein as shown in Figure N-8, perhaps until further data become available.

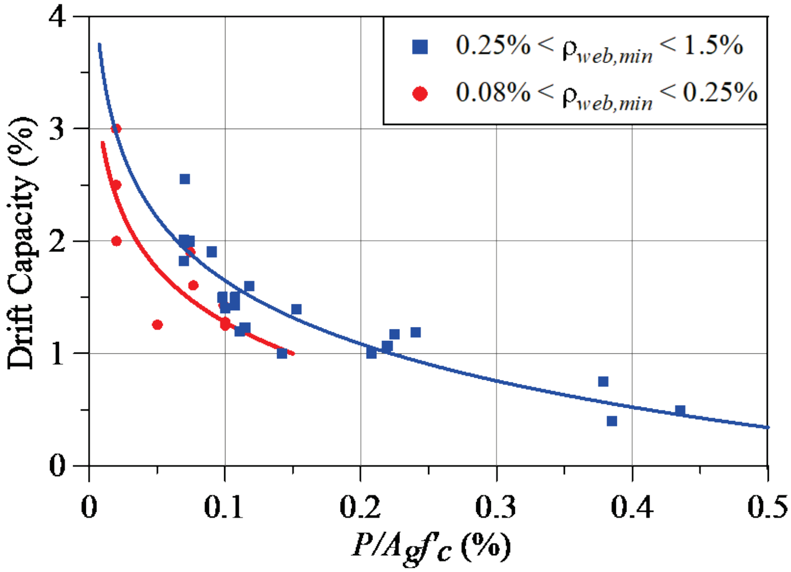

Figure N-7 Drift capacity of shear-controlled walls/piers as a function of $P / A_g f_c'$ and minimum web reinforcement ratio.

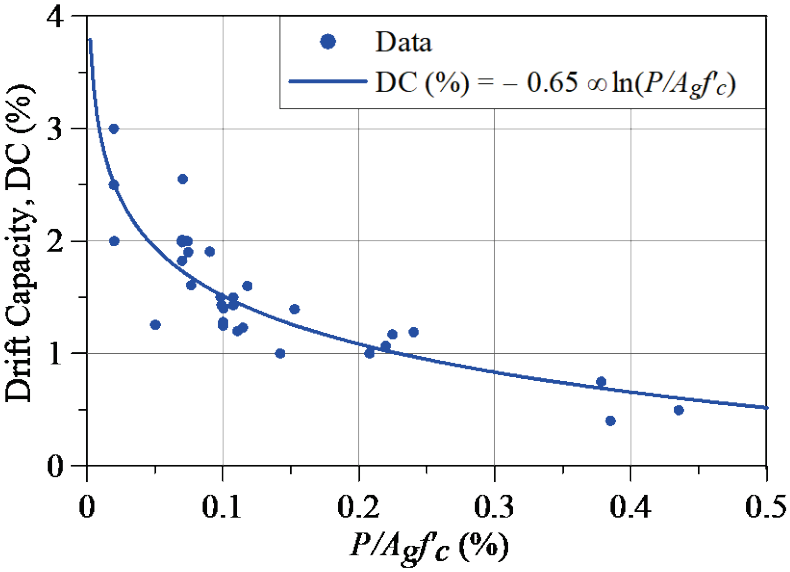

Figure N-8 Drift capacity of shear-controlled walls/piers as a function of $P / A_g f_c'$ with a natural log fit.

A logarithmic fit through the data results in the following predictive equation for drift capacity (DC) at axial failure (Figure N-8):

$$\text{DC}(\%) = -0.65 \times \ln\left(P/A_g f_c'\right) \tag{N-3}$$

Alternatively, a bi-linear curve through data could be used, as shown in Figure N-9, which can be expressed with the following expressions:

$$\begin{aligned} \text{DC}(\%) &= 2.5 - 10\frac{P}{A_g f_c'} \quad \text{for} \quad \frac{P}{A_g f_c'} \le 0.1 \\ \text{DC}(\%) &= 1.75 - 2.6\frac{P}{A_g f_c'} \quad \text{for} \quad \frac{P}{A_g f_c'} > 0.1 \end{aligned} \tag{N-4}$$

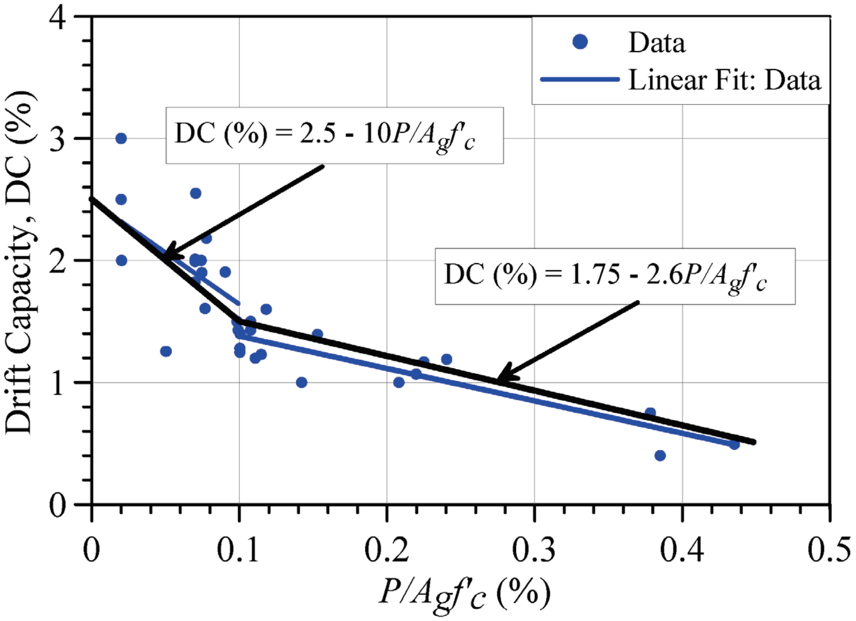

Figure N-9 Drift capacity of shear-controlled walls/piers as a function of $P / A_g f_c'$ with a bi-linear fit.

Table N-2 Drift Capacity for Shear-Controlled Walls/Piers at Axial Collapse

$P/A_g f'_c$	Drift Capacity, DC (%)$^{(1)}$
0.0	2.50
0.05	1.95
0.10	1.40
0.20	1.13
0.30	0.87
0.40	0.60
0.50	0.35

(1) Drift capacity values in this table should be multiplied by a factor of 1.5 for shear-controlled walls with spirally reinforced boundary columns (see Section N.7.2).

The results of Equation N-4 are presented in a tabulated format in Table N-2. Figure N-10 presents a comparison of predicted drift capacities from Equation N-4 with experimentally obtained drift capacities at axial failure from the dataset of 33 shear-controlled wall/pier tests, with a mean and COV of 1.03 and 0.19, respectively.

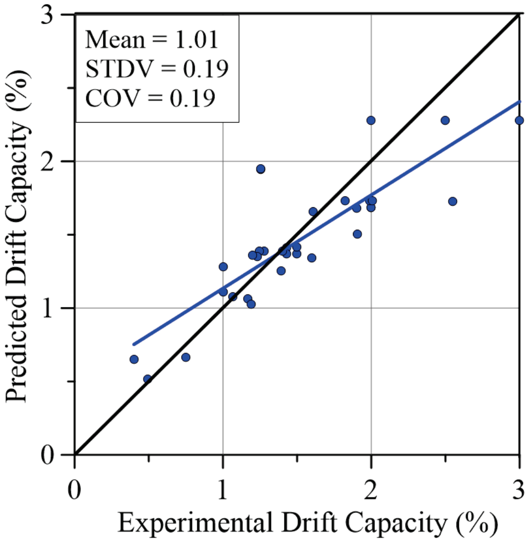

Figure N-10 Comparison of predicted drift capacities from Equation N-4 with experimentally obtained drift capacities at axial failure.

N.5 Drift Capacity of Walls with Inadequate Lap Splices

Review of test results from 10 wall tests that lost lateral strength due to inadequate lap-splice of longitudinal reinforcement (Bimschas, 2010; Hannewald et al., 2013; Elnady, 2008; Jeon and Park, 2016; Paterson and Mitchell, 2003; Woods, 2017) revealed that the bond failure of a lap-splice could actually increase deformation capacity, and that loss of axial load-carrying capacity is unlikely. This is because once the splice fails, the wall becomes very flexible and rocks back and forth as a rigid body when subjected to lateral loads. Therefore, walls with inadequate lap-splices are treated as walls without lap-splices, and the impact of the presence of lap splices is essentially ignored in determining the wall drift capacity at axial failure. However, the potential for overturning instability due to failure of lap-splices should be evaluated (Wallace et al., 2012).

N.6 Drift Capacity of Walls with L-Shaped, T-Shaped, and Half-Barbell Cross-Sections

In the case of walls with asymmetric cross-sections, such as T-shaped, L-shaped, and half-barbell cross-sections (Figure N-11), drift capacity should be evaluated in both directions of loading (i.e., flange in compression and web in compression) and the larger value should be used to determine the wall rating. This is because in cases with a large *b*, where the barbell or flange of the wall is in compression, drift capacity is likely to be relatively large (low λ_b). In such cases, it is unlikely that the wall will lose axial load carrying capacity because the flange or the barbell may remain largely intact and thus could carry the axial load if the web becomes heavily damaged (Figure N-12).

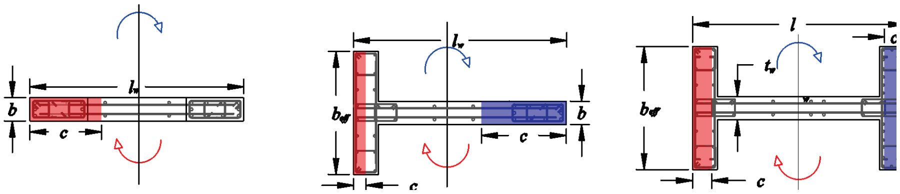

Figure N-11 Examples of asymmetric wall cross-sections.

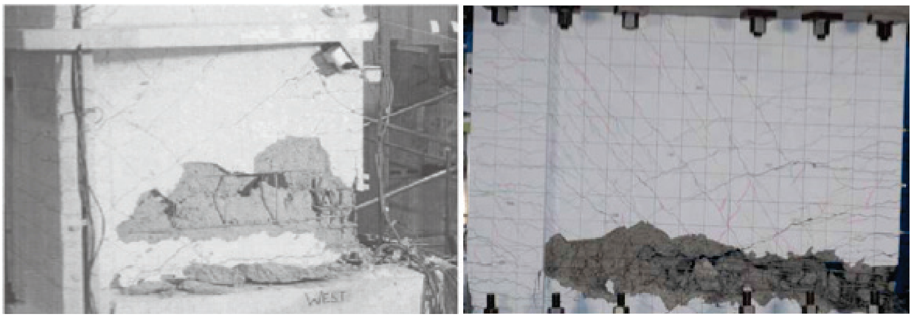

(a) T-shaped
(Thomson and Wallace, 1995)

(b) Half-barbell
(Takahashi et al., 2013)

Figure N-12 Damage in walls with asymmetric wall cross-sections.

N.7 Drift Capacity of Walls Spirally Reinforced Columns at the Boundary Regions

Use of walls with barbell shaped cross-sections (i.e., walls with a thin web and large columns at boundary regions) was common in pre-1971, low-rise and medium-rise, concrete buildings. Typically, boundary columns have spiral transverse reinforcement spaced at, or smaller than, 3 inches center-to-center (Bertero et al., 1975). It is believed that such walls perform better than walls with non-spirally reinforced boundary elements, and, therefore, larger drift capacities are assigned to them.

The UCLA-RCWalls database was filtered to identify walls with boundary columns reinforced with spiral hoops with or without intermediate legs of crossties, and 14 flexure-controlled walls and 28 shear-controlled walls were identified. One important limitation of these tests, which were mostly completed in the 1990s and earlier, is that they are not tested to axial collapse. Some have been tested to peak strength, and others have been tested to some level of lateral strength degradation. In the absence of experimental data for axial collapse of walls with spirally reinforced columns, the drift capacities at axial collapse suggested in the following sections are judged to be appropriate.

N.7.1 Flexure-Controlled Walls with Spirally Reinforced Columns

For the 14 flexure-controlled walls, test results show that the damage includes bar fracture, and in some cases cover spalling of the boundary columns and concrete crushing in the columns and web next to the columns. Figure N-13 shows drift capacity of the dataset at 20% lateral strength loss, which ranges from 2.0 to 5.0% on average (blue dots). This is because the closely spaced spirals prevent early strength degradation due to bar buckling and concrete core crushing. It is noted that since the width of compression zone, b, is relatively large, $l_w c/b^2$ is equal, or smaller, than 15. Abdullah and Wallace (2018c) found that walls with $l_w c/b^2 < 30$ can exhibit moderate to significant post-20% strength loss deformation capacity. Therefore, drift capacity of flexure-controlled walls with spirally reinforced columns at axial failure is taken as drift capacity of non-spirally reinforced walls increased by 25%, as shown in Figure N-13. That is, the results presented in Figure N-4 are increased by 25% for walls with spirally reinforced columns.

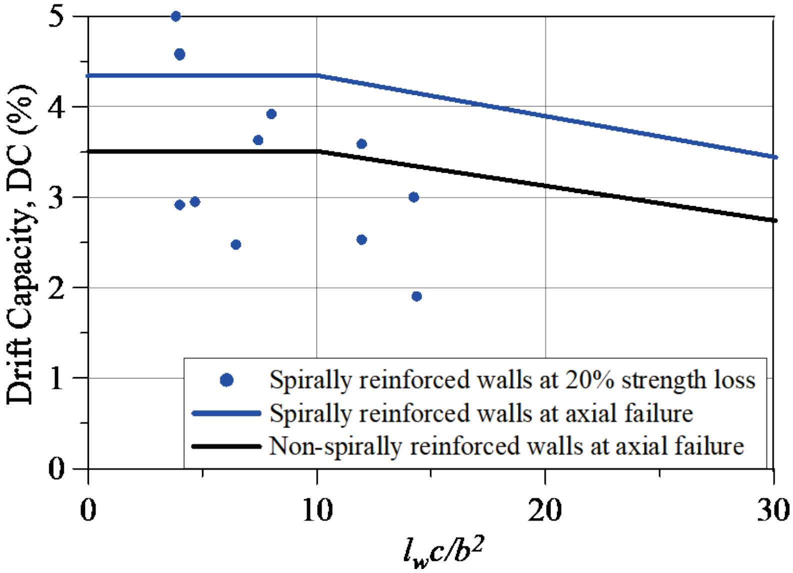

Figure N-13 Drift capacity of flexure-controlled walls with spirally reinforced boundary columns.

N.7.2 Shear-Controlled Walls with Spirally Reinforced Columns

For the 28 shear-controlled walls, test results show that the damage usually includes crushing the concrete in the thinner web, and in some cases spalling concrete cover of the columns, as seen in Figure N-14. However, the core of the boundary columns appears to be perfectly intact and can, therefore, support the axial load on the wall after the web is crushed. Figure N-15 shows drift capacity of the dataset at either peak strength or 20% lateral strength loss. After the web is crushed, it is possible that the wall becomes more flexible and can deform significantly before the columns fail in a sliding shear failure mode along the crushed plane. Therefore, the drift capacity of shear-controlled walls with spirally reinforced boundary columns at axial failure is taken as the drift capacity of non-spirally reinforced walls increased by 50%, as shown in Figure N-15. That is, the results presented in Table N-2 are increased by 50% for walls with spirally reinforced columns.

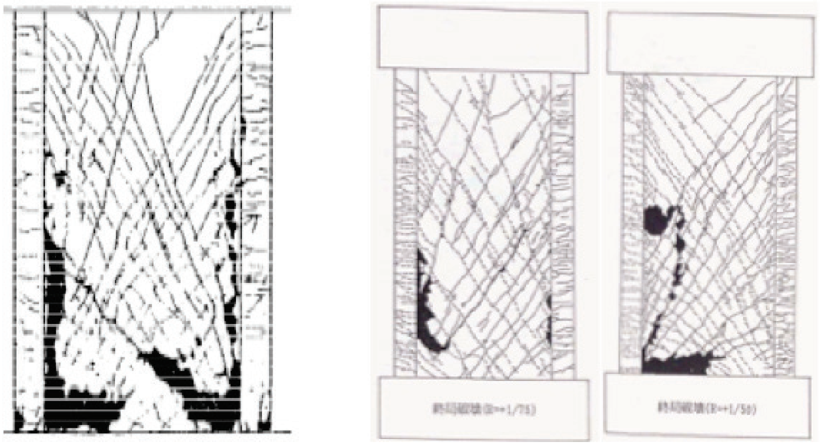

(a) Imanishi, 1996 (b) Kabeyasawa and Matsumoto, 1994

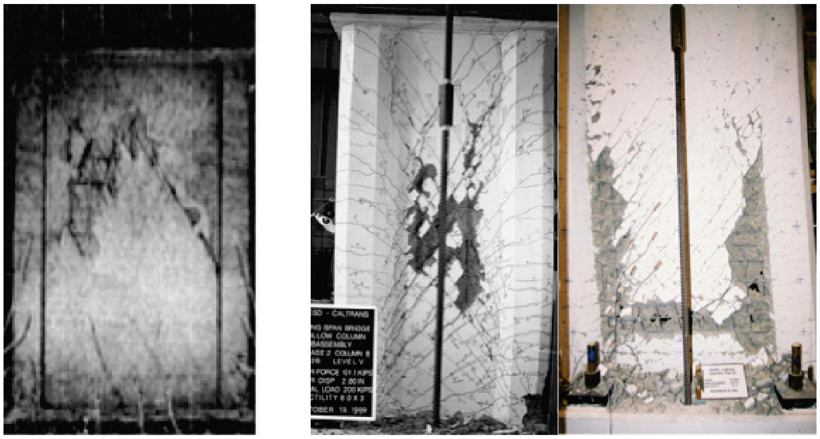

(c) Saitoh et al., 1990 (d) Hines et al., 2002

Figure N-14 Damage of shear-controlled walls with spirally reinforced boundary columns at some level of lateral strength loss.

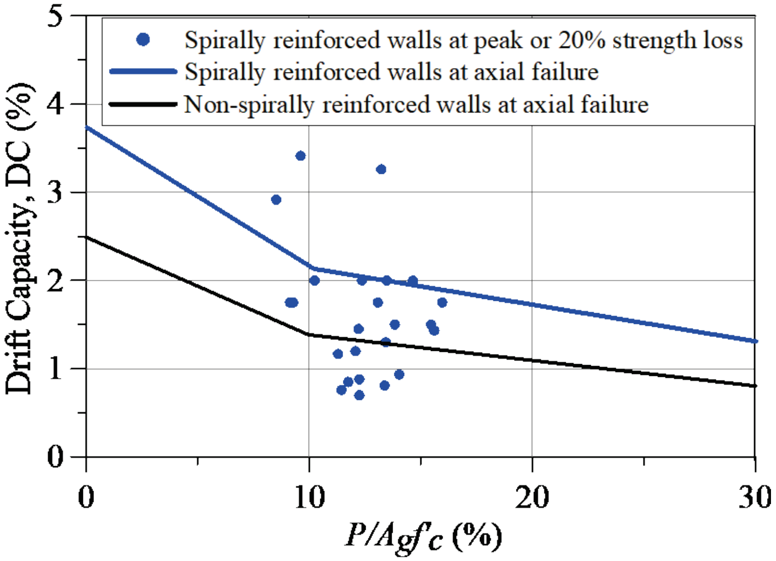

Figure N-15 Drift capacity of shear-controlled walls with spirally reinforced boundary columns.

Appendix O

Studies on Infilled Frames

O.1 Introduction

Masonry infill panels are commonly treated as non-structural elements in analysis and design. However, past earthquakes and laboratory studies have demonstrated that infills can increase the strength and stiffness of the structure considerably, but they can also induce large forces on the bounding frame leading to significant damage, even when subjected to moderate ground shaking (EERI, 1994; EERI, 1999; Brando et al., 2015). As a result, concrete buildings with masonry infill walls are considered rather vulnerable when subjected to seismic forces. The seismic assessment of existing concrete buildings with infills is a challenging task, especially for structures with non-ductile reinforcing details, due to the interaction between the infills and the bounding frame. This interaction can alter the load-transfer mechanism, and cause the brittle shear failure of concrete elements. The goal of the studies conducted herein is to develop reliable, yet efficient, guidelines for the evaluation of the collapse potential of buildings classified as infilled concrete frames. The proposed guidelines follow the assessment approach developed for frame and frame-wall buildings.

The studies discussed in this appendix focus on existing concrete structures with masonry infill walls in the perimeter and bare concrete columns in the interior. Such structures are commonly found in the US and house a variety of uses including hotels, theaters, and warehouses. The studies in this appendix utilize assessment guidelines in ASCE 41-17 (Martin and Stavridis, 2017; 2018) and a recently proposed modeling framework for these buildings (Bose et al., 2018).

The guidelines developed here for infilled frames are included in the evaluation procedures discussed in Chapters 4, 5, and 9. These procedures include the estimation of the plastic mechanism, the shear strength of the critical story, the effective period that allows the estimation of the seismic drift demand, and the rating of the columns and the critical story. In addition, the effects of openings in the infill panels on strength and column shear failures is quantified.

O.2 Simulation of Collapse of Buildings Infilled with Solid Infills

The procedures developed here to evaluate infilled buildings are based on nonlinear dynamic simulations of the seismic response of a set of prototype reinforced concrete buildings with masonry infill panels representing the buildings stock in the U.S. This section discusses the design details of the prototype structures, the numerical models, and the results of the nonlinear analyses.

O.2.1 Details of the Prototype Buildings

The prototype structures considered in this study are based on an actual 6-story warehouse that has infilled bays at the perimeter, and non-infilled interior columns. This is thought to be representative of the building stock of this type found in California. The elevation of the building and a typical floor plan are shown in Figure O-1. This 6-story building, the prototype 3-story structure designed by Stavridis (2009) to represent construction practice of 1920s, and the design guidelines used in 1930s (Caughey, 1933), are the basis for the design of one 8-story and five 4-story buildings. The main features of these prototype structures are summarized in Table O-1. Besides the number of stories, the effect of the relative strength of the infill to that of the interior columns is examined, as well as the effect of a non-infilled weak first story.

Table O-1 Details of the Archetype Models Considered in This Study to Evaluate Seismic Behavior of Infilled Buildings

Model ID	Infill Compressive Strength f_m' (ksi)	Infill Cohesion *C* (psi)	Infill Thickness (in)	Interior Column Shear Strength (kips)	Number of Stories	Non-Infilled Story
M1	1.4	45	12	48	4	No
M2	0.8	30	8			
M3	0.4	22	8			
M4	1.4	45	12	24		
M5	1.4	45	12	102	8	
M6	0.4	22	8	48	8	First Story

To limit the variables between the buildings, all buildings have the floor plan shown in Figure O-2a and uniform story heights of 11 ft. The dimensions and design details of the concrete members of the two bottom stories of the 4-story prototypes are shown in Figure O-2b. The beam details (B1 and B2) are consistent throughout the height of the structures for all buildings as the tributary areas and gravity loads that governed the design in that era do not change. The column sizes and reinforcement details vary along the height according to the warehouse drawings. The column details of the eight-story prototype are summarized in Table O-2. Stories 5-8 in the table reflect the design details of the 4-story prototypes. Tie spacing is 16 in. over the height of the columns for all the structures to represent the non-ductile detailing of old concrete buildings.

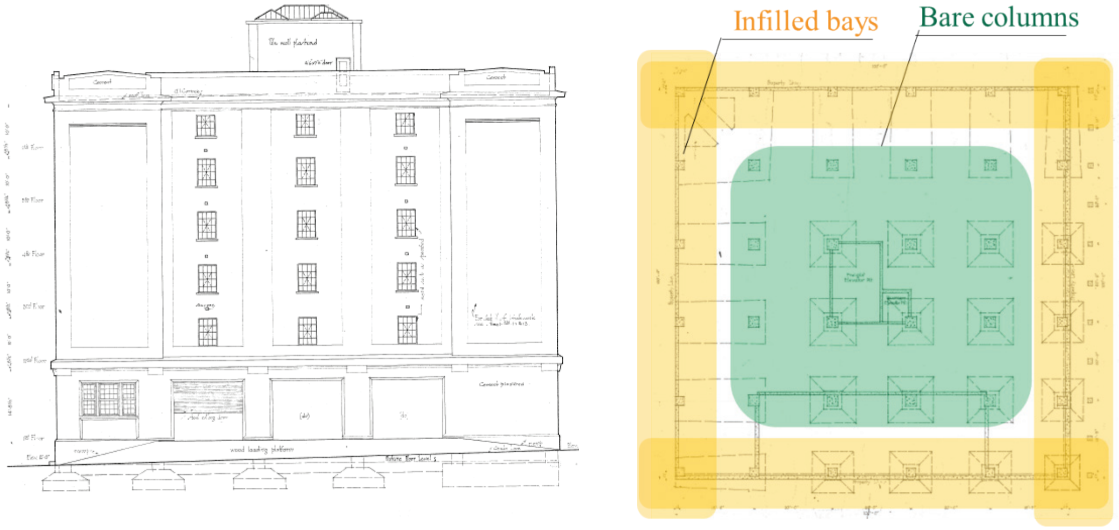
Infilled bays
Bare columns

(a) front view elevation (a) typical floor plan

Figure O-1 Building details of the six-story San Diego warehouse with infilled RC frames.

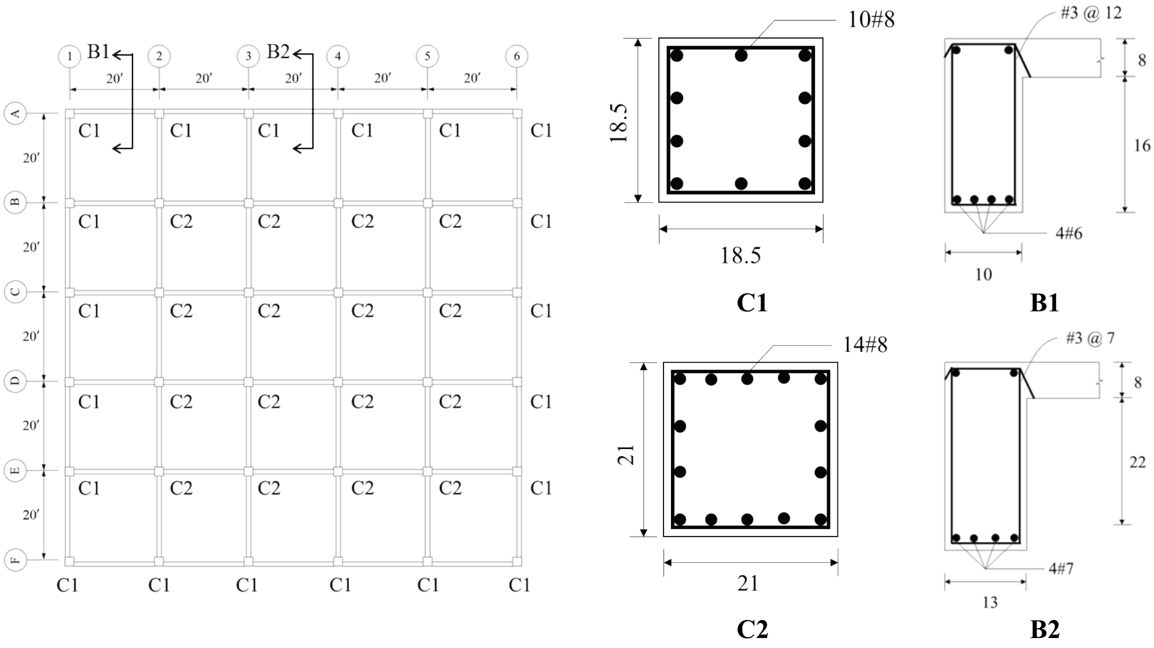
1
2
3
4
5
6
B1
B2
20′
A
B
C
D
E
F
C1
C2
10#8
18.5
#3 @ 12
8
16
4#6
10
14#8
21
#3 @ 7
22
4#7
13
C1
B1
C2
B2

(a) floor plan of archetypes (b) design details

Figure O-2 Floor plans of the prototype structures and design details of the columns and the beams of the first two stories of the 4-story prototype.

Model M-1 is the baseline model for this study. The masonry compressive strength, number of wythes (or wall thickness), and cohesion, of the infill walls are varied in the models M2 and M3, with the strongest infill in M1 representing a triple-wythe brick masonry and the weakest infill in M3 representing a double-wythe wall of hollow clay tiles. Model M4 has the same material properties as that of M1, however, the interior columns are weak with half the lateral resistance of the columns in Table O-2. The 8-story prototype, M5, has the strongest infill, similar to M1. Model M6 has the infill from the bottom story of the M3 model removed to represent buildings with weak infill and open ground stories. The masonry and concrete material properties are those measured through in-situ and laboratory tests in a structure of this type in El Centro, California (Yousefianmoghadam and Stavridis, 2016).

Table O-2 Column Dimensions and Design Details of the Prototypes

	Column Dimensions (in.)		Reinforcement Details	
Stories	Interior	Exterior	Interior	Exterior
8-S1	30.0	28.0	20#11	16#11
8-S2	28.0	26.0	18#11	14#11
8-S3	26.0	24.0	18#10	14#10
8-S4	23.0	21.0	16#9	12#9
8-S5 / 4-S1	21.0	18.5	14#8	10#8
8-S6 / 4-S2	18.5	17.0	12#8	8#8
8-S7 / 4-S3	18.0	16.0	14#7	10#7
8-S8 / 4-S4	18.0	16.0	14#7	10#7

O.2.2 Development of Numerical Models

Three-dimensional numerical models of M1-M6 are developed using beam-column elements for the RC members and diagonal truss elements for the infill walls. The struts are calibrated using a recently proposed framework for the nonlinear simulation of infilled RC buildings (Bose et al., 2018). According to this framework, the backbone force-displacement response for each infilled bay is estimated based on the anticipated failure pattern following the methodology proposed by Martin and Stavridis (2017; 2018) for frames with solid infill panels, now adopted by ASCE 41-17. The obtained backbone curves for a typical infilled bay in the ground floor of each building are illustrated in Figure O-3a. The backbone curves for M4 are the same as those of M1. To account for the deterioration of the buildings, the initial stiffness is reduced to 40% (ACI, 2011b).

The envelop force-displacement responses are used to calibrate the struts representing the masonry infill panels according to the methodology proposed by Bose et al. (2018). This modeling method for the struts does not account explicitly for the shear-dominated failure patterns of infilled frames. However, the backbone curves used to calibrate the struts take into account the anticipated failure mechanisms, including the aforementioned brittle shear failures. An example of a calibrated strut model for Model M1 is shown in Figure O-3b, while the material properties for concrete and masonry for all models are presented in Table O-3.

The interior columns of the buildings are not infilled. Therefore, a uniaxial material model combined with shear axial springs developed by Elwood (2005) is used to capture the response of the interior RC columns during shear and axial load failure.

Table O-3 Calibrated Concrete and Strut Properties of the Models' Elements

Panels		Peak Compressive Strength MPa (ksi)	Residual Strength MPa (ksi)	Tensile Strength MPa (ksi)	Strain at Peak Strength	Strain at Residual Strength	Strut Width mm (in)	Tension Softening Stiffness MPa (ksi)	Lamda*
Concrete		24.1 (3.5)	2.4 (0.35)	3.4 (0.5)	0.003	0.006	-	431 (62.5)	0.1
Masonry	M1	9.6 (1.4)	0.4 (0.06)	3.2 (0.5)	0.0007	0.0011	9.2	431 (62.5)	0.1
	M2	5.5 (0.8)	0.8 (0.12)	1.8 (0.3)	0.0013	0.0023	15.6	258 (37.5)	
	M3	2.8 (0.4)	0.3 (0.04)	0.9 (0.1)	0.0016	0.0023	25.0	86 (12.5)	
	M5	24.1 (3.5)	2.4 (0.35)	3.4 (0.5)	0.0012	0.0022	11.8	431 (62.5)	

* ratio between unloading slope and initial slope at onset of residual strength

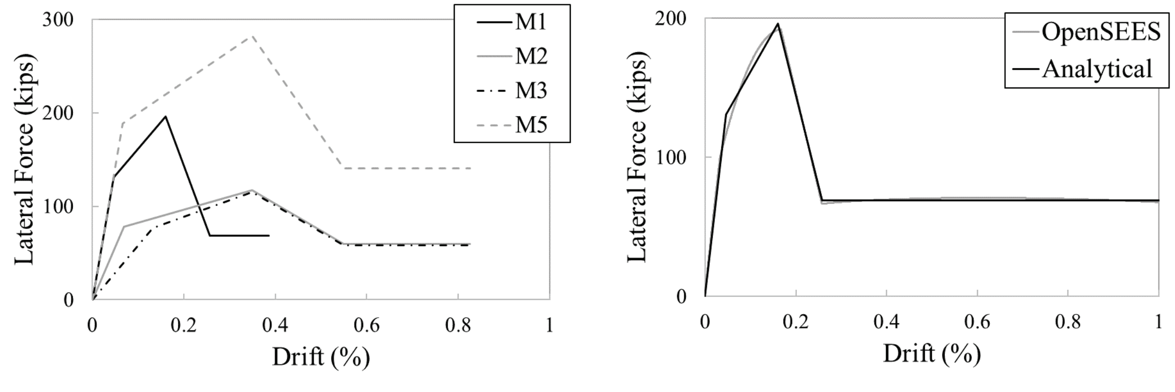

(a) envelop curves estimated using ASCE 41-17 (b) calibration of struts of M1

Figure O-3 Lateral force-drift ratio curves for the infilled bays and calibration of struts.

Once the diagonal struts simulating the effect of the masonry panels and the shear axial springs are calibrated, the three-dimensional model of the entire building is assembled, as shown in Figure O-4. The floor diaphragms are assumed to be rigid, and all structures are fixed at their base. The damping of the structure is modeled using the Rayleigh formulation, considering 3% of critical damping for the first two modes.

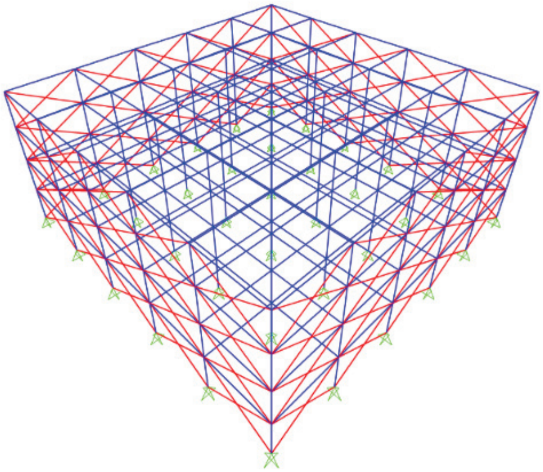

Figure O-4 Three-dimensional numerical model with infill struts.

O.2.3 Nonlinear Time-History Analyses

Each building model is subjected to pushover analyses in the two principal directions independently to evaluate its strength and stiffness. The nodes over each slab are constrained to the node at the centroid of the each floor for this purpose. These master nodes are subjected to monotonically increasing triangular load pattern along the height during a displacement-controlled analysis in the direction of interest.

The three-dimensional numerical models of the buildings are then excited with two components of the ground motions to account for the effects of bidirectional dynamic loading. Each building is subjected to incremental dynamic analyses using the horizontal components of the 22 far-field pairs of ground motions defined in the FEMA P-695 document (FEMA, 2009). The ground motion intensities are gradually increased until collapse, which is considered to occur: (i) when a small increase of the ground motion intensity results in drastic increase of the inter-story drift ratio; or (ii) when the inter story drift exceeds 1.5%. This limit for infilled frames is determined based on the tests conducted by Gao et al. (2018) and Stavridis et al. (2012). The six prototype structures were also dynamically analyzed with all the infills removed to obtain the bare frame response. In that case, the second collapse criterion is adjusted so that collapse is considered to occur when the drift demand reaches or exceeds 3.0%.

O.2.4 Detailed Results for Prototype Buildings

The results from the monotonic pushover analyses of models M1 to M5 are presented in Figure O-5a., while the peak base shear strength reached by each model and the corresponding bare frame is reported in Table O-4. As expected, the infills increase the strength of the buildings, with the most dramatic increase reported for models M1 and M4 which have strong infills (CMU). From Figure O-5a, it can be observed that the numerical models reach the peak strength at a very low drift ratio, prior to a sudden loss in strength. This loss of strength is followed by gradual increase of the shear resistance. The first peak is reached when the infills in the exterior bays reach their peak strength. At that point, the interior bare columns only contribute a fraction of their peak shear capacity, which they reach at considerably larger drifts as indicated in Figure O-5b. The figure presents the disaggregated contributions of the interior and the exterior frames for models M1, and M3. For Model M4, which has weaker interior columns, this post-peak increase in strength is not as drastic compared to model M1 due to the limited strength of the interior columns. In summary, in all cases, the exterior frames determine the peak resistance, while the bare columns in the interior frames govern the post-peak response.

Figure O-6 summarizes the results from the dynamic analyses for models M1 to M6. The median spectral accelerations at collapse of the infilled buildings are compared with their bare frame counterparts in Table O-5. The results indicate that collapse is anticipated to occur for lower values of spectral acceleration regardless of which of the three demand metrics (spectral acceleration at the initial period of the structure, spectral acceleration at a period of 0.5 sec, and peak ground acceleration) is considered as the masonry weakens from M1 to M3. This is expected as the compressive strength, f'_m, of the masonry decreases from model M1 to M3. In fact, the collapse potential of M3 is similar to that of the corresponding bare frame, with the two buildings expected to collapse at a similar PGA and spectral acceleration at 0.5s. Therefore, the weak masonry infills of M3 do not affect the overall collapse potential of the frame. However, when the ground story of the model M3 is removed to obtain model M6, the spectral acceleration at which collapse is anticipated further decreases. The lack of infill in the bottom story of this building increases the vulnerability of the structure, and slightly worsens the behavior compared to the bare frame. M4 has similar material properties for infill as M1, but weaker interior columns. As a result, it is expected to collapse at significantly lower excitation level compared to M1.

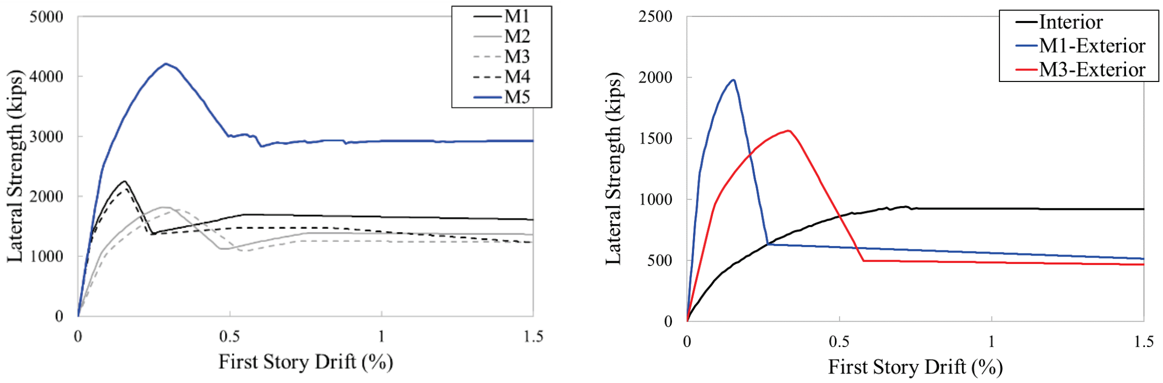

(a) monotonic pushover analyses (b) contribution of interior and exterior frames

Figure O-5 Pushover analyses results of the models (M1 to M5) and deaggregated response of interior and exterior frames for models M1 and M3.

Table O-4 Collapse Potential of the Infilled Buildings and Frame Counterparts

	Peak Base Shear Resistance (kips)	
Models	**Infilled Frame**	**Bare Frame**
M1	2250	1200
M2	1819	
M3	1776	
M6	1200	
M4	2114	1040
M5	4208	2604

Table O-5 Collapse Potential of the Infilled Buildings and Frame Counterparts

	Median Collapse Intensity (g)					
	Infilled Frame			**Bare Frame**		
Models	**SA[T_1]**	**SA[0.5]**	**PGA**	**SA[T_1]**	**SA[0.5]**	**PGA**
M1	0.89	0.77	0.40	0.54	0.62	0.30
M2	0.73	0.69	0.35			
M3	0.66	0.62	0.31			
M6	0.54	0.58	0.29			
M4	0.72	0.70	0.36	0.45	0.60	0.28
M5	0.65	0.75	0.37	0.35	0.61	0.30

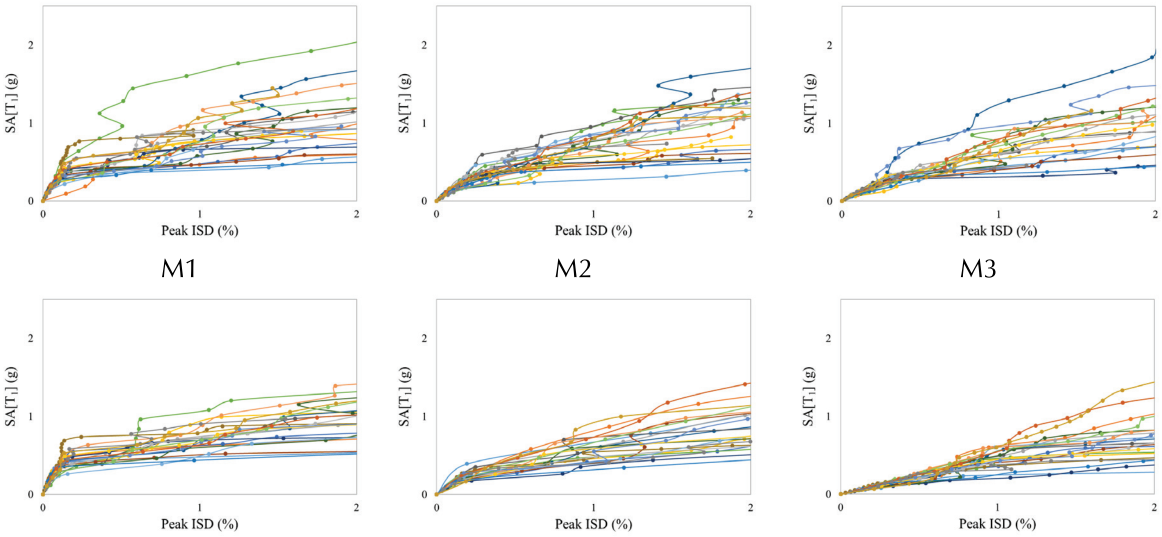

M1 M2 M3

M4 M5 M6

Figure O-6 Incremental dynamic analysis results of the infilled frame models M1 to M6.

O.3 Calculation of Strength of Infilled Frame Buildings

This section discusses the procedures proposed for the estimation of the strength of these buildings based on the results of the nonlinear time-history analyses discussed in the previous section. In some cases, detailed finite element analyses of single bays were also run to provide further insight needed for the development of the proposed methodology.

O.3.1 Default Material Properties

There is great uncertainty regarding the exact values of masonry properties which depend on the construction materials and practice, deterioration and other factors. Without *in situ* testing, estimating the material properties of masonry infills is challenging, as they tend to vary considerably. The most important properties are the compressive strength, cohesion, and the coefficient of friction. It is outside the scope of this methodology to require testing that would provide better estimates of these factors. Therefore, a table of default material property values (Table 3-1) is provided despite these uncertainties.

The values for expected cohesion, friction, and f'_m in Table 3-1 are based on values provided in NZSEE (2017), taken in the middle of the range, and converted from MPa to psi. These values are based on unreinforced masonry construction in New Zealand. Values were revised based on engineering judgement, through consultation with the Project Review Panel and others with expertise in masonry construction. Users are cautioned that it is not conservative to assume the weakest (worst) conditions. If more detailed information is available, it should be used in lieu of the values provided in Table 3-1.

O.3.2 Plastic Mechanism of Infilled Frames

Typical displacement profiles of the prototype buildings (M1 to M6) are presented in Figure O-7. In each subplot, the displacement profiles at the instants of peak strength, peak deformation, as well as the residual deformation profiles are illustrated. In all cases, the selected motion represents the intensity just before collapse, according to the collapse criteria discussed in Section O.2.3. It is evident from the deformation profiles that once these structures become nonlinear, the deformation mostly concentrates in the first story. Therefore, it can be concluded that in case of infilled frames without plan or height irregularities, mechanism 1 develops and the first story above ground is the critical story. For buildings with an obvious strength irregularity along the height, the critical story may be an upper story. This may occur due to reduction in strength of concrete columns, infills, or both. In that case, mechanism 3 governs. Mechanisms 2 and 4 as described in Section 5.5.1 are not considered feasible options, as they are not expected to govern the behavior of infilled buildings with infills strong enough not to be ignored according to this methodology.

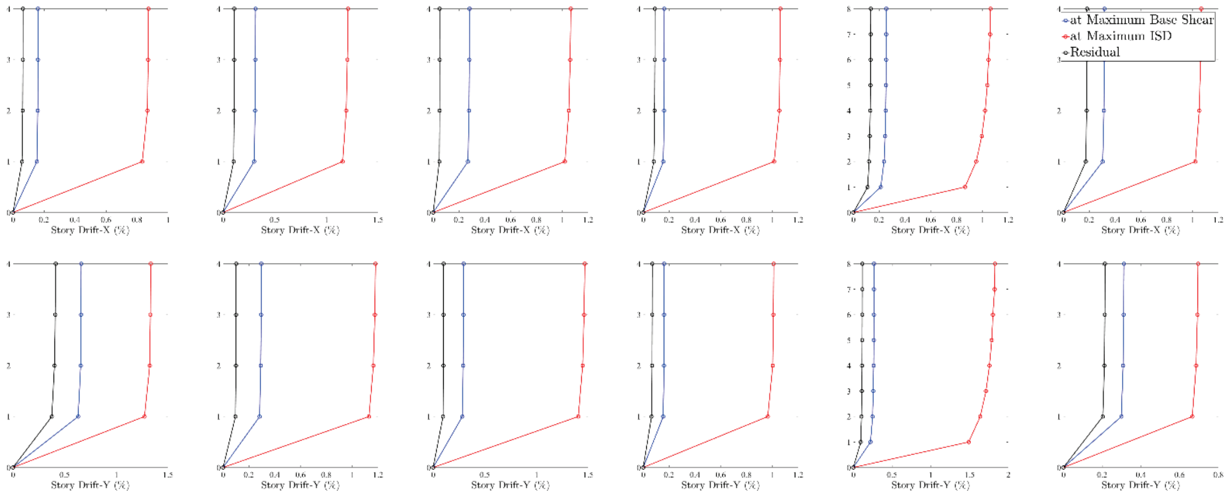

M1 M2 M3 M4 M5 M6

Figure O-7 Displacement profiles of the buildings M1 to M6 just before collapse.

O.3.3 Column Effective Length

Infill panels can shorten the effective length of a column, potentially precipitating shear failure in a column that would otherwise fail in flexure. To account for these effects, in this methodology, infills are assumed to shorten the effective height of the adjacent columns. This shorter effective height must be considered in the calculation of the column shear strength ratio to determine whether flexure or shear governs the behavior. The infill also effectively reduces the column drift capacity in Chapter 9.

The effective heights of the columns are defined in Table O-6 (repeated from Table 9-5), where l_u is the clear height of the column. The recommendation of $l_u/2$ is based on Martin and Stavridis (2018). Although they distinguish between strong and weak infill in definition of effective height, here, for simplicity, one value is recommended. For openings that are close to the column, Table O-6 suggests an effective height equal to the height of the opening. This suggestion is based on earthquake damage, which often causes shear failure in columns adjacent to openings, as shown in Figure O-8.

Table O-6 Effective Height of Columns in Infilled Frame

Effective Height of Column	$l_{u,inf}$
Bare column	l_u
Columns with infill abutting on one or more sides in the direction of loading	$l_u/2$
Partial height infills	Clear height of the column that does not have abutting infill
Columns with infill with openings abutting on one or more sides in the direction of loading	Where an opening exists within a distance of $d_{op} < h_{inf}/2$ of the column, the effective height of the column is taken as the height of the opening, h_{op}. Otherwise, use $l_u/2$.

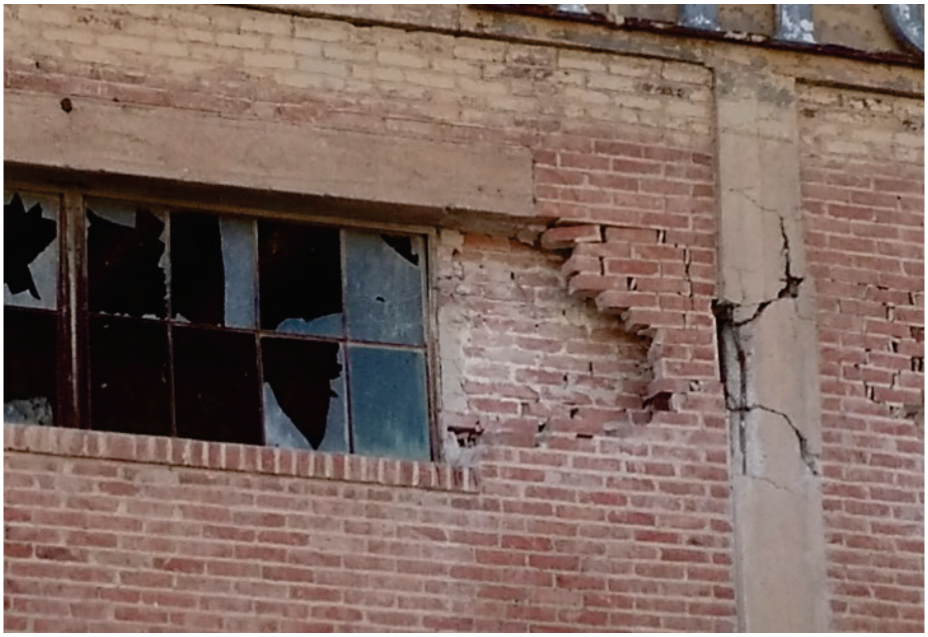

Figure O-8 Damage in infill panel with opening causing shear failure in bounding column (Yousefianmoghadam and Stavridis, 2018).

O.3.4 Classification of Infilled Frames based on Failure Mechanism

The infilled concrete frames are classified here in terms of the relative strengths of the infill and the column as strong infill or weak infill. For this methodology, the infill with solid panel is classified in terms of the anticipated failure mechanism as

- 'strong' relative to the frame if $V_m / V_{lc} > 3.0$, and
- 'weak' otherwise

where V_{lc} is the shear resistance of the weakest of the two columns bounding the infill panel, V_m is the strength of the masonry infill calculated based on Equation (O-2).

In section O.3.7 these definitions of 'weak' and 'strong' infills are revisited to: (a) account for openings, if present; and (b) to identify extremely weak infills not contributing substantially to the strength. The later are ignored from the strength calculations.

The effectiveness of the proposed criterion is compared with the criteria adopted by ASCE 41-17, which are based on stiffness, by considering the structures considered by Martin and Stavridis (2018) for the development of the ASCE 41-17 methodology. The comparison of Figures O-9 and O-10 demonstrates that, with few exceptions, the proposed criteria provide consistent classification with ASCE 41-17.

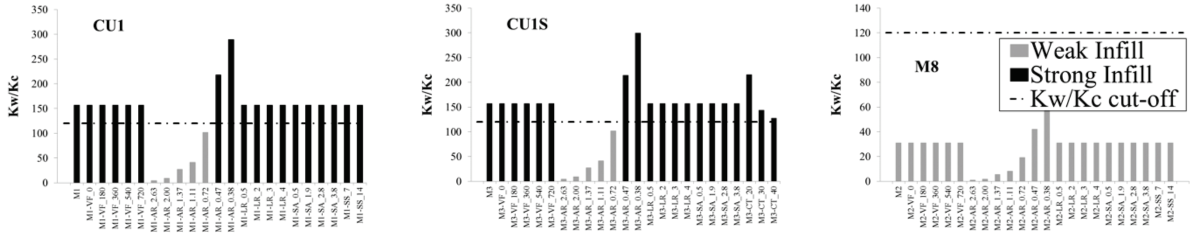

Figure O-9 Classification of infills based on relative stiffness of infill and bounding frame.

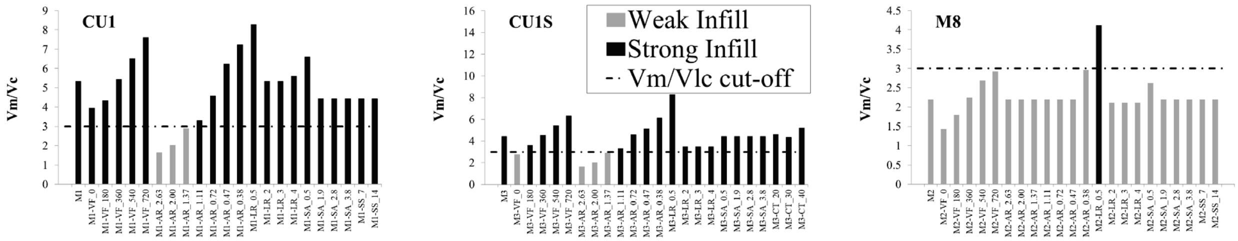

Figure O-10 Classification of infills based on relative strength of infill and bounding frame.

O.3.5 Strength of Single Infilled Bay with Solid Panel

Detailed finite element models of the single-story single-bay frames for the typical infilled bays of the prototype buildings are created following a modeling methodology that combines the smeared-crack and interface elements (Stavridis and Shing, 2010). This methodology can simulate dominant shear and diffused flexural cracks in the concrete members, the crushing and tensile splitting of the masonry units, and the mixed-mode failure of the mortar joints. The deformed mesh of a panel from model M1 and the lateral strength-vs.-drift curves obtained from the detailed FE models subjected to pushover analyses are presented in Figure O-11.

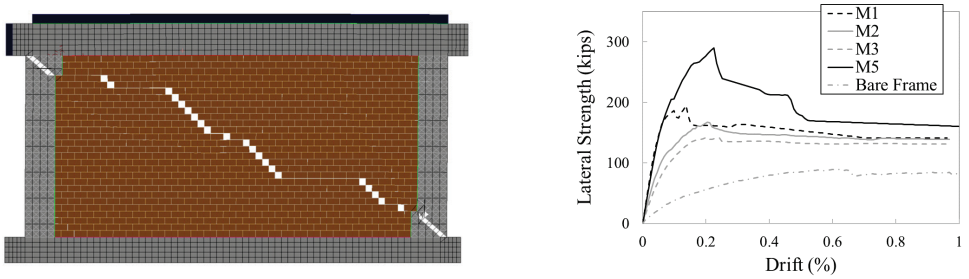

(a) deformed mesh of panel in M1

(b) backbone curves of single-story single bays for all prototypes

Figure O-11 Results of detailed FE analyses single-story single bay frames for the prototypes structures considered here.

As the infilled frames are loaded laterally, the internal forces are redistributed and the vertical load carried by the infill changes. The values of the vertical load carried by the infill initially, and at the instant when the peak vertical load is reached, are summarized in Table O-7. The values provided in the table are indicative of this fluctuation.

Table O-7 P_{inf}^{grav} and P_{inf}^{max} Values of the Models

Models	P_T (kips)	P_{inf}^{grav} (kips)	P_{inf}^{grav} / P_T	P_{inf}^{max} (kips)	P_{inf}^{max} / P_T
M1	130.6	83.0	0.63	91.2	0.70
M2	110.6	44.2	0.40	75.7	0.68
M3	110.6	27.6	0.25	75.7	0.68
M4	124.5	79.1	0.63	89.2	0.72
M5	299.2	126.3	0.42	199.2	0.67

The strength of a single infilled bay can be estimated according to the equations proposed by Martin and Stavridis (2017; 2018), which are adopted in the ASCE 41-17 (2017). By focusing on the structures examined here and making a series of appropriate assumptions, the following simplified provisions are proposed for this methodology.

$$V_{inf,sol} = max(V_m,\ P_{inf}^{max}\mu + V_{lc}) \leq f'_m t_{inf} n_s h_{inf}\ /\ 6 \tag{O-1}$$

$$V_m = P_{inf}^{grav}\mu + A_w C \tag{O-2}$$

where, μ is the initial friction coefficient, C is the cohesion, f'_m is the compressive strength of the masonry assembly, L_{inf} is the length of the infill wall, h_{inf} is the height of the infill panel, t_{inf} is the net thickness of the panel, A_w is the horizontal cross-sectional area of an infill panel ($t_{inf} L_{inf}$), n_s is the number of developed struts in the infill, equal to 1 for panels with aspect ratio (L_{inf}/h_{inf}) < 1.0 and 2 otherwise, P_{inf}^{grav} is the vertical load carried by the infill, calculated from the total gravity load, P_T, above the story of interest, P_{inf}^{max} is the total axial load supported by the infill when the maximum lateral strength is reached. Finally, V_{lc} is the strength of the weaker of the two columns bounding the bay of interest. The calculation of V_{lc} considers both flexure- and shear-critical behavior to determine the governing value of shear strength. For the estimation of the flexural strength of the column, one should consider the reduced clear column height, defined in Table 9-5 of the document.

Based on Table O-7, and additional calculations not shown for conciseness, the initial gravity load carried by the infill can be assumed to be equal to 50% of the total load, P_T, while the vertical load at the instant of peak lateral resistance can be assumed to be equal to 70% of the total vertical load, P_T. These recommendations apply to the cases with wall lengths between 15 ft. and 25 ft., and for story heights between 10 ft. and 14 ft. Otherwise, the vertical loads can be calculated according to ASCE 41-17 Table 11-9.

The maximum shear strength of a single-bay infilled frame obtained from Equation O-1 and the detailed FE analyses are summarized in Table O-8 (M4 and M6 have the same infilled frame as that of M1 and M3, respectively). The table indicates that the analytical equations proposed here predict the peak strength with sufficient accuracy.

Table O-8 Comparison of Strength of Single Infilled Bays Obtained

	Strength (kips) of Single Infilled Bay	
Models	Finite Element Analyses	ATC-78 Calculations (Equations O-1 and O-2)
M1 and M4	194.6	195.9
M2	167.1	127.3
M3 and M6	141.4	125.2
M5	289.7	282.5

O.3.6 Strength of Single Infilled Bay with Openings

Assessing the effect of openings on the response of infilled frames is rather challenging. A parametric study using nonlinear finite element models is conducted to examine the influence of the opening size and location within the masonry panel. For consistency, the frame detailing of the baseline model M1 (same as in M2,3,4, and 6) is used in all the analyses presented in this section. Four different opening sizes are considered, and the windows are placed in the center of the panel or eccentrically. The opening sizes and locations considered in the parametric study are summarized in Table O-9. Masonry with compressive strength of 1.4 ksi (triple wythe), 0.8 ksi (double wythe), and 0.4 ksi (double wythe) is considered to represent the infills in each of the models M1, M2 and M3, respectively. The first part of the nomenclature of the models indicates the opening size: O1 (60 in. × 48 in.), O2 (100 in. × 48 in.), O3 (124 in. × 60 in.) and O4 (148 in. × 64 in.), while the second part indicates the window location: M – concentrically placed opening which is symmetric for the two directions of loading, and two eccentric locations, denoted as L and R. Since the analysis is monotonic, L and R configurations are essentially the same structure loaded laterally from the two opposite directions with R representing the loading direction in which the longer masonry pier is on the windward side of the structure. To facilitate the comparison of the deformed meshes and the load distributions, all analyses are presented with the load applied on the left side of the specimen.

Table O-9 Geometric Details of the Openings Considered in the Parametric Study (all dimensions are in inches)

Model Name	Opening Area	Length			Height		
		From Leeward Column	Opening	From Windward Column	From Top	Opening	From Bottom
MO1-M	(60 in. × 48 in.) 11.7%	80	60	80	32	48	32
MO1-L		16	60	144	32	48	32
MO1-R		144	60	16	32	48	32
MO2-M	(100 in. × 48 in.) 19.3%	60	100	60	32	48	32
MO2-L		16	100	104	32	48	32
MO2-R		104	100	16	32	48	32
MO3-M	(124 in. × 60 in.) 30.2%	48	124	48	28	60	28
MO3-L		16	124	80	28	60	28
MO3-R		80	124	16	28	60	28
MO4-M	(148 in. × 64 in.) 38.4%	36	148	36	24	64	24
MO4-L		16	148	56	24	64	24
MO4-R		56	148	16	24	64	24

The deformed meshes of the FE models at 1.0% drift ratio are presented in Figures O-12 to O-14. It can be observed from the figures, that both the size and location of the openings considerably affect the failure pattern and, therefore, the maximum lateral force that the infilled frame can withstand. These observations are in agreement with earlier observations (Stavridis, 2009), which indicate that the lengths of the piers between the opening and the columns determine the level of the diagonal compressive forces that can develop in the infill, and, eventually, affect the maximum resistance and failure pattern of the infilled frames. The lateral force-drift responses of the FE models are presented in Figure O-15. The backbone curves of the frames without an infill and with a solid infill are also presented for reference. The strength reduction of the infilled frames due to the presence of openings as a function of opening location and size is presented in Figures O-16 and O-17, respectively.

For the models with the opening close to one of the columns, the short masonry pier does not allow the development of the diagonal compressive strut. When the masonry piers are wide enough, for instance, in the case of smaller openings in the center of the panel, the openings do not affect the load-transfer mechanism significantly, as the struts can develop in a similar fashion as in the solid panel. However, for the larger windows, the effective struts could not develop even when the opening is located at the center of the panel due to the narrow masonry piers. Figure O-15 indicates that the lateral behavior of the infilled frame with opening at the middle is closer to that of the solid panel and gradually converges to the behavior of the bare frame as the opening size increases; and especially when the openings are close to one of the columns.

Although this trend has been identified, its precise quantification is rather complex and outside the scope of this document. Hence, the strength of infilled frames with openings is calculated based on Equation O-3.

$$V_{inf,op} = V_{inf,sol}(1 - A_{op}/A_{inf}) \tag{O-3}$$

where, $V_{inf,sol}$ is taken from Equation O-1, A_{op} is the elevation area of the openings ($A_{op} = \Sigma_{op} L_{op} h_{op}$), h_{op} and L_{op} are the height and length of the opening, respectively, and $A_{inf} = L_{inf} h_{inf}$. If $A_{op}/A_{inf} > 0.6$, the infills can be ignored for the calculation of shear strength. However, the openings, even when ignored in the strength calculations, should be considered in the column ratings for inducing possible short column effects. The comparison of the strengths estimated using Equation O-3 and those obtained from the detailed finite element analyses presented in Figure O-18, indicates that the proposed equation can predict the peak strength efficiently and with reasonable accuracy.

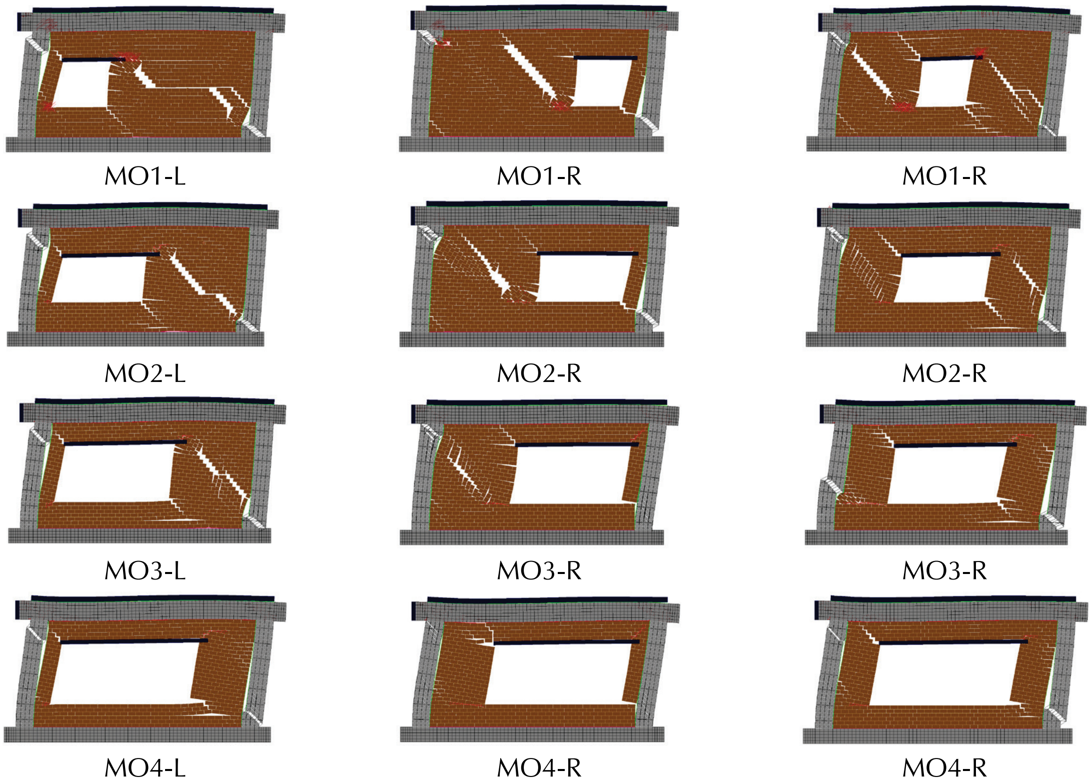

MO1-L MO1-R MO1-R

MO2-L MO2-R MO2-R

MO3-L MO3-R MO3-R

MO4-L MO4-R MO4-R

Figure O-12 Deformed meshes at 1.0% drift of panels with openings for $f'_m = 0.4$ ksi.

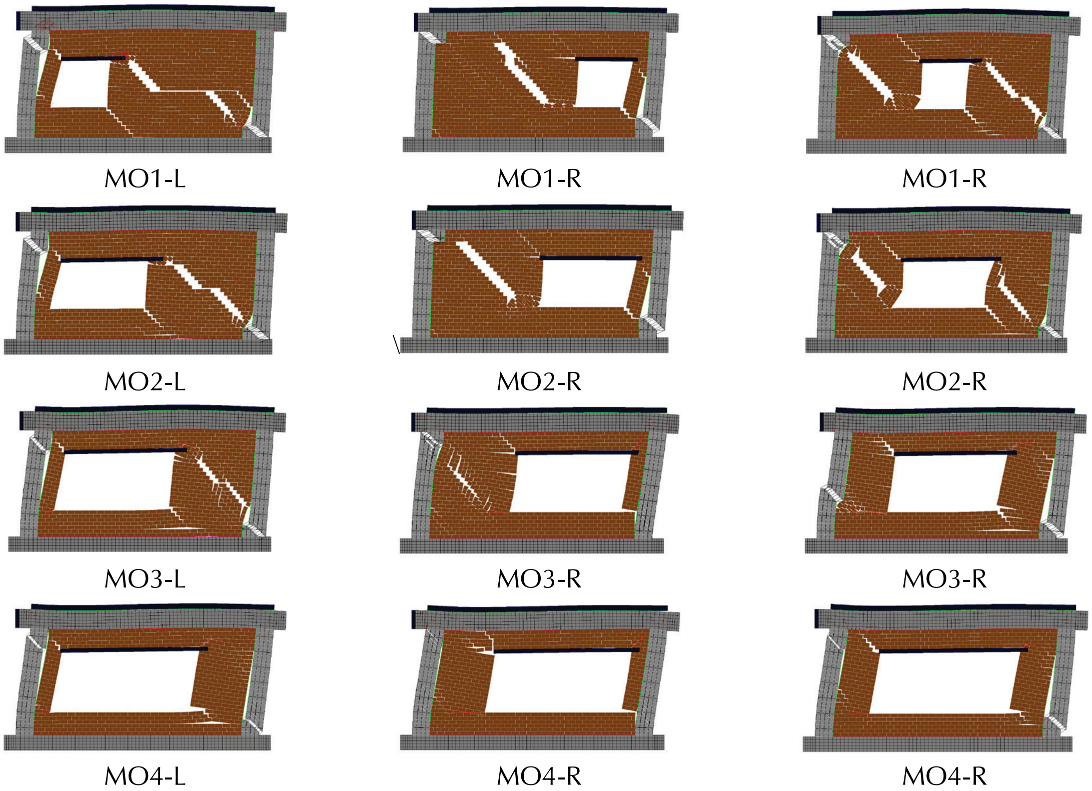

MO1-L MO1-R MO1-R

MO2-L MO2-R MO2-R

MO3-L MO3-R MO3-R

MO4-L MO4-R MO4-R

Figure O-13 Deformed meshes at 1.0% drift of panels with openings for $f'_m = 0.8$ ksi.

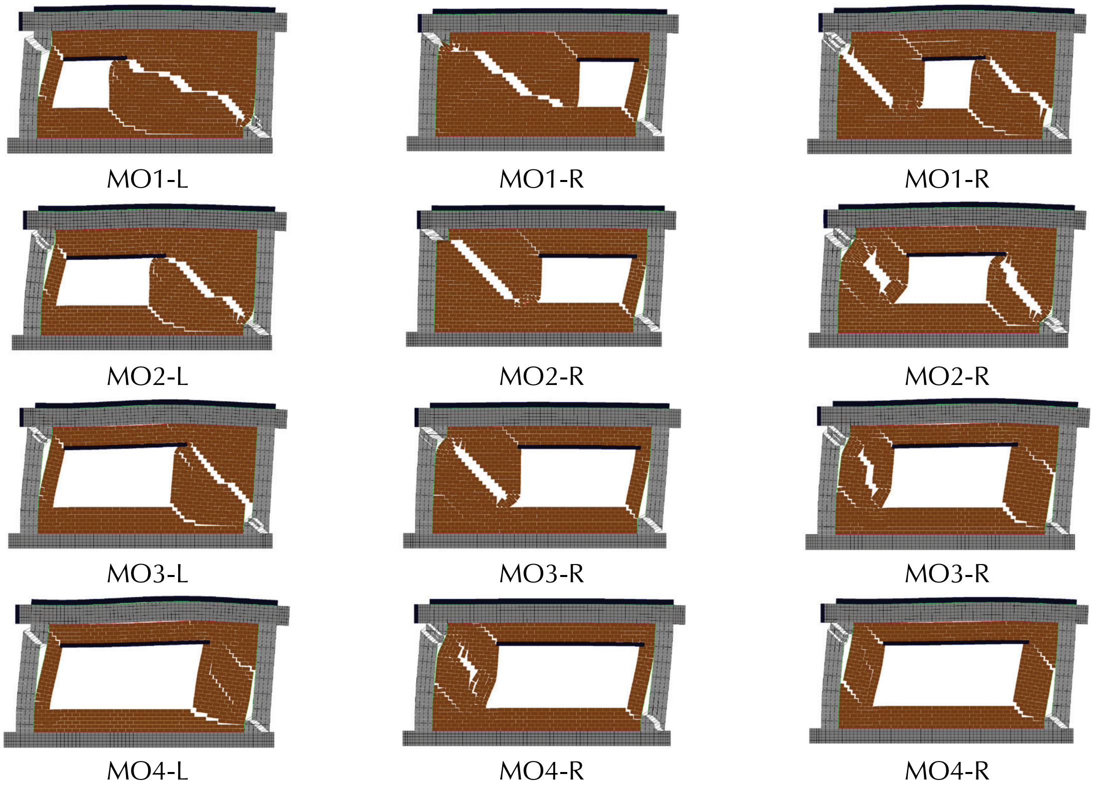
MO1-L MO1-R MO1-R

MO2-L MO2-R MO2-R

MO3-L MO3-R MO3-R

MO4-L MO4-R MO4-R

Figure O-14 Deformed meshes at 1.0% drift of panels with openings for $f'_m = 1.4$ ksi.

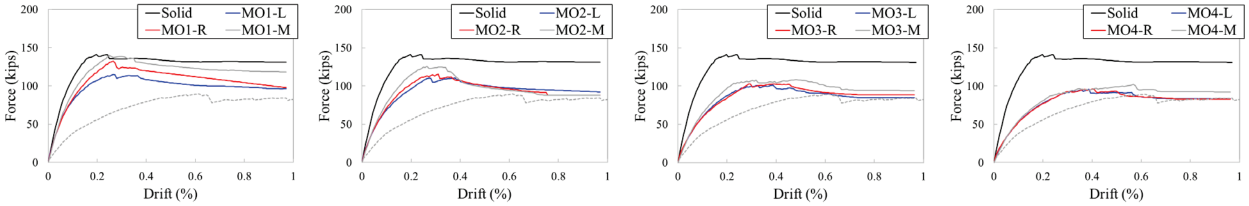

(a) $f'_m = 0.4$ ksi

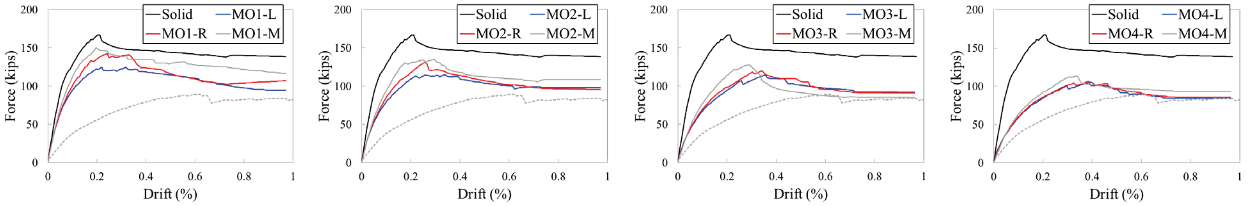

(b) $f'_m = 0.8$ ksi

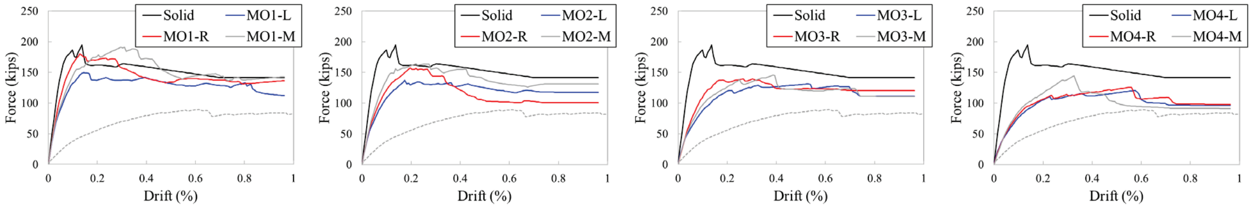

(c) $f'_m = 1.4$ ksi

Figure O-15 Lateral force-vs.-drift behavior of the infilled panels with openings of different size and locations.

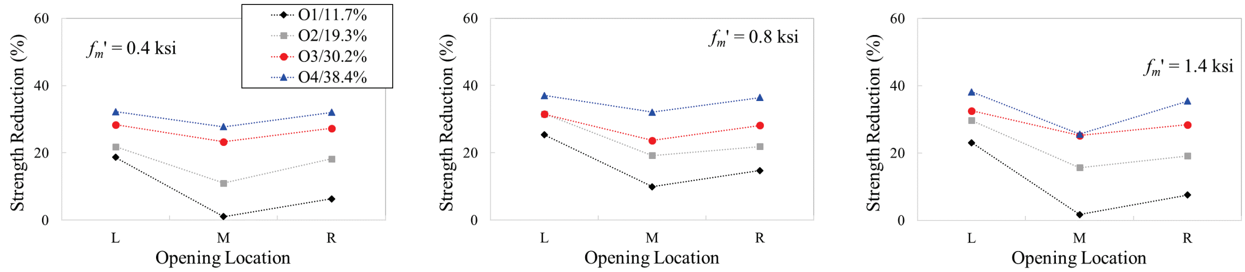

Figure O-16 Strength reduction of infilled frames as a function of opening location compared to the frame with a solid panel.

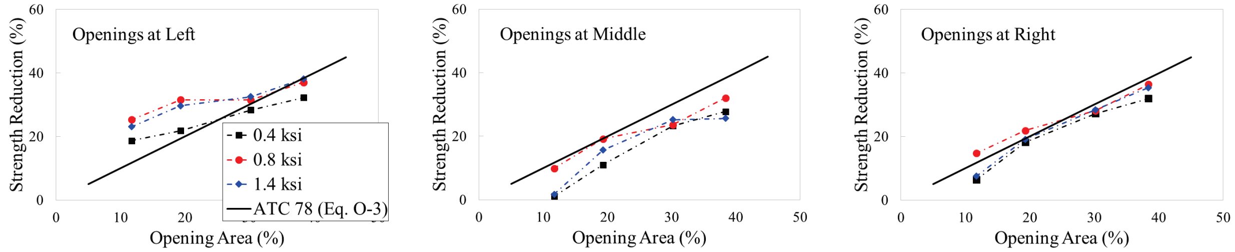

Figure O-17 Strength reduction of infilled frames as a function of opening area compared to the frame with a solid panel.

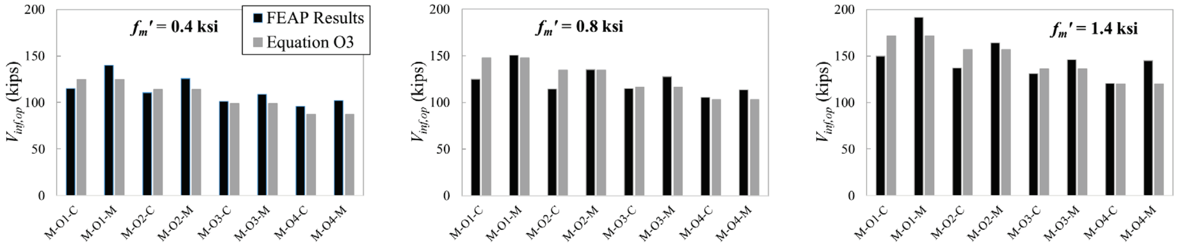

Figure O-18 Comparison of strength of infilled bays with openings obtained from Equation O-3 and detailed FE analyses in FEAP.

O.3.7 When to Ignore Infills in Strength

As indicated by the results of incremental dynamic analyses in Section O.2.4, the collapse potential of the model M3, which incorporates double wythe masonry panels with a low compressive strength, f_m', of 0.4 ksi, is similar to that of the corresponding bare frame. Based on this observation, it can be concluded that the masonry infill in Model M3 is weak enough to not affect the behavior of the building frame in terms of its collapse potential. The strength ratio of the infill and bounding frame is 1.4 for M3. Hence, this value of the strength ratio is adopted here as a criterion to define an infill that can be ignored in the strength calculations ($V_m/V_{lc} < 1.4$). This observation together with Equation O-3 results in Table O-10 which provides guidance as to the classification of infilled frames (with and without openings) in terms of their contribution to the lateral resistance.

Since the collapse potential of M3 is similar with or without the infills in the perimeter bays, the strength of a solid panel with the masonry properties same as model M3 (141 kips) is considered as the criteria to ignore infills for strength. Therefore, panels with openings that have strength less than 141 kips can be ignored for strength calculations. The criterion proposed here is consistent with the detailed FE analyses summarized in Table O-11, with very few exceptions, marked in red in the table.

Table O-10 Classification of Infill in Each Infilled Bay

Ratio of Masonry Panel to Column Strength	Infill Classification	Implication
$\frac{V_m\left(1-{}^{A_{op}}/_{A_{inf}}\right)}{V_{lc}} \geq 3$	Strong	Panel requires full consideration
$3 > \frac{V_m\left(1-{}^{A_{op}}/_{A_{inf}}\right)}{V_{lc}} \geq 1.4$	Weak	Panel requires full consideration
$\frac{V_m\left(1-{}^{A_{op}}/_{A_{inf}}\right)}{V_{lc}} < 1.4$	Very weak due to opening(1)	Neglect in strength calculations, but consider for column rating
$V_m/V_{lc} < 1.4$	Ineffective	Panel can be ignored throughout this methodology

(1) This case also applies when $A_{op}/A_{inf} > 0.6$, but not $V_m/V_{lc} < 1.4$, or if $A_{op}/A_{inf} > 0.2$ with an opening within 2 ft. of the column.

Table O-11 When Infill Panels with Openings Can Be Ignored for Calculation of Strength?

Model ID		Analytical Calculations			FEAP Results			Can Ignore?
		A_{op}/A_{inf} (%)	$V_{m,op}$ (kips)	$V_{m,op}/V_{lc}$	V_{inf} (kips)	Eff. V_{inf} (kips)	$V_{inf,sol}$	
$f_m' = 0.40$ ksi	M-O1-L	0.117	57	1.2	115	115	141	Yes
	M-O1-R		57	1.2	132			
	M-O1-M		57	1.2	140	140		yes
	M-O2-L	0.193	52	1.1	111	111		yes
	M-O2-R		52	1.1	116			
	M-O2-M		52	1.1	126	126		yes
	M-O3-L	0.302	45	1.0	101	101		yes
	M-O3-R		45	1.0	103			
	M-O3-M		45	1.0	108	108		yes
	M-O4-L	0.384	40	0.9	96	96		yes
	M-O4-R		40	0.9	96			
	M-O4-M		40	0.9	102	102		yes

Table O-11 When Infill Panels with Openings Can Be Ignored for Calculation of Strength? (continued)

		Analytical Calculations			FEAP Results			
	Model ID	A_{op}/A_{inf} (%)	$V_{m,op}$ (kips)	$V_{m,op}/V_{lc}$	V_{inf} (kips)	Eff. V_{inf} (kips)	$V_{inf,sol}$	Can Ignore?
f_m' = 0.80 ksi	M-O1-L	0.117	83	1.8	125	125	167	yes
	M-O1-R		83	1.8	142			
	M-O1-M		83	1.8	150	150		no
	M-O2-L	0.193	76	1.6	114	114		yes
	M-O2-R		76	1.6	130			
	M-O2-M		76	1.6	135	135		yes
	M-O3-L	0.302	66	1.4	114	114		yes
	M-O3-R		66	1.4	120			
	M-O3-M		66	1.4	128	128		yes
	M-O4-L	0.384	58	1.2	105	105		yes
	M-O4-R		58	1.2	106			
	M-O4-M		58	1.2	113	113		yes
f_m' = 1.40 ksi	'M-O1-L	0.117	172	3.6	150	150	194.61	no
	M-O1-R		172	3.6	180			
	M-O1-M		172	3.6	191	191		no
	M-O2-L	0.193	157	3.3	137	137		yes
	M-O2-R		157	3.3	157			
	M-O2-M		157	3.3	164	164		no
	M-O3-L	0.302	136	2.9	131	131		yes
	M-O3-R		136	2.9	139			
	M-O3-M		136	2.9	146	146		no
	M-O4-L	0.384	120	2.5	120	120		yes
	M-O4-R		120	2.5	126			
	M-O4-M		120	2.5	145	144.77		no

O.3.8 *Calculation of Story-Shear Strength*

As indicated in Section O.2.4, the exterior infilled frames reach their peak strength at significantly lower drift ratios compared to the interior columns, which are not infilled. The different drift ratios at which the various components reach their strength are depicted in Figure O-19 for models M1 (strongest infill) and M3 (weakest infill). The figure indicates that when the exterior frames reach their peak strength, the interior frames have reached only 40% of their peak strength in the case of M1 and 80% in M3. This difference is expected as M1 has much stronger infill (f_m' = 1.40 ksi and 3 wythes) compared to M3 (f'_m = 0.40 ksi and 2 wythes), and as a result it reaches its peak strength at significantly lower drift.

This observation indicates that when estimating the strength of buildings with infilled frames in the perimeter and bare columns in the interior, only a fraction of the interior columns' strength should be considered when estimating the peak shear strength of the critical story. This fraction depends on the drift at which the exterior frames reach peak resistance, as indicated in Figure O-19. Based on these observations, the story-shear strength is calculated for the critical story based on Equation O-4.

$$V_{px} = \sum_{i=1}^{n_{inf}} V_{inf,op} + \beta \sum_{i=1}^{n_c} V_{ncx} + \sum_{i=1}^{n_{wall}} V_{nw,i} \tag{O-4}$$

where, n_{inf} is the number of infilled bays at the critical story, n_{wall} is the number of structural concrete walls, n_c is the total number of interior columns that do not have infill panels abutting either side of the column in the direction of loading and the columns in the exterior frames next to infills whose strength is ignored. For each column, V_{nc} may be governed by the columns, or slab-column or beam strength, whichever is lower.

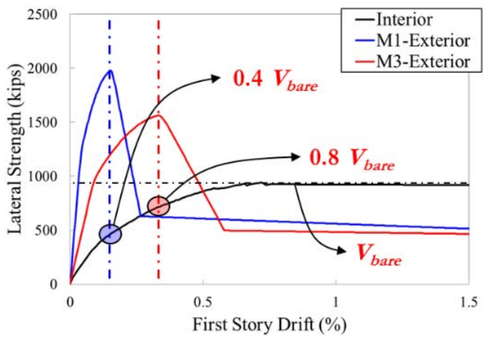

Model	*Contribution of non-infilled columns*
M1	**0.41**
M2	**0.85**
M3	**0.80**
M4	**0.45**
M5	**0.84**

Figure O-19 Contribution of non-infilled columns at the peak strength of infilled frames.

The β-factor determines the contribution of the non-infilled columns to the total strength. It is a function of the drift at which the strongest infilled frame reaches its peak shear resistance (i.e., the minimum of the Δ_{peak} values computed for all of the infilled bays at the critical story in each loading direction). Δ_{peak} can be evaluated based on the ASCE 41-17 provisions, which are also provided in Chapter 5 of this methodology. As shown in Figure O-19, β varies linearly from 0.4 to 0.9 for Δ_{peak} from 0.15% to 0.4%, and it is equal to 0.9 for $\Delta_{peak} > 0.4\%$.

The maximum base shear for each prototype computed using Equation O-4 is compared to the strength estimated by the pushover analyses in Table O-12 obtained following the ASCE 41-17 framework and its extension by Bose et al. (2018). The comparison indicates that the proposed equation, though simple, provides a good estimate of the strength of the structures obtained from more sophisticated nonlinear analysis.

Table O-12 Collapse Potential of the Infilled Buildings and Frame Counterparts

Models	Base Shear Strength (kips)	
	Pushover Analyses	Equation O-4
M1	2250	2261
M2	1819	1789
M3	1776	1757
M6	1200	1274
M4	2114	2101
M5	4208	4156

O.4 Estimation of Effective Periods

The effective fundamental period is the period which, when used with Equation 9-1 and an elastic response spectrum with 5% critical damping, can yield the peak displacement the structure will experience at, or close to, 2/3 of its height (here the displacement of the 4th floor is selected for the 4-story buildings, and the displacement of the 7th floor story is selected for the 8-story prototype). This period cannot be obtained with an eigenvalue analyses or other analytical methods. Hence, a parameter sweep is conducted varying the effective period (T_e) from 0.01s to 10s to calculate δ_{eff} and compare it with the 4th floor displacement for models M1 to M4, M6 and the 7th floor displacement for model M5. As shown in Figure O-20, the effective period increases with increasing excitation level and induced damage.

As this method focuses on the prediction of collapse, the effective period corresponding to the collapse initiation (i.e., peak drift of 1.5%) is considered here and the effective periods summarized in Figure O-21 are obtained. The figure indicates that the effective periods of the infilled frames at collapse can be related to the effective period ($T_{e,bare}$) of the bare frame (Equation 5-17), adjusted by the ratio of strengths of the infilled frame to that of the bare frame ($V_{p1}/V_{p1,bare}$) using Equation (O-5). For an infilled frame system, $V_{p1}/V_{p1,bare}$ shall not be taken greater than 2.0.

$$T_e = \left(1.6 - 0.6\frac{V_{p1}}{V_{p1,bare}}\right)T_{e,bare} \qquad \text{(O-5)}$$

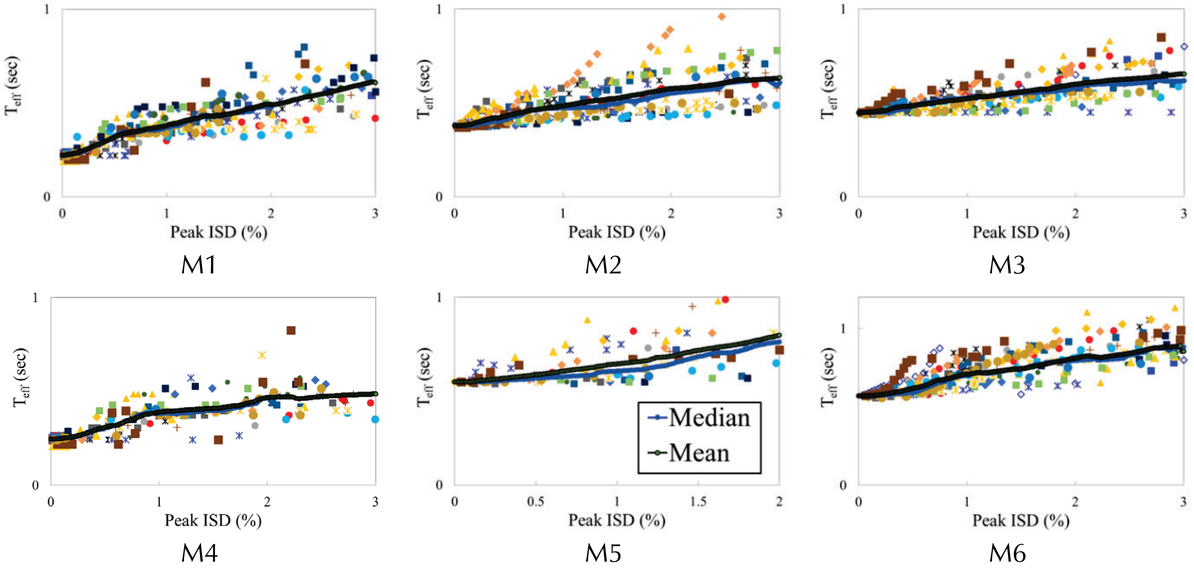

M1 M2 M3

M4 M5 M6

Figure O-20 Variation of T_e with increase in seismic excitation of the infilled frame models M1 to M6.

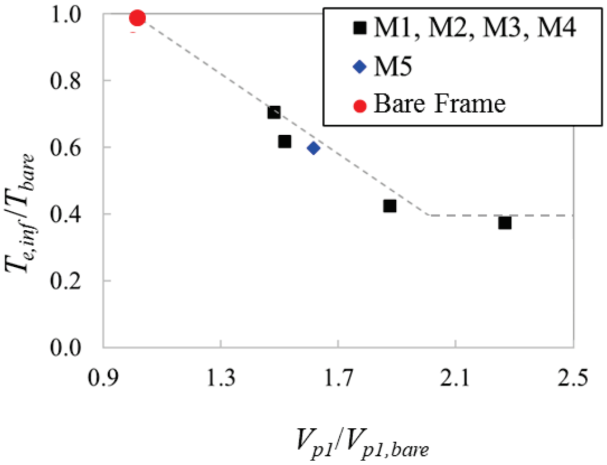

Figure O-21 Estimation of effective period of infilled frames.

O.5 Determination of Story-Drifts

The estimation of effective period, T_e, according to Equation O-5 facilitates the calculation of global effective seismic demand, δ_{eff}, based on Equation 9-1. The story drift demand, δ_x, is calculated based on Equation 9-4 which uses the α-factors to modify the story drifts considering the number of stories in a building and the yield mechanism. The displacement profiles of models M1 to M6 at collapse are normalized such that the δ_{eff} (4th floor displacement in the 4-story buildings and the 7th floor in M5) is equal to 1, and are presented in Figure O-22. The figures present the median normalized displacement profiles. The fractions of δ_{eff} concentrated in the bottom story for the infilled buildings are summarized in Table O-13. It can be observed from the table that the displacement at the first story of the models varies from 81 to 98% of δ_{eff}. In addition, the maximum and the minimum values indicate that there is small variability in the values. For consistency with the other structural systems, the coefficient α is determined according to Table 9-1. This table is similar to Table 7-1 developed for shear wall buildings, which assumes the drift demand at the critical story is 0.8 times the effective global drift demand.

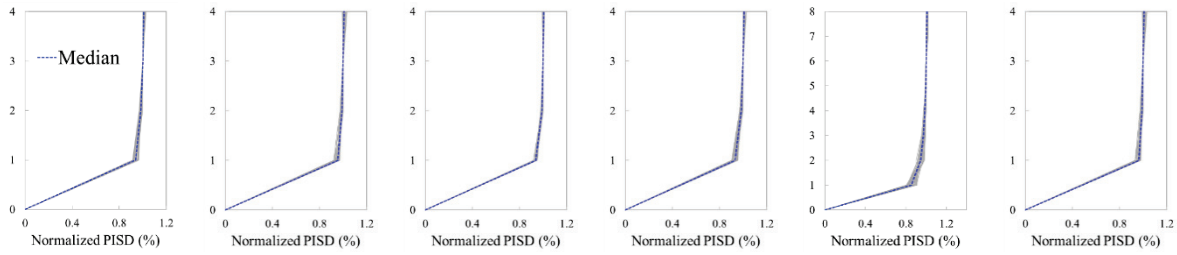

M1 M2 M3 M4 M5 M6

Figure O-22 Normalized displacement profile of the infilled frame buildings with δ_{eff} = 1.0.

Table O-13 Fraction of the Drift Demand in the First Story

Models	Min of 22 GMs	Max of 22 GMs	Median
M1	0.91	0.96	0.94
M2	0.92	0.97	0.95
M3	0.92	0.95	0.94
M4	0.90	0.96	0.93
M5	0.81	0.91	0.85
M6	0.93	0.98	0.96

O.6 Impact of Infill on Column Ratings

The rating of the building in this methodology is based on ratings of critical components (e.g., columns, walls, slab-column connections), which are used to determine the story and building ratings. Infill panel walls are not considered critical components and therefore are not rated. The effect of infill panels on column shear failure is considered by shortening the effective height of the column. In addition, infill panels can support substantial gravity loads, essentially preventing collapse of columns even if they are failed in shear. An example of this phenomenon is shown in Figure O-23.

In this methodology, the ability of infill to carry gravity loads is considered by applying a reduction in the column rating (indicating a better performing column) if infill is likely to be intact and load bearing at the drift levels under consideration, as shown in Table 9-8. Two factors are considered in evaluating an infill's capacity to bear gravity loads. First, panels that are very slender (high h_{inf}/t_{inf}) are likely to fail out of plane and, therefore, are not expected to carry vertical loads following a damaging earthquake. Two limits on h_{inf}/t_{inf} are proposed. h_{inf}/t_{inf} of 25 is based on FEMA 273. The value of h_{inf}/t_{inf} of 35 is based on test results from Angel et al. (1994). Second, panels that have experienced large in-plane deformations are also unlikely to carry significant gravity loads. The limits on in-plane deformations are based on studies by Martin and Stavridis (2017; 2018), which quantified the deformation at which residual strength is reached for infilled frame bays with various configurations. The reduction in column rating applied is based on judgment.

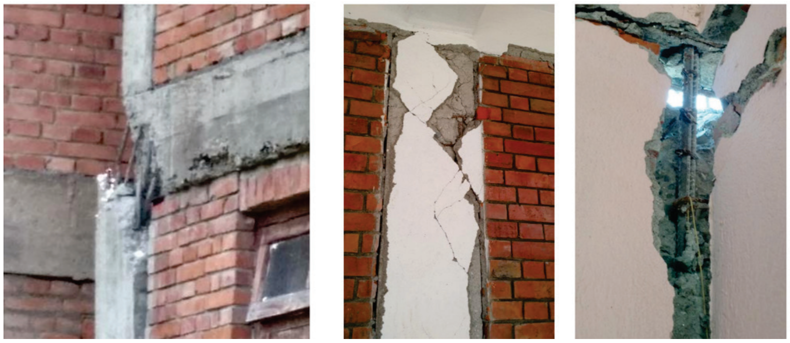

Figure O-23 Damage to an infilled frame building, showing severely damaged columns, but no collapse. Infill panels are likely carrying significant portion of the gravity loads (Bose et al., 2017).

Symbols

a	site class factor, or coefficient for calculation of neutral axis depth of a wall
A_b	area of an individual reinforcing bar, in^2
A_{base}	area of the base of a structure, ft^2
A_f	total area of floors above the story under consideration, ft^2
A_g	gross area of concrete section, in^2
A_{inf}	area of infill panel, in elevation, ft^2
A_j	effective cross-sectional area of a joint, in^2
A_{op}	area of openings in infill panel, in elevation, ft^2
A_s	area of longitudinal tension reinforcement, in^2
A_{sb}	total area of main slab bottom reinforcement passing through, or anchored within, a column cage, in^2
$A_{T, max}$	maximum torsional amplification factor
A_T	torsional amplification factor
A_v	area of shear or transverse reinforcement within spacing s, in^2
A_w	area of webs and associated boundary elements in structural walls in a story in the direction under consideration, ft^2
$A_{w,inf}$	horizontal cross-sectional area of infill panel, in^2 or ft^2
b	plastic rotation at loss of gravity load-carrying ability (from ASCE/SEI 41), or coefficient for calculation of neutral axis depth of a wall
b_c	overall width of a column in the direction perpendicular to shear, inches
BR	building rating
b_w	web width (or thickness) of a beam, column, or wall segment, inches
b'_w	web width of a beam, excluding portions of the web that extend beyond the width of a column, inches

c	neutral axis depth in wall, feet or inches
C	expected cohesion of masonry mortar joint, psi
C_1	modification factor to relate expected maximum inelastic displacement to displacement calculated for linear elastic response
C_2	modification factor to represent the effect of pinched hysteresis shape, cyclic stiffness degradation, and strength deterioration on maximum displacement response
C_m	effective mass factor
CMU	concrete masonry unit
COV	the standard deviation of all column ratings at a story divided by the weighted mean column rating at that story
CR	column rating
CR_{adj}	adjusted average column rating in a story
$\overline{CR}$	the mean column rating for all columns in the story
C_{vx}	vertical distribution factor for story forces
C_w	coefficient for effective fundamental period of frame-wall structures
d	effective depth or the distance from extreme compression fiber to centroid of longitudinal tension reinforcement, inches
d_{op}	distance between opening in infill panel and the nearest column, inches or feet
$DCR_{(avg)}$	average value of DCR_x over the height of the building
$DCR_{(max)}$	maximum value of DCR_x over the height of the building
DCR_x	relative demand-to-capacity ratio for story x
e	real (inherent) eccentricity between the center of mass and the center of strength, feet
E_c	modulus of elasticity of concrete, psi
f'_c	specified compressive strength of concrete, psi
f'_{ce}	expected compressive strength of concrete, psi
f_{col}	fraction of gravity loads supported by columns in a story
f'_m	expected compressive strength of the masonry assembly
f_y	specified yield strength of reinforcement, psi or ksi
f_{ye}	expected yield strength of reinforcement, psi or ksi

f_{wall}	fraction of gravity loads in a story supported by wall
g	acceleration of gravity, in/sec^2
G	limit state function defining failure of a column
h_b	overall depth of a beam, inches
h_c	overall dimension of a column in the direction of shear, inches
h_{eff}	effective height of the building, taken as the height from the base to the centroid of lateral forces (same as the effective height of an equivalent single-degree-of-freedom system), feet or inches
h_i, h_x	height from the base of the building to level i or level x, feet
h_{inf}	height of the infill panel, inches or feet
h_n	height from the base of the building to the highest level of the seismic force-resisting system, feet or inches
h_{op}	height of opening in an infill panel, inches or feet
h_{sx}	height of story x
h_x	height from the base of a building to level x
h_w	height of shear wall, feet; clear height of wall segment, inches
I_e	effective moment of inertia of a concrete section, in^4
I_g	moment of inertia of gross concrete section about centroidal axis, neglecting reinforcement, in^4
k	factor related to ductility demand for computing column shear strength
K_e	effective stiffness of a building, k/in
l_{inf}	height of an equivalent cantilever column, from the face of a joint to the point of inflection (or zero moment), inches
l_n	clear span of beam measured face-to-face of supports, inches
l_u	clear height of a column, inches or feet
$l_{u,inf}$	clear height of a column with abutting infill on either side in the direction of loading, inches or feet
l_w	length of shear wall or wall segment, inches or feet
L	overall building plan dimension, or plan dimension between the outermost frame columns in a story, feet
L_{inf}	length of the infill panel, inches or feet

L_{op}	length of opening in an infill panel, inches or feet
L_1	longer dimension between the edge of the building and the center of strength
L_2	shorter dimension between the edge of the building and the center of strength
M_{cB}	flexural strength at the bottom of a column, kip-inches
M_{cT}	flexural strength at the top of a column, kip-inches
M_n	expected flexural strength of a column, wall, or beam, calculated using expected material properties and strength reduction factor (ϕ) equal to 1.0, kip-inches
M_{nb}	flexural strength of a beam, in mechanism calculations, kip-inches
M_{nc}	flexural strength of a column, in mechanism calculations, kip-inches
M_{nj}	flexural strength of beam-column, slab-column, beam-wall, and slab-wall connections (joints), in mechanism calculations, kip-inches
M_{ns}	moment transfer strength of slab-column connections, in mechanism calculations, kip-inches
M_{nw}	flexural strength of a wall, in mechanism calculations, kip-inches
M_{OT}	overturning moment at the base of a building, kip-feet
M_{OTi}	overturning resistance provided by an individual frame in a building, kip-feet
ΣM_c	summation of column expected flexural strengths, kip-inches
ΣM_b	summation of beam expected flexural strengths, kip-inches
n	number of levels or number of stories in a building
n_c	number of interior columns that do not have abutting infill panels on either in the direction of loading
n_{col}	number of columns in story x
n_f	number of frame or wall lines in story x
n_{inf}	number of infilled bays at the critical story
n_s	number of struts developed in an infill panel
n_{wall}	number of walls in story x
p_f	probability of column drift demand exceeding column drift capacity
P	total column axial load, kips

P_D	axial load due to tributary dead loads, kips
P_{eq}	axial load due to earthquake overturning effects, kips
P_g	axial load due to gravity effects, kips or pounds
P_{inf}^{grav}	vertical load initially supported by an infill panel, kips
P_L	axial load due to unreduced tributary live loads, kips
P_{inf}^{max}	vertical load supported by an infill panel when the maximum (lateral) strength is reached, kips
P_{OT}	axial load due to earthquake overturning effects on corner columns, kips
P_T	total gravity load above story under consideration, kips
R_{adj}	adjusted average of column ratings in a story
R_{avg}	weighted average column rating for all columns in the story, where the average is weighted by the gravity load taken by each column
R_{fi}	perpendicular distance from frame or wall line to the center of strength (for torsion), feet
s	spacing of transverse reinforcement, inches
S_a	spectral acceleration at the effective fundamental period of the building, percentage of g
$S_{a,\,collapse}$	spectral acceleration at collapse at the effective fundamental period of the building, percentage of g
S_d	spectral displacement at the effective fundamental period of the building
SR	story rating
S_S	mapped spectral response acceleration parameter at short periods, percentage of g
S_1	mapped spectral response acceleration parameter at a period of one second, percentage of g
S_{XS}	site class adjusted spectral response acceleration parameter at short periods, percentage of g
S_{X1}	site class adjusted spectral response acceleration parameter at a period of one second, percentage of g
t_{inf}	net thickness of infill panel, inches or feet

T_{bare}	upper bound period of an infilled frame evaluated without any infill panels, s
T_{Cx}	torsional capacity of story x, kip-feet
T_{Dx}	torsional demand at story x, kip-feet
T_e	effective fundamental period of a building, seconds
TR	torsional ratio at the critical story
v	shear stress, psi
V_b	expected shear strength of a beam, kips
V_c	punching shear strength of concrete
$V_{inf,solid}$	strength of single infilled bay with solid infill, kips
$V_{inf,open}$	strength of single infilled bay adjusted for openings, kips
V_g	unfactored gravity shear demand, kips
V_{lc}	strength of the weaker of the two columns bounding an infill panel of interest, kips
V_m	shear strength of a single masonry infill panel, kips
V_n	expected shear strength of a column, wall, or beam, kips or pounds
V_{nc}	shear strength of a column, in mechanism calculations, kips
V_{nj}	expected joint shear strength, kips or pounds
V_{nw}	shear strength of a wall, in mechanism calculations, kips
V_p	column capacity-limited (plastic) shear strength, pounds or kips
V_{pf}	plastic shear capacity of a frame or wall line, kips or pounds
V_{pMx}	column shear capacity controlled by flexure in story x, kips
V_{p1}	plastic mechanism base-shear strength at story 1, kips or pounds
$V_{p1,bare}$	plastic mechanism base-shear strength of an infilled frame evaluated without infill panels, kips
V_{px}	plastic mechanism shear strength at story x, kips or pounds
V_{rx}	relative story shear demand at story x, kips or pounds
V_y	effective yield strength of a structure, kips or pounds
W	total effective seismic weight of a building, kips
W_x	effective seismic weight above story x, kips
WI	wall index

WR	wall rating
WSI	wall strength index
w_x	portion of the total effective seismic weight tributary to level x, kips
x, y	distance from center of strength to column or wall line of interest, feet
x	story under consideration
α_x	coefficient to modify story drifts at story x for building configuration and strength characteristics
α	ratio of post-yield stiffness to initial effective stiffness before yield
α'	coefficient to modify story drifts at a given story for building configuration, recalculated from α considering only the simulations in which the story collapsed
β	reliability index for a given column (Appendix A)
β	contribution of frame elements to the total strength of an infilled frame system
γ	drift factor representing the fraction of story drift affecting the critical component
δ_{eff}	global displacement demand of an equivalent single degree-of-freedom system, inches
δ_{col}	column drift demand, inches
δ_x	story drift demand at story x, inches
δ_{x1}	story drift demand at story x amplified for P-delta effects, inches
δ_y	yield displacement at the roof of a building, inches
$\mathit{\Delta}_C$	drift capacity of a column, slab-column connection, beam-column corner connection, wall, or vertical wall segment, inches or percent
$\mathit{\Delta}_D$	adjusted column drift demand, inches
$\tilde{\mathit{\Delta}}_C$	median drift capacity of a particular column, inches
$\tilde{\mathit{\Delta}}_D$	median drift demand on a particular column, inches
$\mathit{\Delta}_{peak}$	drift at which the peak strength of the infilled bays is reached, percent
$\mathit{\Delta}_{res}$	drift at onset of residual strength for infilled bays, inches or feet
ϕ	strength reduction factor

λ	modification factor for lightweight concrete
μ	expected initial friction coefficient of masonry mortar joints
$\mu_{strength}$	global demand-to-capacity ratio
θ_c	column plastic rotation capacity, radians
ρ_n	transverse reinforcement ratio of a wall
ρ_t	shear reinforcement ratio of a column
$\sigma_{\ln,\Delta_C}$	standard deviation of the drift capacity (in log space)
$\sigma_{\ln,\Delta_D}$	standard deviation of the drift demand (in log space)

References

Abdullah, S.A., and Wallace, J.W., 2018a, "UCLA-RCWalls database for reinforced concrete structural walls," *Proceedings, 11th National Conference in Earthquake Engineering*, Earthquake Engineering Research Institute, Los Angeles, California.

Abdullah, S.A., and Wallace J.W., 2018b, "Drift capacity of RC structural walls with special boundary elements," *ACI Structural Journal*, accepted for publication, 33pp.

Abdullah, S.A., and Wallace J.W., 2018c, "A reliability-based design methodology for RC structural walls with special boundary elements," *ACI Structural Journal*, submitted for review and possible publication, May 4, 2018, 33pp.

ACI, 1977, *Building Code Requirements for Reinforced Concrete*, ACI 318-77, American Concrete Institute, Detroit, Michigan.

ACI, 2008, *Guide to Durable Concrete*, ACI 201.2R-08, American Concrete Institute, Farmington Hills, Michigan.

ACI, 2011, *Building Code Requirements for Structural Concrete and Commentary*, ACI 318-11, American Concrete Institute, Farmington Hills, Michigan.

ACI, 2011b, *Guide for Seismic Rehabilitation of Existing Concrete Frame Buildings and Commentary*, ACI 369R-11, American Concrete Institute, Farmington Hills, Michigan.

ACI, 2014, *Building Code Requirements for Structural Concrete and Commentary*, ACI 318-14, American Concrete Institute, Farmington Hills, Michigan.

Angel, R., Abrams, D.P., Shapiro, D., Uzarski, J., Webster, M., 1994, *Behavior of Reinforced Concrete Frames with Masonry Infills*, Civil Engineering Studies—Structural Engineering Research Series No. 589, University of Illinois, Urbana-Champaign, Illinois.

Arteta, C.A., and Abrahamson, N.A., 2017, "Methodology based on conditional scenario spectra to estimate engineering demand parameter risk," *Proceedings, 16th World Conference on Earthquake Engineering*, Santiago, Chile.

ASCE, 2003, *Seismic Evaluation of Existing Buildings*, ASCE/SEI 31-03, American Society of Civil Engineers, Structural Engineering Institute, Reston, Virginia.

ASCE, 2007, *Seismic Rehabilitation of Existing Buildings*, ASCE/SEI 41-06, American Society of Civil Engineers, Structural Engineering Institute, Reston, Virginia.

ASCE, 2010, *Minimum Design Loads for Buildings and Other Structures*, ASCE/SEI 7-10, American Society of Civil Engineers, Structural Engineering Institute, Reston, Virginia.

ASCE, 2013, *Seismic Evaluation and Retrofit of Existing Buildings*, ASCE/SEI 41-13, American Society of Civil Engineers, Structural Engineering Institute, Reston, Virginia.

ASCE, 2017a, *Minimum Design Loads and Associated Criteria for Buildings and Other Structures, Provisions*, ASCE/SEI 7-16, American Society of Civil Engineers, Structural Engineering Institute, Reston, Virginia.

ASCE, 2017b, *Seismic Evaluation and Retrofit of Existing Buildings*, ASCE/SEI 41-17, American Society of Civil Engineers, Structural Engineering Institute, Reston, Virginia.

Aslani, H., 2005, *Probabilistic Earthquake Loss Estimation and Loss Disaggregation in Buildings*, Ph.D. Dissertation, Stanford University, Stanford, California.

ATC, 2000, *Database on the Performance of Structures Near Strong-Motion Recordings: 1994 Northridge Earthquake*, ATC-38, Applied Technology Council, Redwood City, California.

ATC, 2011, *Identification and Mitigation of Seismically Hazardous Older Concrete Buildings: Interim Methodology Evaluation*, ATC-78, Applied Technology Council, Redwood City, California.

ATC, 2012, *Evaluation of the Methodology to Select and Prioritize Collapse Indicators in Older Concrete Buildings*, ATC-78-1, Applied Technology Council, Redwood City, California.

ATC, 2013, *Seismic Evaluation for Collapse Potential of Older Concrete Frame Buildings*, ATC-78-2, Applied Technology Council, Redwood City, California.

ATC, 2015, *Seismic Evaluation of Older Concrete Frame Buildings for Collapse Potential*, ATC-78-3, Applied Technology Council, Redwood City, California.

ATC, 2016, *Seismic Evaluation of Older Concrete Frame and Shear Wall Buildings for Collapse Potential*, ATC-78-4, Applied Technology Council, Redwood City, California.

ATC, 2016, *Seismic Evaluation of Older Concrete Frame, Wall, and Frame-Wall Buildings for Collapse Potential*, ATC-78-5, Applied Technology Council, Redwood City, California.

ATC, 2017, *Seismic Evaluation of Older Concrete Frame, Frame-Wall, and Bearing Wall Buildings for Collapse Potential*, ATC-78-6, Applied Technology Council, Redwood City, California.

Baker, J.W., 2011, "Conditional mean spectrum: Tool for ground-motion selection," *Journal of Structural Engineering*, Vol. 137, No. 3, pp. 322-331, doi:10.1061/(Asce)St.1943-541x.0000215.

Baker, J.W., 2015, "Efficient analytical fragility function fitting using dynamic structural analysis," *Earthquake Spectra*, Vol. 31, No. 1, pp. 579-599, doi:10.1193/021113eqs025m.

Beres, A., White, R.N., and Gergely, P., 1992, *Seismic Performance of Interior and Exterior Beam-to-Column Joints Related to Lightly Reinforced Concrete Frame Buildings: Detailed Experimental Results*, NCEER-92-0007, National Center for Earthquake Engineering Research, State University of New York, Buffalo, New York.

Berry, M., Parrish, M., and Eberhard, M., 2004, *PEER Structural Performance Database User's Manual*, Version 1.0, Pacific Earthquake Engineering Research Center, University of California, Berkeley, California.

Bimschas, M., 2010, *Displacement-Based Seismic Assessment of Existing Bridges in Regions of Moderate Seismicity*, Ph.D. Dissertation, Institute of Structural Engineering, Swiss Federal Institute of Technology Zurich.

Blume, J.A., Newmark, N.M., and Corning, L.M., 1961, *Design of Multi-story Reinforced Concrete Buildings for Earthquake Motions*, Portland Cement Association, Chicago, Illinois.

Bose, S., Martin, J., Stavridis, A., 2018, "Simulation framework for infilled RC frames subjected to seismic loads," *Earthquake Spectra* (under review).

Bose, S., Nozari, A., Mohammadi, M.E., Stavridis, A., Babak, M., Wood, R.L., Gillins, D., and Barbosa, A., 2016, "Structural assessment of a school building in Sankhu, Nepal damaged due to torsional response during the 2015 Gorkha earthquake," *Proceedings, A Conference and Exposition on Structural Dynamics of Multiphysical Systems: From Active Materials to Vibroacoustic*s, 34th IMAC, Orlando, Florida.

Bose, S., Nozari, A., Stavridis, A., and Moaveni, B., 2017, "Nonlinear modeling of the seismic performance of a building at Sankhu Nepal during the 2015 Nepal Earthquake," *Proceedings*, 16th World Conference on Earthquake Engineering, Santiago, Chile.

Brando, G., Rapone, D., Spacone, E., Barbosa, A., Olsen, M., Gillins, D., Soti, R., Varum, H., Arede, A., Vila-Pouca, N., Furtado, A., Oliveira, J., Rodriges, H., Stavridis, A., Bose, S., Faggella, M., Gigliotti, R., and Wood, R.L., 2015, *Reconnaissance report on the 2015 Gorkha earthquake effects in Nepal 2015*, XVI Congegno ANIDIS, L'AQUILA, Italy.

Canbolat, B.B., and Wight, J.K., 2008, "Experimental investigation on seismic behavior of eccentric reinforced concrete beam-column-slab connections," *ACI Structural Journal*, Vol. 105, No. 2, pp. 154-162.

Canterbury Earthquakes Royal Commission, 2012, *Final Report*, Canterbury Earthquakes Royal Commission, Christchurch, New Zealand, http://canterbury.royalcommission.govt.nz/Commission-Reports.

Caughey, R.A., 1933, *Reinforced Concrete*, Edwards Brothers Inc., Ann Arbor, Michigan.

Ciampi, V., and Carlesimo, L., 1986, "A nonlinear beam element for seismic analysis of structures," *Proceedings, 8th European Conference on Earthquake Engineering*, Lisbon, Portugal.

DeBock, D.J., Liel, A.B., Haselton, C.B., Hooper, J.D., and Henige, R.A., 2014, "Importance of seismic design accidental torsion requirements for building collapse capacity," *Earthquake Engineering and Structural Dynamics*, Vol. 43, No. 6, pp. 831-850.

DeBock, D.J., 2017, *New Studies on Effects of Torsional Irregularities*, ATC-123 Project unpublished manuscript, Applied Technology Council, Redwood City, California.

De Souza, R.M., 2000, *Force-based Finite Element for Large Displacement Inelastic Analysis of Frames*, Ph.D. Dissertation, University of California, Berkeley, California.

Dhakal, R., and Maekawa, K., 2002, "Modeling for postyield buckling of reinforcement," *Journal of Structural Engineering*, Vol. 128, No. 9, pp. 1139-1147.

EERI, 1996, "Northridge earthquake of January 17, 1994 reconnaissance report," *Earthquake Spectra*, Vol. 12, No. S1.

EERI, 2000, "Kocaeli, Turkey earthquake of August 17, 1999 reconnaissance report," *Earthquake Spectra*, Vol. 16, No. S1.

Ellingwood, B., Galambos, T.V., MacGregor, J.G., and Cornell, C.A., 1980, *Development of a Probability Based Load Criterion for American National Standard A58*, National Bureau of Standards, Special Publication 577, Washington, D.C.

Elnady, E.M.M., 2008, *Seismic Rehabilitation of RC Structural Walls*, Ph.D. Dissertation, McMaster University, Hamilton, Ontario, Canada.

Elwood, K.J., 2004, "Modelling failures in existing reinforced concrete columns," *Canadian Journal of Civil Engineering*, Vol. 31, No. 5, pp. 846-859.

Elwood, K.J., 2005, "Modeling failures in existing reinforced concrete columns," *Canadian Journal of Civil Engineering*, Vol. 31, No. 5, pp. 846-859.

Elwood, K.J. and Eberhard, M.O., 2009, "Effective stiffness of reinforced concrete columns," *ACI Structural Journal*, Vol. 106, No.4, pp. 476-484.

Elwood, K.J., Matamoros, A.B., Wallace, J.W., Lehman, D.E., Heintz, J.A., Mitchell, A.D., Moore, M.A., Valley, M.T., Lowes, L.N., Comartin, C.D., and Moehle, J.P., 2007, "Update to ASCE/SEI 41 concrete provisions," *Earthquake Spectra*, Vol. 23, No. 3, pp. 493-523.

Elwood, K.J., and Moehle, J.P., 2005, "An axial capacity model for shear-damaged columns," *ACI Structural Journal*, Vol. 102, No. 4, pp. 578-587.

Elwood, K.J., and Moehle, J.P., 2008, "Dynamic shear and axial-load failure of reinforced concrete columns," *Journal of Structural Engineering*, Vol. 134, No. 7, pp. 1189-1198, doi:10.1061/(Asce)0733-9445(2008) 134:7(1189).

FEMA, 1998, *Evaluation of Earthquake Damaged Concrete and Masonry Wall Buildings*, FEMA 306, prepared by the Applied Technology Council for the Federal Emergency Management Agency, Washington, D.C.

FEMA, 2000, *Prestandard and Commentary for the Seismic Rehabilitation of Buildings*, FEMA 356, prepared by the American Society of Civil Engineers for the Federal Emergency Management Agency, Washington, D.C.

FEMA, 2009, *Quantification of Building Seismic Performance Factors*, FEMA P-695, prepared by the Applied Technology Council for the Federal Emergency Management Agency, Washington, D.C.

FEMA, 2012, *Seismic Performance Assessment of Buildings, Methodology, and Implementation*, FEMA P-58, prepared by the Applied Technology Council for the Federal Emergency Management Agency, Washington, D.C.

FEMA, 2016, *Rapid Visual Screening of Buildings for Potential Seismic Hazards: A Handbook, Third Edition*, FEMA P-154, prepared by the Applied Technology Council for the Federal Emergency Management Agency, Washington, D.C.

FEMA, 2018, *Seismic Performance Assessment of Buildings, Methodology, and Implementation*, FEMA P-58 (Second Edition), prepared by the Applied Technology Council for the Federal Emergency Management Agency, Washington, D.C.

Filippou, F.C., Popov, E.P., and Bertero, V.V., 1983, *Effects of Bond Deterioration on Hysteretic Behavior of Reinforced Concrete Joints*, UCB/EERC-83/19, University of California, Berkeley, California.

Galanis, P.H., and Moehle, J., 2015, "Development of collapse indicators for risk assessment of older-type reinforced concrete buildings," *Earthquake Spectra*, Vol. 31, No. 4, pp. 1991-2006, doi:10.1193/080613EQS225M.

Gao, X., Stavridis, A., Bolis, V., and Preti, M., 2018, "Experimental study on the seismic performance of non-ductile RC frames infilled with sliding subpanels," *Proceedings, 11th National Conference on Earthquake Engineering*, Los Angeles, California.

Ghannoum, W.M., 2017, "Updates to modeling parameters and acceptance criteria for non-ductile and splice-deficient concrete columns," *Proceedings, 16th World Conference on Earthquake Engineering, Santiago*, Chile.

Ghannoum, W.M., and Matamoros, A.B., 2014, *Nonlinear Modeling Parameters and Acceptance Criteria for Concrete Columns*, American Concrete Institute, ACI Special Publication 297, Farmington Hills, Michigan.

Ghannoum, W.M., and Sivaramakrishnan, B., 2012a, "ACI 369 Rectangular Column Database: Network for Earthquake Engineering Simulation (NEES)," https://nees.org/resources/3658.

Ghannoum, W.M., and Sivaramakrishnan, B., 2012b, "ACI 369 Circular Column Database: Network for Earthquake Engineering Simulation (NEES)," https://nees.org/resources/3659.

Goel, R., and Chopra, A.K., 1997a, *Vibration Properties of Buildings Determined from Recorded Earthquake Motions*, Earthquake Engineering Research Center, University of California, UCB/EERC-97/14, Berkeley, California.

Goel, R., and Chopra, A.K., 1997b. "Period formulas for moment-resisting frame buildings," *Journal of Structural Engineering*, Vol. 123, No. 11, pp. 1454-1461.

Goel, R., and Chopra, A.K., 1998, "Period formulas for concrete shear wall buildings," *Journal of Structural Engineering*, Vol. 124, No. 4, pp. 426-433.

Gogus, A., and Wallace, J.W., 2015, "Fragility assessment of slab-column connections," *Earthquake Spectra*, Vol. 31, No. 1, pp. 159-177.

Haindl, M., Hube, M., and Arteta, C.A., 2015, "*Seismic Performance Assessment of a Reinforced Concrete Shear Wall House*," VII Congreso Nacional de Ingenieria Sismica, Bogota, Columbia.

Hannewald, P., Bimschas, M., and Dazio, A., 2013, *Quasi-Static Cyclic Tests on RC Bridge Piers with Detailing Deficiencies*, Institut fur Baustatik und Konstruktion, Bericht Nr. 352, ETH Zurich, Zürich, Switzerland.

Haselton, C.B., Liel, A.B., Lange, S., and Deierlein, G.G., 2007, *Beam-Column Element Model Calibrated for Predicting Flexure Response Leading to Global Collapse of RC frame Buildings*, PEER Report 2007/03, Pacific Earthquake Engineering Research Center, University of California, Berkeley, California.

Hassan, W.M., 2011, *Analytical and Experimental Assessment of Seismic Vulnerability of Beam-Column Joints without Transverse*

Reinforcement in Concrete Buildings, Ph.D. Dissertation, University of California, Berkeley, California.

Henkhaus, K., 2010, *Axial Failure of Vulnerable Reinforced Concrete Columns Damaged by Shear Reversals*, Ph.D. Dissertation, Purdue University, West Lafayette, Indiana.

Hines, E.M., Seible, F., and Priestley, M.J.N., 1999, *Seismic Performance of Hollow Rectangular Reinforced Concrete Piers with Highly Confined Corner Elements—Phase I: Flexural Tests, and Phase II: Shear Tests*, Structural Systems Research Project 99/15, University of California, San Diego, California.

ICBO, 1967, *Uniform Building Code*, International Council of Building Officials, Whittier, California.

ICBO, 1976, *Uniform Building Code*, International Council of Building Officials, Whittier, California.

Ibarra, L.F., Medina, R.A., and Krawinkler, H., 2005, "Hysteretic models that incorporate strength and stiffness deterioration," *Earthquake Engineering and Structural Dynamics*, Vol. 34, No. 12, pp. 1489-1511, doi:10.1002/eqe.495.

Imanishi, T., 1996, "Post-yield behavior of multistory reinforced concrete shear walls subjected to bilateral deformations under axial loading," *Proceedings, 11th World Conference on Earthquake Engineering*, Acapulco, Mexico.

Joh, O., Goto, Y., and Shibata, T., 1991, "Behavior of Reinforced Concrete Beam-Column Joints with Eccentricity," *Design of Beam-Column Joints for Seismic Resistance*, *SP-123*, American Concrete Institute, Farmington Hills, Michigan.

Jeon, S.H., and Park, J.H., 2016, "Experimental assessment of numerical models for reinforced concrete shear walls with deficient details," *Journal of the Earthquake Engineering Society of Korea*, Vol. 20, No. 4, pp. 211-222.

Johnston, R.G., 1973, "Veterans Administration Hospital," *San Fernando, California, Earthquake of February 9, 1971*, Vol. I, Pt. B, N.A. Benfer and J.L. Coffman, Editors, L.M. Murphy, Scientific Coordinator, National Oceanic and Atmospheric Administration, Washington, D.C.

Kabeyasawa, T., and Matsumoto, K., 1992, "Tests and analyses of ultra-high strength reinforced concrete shear walls," *Proceedings, 10th World*

Conference on Earthquake Engineering, Madrid, Spain, pp. 3291-3296.

Kent, D.C., and Park, R., 1971, "Flexural members with confined concrete," *Journal of the Structural Division*, Vol. 97, No. 7, pp. 1969-1990.

Kleinbaum, D.G., and Klein, M, 2005, *Survival Analysis: A Self-Learning Text*, Springer Science + Business Media, Inc., New York, New York.

LaFave, J.M., Bonacci, J.F., Burak, B., and Shin, M., 2005, "Eccentric beam-column connections," *Concrete International*, Vol. 27, No. 9, pp. 58-62.

Lew, H.S., Leyendecker, E.V., and Dikkers, R.D., 1971, *Engineering Aspects of the 1971 San Fernando Earthquake*, National Bureau of Standards, Building Science Series 40, Washington, D.C.

Li, Y., Elwood K.J., and Hwang S.-J., 2014, *Assessment of ASCE/SEI 41 Concrete Column Provisions using Shaking Table Tests*, American Concrete Institute, ACI Special Publication 297, Farmington Hills, Michigan.

Looi, D.T.W., Su, R.K.L., Cheng, B., and Tsang, H.H., 2017, "Effects of axial load on seismic performance of reinforced concrete walls with short shear span," *Engineering Structures,* Vol. 151, pp. 312-326.

Luco, N., Mori, Y., Funahashi, Y., Cornell, A., and Nakashima, M, 2003, "Evaluation of predictors of non-linear seismic demands using 'fishbone' models of SMRF buildings," *Earthquake Engineering and Structural Dynamics*, Vol. 32, pp. 2267–2288, doi:10.1002/eqe.331.

Lynn, A., 1999, *Seismic Evaluation of Existing Reinforced Concrete Building Columns*, Ph.D. Dissertation, University of California, Berkley, California.

Marcilla, T., Uma, S.R., and Liel, A., 2017, "Critical structural weaknesses exposed in older RC wall-frame structures during the Christchurch earthquakes," *Proceedings, 16th World Conference on Earthquake Engineering,* Santiago, Chile.

Martin, J., and Stavridis, A., 2017, "Simplified method to assess lateral resistance of infilled reinforced concrete frames," *Proceedings, 16th World Conference on Earthquake Engineering*, Santiago, Chile.

Martin, J., Stavridis, A., 2018, "Lateral resistance of infilled RC frames," *Bulletin of Earthquake Engineering* (under review).

Melchers, R.E., 1999, *Structural Reliability Analysis and Prediction*, Second Edition, John Wiley and Sons Ltd., West Sussex, England.

Melek, M., and Wallace, J.W., 2004, "Cyclic behavior of columns with short lap splices," *ACI Structural Journal*, Vol. 101, No. 6, pp. 802-811.

Moehle, J., 2014, *Seismic Design of Reinforced Concrete Buildings*, McGraw-Hill, New York, New York.

Mohd Yassin, M.H., 1994, *Nonlinear Analysis of Prestressed Concrete Structures under Monotonic and Cyclic Loads*, Ph.D. Dissertation, University of California, Berkeley, California.

Mori, Y., and Ellingwood, B.R., 1993, "Reliability-based service-life assessment of aging concrete structures," *Journal of Structural Engineering*, Vol. 119, No. 5, pp. 1600-1621.

Murphy, L. M., Steinbrugge, K. V., and Duke, C. M., 1973, "The San Fernando earthquake," *San Fernando, California, Earthquake of February 9, 1971*, Vol. I, Part A, L.M. Murphy, Scientific Coordinator, National Oceanic and Atmospheric Administration, Washington, D.C.

MSJC, 2013, *Building Code Requirements and Specification for Masonry Structures,* TMS 402/ACI 530/ASCE 5 and TMS 602/ACI 530.1/ASCE 6, Masonry Standards Joint Committee (MSJC) of The Masonry Society, Boulder, Colorado; the American Concrete Institute, Farmington Hills, Michigan; and the American Society of Civil Engineers, Reston, Virginia.

NEES, 2010, *Mitigation of Collapse Risk in Older Concrete Buildings*, Grand Challenge Research, Pacific Earthquake Engineering Research Center and the Network for Earthquake Engineering Simulation, http://peer.berkeley.edu/grandchallenge/index.html, last accessed November 5, 2014.

NIST, 2010a, *Concrete Model Building Subtypes Recommended for Use in Collecting Inventory Data*, NIST GCR 10-917-6, prepared by the Building Seismic Safety Council for the National Institute of Standards and Technology, Gaithersburg, Maryland.

NIST, 2010b, *Program Plan for the Development of Collapse Assessment and Mitigation Strategies for Existing Reinforced Concrete Buildings*, NIST GCR 10-917-7, prepared by the NEHRP Consultants Joint Venture, a partnership of the Applied Technology Council and the Consortium of Universities for Research in

Earthquake Engineering, for the National Institute of Standards and Technology, Gaithersburg, Maryland.

NIST, 2010c, *Evaluation of the FEMA P-695 Methodology for Quantification of Building Seismic Performance Factors*, NIST GCR 10-917-8, prepared by the NEHRP Consultants Joint Venture, a partnership of the Applied Technology Council and the Consortium of Universities for Research in Earthquake Engineering, for the National Institute of Standards and Technology, Gaithersburg, Maryland.

NIST, 2014, *Review of Past Performance and Further Development of Modeling Techniques for Collapse Assessment of Existing Reinforced Concrete Buildings*, NIST GCR 14-917-28, prepared by the NEHRP Consultants Joint Venture, a partnership of the Applied Technology Council and the Consortium of Universities for Research in Earthquake Engineering, for the National Institute of Standards and Technology, Gaithersburg, Maryland.

NZSEE, 2017, *Seismic Assessment of Existing Buildings*, New Zealand Society of Earthquake Engineering, http://www.eq-assess.org.nz.

Paterson, J., and Mitchell, D., 2003, "Seismic retrofit of shear walls with headed bars and carbon fiber wrap," *Journal of Structural Engineering*, Vol. 129, No. 5, pp. 606–614.

Paulay T., and Priestley M.J.N., 1992, *Seismic Design of Reinforced Concrete Masonry Buildings*, John Willey & Sons, New York, USA.

Pessiki, S.P., Conley, C.H., Gergely, P., and White, R.N., 1990, *Seismic Behavior of Lightly-Reinforced Concrete Column and Beam-Column Joint Details*, NCEER-90-0014, National Center for Earthquake Engineering Research, State University of New York, Buffalo, New York.

Renouard, F., 2014, *Evaluation of a Methodology to Assess the Collapse Risk of Older Reinforced Concrete Buildings*, M.S. Thesis, University of California, Berkeley.

Saitoh, F., Kuramoto, H., and Minami, K., 1990, "Shear behavior of shear walls using high strength concrete," *Summaries of Technical Papers of Annual Meeting, Architectural Institute of Japan*, pp. 605-606 (in Japanese).

Scott, B.D., Park, R., and Priestley, M.J.N., 1982, "Stress-strain behavior of concrete confined by overlapping hoops at low and high strain rates," *ACI Journal Proceedings*, Vol. 79, No. 1, pp. 13-27, doi:10.14359/10875.

Scott, M.H., and Fenves, G.L., 2006, "Plastic hinge integration methods for force-based beam-column elements," *Journal of Structural Engineering*, Vol. 132, No. 2, pp. 244-252, doi:10.1061/(Asce)0733-9445(2006)132:2(244).

Scott, M.H., and Hamutçuoğlu, O.M., 2008, "Numerically consistent regularization of force-based frame elements," *International Journal for Numerical Methods in Engineering*, Vol. 76, No. 10, pp. 612-1631, doi:10.1002/nme.2386.

Sezen, H., and Moehle, J.P., 2004, "Shear strength model for lightly reinforced concrete columns," *Journal of Structural Engineering*, Vol. 130, No. 11, pp. 1692-1703, doi:10.1061/(ASCE)0733-9445(2004)130:11(1692).

Sozen, M.A., 2014, "Surrealism in facing the earthquake risk," *Seismic Evaluation and Rehabilitation of Structures*, Vol. 26, pp. 1-13.

Spacone, E., Filippou, F.C., and Taucer, F.F., 1996, "Fibre beam-column model for non-linear analysis of R/C frame: Part I. Formulation," *Earthquake Engineering and Structural Dynamics*, Vol. 25, pp. 711-725.

Stavridis, A., 2009, *Analytical and Experimental Study of Seismic Performance of Reinforced Concrete Frames Infilled with Masonry Walls*, Ph.D. Dissertation, University of California, San Diego, California.

Stavridis, A., Koutromanos, I., and Shing, P., 2012, "Shake-table tests of a three-story reinforced concrete frame with masonry infill walls," *Earthquake Engineering and Structural Dynamics*, Vol. 41, No. 6, pp. 1089-1108.

Stavridis, A., and Shing, P., 2010, "Finite element modeling of nonlinear behavior of masonry-infilled RC frames," *Journal of Structural Engineering*, Vol. 136, No. 3, pp. 285-296.

Takahashi, S., Yoshida, K., Ichinose, T., Sanada, Y., Matsumoto, K., Fukuyama, H., and Suwada, H., 2013, "Flexural drift capacity of reinforced concrete wall with limited confinement," *ACI Structural Journal*, Vol. 110, No. 1, pp. 95-104.

Thomsen, J.H., and Wallace, J.W., 1995, *Displacement-Based Design of Reinforced Concrete Structural Walls: Experimental studies of walls* *with rectangular and T-shaped cross sections,* Report No. CU/CEE-95/06, Department of Civil and Environmental Engineering, Clarkson University, Potsdam, New York.

Vamvatsikos, D., and Cornell, C.A., 2002, "Incremental dynamic analysis," *Earthquake Engineering and Structural Dynamics*, Vol. 31, No. 3, pp. 491-514, doi:10.1002/eqe.141.

Wallace, J.W., Elwood, K.J., and Massone, L.M., 2008, "Investigation of the axial load capacity for lightly reinforced wall piers," *Journal of Structural Engineering*, Vol. 134, No. 9, pp. 1548-1557.

Wallace, J.W, Massone, L.M., Bonelli, P., Dragovich, J., Lagos, R., Luders, C., and Moehle, J., 2012, "Damage and implications for seismic design of RC structural wall buildings," *Earthquake Spectra*, Vol. 28, No. S1, pp. 281-289.

Wang, T.Y., Betero, V.V., and Popov, E.P., 1975, *Hysteretic Behavior of Reinforced Concrete Framed Walls*, Report No. EERC 75-23, Earthquake Engineering Research Center, University of California, Berkeley, California.

Woods, C., and Matamoros, A., 2010, "Effect of longitudinal reinforcement ratio on the failure mechanism of R/C columns most vulnerable to collapse," *Proceedings, 9th U.S. National and 10th Canadian Conference on Earthquake Engineering*, Toronto, Canada.

Woods, J.E., Lau, D.T., Cruz-Noguez, C.A., and Shaheen, I.K., 2017, "Repair of earthquake damaged squat reinforced concrete shear walls using externally bonded CFRP sheets," *Proceedings, 16th World Conference on Earthquake Engineering*, Santiago, Chile.

Yousefianmoghadam, S., and Stavridis, A., 2016, "Nonlinear response of a dynamically tested two story infilled RC structure at different damage levels," *Proceedings of 2nd Huixian International Forum on Earthquake Engineering for Young Researchers*, Beijing, China.

Project Participants

FEMA Emergency Management Agency

Michael Mahoney (Project Officer)
Federal Emergency Management Agency
400 C Street, SW
Washington, DC 20472

Robert D. Hanson (Technical Monitor)
Federal Emergency Management Agency
5885 Dunabbey Loop
Dublin, Ohio 43017

Applied Technology Council

Jon A. Heintz (Project Manager)
Applied Technology Council
201 Redwood Shores Parkway, Suite 240
Redwood City, California 94065

Project Technical Committee

William T. Holmes (Project Technical Director)
Rutherford + Chekene
375 Beale Street, Suite 310
San Francisco, California 94105

Abbie Liel
University of Colorado, Boulder
Dept. of Civil, Environ., and Arch. Engineering
ECOT 441, UCB 428
Boulder, Colorado 80309

Michael Mehrain
Mehrain Naeim International, Inc.
100 Spectrum Center Drive, Suite 900
Irvine, California 92618

Jack P. Moehle
University of California, Berkeley
Dept. of Civil and Environmental Engineering
3444 Echo Springs Road
Lafayette, California 94549

Peter Somers
Magnusson Klemencic Associates
1301 Fifth Avenue, Suite 3200
Seattle, Washington 98101

Project Review Panel

Terry Lundeen (Chair)
Coughlin Porter Lundeen, Inc.
801 Second Avenue, Suite 900
Seattle, Washington 98104

Michael Cochran
Thornton Tomasetti
4551 Glencoe Avenue, Suite 350
Marina del Rey, California 90292

Gregory G. Deierlein
Stanford University
Dept. of Civil and Environmental Engineering
318 Parkside Drive
Palo Alto, California 94306

Ken Elwood
The University of Auckland
Dept. of Civil and Environmental Engineering
3 Grafton Road
Auckland, New Zealand

Josh Gebelein
Parsons
100 West Walnut Street, C4-03-01
Pasadena, California 91124

Laura N. Lowes
University of Washington
Dept. of Civil and Environmental Engineering
233C More Hall, Box 352700
Seattle, Washington 98195

Khalid Mosalam
University of California, Berkeley
Structural Engineering, Mechanics, and Materials
Civil and Environmental Engineering
723 Davis Hall
Berkeley, California 94720

Robert Pekelnicky
Degenkolb Engineers
375 Beale Street, Suite 500
San Francisco, California 94105

Pui-Shum (Benson) Shing
University of California, San Diego
Dept. of Structural Engineering
9500 Gilman Drive, MC0085
La Jolla, California 92093

Bill Tremayne
Holmes Structures
235 Montgomery Street
San Francisco, California 94104

Fred Turner
1516 40th Street
Sacramento, California 95819

John W. Wallace
University of California, Los Angeles
Dept. of Civil and Environmental Engineering
5731 Boelter Hall
Los Angeles, California 90095

Working Group Members

Saman A. Abdullah
University of California, Los Angeles
2541 Boelter Hall
Los Angeles, California 90095

Carlos Arteta
Universidad del Norte
Km.5 Vía Puerto Colombia, Of. 8-28K
Barranquilla, Colombia

Supratik Bose
University at Buffalo
82 Springville Avenue
Buffalo, New York 14226

Panagiotis Galanis
University of California, Berkeley
760 Davis Hall
Berkeley, California 94720

Cody Harrington
University of Colorado, Boulder
ECOT 441, UCB 428
Boulder, Colorado 80309

Travis Marcilla
University of Colorado, Boulder
4362 Ohio Street
San Diego, California 92104

Pablo Parra
Universidad Adolfo Ibáñez
Avenida Quebrada de Macul #8600
Santiago, Chile

Siamak Sattar
National Institute of Standards and Technology
Engineering Laboratory (MS 8604)
100 Bureau Drive
Gaithersburg, Maryland 20899

Andreas Stavridis
University at Buffalo
Dept. of Civil, Structural, and Environ. Engin.
224 Ketter Hall
Buffalo, New York 14260

Duy Vu To
University of California, Berkeley
15662 Jefferson Street
Midway City, California 92655

Trial Evaluation Participants

Brandow & Johnston, Inc.
Josh Gebelein
700 South Flower Street, Suite 1800
Los Angeles, California 90017

Coughlin Porter Lundeen, Inc.
Terry Lundeen, Rebecca Hix Collins, and Alex Barnes
801 Second Avenue, Suite 900
Seattle, Washington 98104

Degenkolb Engineers (Los Angeles)
Daniel Zepeda and Garrett Hagen
300 South Grand Avenue, Suite 3850
Los Angeles, California 90071

Degenkolb Engineers (San Francisco)
Insung Kim
375 Beale Street, Suite 500
San Francisco, California 94105

Gilsanz Murray Steficek LLP
Ramon Gilsanz, Joe Mugford, and Yuxing Yang
129 W 27th Street
New York, New York 10001

Holmes Structures
Nina Mahjoub and Dion Marriott
523 West 6th Street, Suite 1122
Los Angeles, California 90014

IDS Group
Rami Elhassan, David Pomerleau, and Yangbo Chen
1 Peters Canyon Road, Suite 130
Irvine, California 92606

Murphy Burr Curry, Inc.
David Murphy and Pak Hui
85 Second Street
San Francisco, California 94105

Nishkian Chamberlain
Craig Chamberlain, Jack Hadjian, and Eugene Ungermann
3710 S. Robertson Blvd., Suite 220
Culver City, California 90232

Rutherford + Chekene
Afshar Jalalian, Brett Lizundia, Lawrence Burkett, and Francisco, Parisi
375 Beale Street, Suite 310
San Francisco, California 94105

Simpson Gumpertz & Heger
Kevin O'Connell
1055 W. Seventh Street, Suite 2500
Los Angeles, California 90017

Thornton Tomasetti
Chukwuma G. Ekwueme
4551 Glencoe Avenue, Suite 350
Marina del Rey, California 90292

Thornton Tomasetti (Los Angeles)
Albert Chen, Jeffrey Shoemaker, and Mark Ellis
707 Wilshire Blvd., Suite 4450
Los Angeles, California 90017

Thornton Tomasetti (San Francisco)
Jaime Neilson
650 California Street, Suite 1400
San Francisco, California 94108

University of California, Los Angeles
John W. Wallace, Sofia Gavridou, and Elham Moore
5731 Boelter Hall
Los Angeles, California 90095

University of Washington
Dawn Lehman and Jakob Sumearll
214B More Hall, Box 352700
Seattle, Washington 98195

ZFA Structural Engineers
Mark Moore and Ryan Bogart
100 Bush Street, Suite 1850
San Francisco, California 94104

U.S. DEPARTMENT OF HOMELAND SECURITY

FEMA

FEMA P-2018
Catalog No. 18233-1